

AD-A058 441 MASSACHUSETTS INST OF TECH CAMBRIDGE DEPT OF PHYSICS F/G 17/5
MEASUREMENT OF FREQUENCY OF LIGHT AND ITS APPLICATION. (U)
AUG 78 A JAVAN, M S FELD DAAG29-75-C-0026

MASSACHUSETTS INST OF TECH CAMBRIDGE DEPT OF PHYSICS
MEASUREMENT OF FREQUENCY OF LIGHT AND ITS APPLICATION. (U)
AUG 78 A JAVAN, M S FELD DAAG29-75

F/G 17/5

DAAG29-75-C-0026

ARO-13227.12-P

NL

1 OF 3

AD
A068441

6
MEASUREMENT OF FREQUENCY OF LIGHT
AND ITS APPLICATION,

9
Final Report

Covering the Period June 1, 1975 to May 31, 1978

Submitted by:
Professors Ali Javan
and
Michael S. Feld

11
August 1, 1978

12
225p.

18 ARO

19 13227.12-P

U.S. Army Research Office
Post Office Box 12211
Research Triangle Park, North Carolina 27709

15 DAHGA-75-C-0020

Massachusetts Institute of Technology
Physics Department
Cambridge, Massachusetts 02139

DDC
RECEIVED
SEP 8 1978
E

Approved for public release;
distribution unlimited

78 09 01 071
401 735
j/b

Unclassified

SECURITY CLASSIFICATION OF THIS PAGE (When Data Entered)

REPORT DOCUMENTATION PAGE		READ INSTRUCTIONS BEFORE COMPLETING FORM
1. REPORT NUMBER DRXRO-PT-L-13227-P <i>per ARO office symbol put on by MIT</i>	2. GOVT ACCESSION NO.	3. RECIPIENT'S CATALOG NUMBER
4. TITLE (and Subtitle) Measurement of Frequency of Light and its Application		5. TYPE OF REPORT & PERIOD COVERED Final: 6/1/75-5/31/78
		6. PERFORMING ORG. REPORT NUMBER
7. AUTHOR(s) Professor Ali Javan and Professor M.S. Feld		6. CONTRACT OR GRANT NUMBER(s) DAHC 04 74 C 0017 <i>new</i> DAAG29 75 C0026
9. PERFORMING ORGANIZATION NAME AND ADDRESS Physics Department Massachusetts Institute of Technology Cambridge, MA 02139		10. PROGRAM ELEMENT, PROJECT, TASK AREA & WORK UNIT NUMBERS <i>MIT</i>
11. CONTROLLING OFFICE NAME AND ADDRESS U. S. Army Research Office P. O. Box 12211 Research Triangle Park, NC 27709		12. REPORT DATE August 1, 1978
14. MONITORING AGENCY NAME & ADDRESS (if different from Controlling Office)		13. NUMBER OF PAGES 222
		15. SECURITY CLASS. (of this report) unclassified
		15a. DECLASSIFICATION/DOWNGRADING SCHEDULE
16. DISTRIBUTION STATEMENT (of this Report) Approved for public release; distribution unlimited.		
17. DISTRIBUTION STATEMENT (of the abstract entered in Block 20, if different from Report)		
18. SUPPLEMENTARY NOTES The findings in this report are not to be construed as an official Department of the Army position, unless so designated by other authorized documents.		
19. KEY WORDS (Continue on reverse side if necessary and identify by block number) Speed of light, superradiance, adiabatic rapid passage, free induction decay, far infrared, infrared tunneling resonances, dielectric formation, oxide studies, photoemission, nonlinear spectroscopy, molecular relaxation dynamics, time delayed laser saturation spectroscopy, Raman processes		
20. ABSTRACT (Continue on reverse side if necessary and identify by block number) This three-year contract has covered many rich areas of physics. Measurement of the velocity of light provided equipment and techniques for studying the anomalous Zeeman effect. Several important theoretical studies on superradiance were conducted. The whole field of time delayed laser saturation spectroscopy was opened. A study has been made of the mechanism of optically pumping far infrared lasers. The metal-oxide-metal diode was analysed theoretically and results verified experimentally. Guidelines are given for litho-		

DD FORM 1 JAN 73 1473

EDITION OF 1 NOV 65 IS OBSOLETE

Unclassified

401 735

Count Page

Unclassified

SECURITY CLASSIFICATION OF THIS PAGE (When Data Entered)

Block 20

graphic fabrication of thin film structures to operate in the 10 micron region of the infrared spectrum.

ACCESSION for	
NTIS	White Section <input checked="" type="checkbox"/>
DDC	Buff Section <input type="checkbox"/>
UNANNOUNCED	<input type="checkbox"/>
JUSTIFICATION	
BY	
DISTRIBUTION/AVAILABILITY CODES	
Dist.	AVAIL. and/or SPECIAL
A	

Unclassified

SECURITY CLASSIFICATION OF THIS PAGE (When Data Entered)

Table of Contents

Papers appear in the order listed below

I. Measurement of the speed of light

1. J.-P. Monchalin, M.J. Kelly, J.E. Thomas, N.A. Kurnit, A. Szoke, A. Javan, F. Zernike and P.H. Lee, Determination of the Speed of Light by Absolute Wavelength Measurement of the R(14) line of the CO₂ 9.4- m Band and the Known Frequency of this Line, Optics Letters 1, 5 (1977).

II. Superradiance

2. J.C. MacGillivray and M.S. Feld, Superradiance in Experimentally Relevant Regimes, Cooperative Effects in Matter and Radiation, Plenum Publishing Corporation (1977).
3. J.C. MacGillivray and M.S. Feld, Theory of Superradiance in an Extended, Optically Thick Medium, Phys. Rev. A, 14, 1169 (1976).
4. J.C. MacGillivray and M.S. Feld, Criteria for X-ray Superradiance, Appl. Phys. Lett. 31, 74 (1977).

III. Laser Saturation Spectroscopy

5. S.M. Hamadani, A.T. Mattick, N.A. Kurnit and A. Javan, Observation of Adiabatic Rapid Passage Utilizing Narrow Infrared Saturation Resonances, Appl. Phys. Lett. 27, 21 (1975).
6. J.R.R. Leite, M. Ducloy, A. Sanchez, D. Seligson and M.S. Feld, Measurement of Molecular-Alignment Relaxation Rate in NH₃ Using Non-Lorentzian Laser-Induced Saturation Resonances, Phys. Rev. Lett. 39, 1465 (1977).
7. R.E. McNair, R. Forber, S.F. Fulghum, G.W. Flynn, M.S. Feld and B.J. Feldman, (to be submitted).
8. M. Ducloy and M.S. Feld, Laser Saturation Spectroscopy in the Time-Delayed Mode
9. J.R.P. Leite, M. Ducloy, A. Sanchez, D. Seligson and M.S. Feld, Laser Saturation Resonances in NH₃ Observed in the Time-Delayed Mode, Phys. Rev. Lett. 39, 1469 (1977).
10. M. Ducloy, J.R.R. Leite and M.S. Feld, Laser Saturation Spectroscopy in the Time-Delayed Mode. Theory of Optical Free Induction Decay in Coupled Doppler-Broadened Systems, Phys. Rev. A, 17, 623 (1978).

Table of Contents
Page 2

11. J.R.R. Leite, A. Sanchez, M. Ducloy and M.S. Feld,
Saturated Absorption Spectroscopy of CH_3OH

IV. Optically Pumped Far Infrared Lasers

12. J.R.R. Leite, D. Seligson, J.J. Mickey, M. Ducloy,
A. Sanchez and M.S. Feld, Quantum Mechanical Features
of Optically Pumped FIR C.W. Lasers
13. D. Seligson, M. Ducloy, J.R.R. Leite, A. Sanchez and
M.S. Feld, Quantum Mechanical Features of Optically
Pumped CW FIR Lasers, IEEE J. of Quantum Electronics,
QE-13, 468 (1977).
14. R.E. McNair, S.F. Fulghum, G.W. Flynn, M.S. Feld and
B.J. Feldman, Energy Storage and Vibrational Heating
in CH_3F Following Intense Laser Excitation, Chem. Phys.
Lett. 48, 241 (1977).

V. Non-Linear Characteristics of Tunneling Diodes

15. C.F. Davis, Jr., G. Elchinger, A. Sanchez, K.C. Liu and
A. Javan, Optical Electronics, Extension of Microwave
Techniques into the Optical Region, Proceedings of the
31st Annual Frequency Control Symposium, Fort Monmouth,
N.J. (1977).
16. A. Sanchez, C.F. Davis, K.C. Liu and A. Javan, The MOM
Tunneling Diode: Theoretical Estimate of its Performance
at Microwave and Infrared Frequencies, J. Appl. Phys.
(to be published, August 1978).

VI. Theses

- 17 J.J. Mickey, Study of CH_3OH Far Infrared Pump Transitions
Using Stark Effect and Saturated Absorption Techniques
18. D. Seligson, Saturated Absorption Studies of Methyl Alcohol
Far Infrared Laser Pump Transitions
19. J-P Monchalin, Development of a Precise Wavelength Measure-
ment Technique for Lasers and its Application to the
Measurement of the Speed of Light and Spectroscopy

Table of Contents

Page 3

20. M.J. Kelly, Lineshapes of Narrow Doppler-Free Saturation Resonances and Observation of Anomalous Zeeman Splitting Arising from Rotational Magnetic Moment in $^{13}\text{C}^{18}\text{O}_2$ and N_2O Molecules
21. J. C. MacGillivray, Theory of Superradiance in an Extended, Optically Thick Medium
22. S.M. Hamadani, Investigation of Transient Coherent Optical Phenomena in Resonant Media
23. J.R.R. Leite, Coherent Transient and Steady State Phenomena in Coupled Molecular Transitions
24. R. Francke, Study of Relaxation Processes in He_2 Using Pulsed Dye Laser Techniques
25. R.E. McNair, Energy Absorption and Vibrational Heating in Molecules Following Intense Laser Excitation
26. G. Elchinger, Properties of High Speed Metal-Barrier-Metal Tunneling Junctions responding to Infrared and Visible Radiations

This final report consists of selected papers describing research work performed in the MIT Optical and Infrared Laser Laboratory with the support of Army Research Office Contract Number DAHC 04-74-C-0017. *3493 x cover*

The areas discussed are: Measurement of the speed of light, superradiance, laser saturation spectroscopy, optically pumped far infrared lasers and non-linear characteristics of tunneling diodes.

For brevity and economy, thesis work performed under the contract is represented by the respective abstracts. The whole theses are available from MIT Microreproduction or this laboratory.

I. Measurement of the Speed of Light

Determination of the speed of light by absolute wavelength measurement of the $R(14)$ line of the CO_2 9.4- μm band and the known frequency of this line

J.-P. Monchalín, M. J. Kelly, J. E. Thomas, N. A. Kurnit, A. Szöke, and A. Javan

Department of Physics, Massachusetts Institute of Technology, Cambridge, Massachusetts 02139

F. Zernike

P. H. Lee

Perkin-Elmer Corporation, Norwalk, Connecticut

Physics Department, University of California, Santa Barbara, California

Received April 12, 1977

A precision long-arm scanning Michelson interferometer system is described that is capable of measuring absolute laser wavelength to within several parts in 10^9 in the 10- μm spectral range and to within several parts in 10^{11} in the visible range. The $R(14)$ line of the CO_2 9.4- μm band is measured to be 9.305 385 613 (70) μm . This measured value and the known frequency of this line give a value for the speed of light: $c = 299\,792\,457.6$ (2.2) m/sec, in agreement with the recent independent measurements of c and its recommended value.

Since the late 1960's, in a continuing experimental program at MIT, a precision scanning long-arm vacuum Michelson interferometer has been developed and perfected for an accurate comparison of two widely different laser wavelengths, one of them lying in the far infrared or the infrared and the other in the visible region. In the experiment, the visible laser is a frequency-stabilized He-Ne 633-nm laser having an accurately calibrated wavelength with respect to a Kr standard. The measurements are performed by simultaneous fringe counting and relative fringe-phase comparison at the two wavelengths, while the scanning arm of the interferometer is varied over a path length of about 50 cm. The precise absolute wavelength of the far-infrared or the infrared laser is obtained from this simultaneous fringe counting and the calibrated wavelength of the He-Ne laser. On-line data processing has made possible measurements of relative phases to within a small fraction of the He-Ne red fringe. The limiting accuracy of these measurements is set by the ability to make correction for the systematic fringe shift caused by diffraction. These shifts were minimized by using large-aperture optical components. Other major practical limitations to the accuracy arise from the laser-beam quality, the quality of optical surfaces, and the ability to align the two laser beams collinearly.

Over the past several years, the design of the interferometer and the measuring procedures have been refined to obtain higher accuracy.^{1,2} Our accuracy limit at this time is several parts in 10^9 in the 10- μm region of the spectrum. In the visible region (where the diffraction fringe shift is appreciably less), the interferometer can be adapted and applied to the absolute laser-wavelength measurements to within a few parts in 10^{11} . Because of its low- Q and broadband operating capability, it can be used as a broadband spectrometer for precise spectroscopic studies through accurate laser wavelength measurements over the entire wavelength

region permitted by its transmitting optics (the beam-splitter, the windows, and the compensator). An application of this has recently been reported³ in a spectroscopic study of the CO_2 $01^{11}-(11^{10},03^{10})_I$ band, which oscillates in the 11.2- μm region.

The first use of this interferometer in a precision determination of c by simultaneous measurements of the absolute laser wavelength and frequency was reported¹ in 1969. In that experiment the interferometer was used to measure the absolute wavelength of a D_2O 84- μm laser radiation: this, together with the precise measured frequency⁴ of that laser line, gave a value for the speed of light to within an accuracy of 2 parts in 10^6 , comparable at that time with the best previous measurements. This Letter reports the application of the interferometer with the improved precision to an independent determination of c to within an accuracy of 7 parts in 10^9 ; the measurement is done by precise wavelength determination of the center of the Doppler-free resonance of the $R(14)$ line of the CO_2 9.4- μm $(00^01)-(10^00,02^00)_{II}$ band.⁵ The known absolute frequency of this line⁶ and the measured wavelength give a precise value of c . Our measured value agrees with the recent measurements of c with a comparable accuracy.⁷

Figure 1 is a block diagram of the experiment. An important feature of the interferometer is the use of a flat mirror on one arm and a corner reflector on the variable arm: with this configuration the two beams having different wavelengths can be made accurately parallel, since flat interference patterns are obtained only when the beams corresponding to each wavelength are perpendicular to the flat mirror.

The wavelength measurements reported here were performed using a frequency-stabilized CO_2 laser oscillating at the center of the narrow Doppler-free resonance belonging to the $R(14)$ line. This Doppler-free resonance is obtained by a well-known method⁸ in which

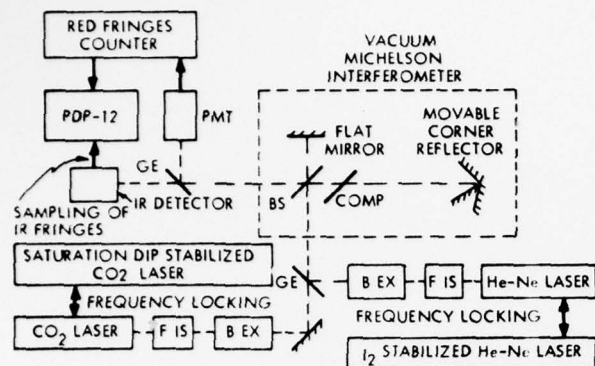


Fig. 1 Simplified block diagram of the experimental setup: BS = beam splitter, COMP = compensator, GE = germanium slab (reflects the red and transmits the infrared), BEX = beam expander, FIS = feedback-isolation optics (polarizer, quarter-wave plate, attenuator). All the optics have a large size with a useful aperture of 50 mm. The corner reflector carriage rides on two carefully polished stainless steel rods, and its surface in contact with the rods is coated with Teflon. The translation is obtained by the motion of an ac-synchronous motor with this motion transferred to the carriage by the use of gears, pulleys, and a strong steel cable. A heavy fly-wheel (inside the vacuum-interferometer assembly) attached to the main pulley gives a highly uniform and jitter-free translation over a length of about 50 cm.

the laser-induced fluorescence at the $(001) \rightarrow (000)$ $4.3\text{-}\mu\text{m}$ CO_2 emission band is used in the detection system. Resonance full widths of 1 part in 10^8 were typical in this experiment.⁹ The laser frequency was stabilized at the line center to within one tenth of the resonance width.

In order to avoid fringe modulation, the CO_2 laser used in the measurement was stabilized to its zero beat with respect to a frequency-modulated laser, which was first-derivative locked to the center of the $R(14)$ Doppler-free resonance.

The He-Ne laser used was likewise stabilized to the center frequency of a second laser locked to the inverted Lamb dip obtained with a low-pressure intracavity iodine cell. Two He-Ne lasers similarly and independently locked to the center frequency of the iodine inverted Lamb dip were used to determine the He-Ne laser frequency resetability. From the beat note obtained by mixing the output of the two lasers, their frequency resetability was estimated¹⁰ to be ± 5 parts in 10^{10} .

The largest systematic error requiring correction arises from the fringe shift due to diffraction of the spatially limited beam propagating in the interferometer (without an aperture in its beam path). Since this error scales as λ^2 , the dominant diffraction correction is introduced by the CO_2 infrared beam.

It is known that, for the lowest-order propagation mode consisting of a TEM_{00} Gaussian beam, this correction is given by $(\lambda - \lambda_{\text{exp}})/\lambda = -\lambda^2/(4\pi^2 w_0^2)$, where λ_{exp} is the experimental value given by the ratio of the fringe counts and w_0 is the beam radius at $1/e$ of its E -field distribution.^{11,12}

With the laser optimally aligned for operation on its

lowest-order mode, the beam profile was carefully measured at the input of the interferometer. It was found that this beam profile reproducibly and dominantly consisted of the TEM_{00} mode with a small admixture of the high-order modes in such a way as to cause a slightly astigmatic beam with, in fact, perfect collimation along its two principal axes. (This profile was characteristic of the CO_2 laser used in the experiment; it utilized one Brewster-angle polarizing plate in its cavity.) It can be shown that, for this astigmatic beam, the diffraction correction has the same form as the TEM_{00} mode given above after substituting for $1/w_0^2$, the quantity $\frac{1}{2}(1/w_{0x}^2 + 1/w_{0y}^2)$, where w_{0x} and w_{0y} are the beam radii along the two principal directions.¹³

Since the corner reflector is used at its center, the small empty spaces existing between its adjacent mirrors cause diffraction resulting in an additional small correction. This correction can be estimated by the scalar diffraction theory.¹³ Correcting for this and the diffraction effect, one obtains

$$\frac{\lambda - \lambda_{\text{exp}}}{\lambda} = -\frac{\lambda^2}{8\pi^2} \left(\frac{1}{w_{0x}^2} + \frac{1}{w_{0y}^2} \right) \left(1 - \frac{9a_0}{2\sqrt{\pi}w_0} \right),$$

wherein the last factor, a_0 , is the width of the empty space at the junction of the corner reflector's mirrors, which is much smaller than the quantity w_0 given by $(w_{0x} + w_{0y})/2$. Inspection shows that other diffraction fringe shifts are much smaller, and their contributions lie below our experimental error.

The measurements of the beam widths were performed with a detector, a pinhole, and a two-dimensional beam-steering mechanism displaying the CO_2 beam profile at the input of the interferometer. The spacing a_0 was estimated from a large-scale photograph of the corner reflector.

From the above studies, the final diffraction correction is found to be $[(\lambda - \lambda_{\text{exp}})/\lambda] = -1.89 \times 10^{-8}$, corresponding to $(\lambda - \lambda_{\text{exp}}) = -1.76 \times 10^{-7} \mu\text{m}$. The uncertainty of this result is conservatively estimated to be $\pm 20\%$ according to the following: 8% comes from w_{0x} and w_{0y} measurements (which were performed with $\pm 4\%$ precision); another 8% originates from a_0 determination (which was measured with $\pm 25\%$ uncertainty for $w_0 \approx 10 \text{ mm}$ and $a_0 \approx 0.6 \text{ mm}$).

The experimental results are plotted in Fig. 2. For each point of the plot, the red and infrared fringes have been maximized before scanning. For each group of six data points (separated by vertical lines on the plot), the red and infrared beams have been carefully recentered on the corner reflector for any position along the scan by realigning the entire interferometer. This centering on the corner reflector (for any position along the scan) was used to obtain the required parallelism of the red and the infrared beams with respect to the axis of the reflector translation. In the absence of this parallelism, as the interferometer arm is varied, the wavefront of the beam reflected by the corner reflector moves across the fixed wavefront of the beam reflected by the flat mirror; this introduces an error if these wavefronts are not perfectly flat. The experimental scatter seen in Fig. 2 is in part caused by this effect. (The slight deviation from a perfectly flat wavefront is caused by the lack of

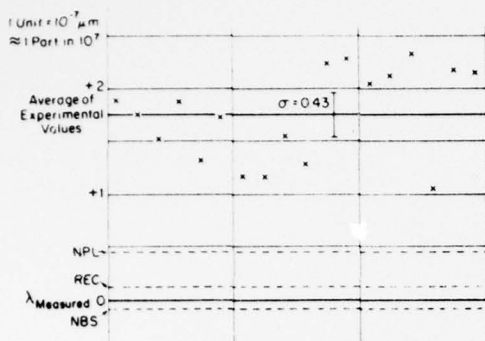


Fig. 2 Plot of the experimental results obtained directly from the ratio of the fringe counts. The origin of the vertical axis is chosen at the final result ($\lambda_{\text{MEASURED}}$), which is obtained by subtracting the diffraction correction ($1.76 \times 10^{-7} \mu\text{m}$) from the average of the experimental data. One standard deviation ($\sigma = 0.43 \times 10^{-7} \mu\text{m}$) is indicated by an error bar. The lines marked NPL, NBS, and REC correspond, respectively, to values of the wavelength of the $R(14)$ line calculated by using the values of the speed of light given by the National Physical Laboratory, Teddington (England), the National Bureau of Standards, Boulder (Colorado) and the recommended value of c (see Ref. 7).

perfect flatness of our beam splitter and the compensator, which were made of sodium chloride.) The precision of each data point is typically 1–2 parts in 10^9 , as determined by a least-squares fit to a straight line of the relative fringe phases determined at 38 equally spaced intervals during a scan.

In the measured value $\lambda_{\text{MEASURED}}$, we use the recommended¹⁴ value for the i component of iodine-127: $0.632\,991\,399 \mu\text{m}$ (uncertainty ± 4 parts in 10^9). The experimental standard deviation is $4.3 \times 10^{-8} \mu\text{m}$. By combining quadratically the standard deviation and the uncertainty of the diffraction correction, one finds that the uncertainty of the ratio $\lambda_{\text{CO}_2}/\lambda_{\text{He-Ne}}$ is ± 6 parts in 10^9 . The uncertainty of $\lambda_{R(14)}$ is $\pm 7.2 \times 10^{-9}$, and the result is found to be: $\lambda_{R(14)} = 9.305\,385\,613 (70) \mu\text{m}$.

This gives a value for the speed of light $c = 299\,792\,457.6 (2.2) \text{ m/s}$ (relative uncertainty ± 7.3 parts in 10^9). This is in excellent agreement with the recommended¹⁴ value of c ($299\,729\,458 \text{ m/sec}$) based on the previous independent measurements of this quantity.⁷

The ratio found for $\lambda_{R(14)}/\lambda_{I(2i)}$ also compares very well with the ratio of their frequencies calculated from the frequency of the $R(14)$ line and the frequency of the i component of the iodine transition deduced from the recent wavelength comparison¹⁵ of an iodine-stabilized He-Ne 633-nm laser with the wavelength of a methane-stabilized 3.39- μm He-Ne laser. The difference between the two ratios is 2.8 parts in 10^9 .

This work was supported by the Air Force Cambridge Research Laboratories, the National Science Foundation, and the U.S. Army Research Office, Durham, North Carolina. J.-P. Monchalín is now at École Polytechnique, Université de Montréal; M. J. Kelly at Physics Department, University of California, Berkeley; N. A. Kurnit at Los Alamos Scientific Laboratory, Los Alamos, New Mexico; A. Szöke at Lawrence Livermore

Laboratory, University of California, Livermore; and F. Zernike at Philips Laboratories, Briarcliff Manor, New York. J. E. Thomas is a Hertz Predoctoral Fellow.

References

1. V. Daneu, L. O. Hocker, A. Javan, D. Ramachandra Rao, A. Szöke, and F. Zernike, *Phys. Lett.* **29A**, 319 (1969).
2. J.-P. Monchalín, A. Javan, N. A. Kurnit, A. Szöke, and F. Zernike, *Bull. Am. Phys. Soc.* **16**, 1403 (1971); N. A. Kurnit, in *Fundamental and Applied Laser Physics*, Proceedings of the Esfahan Symposium, 1971, M. S. Feld, A. Javan, and N. A. Kurnit, eds. (Wiley-Interscience, New York, 1973), p. 479; J.-P. Monchalín, M. J. Kelly, J. G. Small, F. Keilmann, N. A. Kurnit, A. Javan, and F. Zernike, *Proceedings of the Conference on Precision Electromagnetic Measurements* (Boulder, Colorado, 1972); J.-P. Monchalín, M. J. Kelly, J. E. Thomas, N. A. Kurnit, and A. Javan, *Proceedings of the Atomic Spectroscopy Symposium 1975* (NBS, Washington, D.C.).
3. J.-P. Monchalín, M. J. Kelly, J. E. Thomas, N. A. Kurnit, and A. Javan, *J. Mol. Spectrosc.* **64**, 491 (1977).
4. L. O. Hocker, J. G. Small, and A. Javan, *Phys. Lett.* **29A**, 321 (1969).
5. The reason for the choice of this $R(14)$ line relates to the frequency-measurements chain. See A. Javan in *Fundamental and Applied Laser Physics*, p. 295.
6. K. M. Evenson, J. S. Wells, F. R. Petersen, B. L. Danielson, and G. W. Day, *Appl. Phys. Lett.* **22**, 192 (1973); T. G. Blaney, C. C. Bradley, G. J. Edwards, D. J. E. Knight, P. T. Woods, and B. W. Jolliffe, *Nature* **244**, 504 (1973); F. R. Petersen, D. G. McDonald, J. D. Cupp, and B. L. Danielson, *Laser Spectroscopy*, Proceedings of the Vail (Colorado) Conference, R. G. Brewer and A. Mooradian, eds., p. 555.
7. K. M. Evenson, J. S. Wells, F. R. Petersen, B. L. Danielson, G. W. Day, R. L. Barger, and J. L. Hall, *Phys. Rev. Lett.* **29**, 1346 (1972); T. G. Blaney, C. C. Bradley, C. J. Edwards, B. W. Jolliffe, D. J. E. Knight, W. R. C. Rowley, K. C. Shotton, and P. T. Woods, *Nature* **251**, 46 (1974).
8. C. Freed and A. Javan, *Appl. Phys. Lett.* **17**, 53 (1970). For an experimental arrangement similar to the one used here see M. J. Kelly, J. E. Thomas, J.-P. Monchalín, N. A. Kurnit, and A. Javan, "Observation of anomalous Zeeman effect in infrared transitions of $^1\Sigma \text{CO}_2$ and N_2O molecules," *Phys. Rev. Lett.* **37**, 686 (1976).
9. Much narrower linewidths have been observed when the laser beam is expanded and the pressure reduced. See M. J. Kelly, J. E. Thomas, J.-P. Monchalín, N. A. Kurnit, and A. Javan, *Proceedings of the 29th Annual Symposium on Frequency Control* (1975), and M. J. Kelly, Ph.D. Thesis (MIT, 1976) (unpublished).
10. A first-derivative locking technique was used. An improvement by more than one order of magnitude can readily be obtained.
11. H. Kogelnik and T. Li, *Appl. Opt.* **5**, 1550 (1966).
12. J.-P. Monchalín, M. J. Kelly, J. E. Thomas, N. A. Kurnit, A. Szöke, F. Zernike, P. H. Lee, and A. Javan, *Frontiers in Laser Spectroscopy*, Les Houches, 1975, Session 27 (North-Holland, Amsterdam, 1976).
13. J.-P. Monchalín, Ph.D. Thesis (MIT, 1976) (unpublished).
14. Fifth Meeting of the Comité Consultatif pour la Définition du Mètre, *Metrologia* **10**, 75 (1974); J. Terrien, *Nouv. Rev. Opt.* **4**, 215 (1973).
15. H. P. Layer, R. D. Deslattes, and W. G. Schweitzer, Jr., *Appl. Opt.* **15**, 734 (1976).

II. Superradiance

Reprinted from: COOPERATIVE EFFECTS IN MATTER AND RADIATION (1977)
Edited by Charles M. Bowden, D. W. Howgate and Hermann R. Robl
Book available from: Plenum Publishing Corporation
227 West 17th Street, New York, N.Y. 10011

SUPERRADIANCE IN EXPERIMENTALLY RELEVANT REGIMES*

J. C. MacGillivray and M. S. Feld[†]

Department of Physics and Spectroscopy Laboratory
Massachusetts Institute of Technology
Cambridge, Massachusetts 02139

Abstract: This paper explores the assumptions made in the semiclassical description of superradiance. Simple expressions for observable output parameters in several experimentally relevant regimes are given. Implications of these results to some possible applications of superradiance are discussed.

I. INTRODUCTION

In view of the renewed experimental interest in superradiance,¹⁻⁴ a detailed list of specific limiting conditions⁵ for the applicability of the simple theoretical model^{6,7} which accurately described the results of the initial experiments⁸ seems appropriate. In this paper the semiclassical model and its exact solution in the "ideal superradiance" limit will be briefly reviewed. The effect of relaxing each of the assumptions made in obtaining this limit will be described, emphasizing the amount by which the parameters of an actual system can depart from ideality without significantly altering the analytical expressions for the expected output radiation. The changes in these expressions which occur when some of the constraints are further relaxed will then be discussed. Finally, the implications of these results to some potential applications of superradiance will be mentioned.

*Work supported in part by National Science Foundation and US Army Research Office (Durham).

[†]Alfred P. Sloan Fellow.

These considerations should be of particular interest to those attempting to observe superradiance in other systems, and are relevant to the problems of x-ray laser system design⁹ and ultrashort pulse generation.

Superradiance is the spontaneous radiative decay of an assembly of atoms or molecules in the collective mode. It is the optimal process for extracting coherent energy from an inverted system. In this process incoherent emission induces a small macroscopic polarization in an inverted two-level medium which gives rise to a growing electric field and consequently an increasing polarization in space and time. After a long delay, a highly directional pulse is emitted, often accompanied by ringing. The peak output power is proportional to the square of the number of radiators, N .

In our theoretical model⁷ the semiclassical approach (classical fields, quantized molecules) has been adopted in order to take propagation effects fully into account. Semiclassical discussions have also been given by Burnham and Chiao,¹⁰ Friedberg and Hartmann,¹¹ Arecchi and Courtens,¹² and Bullough.¹³ In fact, Dicke¹⁴ gave a semiclassical description in his original paper. For a discussion of quantized field models, see Bonifacio and Lugiato¹⁵ and references contained therein.

The coupled Maxwell-Schrödinger equations in the slowly-varying envelope approximation, written in complex form, are^{7,16}

$$\partial E / \partial x = -\nu E + 2\pi k \sum_{v,M} P_{v,M} \quad (1a)$$

$$\partial P / \partial T = -\left(\frac{1}{T_2} - ik\nu\right)P + \frac{\mu_z^2}{\hbar} En + \Lambda_p \quad (1b)$$

$$\partial n / \partial T = \Lambda - n/T_1 - (1/\hbar) \operatorname{Re}(EP^*) \quad (1c)$$

Here $P(x, T, v, M)$ and $E(x, T)$ are the complex, slowly varying envelopes of the polarization density per velocity interval dv in degenerate M_J -state M and of the electric field, respectively, at position x and retarded time $T = t - x/c$; $n(x, T, v, M)$ is the inversion density; κ accounts for diffraction or other loss; T_1 is the population decay time; T_2 is the polarization decay time; Λ is a source term describing the rate of production of n ; μ_z is the dipole moment component parallel to the direction of polarization; and $\sum_{v,M}$ denotes a velocity integral and a sum over degenerate M -states. The remaining notation is the same as in Ref. 7.

SUPERRA

Sp
this me
describ
given i
either
ever, c
since l
relativ
experim

Th
implic

1)
to sim
field

2)
associ

3)
is ign

C
compar
tical
result
are us
an aid

4)
can be
observ
delay
of a p
system

7
limit,
 $1/T_1 =$
 $P(t =$
transi
degene
excita
throug

Spontaneous emission from the excited state is simulated in this model by a randomly phased polarization source term Λ_p which describes the rate of production of P . (The expression for Λ_p is given in Ref. 7.) The superradiant process can be initiated by either spontaneous emission or background thermal radiation. However, only spontaneous emission will be considered in this paper, since blackbody radiation (described in detail in Ref. 7) is relatively unimportant at wavelengths shorter than 50 μ , as in the experiments of current interest.

Three basic assumptions are incorporated in Eqs. (1), the implications of which will be discussed below:

- 1) The semiclassical model with a polarization source term to simulate spontaneous emission is used, instead of a quantized field model.
- 2) The plane wave approximation is utilized. Thus, effects associated with finite beam diameter are neglected.
- 3) The interaction of forward and backward travelling waves is ignored.

Computer solutions of Eqs. (1) should be used for precise comparisons with experimental data. However, approximate analytical solutions which are in close agreement with the computer results can be obtained in certain limiting cases. These results are useful in estimating relevant experimental parameters and as an aid to understanding the underlying physical processes.

II. IDEAL SUPERRADIANCE

In this limit an exact solution of the resulting equations can be obtained, with simple expressions for experimentally observable quantities such as output intensity, pulse width, and delay time. These can be useful in determining the feasibility of a proposed superradiant scheme and in optimizing an existing system.

The assumptions made to obtain the "ideal superradiance" limit, in addition to those built into Eqs. (1), are: (4) $1/T_1 = 1/T_2 = 1/T_2^* = 0$, where T_2^* is the dephasing time; (5) $P(t=0) = 0$ (no initial polarization at the superradiant transition); (6) $i = 0$; (7) no level degeneracy (n is summed over degenerate M states and μ_z is averaged over M states); (8) swept excitation (system inverted by a pulse travelling longitudinally through the medium at the speed of light); (9) zero inversion

time (system inverted instantaneously); and (10) no feedback. Furthermore, (11) Λ_p is set equal to zero and replaced by an equivalent delta-function input electric field. Each of these assumptions is discussed below.

Given these assumptions, Eqs. (1) become⁷

$$\partial E / \partial x = 2\pi k P, \quad (2a)$$

$$\partial P / \partial T = \mu_z^2 n E / \hbar, \quad (2b)$$

$$\partial n / \partial T = -EP / \hbar, \quad (2c)$$

and n , E , and P are all real. The solution of these equations is $n = n_0 \cos \psi$, $P = \mu_z n_0 \sin \psi$, $n_0 = n(t=0)$, and

$$d\psi/dT = \mu_z L / \hbar, \quad (3)$$

where

$$\psi(x, T) = \int_{-\infty}^T (\mu_z / \hbar) E(x, T') dT' \quad (4)$$

is the partial area of the pulse. (The total area $\theta(x) \equiv \psi(x, \infty)$.) Applying the transformation $w = \sqrt{2xT}$ to Eqs. (2a) and (3) gives the pendulum equation,¹⁷

$$\psi'' + (1/w)\psi' = \sin \psi / (T_R L), \quad (5)$$

where $\psi = \psi(w)$ and

$$T_R = \frac{\lambda}{2\pi} \frac{\hbar}{2\pi} \frac{1}{\mu_z^2 n_0 L} \quad (6)$$

is the characteristic radiation damping time of the collective system.

Equations (2b-c) give rise to the familiar Bloch vector picture. As can be seen from the zI dependence of Eq. (5), this system is analogous to a spatial array of coupled pendula, initially tipped at a uniform small angle $\psi(w=0) = \theta(x=0) = \theta_0$,¹⁸ which fall as a phased array.

The solution of Eq. (5) is completely determined by two parameters,¹⁰ T_R and the initial tipping angle θ_0 . For a given value of θ_0 , a single curve relates $T_R^2 I_p$ to T/T_R (see Fig. 4 of Ref. 7), and approximate expressions in terms of $\phi \equiv \ln(2\pi/\theta_0)$ can be derived for the peak output power

$$I_p \approx 4N\hbar\omega/T_R \phi^2 \propto N^2, \quad (7a)$$

the width of the output pulse

$$T_w \approx T_R \phi \propto N^{-1}, \quad (7b)$$

and the energy contained in the first lobe of emitted radiation

$$E_p \approx 4N\hbar\omega/\phi \propto N. \quad (7c)$$

The delay time from the inversion to I_p is

$$T_D \approx T_R \phi^2/4 \propto N^{-1}, \quad (7d)$$

so that $T_D \approx T_w \phi/4$. Typically, $10 < \phi < 20$.

III. APPLICABILITY OF IDEAL SUPERRADIANCE

The regions of validity of each of the assumptions listed above will now be discussed.

A. Simplifying Assumptions Which Have Little Effect on Output

We first consider those assumptions which can be completely removed without significantly affecting the ideal solution.

a) The semiclassical approach describes the system for $T \gg T_R$, since at T_R there is one photon in each mode of the radiation field.⁷ Although, strictly speaking, the semiclassical description breaks down for $T < T_R$, we are only interested in the output at T_D , which is typically 25-100 T_R . Fluctuations in the fields during the first T_R will have little effect on the output at T_D due to the logarithmic dependence of the output on the initial conditions through ϕ . Thus, the randomly phased polarization source, constructed to be consistent with the requirements of thermal equilibrium,⁷ should give correct results for $T \gg T_R$.

b) Computer analysis shows that the effect of Λ_p on the evolution of the system is almost identical to that of a delta-function input field of appropriate magnitude to give $\phi = \ln [\sqrt{2\pi N} (2\alpha L)^{3/4}]$, where αL is the small-signal field gain, so that $\alpha L = T_2^2/T_R$, where T_2 is the inverse linewidth. This is understandable since fluctuations at the far end of the medium are amplified over the greatest length and therefore dominate.

c) Computer analysis of the interaction between forward and backward travelling waves shows that this effect is virtually negligible in all swept excitation systems, and it is also negligible in uniformly excited systems for which $L/c \leq T_D$.

(This latter case is discussed below.) This is so because the forward and backward waves only become sizable in the same region after much of the stored energy has been radiated.¹⁹

d) Computer calculations show that replacing μ_z^2 by its average value over M states and n by its sum over M states has little effect on the output radiation. Therefore, the influence of level degeneracy is insignificant.

B. Assumptions Which Can Significantly Affect Output

For the remaining assumptions, small deviations from ideality are of little importance but large deviations can cause significant changes in the output. The following conclusions have been verified by computer solutions of Eqs. (1).⁵

a) The lifetimes need not be infinite, which would imply infinite gain:

i) The net gain (gain minus loss) must be large enough so that the total area of the output pulse can grow to π . This leads to the requirement⁵

In
be
ene
we
eff
reg
can
thi

pop
coh

The
lar
gai

del
oth
 T_D

If
ter
can
cas
emi

and

$$(\alpha - \kappa)L \geq \phi \quad (10a)$$

In the opposite limit where $(\alpha - \kappa)L < 1$, collective effects can still be important (since $T_R \ll T_{sp}$) but only a small fraction of the energy is radiated coherently (since $T_2' \ll T_R$); this regime, which we refer to as "limited superradiance",⁷ includes such familiar effects as free induction decay and echos. In the intermediate regime, where $1 < (\alpha - \kappa)L < \phi$, the peak intensity will be significantly less than that given by Eq. 7(a); analytical results in this regime can be obtained from the linear theory of Crisp.²⁰

ii) T_1 must be greater than T_D [Eq. 7(d)], otherwise the population will decay incoherently and reduce the amount of coherent output. This leads to the condition for efficient output

$$\alpha L > (\phi^2/4)T_2'/T_1 \quad (10b)$$

There is no similar requirement on T_2 or T_2^* since effects due to large dephasing or polarization decay rates are offset by high gain.⁷

b) As long as the inversion time τ is less than the observed delay time, a non-zero τ will have little effect on the output other than to increase the observed delay time from T_D to $T_D + \tau/2$. This gives the requirement

$$\tau \leq 2T_D \quad (10c)$$

If the superradiant output occurs before the inversion process terminates, then only the early part of the population inversion can contribute to the first burst of radiation.²¹ In the simple case where the inversion density in the absence of superradiant emission is equal to Λt , Λ constant, then⁹

$$(T_D)_{\text{observed}} = \sqrt{4\pi T_{sp} \phi^2 / \lambda^2 L \Lambda} \quad ,$$

$$I_p = 2h\nu \Lambda L \Lambda \quad ,$$

and

$$T_w = 8\sqrt{\pi T_{sp}/\lambda^2 L \Lambda}.$$

Simple forms other than Λt can also be solved analytically, and graphical solutions are also possible.⁹

This same method can be used to provide an approximate solution for the case where $T_L < T_D$, in violation of requirement (10b) above.

c) Excessive loss κ can diminish superradiance in two ways. It can reduce the net gain, making requirement (10a) harder to fulfill. Superradiant behavior also requires that

$$\int \kappa dx < \phi/4. \quad (10d)$$

When $\int \kappa dx \geq \phi/4$ the pulse stops narrowing and the intensity no longer grows with length. For constant κ , $I_p = N\hbar\omega/4T_R(\kappa L)^2$.²²

In the case of diffraction of a Gaussian beam, $\int \kappa dx = 1/2 \ln[1 + (\lambda L/\Lambda)^2]$. This quantity is always small when the Fresnel number is larger than unity.

d) Uniform excitation (entire system inverted simultaneously, in contrast to swept excitation) will have little effect on the output as long as the transit time $T_{tr} = L/c$ is less than the observed delay time, other than to increase the observed delay time to $T_D + T_{tr}/2$. When T_{tr} is longer than the delay time, the system will no longer radiate as a single entity; this places a condition on the length L_c ("cooperation length"):

$$L_c = L_e = \sqrt{c T_{sp}} \phi^2 / 2n\lambda^2. \quad (10e)$$

Longer systems will break up into a number of independently radiating segments in a manner described by Arecchi and Courtens.¹² In this limit, the output intensity $I_p = n\hbar\omega c$ and no longer increases with increasing length. Note that requirement (10e) does not apply to swept excitation.

e) The presence of polarization at the superradiant transition $t = 0$ will have little effect provided that

Large
tipp
and
plet
In p
init
ener
be s
medi
and
matt
not
tran
prof

meth
a no
up t
that
pola
in s
popu
This
by c
(to

back
by t
tion
part

long
emis
whic
quan

(F <
tran
Comp

$$P(t = 0) \approx \mu_z n_0^2 \quad (10f)$$

larger values of $P(t = 0)$ are equivalent to increasing the initial tipping angle of the Bloch vector, which shortens the delay time and reduces the ringing. This increases the difficulty of completing the inversion process before coherent emission begins. In principle, a pulse of area exactly π could completely invert an initially absorbing medium without residual polarization. An energy conservation argument shows that such a pulse would have to be shorter than T_R in order not to lose area as it traverses the medium; for longer pulses, the effects of self-induced transparency and pulse propagation become relevant.^{10,12,16,23,24} As a practical matter, schemes to directly invert two-level systems are probably not feasible due to problems associated with loss, level degeneracy, transverse variations in the electric field associated with beam profile, and the difficulty of generating a pulse of exactly area π .

These problems can be circumvented by using indirect excitation methods such as three level pumping⁸ and two photon excitation with a nonresonant intermediate state. All observations of superradiance up to now have employed such schemes. However, the problem remains that when the pump radiation is turned off, a large residual polarization could be left at the pump transition. This can result in superradiance at this transition, which would deplete the population available for superradiance at the desired wavelength. This problem can be overcome by using an incoherent pump pulse, or by choosing a much shorter wavelength for the pump transition (to increase its T_R).

One should also note that in indirect excitation schemes the background emission which initiates superradiance can be modified by the presence of the pump field through multiple quantum transitions. This would increase the effective initial tipping angle, particularly if τ is long.

1) The effect of feedback on the output is negligible as long as the output field due to the initializing spontaneous emission is significantly greater than the additional output which results from the feedback process. Comparing these two quantities gives a condition on the feedback fraction F :

$$F \ll 4 / (c^0 \cdot 3 \phi \phi^2) \quad (10g)$$

($F \approx 10^{-4}$ in the HF experiments.^{8,25}) In long systems, where transit time is appreciable, the influence of feedback decreases. Computer calculations in this regime have not yet been made.

The effect of significant feedback is to drastically shorten the delay times and reduce the ringing; the effect is analogous to continuing to push a pendulum after it has started to fall. The system acts as if it were subject to a different, larger initial condition.

g) The plane wave approximation breaks down when the solid angle factor μ of Rehler and Eberly²⁶ (a function of A , L , and λ) falls in the small Fresnel number regime of Fig. 5 of Ref. 26; the break between the two regimes is relatively sharp and occurs near Fresnel number $2A/\lambda L \approx 1/10$.

For small Fresnel number $T_R = T_{sp} 4\pi/nA\lambda$. The output should be independent of length in this regime, but the output intensity should still be proportional to the square of the population inversion density. We have done no computer analysis in the small Fresnel number regime.

To properly account for the spatial variations of E associated with finite beam diameter, and with focusing and defocusing in a high gain medium, a transverse spatial dependence must be added to Eqs. (1). This aspect of the analysis deserves further attention.

IV. SOME APPLICATIONS OF SUPERRADIANCE

A. Spin-Phonon Superradiance

It may be possible to observe an acoustical analog of superradiance in the spin-phonon interaction process in paramagnetic crystals.²⁷ In such a system the paramagnetic spins are coupled to the lattice vibrations (in a manner described by Jacobsen and Stevens²⁸). As shown in Ref. 29, in the slowly varying envelope approximation the coupled spin-phonon equations become almost identical in form to Eqs. (1).³⁰ Acoustical gain can be suitably defined, and so in a high gain medium, it should be possible for an initially inverted ensemble of spins, perturbed by kT fluctuations, to rapidly transfer its stored energy to the lattice. The ensuing acoustic waves should have all the properties of the coherent emission observed in optical superradiance.

Recently, Hahn and Wilson²⁷ proposed a related experiment to observe superradiant emission in a spin-phonon system by preparing the spins in a phased array. The phonon avalanche experiment of Brya and Wagner,³¹ although probably not a true coherent effect, was an interesting advance along these lines.

B. X-ray Lasers

The requirements for efficient superradiant emission should also be of interest to designers of x-ray laser systems. Due to the short lifetimes of the transitions and the lack of suitable mirrors in this regime, most proposed schemes use a single pass high gain swept-excitation system. Thus, x-ray lasers will superradiate. Consequently, the conventional rate equation analysis is not applicable, and the above considerations can be useful to estimate the output behavior. Some of the discussions in Section III are especially relevant to the x-ray regime; in particular, T_1 is usually so short that the inversion process will not be completed by the time superradiance occurs [see Eq. (10c)].

As mentioned above, the rate equation analysis gives incorrect results. For example, in the Na scheme of Duguay and Rentzepis,³² rate equation analysis predicts (at the threshold value) I_p about 10 times smaller and T_w about 10 times larger than the semiclassical predictions.⁹ In addition, the threshold inversion density is a factor of 10 smaller than the corresponding rate equation threshold.

Specific applications of these requirements to x-ray laser schemes are discussed further in Ref. 9.

C. Ultrashort Pulse Generation

Since superradiance is the optimum method for extracting coherent energy from an inverted medium, it is interesting to consider it as a method for generating ultrashort pulses. Although in the ideal case T_w decreases with increasing N , many of the conditions listed above restrict the shortness of output pulses one can hope to achieve. Combining Eqs. (7b), (7d), and (10c) shows that the inversion time places a particularly restrictive limit on the minimum T_w which can be generated superradiantly:

$$T_w \geq 2\tau/\phi \quad (11)$$

Therefore, ultrashort pulse generation by this method requires swept excitation, small τ , and as short an inversion time as possible. Values of T_w/τ less than 1/10 appear possible.

Note that superradiance is a transient process, and so the generation of ultrashort pulses by this method is inherently different from the mode locking approach, where short pulses

are generated by mixing a set of equally-spaced phase correlated modes to synthesize a Fourier spectrum.

References

- (1) M. Gross, C. Fabre, P. Pillet, and S. Harouche, *Phys. Rev. Lett.* **36**, 1035 (1976).
- (2) Q. H. F. Vreken, H. M. J. Hixspoors, and H. M. Gibbs, *Phys. Rev. Lett.*, to be published; H. M. Gibbs, in this volume; and Q. H. F. Vreken, in this volume.
- (3) A. Flusberg, T. Mossberg, and S. R. Hartmann, *Phys. Rev. Lett.*, to be published, and in this volume.
- (4) T. A. DeTemple, in this volume.
- (5) Derivations of these conditions and computer results which support them can be found in J. C. MacGillivray and M. S. Feld (unpublished).
- (6) I. P. Herman, J. C. MacGillivray, N. Skribanowitz, and M. S. Feld, in *Laser Spectroscopy*, edited by R. G. Brewer and A. Mooradian, Plenum, 1974.
- (7) J. C. MacGillivray and M. S. Feld, *Phys. Rev. A* **14**, 1169 (1976).
- (8) N. Skribanowitz, I. P. Herman, J. C. MacGillivray, and M. S. Feld, *Phys. Rev. Lett.* **30**, 309 (1973).
- (9) J. C. MacGillivray and M. S. Feld, *Appl. Phys. Lett.*, to be published.
- (10) D. C. Burnham and R. Y. Chiao, *Phys. Rev.* **188**, 667 (1969).
- (11) R. Friedberg and S. R. Hartmann, *Phys. Lett.* **38A**, 227 (1972) and references contained therein.
- (12) F. T. Arecchi and E. Courtens, *Phys. Rev. A* **2**, 1730 (1970).
- (13) R. Saunders, S. S. Hassan, and R. K. Bullough, *J. Phys. A* **9**, 1725 (1976) and in this volume.
- (14) R. H. Dicke, *Phys. Rev.* **93**, 99 (1954) and in *Proceedings of the Third International Conference on Quantum Electronics, Paris, 1963*, edited by P. Grivet and N. Bloembergen, Columbia U. P., 1964.
- (15) R. (1976)
- (16) The Low level
- (17) The con the
- (18) It fie
- (19) Thi Bul
- (20) M.
- (21) Alt con sma
- (22) F. Q& and Phy
- (23) In sel
- (24) S.
- (25) P. (un)
- (26) N.
- (27) See the 1976
- (28) E. (196
- (29) C. 1 Phys

- (15) R. Bonifacio and L. A. Lugiato, Phys. Rev. A 11, 1507 (1975) and 12, 587 (1975).
- (16) The notation is similar to that of A. Isevski and W. E. Lamb, Jr. [Phys. Rev. 185, 517 (1969)], extended to include level degeneracy and the polarization source term Λ_p .
- (17) The delta-function assumption is needed so that a boundary condition can be written for Eq. (5). It does not affect the derivations of Eqs. (2)-(4).
- (18) It follows from the assumption of a delta-function input E field that $E(x=0, t) = (h/\mu)_0 \delta(t)$.
- (19) This interaction has been studied by R. Saunders, R. K. Bullough, and S. S. Hassan (Ref. 13).
- (20) M. D. Crisp, Phys. Rev. A 1, 1604 (1970).
- (21) Although population inversion created after this time can contribute to later radiation lobes, the contribution is small due to the filling of the lower state.
- (22) F. T. Arecchi and R. Bonifacio, IEEE J. Quantum Electron. QE-1, 169 (1965); A. Isevski and W. E. Lamb, Jr. (Ref. 16); and R. Bonifacio, F. A. Hopf, P. Meystre, and M. O. Scully, Phys. Rev. A 12, 2568 (1975).
- (23) In this sense the condition $t = T_R$ is the dividing line between self-induced transparency pulse evolution and superradiance.
- (24) S. L. McCall and E. L. Hahn, Phys. Rev. 183, 457 (1969).
- (25) P. T. Ho, J. C. MacGillivray, S. Liberman, and M. S. Feld (unpublished).
- (26) N. E. Rehler and J. H. Eberly, Phys. Rev. A 3, 1735 (1971).
- (27) See references contained in E. L. Hahn and R. Wilson, in the proceedings of the XIXth Congress Ampère, Heidelberg, 1976.
- (28) E. H. Jacobsen and K. W. H. Stevens, Phys. Rev. 129, 2036 (1963).
- (29) C. Leonardi, J. C. MacGillivray, S. Liberman, and M. S. Feld, Phys. Rev. B 11, 3298 (1975).

- (30) The similarity between the Maxwell-Schrödinger and spin-phonon equations has also been exploited by N. Shiren [Phys. Rev. B 2, 2471 (1970)] to observe an acoustical analogue of self-induced transparency.
 - (31) W. J. Brya and P. E. Wagner, Phys. Rev. 157, 400 (1967).
 - (32) M. A. Duguay and P. M. Rentzepis, Appl. Phys. Lett. 10, 350 (1967).
-

Reprinted from: COOPERATIVE EFFECTS IN MATTER AND RADIATION (1977)
Edited by Charles M. Bowden, D. W. Howgate and Hermann R. Robl
Book available from: Plenum Publishing Corporation
227 West 17th Street, New York, N.Y. 10011

SUPERRADIANCE IN EXPERIMENTALLY RELEVANT REGIMES^{*}

J. C. MacGillivray and M. S. Feld[†]

Department of Physics and Spectroscopy Laboratory

Massachusetts Institute of Technology

Cambridge, Massachusetts 02139

Abstract: This paper explores the assumptions made in the semiclassical description of superradiance. Simple expressions for observable output parameters in several experimentally relevant regimes are given. Implications of these results to some possible applications of superradiance are discussed.

I. INTRODUCTION

In view of the renewed experimental interest in superradiance,¹⁻⁴ a detailed list of specific limiting conditions⁵ for the applicability of the simple theoretical model^{6,7} which accurately described the results of the initial experiments⁸ seems appropriate. In this paper the semiclassical model and its exact solution in the "ideal superradiance" limit will be briefly reviewed. The effect of relaxing each of the assumptions made in obtaining this limit will be described, emphasizing the amount by which the parameters of an actual system can depart from ideality without significantly altering the analytical expressions for the expected output radiation. The changes in these expressions which occur when some of the constraints are further relaxed will then be discussed. Finally, the implications of these results to some potential applications of superradiance will be mentioned.

^{*}Work supported in part by National Science Foundation and US Army Research Office (Durham).

[†]Alfred P. Sloan Fellow.

These considerations should be of particular interest to those attempting to observe superradiance in other systems, and are relevant to the problems of x-ray laser system design⁹ and ultrashort pulse generation.

Superradiance is the spontaneous radiative decay of an assembly of atoms or molecules in the collective mode. It is the optimal process for extracting coherent energy from an inverted system. In this process incoherent emission induces a small macroscopic polarization in an inverted two-level medium which gives rise to a growing electric field and consequently an increasing polarization in space and time. After a long delay, a highly directional pulse is emitted, often accompanied by ringing. The peak output power is proportional to the square of the number of radiators, N .

In our theoretical model⁷ the semiclassical approach (classical fields, quantized molecules) has been adopted in order to take propagation effects fully into account. Semiclassical discussions have also been given by Burnham and Chiao,¹⁰ Friedberg and Hartmann,¹¹ Arecchi and Courtens,¹² and Bullough.¹³ In fact, Dicke¹⁴ gave a semiclassical description in his original paper. For a discussion of quantized field models, see Bonifacio and Lugliato¹⁵ and references contained therein.

The coupled Maxwell-Schrödinger equations in the slowly-varying envelope approximation, written in complex form, are^{7,16}

$$\partial E / \partial x = -\kappa E + 2\pi k \sum_{v,M} P \quad , \quad (1a)$$

$$\partial P / \partial T = -\left(\frac{1}{T_2} - ikv\right)P + \frac{\mu_z}{\hbar} En + \Lambda_p \quad , \quad (1b)$$

$$\partial n / \partial T = \Lambda - n/T_1 - (1/\hbar) \operatorname{Re} (EP^*) \quad . \quad (1c)$$

Here $P(x, T, v, M)$ and $E(x, T)$ are the complex, slowly varying envelopes of the polarization density per velocity interval dv in degenerate M_j -state M and of the electric field, respectively, at position x and retarded time $T = t - x/c$; $n(x, T, v, M)$ is the inversion density; κ accounts for diffraction or other loss; T_1 is the population decay time; T_2 is the polarization decay time; Λ is a source term describing the rate of production of n ; μ_z is the dipole moment component parallel to the direction of polarization; and $\sum_{v,M}$ denotes a velocity integral and a sum over degenerate M -states. The remaining notation is the same as in Ref. 7.

Spontaneous emission from the excited state is simulated in this model by a randomly phased polarization source term Λ_p which describes the rate of production of P . (The expression for Λ_p is given in Ref. 7.) The superradiant process can be initiated by either spontaneous emission or background thermal radiation. However, only spontaneous emission will be considered in this paper, since blackbody radiation (described in detail in Ref. 7) is relatively unimportant at wavelengths shorter than 50μ , as in the experiments of current interest.

Three basic assumptions are incorporated in Eqs. (1), the implications of which will be discussed below:

- 1) The semiclassical model with a polarization source term to simulate spontaneous emission is used, instead of a quantized field model.
- 2) The plane wave approximation is utilized. Thus, effects associated with finite beam diameter are neglected.
- 3) The interaction of forward and backward travelling waves is ignored.

Computer solutions of Eqs. (1) should be used for precise comparisons with experimental data. However, approximate analytical solutions which are in close agreement with the computer results can be obtained in certain limiting cases. These results are useful in estimating relevant experimental parameters and as an aid to understanding the underlying physical processes.

II. IDEAL SUPERRADIANCE

In this limit an exact solution of the resulting equations can be obtained, with simple expressions for experimentally observable quantities such as output intensity, pulse width, and delay time. These can be useful in determining the feasibility of a proposed superradiant scheme and in optimizing an existing system.

The assumptions made to obtain the "ideal superradiance" limit, in addition to those built into Eqs. (1), are: (4) $1/T_1 = 1/T_2 = 1/T_2^* = 0$, where T_2^* is the dephasing time; (5) $P(t=0) = 0$ (no initial polarization at the superradiant transition); (6) $\kappa = 0$; (7) no level degeneracy (n is summed over degenerate M states and μ_z is averaged over M states); (8) swept excitation (system inverted by a pulse travelling longitudinally through the medium at the speed of light); (9) zero inversion

time (system increased instantaneously); and (10) no feedback. Furthermore, (11) A_p is set equal to zero and replaced by an equivalent delta-function input electric field. Each of these assumptions is discussed below.

Given these assumptions, Eqs. (1) become⁷

$$\partial E / \partial x = 2\pi k P, \quad (2a)$$

$$\partial P / \partial T = \mu_z^2 n E / \hbar, \quad (2b)$$

$$\partial n / \partial T = -EP / \hbar, \quad (2c)$$

and n , E , and P are all real. The solution of these equations is $n = n_0 \cos \psi$, $P = \mu_z n_0 \sin \psi$, $n_0 = n(t = 0)$, and

$$d\psi/dT = \mu_z E / \hbar, \quad (3)$$

where

$$\psi(x, T) = \int_{-\infty}^T (\mu_z / \hbar) E(x, T') dT' \quad (4)$$

is the partial area of the pulse. (The total area $\theta(x) \equiv \psi(x, \infty)$.) Applying the transformation $w = \sqrt{2xT}$ to Eqs. (2a) and (3) gives the pendulum equation,¹⁷

$$\psi'' + (1/w)\psi' = \sin \psi / (T_R L), \quad (5)$$

where $\psi = \psi(w)$ and

$$T_R = \frac{\lambda}{2\pi} \frac{\hbar}{2\pi} \frac{1}{\mu_z^2 n_0 L}, \quad (6)$$

is the characteristic radiation damping time of the collective system.

Equations (2b-c) give rise to the familiar Bloch vector picture. As can be seen from the zT dependence of Eq. (5), this system is analogous to a spatial array of coupled pendula, initially tipped at a uniform small angle $\psi(w=0) = \theta(x=0) = \theta_0$,¹⁸ which fall as a phased array.

The solution of Eq. (5) is completely determined by two parameters,¹⁰ T_R and the initial tipping angle θ_0 . For a given value of θ_0 , a single curve relates $T_R^2 I_p$ to T/T_R (see Fig. 4 of Ref. 7), and approximate expressions in terms of $\phi \equiv \ln(2\pi/\theta_0)$ can be derived for the peak output power

$$I_p \approx 4N\hbar\omega/T_R \phi^2 \propto N^2, \quad (7a)$$

the width of the output pulse

$$T_w \approx T_R \phi \propto N^{-1}, \quad (7b)$$

and the energy contained in the first lobe of emitted radiation

$$E_p \approx 4N\hbar\omega/\phi \propto N. \quad (7c)$$

The delay time from the inversion to I_p is

$$T_D \approx T_R \phi^2/4 \propto N^{-1}, \quad (7d)$$

so that $T_D \approx T_w \phi/4$. Typically, $10 < \phi < 20$.

III. APPLICABILITY OF IDEAL SUPERRADIANCE

The regions of validity of each of the assumptions listed above will now be discussed.

A. Simplifying Assumptions Which Have Little Effect on Output

We first consider those assumptions which can be completely removed without significantly affecting the ideal solution.

a) The semiclassical approach describes the system for $T \gg T_R$, since at T_R there is one photon in each mode of the radiation field.⁷ Although, strictly speaking, the semiclassical description breaks down for $T < T_R$, we are only interested in the output at T_D , which is typically 25-100 T_R . Fluctuations in the fields during the first T_R will have little effect on the output at T_D due to the logarithmic dependence of the output on the initial conditions through ϕ . Thus, the randomly phased polarization source, constructed to be consistent with the requirements of thermal equilibrium,⁷ should give correct results for $T \gg T_R$.

b) Computer analysis shows that the effect of Λ_p on the evolution of the system is almost identical to that of a delta-function input E field of appropriate magnitude to give $\phi \approx \ln [\sqrt{2\pi N} (2\pi\alpha L)^{3/4}]$, where αL is the small-signal field gain, so that $\alpha L = T_2'/T_R$, where T_2' is the inverse linewidth. This is understandable since fluctuations at the far end of the medium are amplified over the greatest length and therefore dominate.

c) Computer analysis of the interaction between forward and backward travelling waves shows that this effect is virtually negligible in all swept excitation systems, and it is also negligible in uniformly excited systems for which $L/c \leq T_D$. (This latter case is discussed below.) This is so because the forward and backward waves only become sizable in the same region after much of the stored energy has been radiated.¹⁹

d) Computer calculations show that replacing μ_z^2 by its average value over M states and n by its sum over M states has little effect on the output radiation. Therefore, the influence of level degeneracy is insignificant.

B. Assumptions Which Can Significantly Affect Output

For the remaining assumptions, small deviations from ideality are of little importance but large deviations can cause significant changes in the output. The following conclusions have been verified by computer solutions of Eqs. (1).⁵

a) The lifetimes need not be infinite, which would imply infinite gain:

i) The net gain (gain minus loss) must be large enough so that the total area of the output pulse can grow to π . This leads to the requirement⁵

$$(\alpha - \kappa)L \geq \phi \quad . \quad (10a)$$

In the opposite limit where $(\alpha - \kappa)L < 1$, collective effects can still be important (since $T_R \ll T_{sp}$) but only a small fraction of the energy is radiated coherently (since $T_2' \ll T_R$); this regime, which we refer to as "limited superradiance",⁷ includes such familiar effects as free induction decay and echos. In the intermediate regime, where $1 < (\alpha - \kappa)L < \phi$, the peak intensity will be significantly less than that given by Eq. 7(a); analytical results in this regime can be obtained from the linear theory of Crisp.²⁰

ii) T_1 must be greater than T_D [Eq. 7(d)], otherwise the population will decay incoherently and reduce the amount of coherent output. This leads to the condition for efficient output

$$\alpha L \geq (\phi^2/4)T_2'/T_1 \quad . \quad (10b)$$

There is no similar requirement on T_2 or T_2^* since effects due to large dephasing or polarization decay rates are offset by high gain.⁷

b) As long as the inversion time τ is less than the observed delay time, a non-zero τ will have little effect on the output other than to increase the observed delay time from T_D to $T_D + \tau/2$. This gives the requirement

$$\tau \leq 2T_D \quad . \quad (10c)$$

If the superradiant output occurs before the inversion process terminates, then only the early part of the population inversion can contribute to the first burst of radiation.²¹ In the simple case where the inversion density in the absence of superradiant emission is equal to Λt , Λ constant, then⁹

$$(T_D)_{\text{observed}} = \sqrt{4\pi T_{sp} \phi^2 / \lambda^2 L \Lambda} \quad ,$$

$$I_p = 2h\omega A L \Lambda \quad ,$$

and

$$T_w = 8\sqrt{\pi T_{sp}} / \lambda^2 L \Lambda \quad .$$

Simple forms other than Λt can also be solved analytically, and graphical solutions are also possible.⁹

This same method can be used to provide an approximate solution for the case where $T_1 < T_D$, in violation of requirement (10b) above.

c) Excessive loss κ can diminish superradiance in two ways. It can reduce the net gain, making requirement (10a) harder to fulfill. Superradiant behavior also requires that

$$\int \kappa dx \leq \phi/4 \quad . \quad (10d)$$

When $\int \kappa dx \geq \phi/4$ the pulse stops narrowing and the intensity no longer grows with length. For constant κ , $I_p = N\hbar\omega/4T_R(\kappa L)^2$.²²

In the case of diffraction of a Gaussian beam, $\int \kappa dx = 1/2 \ln[1 + (\lambda L/A)^2]$. This quantity is always small when the Fresnel number is larger than unity.

d) Uniform excitation (entire system inverted simultaneously, in contrast to swept excitation) will have little effect on the output as long as the transit time $T_{tr} = L/c$ is less than the observed delay time, other than to increase the observed delay time to $T_D + T_{tr}/2$. When T_{tr} is longer than the delay time, the system will no longer radiate as a single entity; this places a condition on the length L_c ("cooperation length"):

$$L \leq L_c = \sqrt{c T_{sp} \phi^2 / 2 n \lambda^2} \quad . \quad (10e)$$

Longer systems will break up into a number of independently radiating segments in a manner described by Arecchi and Courtens.¹² In this limit, the output intensity $I_p \approx n A \hbar \omega c$ and no longer increases with increasing length. Note that requirement (10e) does not apply to swept excitation.

e) The presence of polarization at the superradiant transition $t = 0$ will have little effect provided that

$$P(t = 0) \ll \mu_z n_0^0 \quad (10f)$$

Larger values of $P(t = 0)$ are equivalent to increasing the initial tipping angle of the Bloch vector, which shortens the delay time and reduces the ringing. This increases the difficulty of completing the inversion process before coherent emission begins. In principle, a pulse of area exactly π could completely invert an initially absorbing medium without residual polarization. An energy conservation argument shows that such a pulse would have to be shorter than T_R in order not to lose area as it traverses the medium; for longer pulses, the effects of self-induced transparency and pulse propagation become relevant.^{10,12,16,23,24} As a practical matter, schemes to directly invert two-level systems are probably not feasible due to problems associated with loss, level degeneracy, transverse variations in the electric field associated with beam profile, and the difficulty of generating a pulse of exactly area π .

These problems can be circumvented by using indirect excitation methods such as three level pumping⁸ and two photon excitation with a nonresonant intermediate state. All observations of superradiance up to now have employed such schemes. However, the problem remains that when the pump radiation is turned off, a large residual polarization could be left at the pump transition. This can result in superradiance at this transition, which would deplete the population available for superradiance at the desired wavelength. This problem can be overcome by using an incoherent pump pulse, or by choosing a much shorter wavelength for the pump transition (to increase its T_R).

One should also note that in indirect excitation schemes the background emission which initiates superradiance can be modified by the presence of the pump field through multiple quantum transitions. This would increase the effective initial tipping angle, particularly if τ is long.

f) The effect of feedback on the output is negligible as long as the output field due to the initializing spontaneous emission is significantly greater than the additional output which results from the feedback process. Comparing these two quantities gives a condition on the feedback fraction F :

$$F \lesssim 4/(e^{0.35\phi} \phi^2) \quad (10g)$$

($F < 10^{-4}$ in the HF experiments.^{8,25}) In long systems, where transit time is appreciable, the influence of feedback decreases. Computer calculations in this regime have not yet been made.

The effect of significant feedback is to drastically shorten the delay times and reduce the ringing; the effect is analogous to continuing to push a pendulum after it has started to fall. The system acts as if it were subject to a different, larger initial condition.

g) The plane wave approximation breaks down when the solid angle factor μ of Rehler and Eberly²⁶ (a function of A , L , and λ) falls in the small Fresnel number regime of Fig. 5 of Ref. 26; the break between the two regimes is relatively sharp and occurs near Fresnel number $2A/\lambda L \approx 1/10$.

For small Fresnel number $T_R = T_{sp} 4\pi/nA\lambda$. The output should be independent of length in this regime, but the output intensity should still be proportional to the square of the population inversion density. We have done no computer analysis in the small Fresnel number regime.

To properly account for the spatial variations of E associated with finite beam diameter, and with focusing and defocusing in a high gain medium, a transverse spatial dependence must be added to Eqs. (1). This aspect of the analysis deserves further attention.

IV. SOME APPLICATIONS OF SUPERRADIANCE

A. Spin-Phonon Superradiance

It may be possible to observe an acoustical analog of superradiance in the spin-phonon interaction process in paramagnetic crystals.²⁷ In such a system the paramagnetic spins are coupled to the lattice vibrations (in a manner described by Jacobsen and Stevens²⁸). As shown in Ref. 29, in the slowly varying envelope approximation the coupled spin-phonon equations become almost identical in form to Eqs. (1).³⁰ Acoustical gain can be suitably defined, and so in a high gain medium, it should be possible for an initially inverted ensemble of spins, perturbed by kT fluctuations, to rapidly transfer its stored energy to the lattice. The ensuing acoustic waves should have all the properties of the coherent emission observed in optical superradiance.

Recently, Hahn and Wilson²⁷ proposed a related experiment to observe superradiant emission in a spin-phonon system by preparing the spins in a phased array. The phonon avalanche experiment of Brya and Wagner,³¹ although probably not a true coherent effect, was an interesting advance along these lines.

B. X-ray Lasers

The requirements for efficient superradiant emission should also be of interest to designers of x-ray laser systems. Due to the short lifetimes of the transitions and the lack of suitable mirrors in this regime, most proposed schemes use a single pass high gain swept-excitation system. Thus, x-ray lasers will superradiate. Consequently, the conventional rate equation analysis is not applicable, and the above considerations can be useful to estimate the output behavior. Some of the discussions in Section III are especially relevant to the x-ray regime; in particular, T_1 is usually so short that the inversion process will not be completed by the time superradiance occurs [see Eq. (10c)].

As mentioned above, the rate equation analysis gives incorrect results. For example, in the Na scheme of Duguay and Rentzepis,³² rate equation analysis predicts (at the threshold value) I_p about 10 times smaller and T_w about 10 times larger than the semiclassical predictions.⁹ In addition, the threshold inversion density is a factor of 10 smaller than the corresponding rate equation threshold.

Specific applications of these requirements to x-ray laser schemes are discussed further in Ref. 9.

C. Ultrashort Pulse Generation

Since superradiance is the optimum method for extracting coherent energy from an inverted medium, it is interesting to consider it as a method for generating ultrashort pulses. Although in the ideal case T_w decreases with increasing N , many of the conditions listed above restrict the shortness of output pulses one can hope to achieve. Combining Eqs. (7b), (7d), and (10c) shows that the inversion time places a particularly restrictive limit on the minimum T_w which can be generated superradiantly:

$$T_w \geq 2\tau/\phi \quad . \quad (11)$$

Therefore, ultrashort pulse generation by this method requires swept excitation, small ν , and as short an inversion time as possible. Values of T_w/τ less than 1/10 appear possible.

Note that superradiance is a transient process, and so the generation of ultrashort pulses by this method is inherently different from the mode locking approach, where short pulses

are generated by mixing a set of equally-spaced phase correlated modes to synthesize a Fourier spectrum.

References

- (1) M. Gross, C. Fabre, P. Pillet, and S. Harouche, Phys. Rev. Lett. 36, 1035 (1976).
- (2) Q. H. F. Vrehen, H. M. J. Hikspoors, and H. M. Gibbs, Phys. Rev. Lett., to be published; H. M. Gibbs, in this volume; and Q. H. F. Vrehen, in this volume.
- (3) A. Flusberg, T. Mossberg, and S. R. Hartmann, Phys. Rev. Lett., to be published, and in this volume.
- (4) T. A. DeTemple, in this volume.
- (5) Derivations of these conditions and computer results which support them can be found in J. C. MacGillivray and M. S. Feld (unpublished).
- (6) I. P. Herman, J. C. MacGillivray, N. Skribanowitz, and M. S. Feld, in Laser Spectroscopy, edited by R. G. Brewer and A. Mooradian, Plenum, 1974.
- (7) J. C. MacGillivray and M. S. Feld, Phys. Rev. A 14, 1169 (1976).
- (8) N. Skribanowitz, I. P. Herman, J. C. MacGillivray, and M. S. Feld, Phys. Rev. Lett. 30, 809 (1973).
- (9) J. C. MacGillivray and M. S. Feld, Appl. Phys. Lett., to be published.
- (10) D. C. Burnham and R. Y. Chiao, Phys. Rev. 188, 667 (1969).
- (11) R. Friedberg and S. R. Hartmann, Phys. Lett. 38A, 227 (1972) and references contained therein.
- (12) F. T. Arecchi and E. Courtens, Phys. Rev. A 2, 1730 (1970).
- (13) R. Saunders, S. S. Hassan, and R. K. Bullough, J. Phys. A 9, 1725 (1976) and in this volume.
- (14) R. H. Dicke, Phys. Rev. 93, 99 (1954) and in Proceedings of the Third International Conference on Quantum Electronics, Paris, 1963, edited by P. Grivet and N. Bloembergen, Columbia U. P., 1964.

- (15) R. Bonifacio and L. A. Lugiato, Phys. Rev. A 11, 1507 (1975) and 12, 587 (1975).
- (16) The notation is similar to that of A. Icsevgi and W. E. Lamb, Jr. [Phys. Rev. 185, 517 (1969)], extended to include level degeneracy and the polarization source term Λ_p .
- (17) The delta-function assumption is needed so that a boundary condition can be written for Eq. (5). It does not affect the derivations of Eqs. (2)-(4).
- (18) It follows from the assumption of a delta-function input E field that $E(x=0,t) = (h/\mu)\theta_0\delta(t)$.
- (19) This interaction has been studied by R. Saunders, R. K. Bullough, and S. S. Hassan (Ref. 13).
- (20) M. D. Crisp, Phys. Rev. A 1, 1604 (1970).
- (21) Although population inversion created after this time can contribute to later radiation lobes, the contribution is small due to the filling of the lower state.
- (22) F. T. Arecchi and R. Bonifacio, IEEE J. Quantum Electron. QE-1, 169 (1965); A. Icsevgi and W. E. Lamb, Jr. (Ref. 16); and R. Bonifacio, F. A. Hopf, P. Meystre, and M. O. Scully, Phys. Rev. A 12, 2568 (1975).
- (23) In this sense the condition $\tau = T_R$ is the dividing line between self-induced transparency pulse evolution and superradiance.
- (24) S. L. McCall and E. L. Hahn, Phys. Rev. 183, 457 (1969).
- (25) P. T. Ho, J. C. MacGillivray, S. Liberman, and M. S. Feld (unpublished).
- (26) N. E. Rehler and J. H. Eberly, Phys. Rev. A 3, 1735 (1971).
- (27) See references contained in E. L. Hahn and R. Wilson, in the proceedings of the XIXth Congress Ampère, Heidelberg, 1976.
- (28) E. H. Jacobsen and K. W. H. Stevens, Phys. Rev. 129, 2036 (1963).
- (29) G. Leonardi, J. C. MacGillivray, S. Liberman, and M. S. Feld, Phys. Rev. B 11, 3298 (1975).

- (30) The similarity between the Maxwell-Schrödinger and spin-phonon equations has also been exploited by N. Shiren [Phys. Rev. B 2, 2471 (1970)] to observe an acoustical analogue of self-induced transparency.
- (31) W. J. Brya and P. E. Wagner, Phys. Rev. 157, 400 (1967).
- (32) M. A. Duguay and P. M. Rentzepis, Appl. Phys. Lett. 10, 350 (1967).

Theory of superradiance in an extended, optically thick medium*

J. C. MacGillivray and M. S. Feld†

Department of Physics and Spectroscopy Laboratory, Massachusetts Institute of Technology,
Cambridge, Massachusetts 02139

(Received 21 April 1976)

This paper presents a semiclassical treatment of the evolution of an initially inverted system into a superradiant state in an extended, optically thick medium. In this process spontaneous emission and background thermal radiation initiate the collective radiative decay and produce a superradiant output pulse of intensity proportional to the square of the number of radiators. The treatment is based on the coupled Maxwell-Schrodinger equations, modified to include a fluctuating polarization source properly constructed to account for the effects of spontaneous emission. Computer results show that for a high-gain system only two parameters significantly influence the evolution process: T_R , the characteristic radiation damping time of the collective system, and θ_0 , a function of the conditions which initiate the superradiant process. In this limit one obtains a normalized emission curve and simple analytical expressions for the time delay, pulse width, and peak intensity of the output radiation. These results are in good agreement with experiments. A comparison of our model with previous treatments of superradiance is given.

I. INTRODUCTION

Superradiance, the idea that the spontaneous emission rate of an assembly of atoms (or molecules) can be much greater than that of the same number of isolated atoms, has been the subject of much theoretical discussion since it was originally proposed by Dicke¹ in 1954. In the process of superradiant emission the atoms are coupled together by their common radiation field, and so decay cooperatively. The intensity emitted by N atoms is therefore proportional to N^2 instead of N . Thus, superradiance is a fundamental effect.

Historically, observations of cooperative emission effects go back at least as far as Hahn's spin-echo experiment of 1948.² In the ensuing years experimental observations of free-induction decay, echos, and other cooperative emission effects have been made in both optical³ and longer-wavelength⁴ regimes. Such phenomena can be termed "limited superradiance," in that only a small fraction of the energy stored in the sample is emitted cooperatively, so that the decay of the sample is essentially unaffected by the cooperative radiation.⁵

In 1973 the first observation of "strong superradiance" was made in optically pumped HF gas.⁶ In this experiment virtually all of the energy stored in the sample was emitted cooperatively, and so the decay of the sample was dramatically accelerated. Although the emitted radiation had all the characteristics of superradiance described by Dicke, the detailed behavior (e.g., ringing, time delay of output) differed substantially from that predicted by the theoretical elaborations of Dicke's work then available.⁷⁻¹¹ Guided by the experimental observations, a simple theoretical model was developed^{6,12} which accurately described the features of the emitted radiation. The present paper

is an elaboration of that model. Recent experimental observations and their analysis are presented in another paper.^{15,16}

Dicke considered two regimes, distinguished by whether the sample is small ("point sample") or large ("extended medium") compared to the wavelength of the emitted radiation. The description of superradiant emission in an extended sample, such as occurs in the HF experiments, requires a more complex analysis, since propagation effects must be fully taken into account. Although most theoretical treatments of superradiance have used quantized fields,^{7-12,17-20} propagation effects are more easily included in the semiclassical approach (classical fields, quantized molecules) used by Dicke^{1,21} and a few others.^{6,13,14,22-25} The model presented here makes use of the semiclassical approach which, as discussed below, adequately describes a superradiant system. In fact, there is nothing inherently quantum mechanical about superradiance, as is illustrated by Dicke's description^{1,21} of how a collection of classical dipoles appropriately prepared can exhibit superradiant behavior. Later, our semiclassical results will be compared with some results obtained in quantized field treatments.

The theory developed in this paper is relevant to several potentially useful applications of superradiance. For example, it may be possible to produce ultrashort superradiant pulses of large peak intensity.²⁶ The results of this work should also be applicable to x-ray lasers²⁷ where, owing to the lack of suitable reflective surfaces, feedback is absent and one must depend on single-pass gain. Superradiant emission should also be observable in spin-lattice systems.^{28,29}

In an extremely long (or dense) sample, features of the superradiant output may be modified. The

maximum spatial extent of a system which can superradiate as a whole, and the minimum duration of its output pulses, are limited by effects such as finite transit time, diffraction, and the nature and duration of the excitation process. These effects are discussed in another paper²⁶; they are insignificant in the case of optically pumped HF gas at mTorr pressures in samples shorter than ~ 10 m (about 10 times the sample length of the experiments).

The remainder of this paper contains the following sections: II, Experimental Observation of Superradiance. III, Physical Principles. IV, Theoretical Model with Polarization Source, with sub-sections: A, Introduction; B, Coupled Maxwell-Schrödinger equations; C, Polarization source; D, Blackbody radiation and "equivalent input field." V, Numerical Results. VI, Simplified Theory. VII, Connections with Other Work.

Lengthy mathematical discussions have been placed in the appendixes.

II. EXPERIMENTAL OBSERVATION OF SUPERRADIANCE

In the experiments^{6,14,15} a long sample cell of low-pressure HF gas is pumped by a short intense pulse from an HF laser operating on a single R or P branch transition between the $v=0$ and 1 vibrational levels (Fig. 1). This produces a nearly complete population inversion between two adjacent rotational levels in the first excited vibrational state, corresponding to a transition in the 50–250- μ m range. The infrared radiation from this coupled transition (which is not at the same frequency as the pump transition) is studied as a function of time. There are no mirrors, and care is taken to minimize feedback. A detailed description of the experiments and their comparison with theory is given in Ref. 15.

An example of the observed output intensity is shown in Fig. 2(c). After a considerable delay (~ 1 – 2μ sec) with respect to the ~ 100 -nsec pump pulse [Fig. 2(a)], radiation is emitted in a series of intense, short (~ 100 nsec) bursts of diminishing

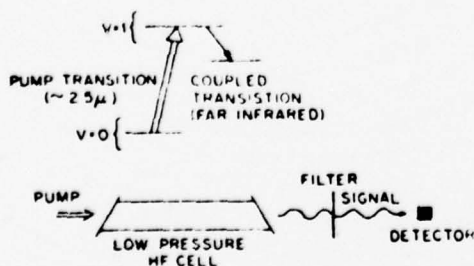


FIG. 1. HF level scheme and schematic of experimental setup.

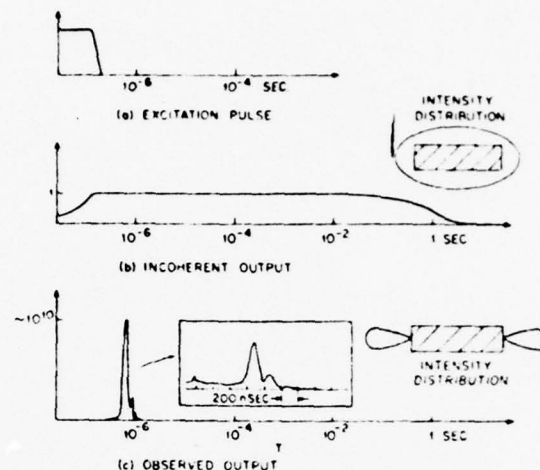


FIG. 2. Comparison of observed output and incoherent spontaneous emission. Time is plotted on a logarithmic scale. (a) Population-inverting laser pulse. (b) Output expected from incoherent spontaneous emission, exhibiting exponential decay and an isotropic radiation pattern. (c) Observed output, exhibiting ringing, a highly directional radiation pattern, and a peak intensity of $\sim 10^{10}$ times that of (b). The inset shows the time evolution of the same pulse with a linear time scale.

size ("ringing"); the process is completed within a few μ sec. The radiation pattern is highly directional; almost all of the radiation is emitted into a very small angle along the axis of the pump beam.

If the radiation emitted by this system were incoherent spontaneous emission, then it would have a long exponential decay (the radiative lifetime of these transitions is in the 1–10-sec range), and the radiation pattern would be isotropic [Fig. 2(b)]. Furthermore, the observed peak intensity is ten orders of magnitude greater than that expected for incoherent radiation. It is therefore clear that the process observed is not incoherent spontaneous emission. It is also clear that the output signal is not "amplified spontaneous emission"^{30–32} in the usual sense, since the pulse evolution time is much longer than the time over which population inversion occurs.

The observed radiation is also distinct from that of an "ordinary" high-gain laser, even one which can oscillate without mirrors, such as a saturated-molecular-nitrogen laser (3300 Å).^{33,34} In the nitrogen system the peak output intensity is directly proportional to the total population difference between the levels of the laser transition. Therefore, when the length or pressure is increased, the peak intensity increases proportionally. In contrast, the peak intensity of the observed output pulses in HF is proportional to the square of the pressure.^{14,15} This proportionality is in agreement

with the theoretical conclusions illustrated in Fig. 4 below.

The observed output radiation is therefore distinct from both incoherent emission and normal laser radiation. The N^2 dependence and the directionality of the observed radiation agree with the predictions of Dicke^{1,21} for the behavior of a superradiant system (Sec. III). The present analysis of a superradiant system is based on the semiclassical formalism³⁵ which, as shown below, predicts the same N^2 dependence and directionality as Dicke's analysis. The semiclassical formalism makes possible a detailed description of the time evolution of the system and allows one to establish the specific conditions under which superradiance can occur in an extended sample. Furthermore, in the special case of "limited superradiance" described below, the results of the present analysis reduce to those obtained in previous theoretical treatments of superradiance.^{11,12,17} The interpretation of the present experiment as the observation of superradiance is based on the connections of the present theory with previous treatments of Dicke and others, and the agreement of this theory with our experiments.

III. PHYSICAL PRINCIPLES

In his original treatment, Dicke¹ considered the radiative decay of an assembly of molecules for both a point sample (where the wavelength of emitted radiation λ is much greater than the sample length L) and an extended medium ($L \gg \lambda$). In a point sample,³⁶ by treating the entire collection of N molecules as a single quantum-mechanical system, he found that an initially totally inverted system will evolve into a "superradiant" state whose intensity is $N^2/4$ times the intensity radiated by a single molecule. This is larger by a factor of $N/4$ than the intensity radiated by N incoherent molecules.

For an extended medium, Dicke¹ showed that an array of quantum-mechanical dipoles phased along an axis could also produce superradiant emission.³⁶ Most of the radiation from the array is emitted into a small solid angle along the axis. For systems in which the Fresnel number $2A/\lambda L \gg 1$ ("disk"), the fraction of solid angle within which the radiation adds coherently is¹¹

$$f = \Delta\Omega/4\pi = \lambda^2/4\pi A, \quad (1)$$

where A is the cross-sectional area of the sample. In our HF system, where the Fresnel number is of order unity, the correct formula¹¹ gives a value only slightly different from that of Eq. (1), and $f \sim 10^{-4}$. The output radiation intensity of the array of dipoles is larger than the radiated intensity of

N incoherent dipoles by a factor $Nf \sim 10^8$.

The power I radiated by this array of N dipoles can be written in the form¹⁵

$$I = N(\frac{1}{4} h\omega/T_R), \quad (2)$$

where T_R is the characteristic radiation damping time of the collective system,³⁷

$$T_R = T_{sp}(8\pi/n\lambda^2 L), \quad (3)$$

$n = N/AL$, and T_{sp} is the lifetime of an isolated molecular dipole. Therefore, the emitted power is proportional to $N^2 f$.

In an extended molecular sample which is evolving to a superradiant state, a macroscopic polarization is established over a region of space. This polarization is equivalent to a phased array of dipoles which can be represented quantum mechanically as coherent mixtures of the stationary states of the molecules.²¹ In the case of a $(J_{upper} = J+1) \rightarrow (J_{lower} = J)$ rotational transition of a diatomic molecule such as HF, T_{sp} is given by

$$h\omega_0/T_{sp} = \frac{4}{3} |\mu|^2 \omega_0^4/c^3, \quad (4)$$

where³⁸

$$|\mu|^2 = \mu_0^2 \frac{J+1}{2J+3}, \quad (5)$$

and μ_0 is the dipole moment of the molecule. Combining Eqs. (3) and (4), we have

$$T_R^{-1} = \frac{2\pi}{\lambda} \frac{2\pi}{h} \mu_0^2 n_T L, \quad (6)$$

where $n(M)$ is the population inversion density between the states $|J_{upper}, M\rangle$ and $|J_{lower}, M\rangle$, n_T is the sum of $n(M)$ over all M levels in J_{upper} , and

$$\mu_0^2 = \langle |\mu_+(M)|^2 \rangle_{J_{lower}} = \sum_{M=-J}^J \frac{|\mu_+(M)|^2 n(M)}{n_T}, \quad (7)$$

where

$$\mu_+(M) \equiv \mu_+[(J+1, M) \rightarrow (J, M)]. \quad (8)$$

In our HF case,

$$\mu_+^2 = \frac{\mu_0^2}{3} \frac{J+1}{2J+3} \quad (9)$$

when the excitation pulse is a P branch transition, and

$$\mu_+^2 = \frac{\mu_0^2}{3} \frac{J+1}{2J+1} \quad (10)$$

for an R branch excitation pulse.

Equation (2) shows that when the sample radiates as a collective system, the lifetime decreases from T_{sp} to $\sim T_R$. T_R can therefore be interpreted as a characteristic radiation damping time of the collective system. For the HF system, $T_{sp} \sim 1$ sec

and $n \sim 10^{11} - 10^{12} \text{ cm}^{-3}$, so $T_R \sim 10^{-8} \text{ sec}$. In order for the system to decay by the collective mode rather than as independent radiators it is necessary that $T_R \ll T_{sp}$. For a "disk" this requires that $n\lambda^2 L \gg 1$; i.e., there must be a large number of molecules in a "diffraction volume" $\lambda^2 L = (\lambda^2/A)AL$. This requirement also insures that there are many molecules in a cylinder of cross section λ^2 and length L , so that a coherent wave front can be properly reconstructed.

Consider next the process by which a macroscopic polarization builds up in an initially inverted system (the two adjacent rotational levels of interest in the HF $v=1$ level). In the Bloch formalism¹¹ for a point sample, a totally inverted system corresponds to a vector pointing straight up, analogous to a rigid pendulum balanced exactly on end. Similarly, our initially inverted extended medium corresponds to a spatial distribution of Bloch vectors all pointing straight up. The individual Bloch vectors of the extended medium, which are coupled together via the common radiation field, may evolve differently owing to propagation effects.

Just as the pendulum is unstable to small fluctuations, so the excited molecular system is unstable to a small perturbing field, initiated by spontaneous emission from one of the excited molecules or by background thermal radiation. This weak propagating electric field induces a small macroscopic polarization in the medium, which acts as a source to create additional electric field in the medium which, in turn, produces more polarization. This regenerative process gives rise to a growing electric field and an increasing polarization throughout the medium [Fig. 3(a)]. Therefore, a superradiant state slowly evolves over a sizable portion of the sample cell.¹¹ This state corresponds to the Bloch vectors pointing sideways over a sizable region of space, at which time radiation is emitted at a greatly enhanced rate. This process leads to a rapid deexcitation of that region of the medium, after which essentially all of the population is in the lower level; i.e., the Bloch vectors all point downward. Deexcited regions can then be reexcited by radiation from other regions, which gives rise to the "ringing" observed in the output radiation.

Figure 3 plots the polarization envelope \mathcal{P} and the population inversion density n , respectively, throughout the sample at several instants of time. These values have been calculated from a theoretical model (developed in the following sections) based on the intuitive picture presented above. Notice that \mathcal{P} and n vary slowly in space and time throughout the medium, giving rise to several regions of locally uniform polarization. These

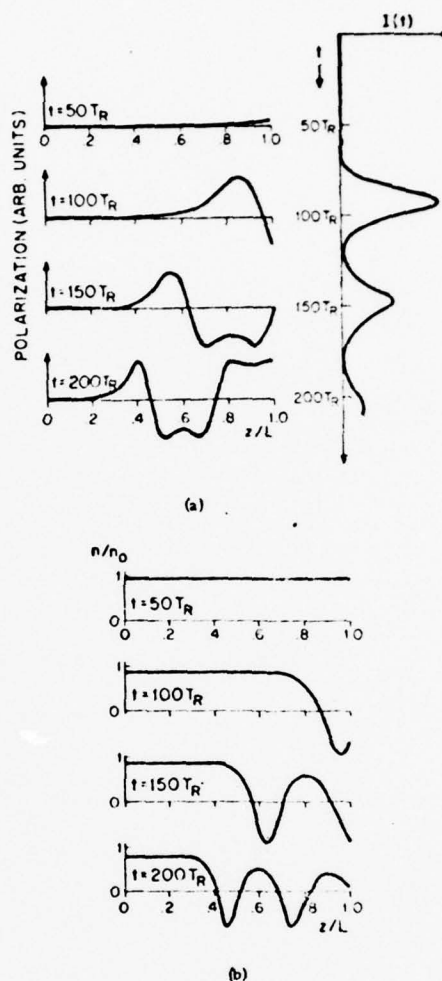


FIG. 3. Sketch of (a) the polarization envelope \mathcal{P} and (b) the population inversion density n in the medium as functions of x at $t = 50T_R, 100T_R, 150T_R,$ and $200T_R$. The corresponding output intensity pattern is shown at the right of (a). The double peaks in \mathcal{P} (c) occur whenever the ringing is sufficiently large (Ref. 40).

spatial variations in \mathcal{P} and n are due to propagation effects in a high-gain medium, a crucial point which was not appreciated in some earlier work. The ringing in the output radiation (Fig. 3) is a direct consequence of these spatial variations (see Sec. VI).

The time evolution of the radiation emitted by an initially inverted system depends on many factors, including broadening, diffraction loss, and level degeneracy. However, as shown in Sec. V, in a high-gain system the major features of the output radiation pulse are determined by T_R and the logarithm of θ_0 (described below), and a normalized curve can be drawn which gives the output intensity $I(T)$ multiplied by T_R^2 as a function of time in units

of T_R (T is the retarded time at the end of the sample). This curve (Fig. 4) depicts a burst of radiation with ringing preceded by a long delay. The scaling of the curve is such that when T_R is halved, the system radiates twice as fast and the peak intensity is quadrupled. This curve exhibits the N^2 intensity dependence which is characteristic of superradiant emission, since the peak intensity is proportional to T_R^{-2} and T_R is proportional to N^{-1} . Experimental data exhibiting this scaling are given in Ref. 15.

The shape of this curve depends on θ_0 , a parameter which is a measure of the conditions which initiate the superradiant pulse [Eq. (20) below]. Whenever $\theta_0 \ll 1$, the delay time T_D from the time of inversion to the peak of the first lobe of emitted radiation is much greater than T_R . This long delay time may be understood by considering a pendulum which is initially balanced exactly on end. The time required for the pendulum to fall following a small perturbation can be much longer than the oscillation period. In an analogous manner, the time necessary for the completely inverted system to develop a macroscopic polarization can be much longer than the collective radiation time T_R . This point will be discussed in Sec. VI.

In the experiments, superradiant pulses are observed simultaneously in both the forward and backward directions with respect to the population-inverting laser pulse. This comes about because in the HF system the transit time through the sample cell is short compared to the time needed for the system to superradiate ($\sim T_D$), so that the electromagnetic waves can grow in both directions simultaneously without interacting appreciably

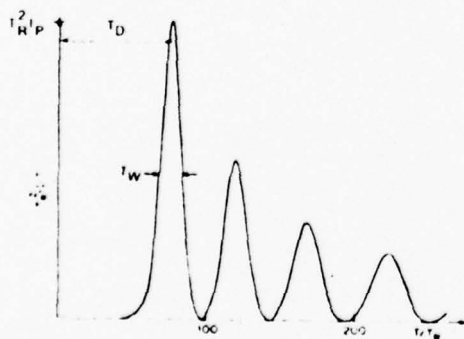


FIG. 4. Normalized output curve. This curve is the output response to a small rectangular input pulse of area θ_0 in a nondegenerate system where $T_2 = T_2^*$ and $\kappa L = 0$. The time scales as T_R and the intensity scales as T_R^{-2} . Note that the shape of the normalized output curve depends on θ_0 . I_R , T_D , and T_R can all be expressed in terms of T_R and θ_0 (see Sec. VI).

during most of the pulse evolution time. (Long transit times and different excitation configurations are discussed in Sec. VI and Ref. 26.) This is so because in order for the waves to interact, either (i) they must become large in the same region of the medium at the same time, so that the coherent interactions which couple the forward and backward waves become important, or (ii) the population depletion by one wave must affect the subsequent growth of the other wave. The former effect is negligible because the buildup of polarization of a given wave is confined to one end of the medium until well after the main pulse has already been emitted [$\sim 150 T_R$, Fig. 3(a)]. The latter effect is negligible because each wave depletes the population inversion primarily at one end of the medium [Fig. 3(b)]. An iterative computer solution using the theoretical model shows that the growth of each wave is almost completely unaffected by the population depletion caused by the other wave. We therefore conclude that for systems with small transit time the two waves will radiate essentially independently without significant correlation, and henceforth, we will only deal with the forward traveling wave. A discussion of the interaction of forward and backward waves in systems with long transit times will be found in Ref. 26.

IV. THEORETICAL MODEL WITH POLARIZATION SOURCE

A. Introduction

In numerous treatment of superradiance the radiation field is quantized and the molecular system is described in terms of collective Dicke states.^{7-12,17-20} As pointed out by Arecchi, Courtens, Gilmore, and Thomas,³⁵ these states can be used to construct a new set of states, Bloch states, which also describe superradiant ensembles. These new states can be treated by means of the semiclassical formalism (coupled Maxwell-Schrödinger equations), in which the molecular system is quantized but the electromagnetic field is treated classically.

One shortcoming of the Maxwell-Schrödinger equations as they are usually written¹² is that there is no mechanism for spontaneous emission, so that an initially inverted system (such as in the HF experiment) cannot evolve.⁴³ This problem can be overcome by adding a phenomenological fluctuating polarization source term to simulate the effect of spontaneous emission. This term can be constructed to be consistent with requirements of thermal equilibrium as well as energy and number conservation.

Let us consider in more detail the initial stage of the evolution of an inverted system to a superradiant state. At first the system undergoes spon-

taneous emission in various directions at random times. Eventually a photon is emitted along the axis of the sample cell, leading to the excitation of one of the modes of the inverted medium. In the case of large Fresnel number (disk) this mode subtends a solid angle $\Delta\Omega = \lambda^2/A$ [Eq. (1)], determined by diffraction. The average number of photons emitted into this mode in a time t is equal to $(N/T_R)(\lambda^2/4\pi A)t = 2t/T_R$, so that the first photon is emitted into the diffraction mode in a time of order T_R .¹³ Therefore, at times greater than T_R there will be many photons per mode, so that the radiation field can be treated classically.

Note that up to time $\sim T_R$, when the medium is starting to evolve, the number of photons per mode is small and one can question the validity of the semiclassical model with polarization source term included. However, in the present problem, in which an initially unstable system is subjected to small perturbations, this model is a good approximation. To justify this conclusion, we note the following:

(i) Computer results (Sec. V) obtained from this model show that the superradiant output of the initially inverted system is insensitive to the specific form of the source fluctuations, depending only on their sum over a time $\sim T_R$. This is easy to understand in terms of the pendulum analogy presented previously: For a system in an unstable initial state, the response to a rapid series of small destabilizing forces depends only on the sum of these forces over a period of time (here, $\sim T_R$) and not on the form of the individual forces.

(ii) The numerical results also show that the contribution of the polarization source term to the evolution of the system becomes negligible for times larger than $\sim T_R$. This can be understood by using Eq. (47) below to show that the time necessary for the output resulting from a small input pulse to become much larger than the input pulse itself is of order T_R . Therefore, for times greater than T_R , the input pulse and, accordingly, the polarization source which gives rise to it, no longer significantly influences the output behavior. (It will be shown in Sec. IVD that the polarization source of this model can be accurately approximated by an equivalent input pulse.)

Since the output radiation becomes independent of the polarization source after a time $\sim T_R$ following the inversion of the medium, phase fluctuations associated with spontaneous emission at subsequent times will have little effect on the output radiation. In other words, the first photon emitted into the diffraction mode initiates the evolution of the system, and phase fluctuations associated with subsequent spontaneous-emission events are unimportant. In effect, the first photon determines

the phase of the output radiation.

(iii) The delay time between the inversion of the medium and the peak of the superradiant output pulse, which is of the order of $100 T_R$ in the HF experiments [see Eq. (49)], is not sensitive to the fluctuations of the spontaneous emission which initiates the superradiant process. This is so because the fluctuation time before the first photon is emitted into the diffraction mode is of order T_R . This time is only $\sim 1\%$ of the delay time in HF, and can be ignored in calculating the delay time.

This explains why the semiclassical formalism with a fluctuating polarization source included gives a good description of the evolution of a superradiant state in an initially inverted medium.

B. Coupled Maxwell-Schrödinger equations

Adopting the semiclassical formalism, we consider a gas of two-level molecules interacting with an electromagnetic wave. As in the discussion following Eq. (1), we confine our attention to a system of large Fresnel number (disk-shaped system) where the electromagnetic field can be approximated by a plane wave. In this limit the two-level system is described by the coupled Maxwell-Schrödinger equations given by many authors.^{22-24,34,45} We shall adopt notation similar to that of Isevgi and Lamb,²⁴ extended to include level degeneracy, as is necessary in treating rotational transitions of a molecular system, and the polarization source described previously. The coupled equations in the slowly-varying-envelope approximation, written in complex form, are

$$\frac{\partial \mathcal{E}}{\partial x} = -\kappa \mathcal{E} + 2\pi k \sum_{v,M} \mathcal{P}, \quad (11a)$$

$$\frac{\partial \mathcal{P}}{\partial T} = -(\gamma - ikv)\mathcal{P} + (\mu_z^2)_M \mathcal{E} n / \hbar + \Lambda_P, \quad (11b)$$

$$\frac{\partial n}{\partial T} = \Lambda - \gamma n - (1/\hbar) \text{Re}(\mathcal{E}\mathcal{P}^*). \quad (11c)$$

Here $\mathcal{E}(x, T)$ and $\mathcal{P}(x, T, v, M)$ are the slowly varying envelopes of the electric field $\tilde{E}(\tilde{r}, t)$ and the polarization density per velocity interval $d\tilde{v}$, $\tilde{P}(\tilde{r}, t, v, M)$, respectively. They are defined by

$$\tilde{E}(\tilde{r}, t) = \hat{z} E(x, t) = \hat{z} \text{Re}[\mathcal{E}(x, T) e^{i(\omega_0 t - kx)}], \quad (12)$$

$$\begin{aligned} \tilde{P}(\tilde{r}, t, v, M) &= \hat{z} P(x, t, v, M) \\ &= \hat{z} \text{Re}[i \mathcal{P}(x, T, v, M) e^{i(\omega_0 t - kx)}], \end{aligned} \quad (13)$$

at position x , time t , and retarded time $T = t - x/c$. The carrier frequency is assumed to be the molecular center frequency ω_0 with no loss of generality. Note that \mathcal{E} and \mathcal{P} are complex, and that $\mathcal{E}(x, T) = |\mathcal{E}(x, T)| e^{i\phi}$ where $\phi(x, T)$ is a slowly varying real phase. In these equations, $n(x, T, v, M)$

$=n_2 - n_1$, where n_2 and n_1 are the number densities per velocity interval dv of molecules in the upper and lower states (J, M) of the superradiant transition, respectively; κ is a loss term which accounts for diffraction (see Sec. V), which can be a function of x but not of δ ; and γ is the decay rate of n_1 , n_2 , and ϕ , assumed equal for simplicity (i.e., $T_1 = T_2 = \gamma^{-1}$).⁴⁶ $\Lambda = \lambda(z, T, M)W(v)$ is a source term describing the rate of production of n , due to optical pumping in our case, where $W(v)$ is the distribution of molecular velocities, normalized to unity [Eq. (15)]. $\Lambda_p(v, T, v, M)$ is the polarization source term describing the rate of production of ϕ due to spontaneous emission. The exact form is discussed in Sec. IV C. The symbol $\sum_{v, M}$ denotes an integral over the velocity distribution and a sum over degenerate M states of the rotational levels:

$$\sum_{v, M} f(v, M) = \int_{-\infty}^{\infty} dv \sum_{M=-J}^J f(v, M). \quad (14)$$

In the experiments the optical pumping process produces excited molecules in the upper level of an initially unpopulated two-level system (Fig. 1) with a Lorentzian velocity distribution,⁴⁷

$$W(v) = u_1 / \pi(v^2 + u_1^2), \quad (15)$$

where

$$u_1 \approx \mu_p \mathcal{E}_p / \hbar k_p. \quad (16)$$

Here k_p is the wave number and μ_p the matrix element of the pump transition, and \mathcal{E}_p is the amplitude of the intense pump field. In HF,^{14,15} $u_1 \sim 10^4$ cm/sec. The total number density of excited molecules in all M_J states is then (for R branch pumping)

$$n_T = \sum_{v, M} n(v, M), \quad (17)$$

$$n_{T0} = n_T(t=0) = \frac{1}{2} \left(\frac{\mu_p \mathcal{E}_p / \hbar}{k_p u / \sqrt{\pi}} \right) n_G, \quad (18)$$

where n_G is the total number of molecules in the rotational level (of the $v=0$ vibrational state) which is being pumped.⁴⁸

Although the growth of the electric field in the medium does not follow simple exponential gain, the time integral of the electric field obeys an exponential law, the area theorem.⁴⁴ This states that for a nondegenerate Doppler-broadened collisionless system subjected to an incident field $\delta(x \approx 0, t)$ of constant phase, the pulse area $\theta(x)$ obeys the equation

$$\tan^{-1} \theta(v) = (\tan^{-1} \theta_0) e^{\alpha_0 x}, \quad (19)$$

where

$$\theta(x) \equiv \frac{\mu_p}{\hbar} \int_{-\infty}^{\infty} \delta(x, t) dt, \quad (20)$$

$\theta_0 = \theta(x=0)$, and α_0 is the small signal field gain at the molecular center frequency ω_0 . For a system whose linewidth contains both homogeneous and inhomogeneous contributions,

$$\alpha_0 L = 2\pi k (\mu_p^2 / \hbar) n_{T0} L T'_2, \quad (21)$$

where n_{T0} is the initial total inversion density. In the Doppler-broadened limit, which applies in the HF system, the characteristic broadening time $T'_2 \approx T_2^* = 1/k u_1$. [Note that in our case, $k u_1$ is an effective Doppler width, given by Eq. (16) above.] Combining Eqs. (6) and (21) gives the relationship⁴⁹

$$\alpha_0 L = T'_2 / T_R, \quad (22)$$

so that $\alpha_0 L$ is independent of the pump field intensity I .

Equation (19) shows that in a high-gain medium the area of a pulse of small initial area begins to grow exponentially,

$$\theta(x) = \theta_0 e^{\alpha_0 x}, \quad (23)$$

but then evolves towards π . In this process the field envelope may develop positive and negative lobes (ringing) whose contributions to the area substantially cancel one another. Accordingly, in a high-gain system the pulse energy continues to grow even though the area remains constant.

The presence of level degeneracy does not invalidate this conclusion, although level degeneracy can inhibit pulse propagation in an absorber. The considerations of Rhodes, Szöke, and Javan⁵⁰ applied to an amplifier show that level degeneracy does not prevent pulse formation, and that pulses of increasing energy and area near π can evolve.

High gain ($\alpha_0 L \gg 1$) is necessary for superradiance to occur. This condition is equivalent [Eq. (22)] to $T_R \ll T'_2$, which is necessary so that collective radiation can occur rapidly with respect to incoherent decay. The requirement $\alpha_0 L \gg 1$ also ensures that $\alpha_0 L \approx |\ln \theta_0|$, so that a π pulse will evolve [Eq. (19)]. The high-gain condition will be discussed further in Sec. VII.

C. Polarization source

As discussed earlier, the superradiant evolution process is initiated by spontaneous emission from the excited molecules and by background thermal radiation. In our model spontaneous emission is simulated by a randomly phased polarization source term Λ_p which is distributed throughout the medium. As is shown below, although Λ_p is essential for initiating the growth of δ , as the δ field evolves in a high-gain system the influence of Λ_p soon becomes unimportant. Therefore, to calculate the

amplitude of Λ_p for a high-gain system, we consider the contribution of Λ_p to the growth of \mathcal{E} only during the first stage of pulse evolution, when \mathcal{E} is small and the field produced by Λ_p is sizable compared to the field already present.

The amplitude of Λ_p will be calculated in the following manner: First, starting from the coupled Maxwell-Schrödinger equations, specialized to the case of weak field and steady state, we obtain an equation for the intensity $I(x)$ as a function of the amplitude of Λ_p . This equation is then compared to an intensity equation derived from thermal equilibrium considerations which also holds for linear steady-state systems. Since these two equations are of the same form, we can evaluate the amplitude of Λ_p in terms of the molecular parameters of the system. The resulting expres-

sion for Λ_p , which is not a function of dynamical variables, can be used in the coupled Maxwell-Schrödinger equations to describe a system not at thermal equilibrium.

We consider the medium to be divided into small regions of volume $A\Delta x$ ($\Delta x \ll L$), and time into intervals $\Delta t < T_R$. Since the spontaneous-emission intensity is proportional to $n_2(x, t)$ and otherwise depends only on molecular constants (except for a linewidth-narrowing effect in high-gain systems, described below), Λ_p is proportional to $(n_2)^{1/2}$. We choose the form of Λ_p to be a series of pulses in space and time with constant amplitude⁵¹ (except for the n_2 dependence) and random phases.⁵² It is convenient to evaluate Λ_p at points separated by Δx in space and ΔT in retarded time. Then Λ_p will be of the form

$$\Lambda_p(x, T, v, M) = B_1 [n_2(x, T, v, M)]^{1/2} \sum_{j=1}^{J'} \delta(x - x_j) \sum_{l=-\infty}^{\infty} \delta(T - T_l) \sum_{k=1}^{K'} \delta(v - v_k) e^{i\phi_{jlkM}}, \quad (24)$$

where B_1 is a (real) constant to be determined, $x_j = (j - \frac{1}{2})\Delta x$, $\Delta x = L/J$, $T_l = l\Delta T$, v_k are k' discrete velocities,⁵³ and ϕ_{jlkM} are independent random phases.

We consider the case where n and \mathcal{E} are independent, \mathcal{E} is very slowly varying in time ($\partial\mathcal{E}/\partial T \ll \gamma\mathcal{E}$),⁵⁴ and n is near a constant value n_0 and is very slowly varying in space and time ($\partial n/\partial T \ll \gamma n$, $\partial n/\partial x \ll \gamma n/c$).⁵⁵ Such a system is linear and nearly steady state ($n \approx n_0$). As shown in Appendix A, the coupled Maxwell-Schrödinger equations [Eqs. (11a) and (11b)] for such a system may be integrated to give an intensity gain equation

$$I(x) = I(x=0) e^{2\alpha_0 x} + K_0 (e^{2\alpha_0 x} - 1), \quad (25)$$

where α_0 is the gain of the system at the molecular center frequency ω_0 , $I(x) = cA |\mathcal{E}(x)|^2/8\pi$ is the power at position x , and

$$K_0 = \frac{\pi}{4} \frac{\omega_0^2}{c} AB^2 \frac{T_2 n_2}{\Delta T} (1 - e^{-2\alpha_0 \Delta x})^{-1}. \quad (26)$$

Equation (25) holds for any linear steady-state system, independent of the sign and magnitude of the gain.

We require that Eq. (25) be consistent with the Einstein intensity equation,^{56,57} which states that throughout the active region of any linear steady-state medium, the total energy per mode $I_\omega(x)$ must satisfy the equation

$$\frac{dI_\omega(x)}{dx} = 2\alpha(\omega) \left(I_\omega(x) + \frac{\hbar\omega n_2}{n_2 - n_1} \right), \quad (27)$$

where $\alpha(\omega)$ is the gain at frequency ω . [Note that

Eq. (27) is consistent with the requirements of thermal equilibrium, since when $I_\omega(x) = \hbar\omega/(e^{\hbar\omega/kT} - 1)$ and $n_2 = n_1 e^{-\hbar\omega/kT}$, Eq. (27) simplifies to $dI_\omega(x)/dx = 0$.] To compare Eq. (27) with Eq. (25), Eq. (27) must be rewritten in terms of the power per unit frequency interval $I(\omega, x)$ in the plane-wave direction. As shown in Appendix B, for a system with Fresnel number not significantly less than unity, Eq. (27) becomes

$$\frac{\partial I(\omega, x)}{\partial x} = 2\alpha(\omega) \left(I(\omega, x) + \frac{\hbar\omega}{4\pi} \frac{n_2}{n_2 - n_1} \right). \quad (28)$$

The integration of Eq. (28) in a high-gain ($\alpha_0 L \gg 1$) linear steady-state system with finite bandwidth is performed in Appendix C. In such a system the linewidth of $I(\omega, x)$ decreases as $\alpha_0 x$ increases ("gain narrowing"). For a high-gain system interacting with a broadband field of input bandwidth $\Delta\omega \gg (T_2')^{-1} (\pi/2\alpha_0 L)^{1/2}$ centered at frequency ω_0 (where $1/T_2'$ is the bandwidth of the gain profile), the total output power $I(x=L)$ can be obtained by integrating Eq. (28) as in Appendix C:

$$\begin{aligned} I(x=L) &= \int I(\omega, x=L) d\omega \\ &\approx \left(I(\omega_0, x=0) + \frac{\hbar\omega_0}{4\pi} \frac{n_2}{n_2 - n_1} \right) (T_2')^{-1} \\ &\quad \times \left(\frac{\pi}{2\alpha_0 L} \right)^{1/2} e^{2\alpha_0 L}. \end{aligned} \quad (29)$$

We can compare this result with the high-gain limit ($e^{2\alpha_0 x} \gg 1$) of Eq. (25) to obtain⁵⁸

$$I(x=0) = I(\omega_0, x=0) (T'_2)^{-1} (\pi/2\alpha_0 L)^{1/2} \quad (30)$$

and

$$K_0 = \frac{n_2}{n_2 - n_1} (T'_2)^{-1} \left(\frac{\pi}{2\alpha_0 L} \right)^{1/2} \frac{\hbar \omega_0}{4\pi} \quad (31)$$

Equation (30) tells us what the input power $I(x=0)$ in the intensity gain equation [Eq. (25)] must be for a high-gain system in order to be consistent with the Einstein equation. Equation (30) can be rewritten in the form

$$I(x=0) = I(\omega_0, x=0) (\Delta\omega)_{\text{eff}}, \quad (32)$$

where $(\Delta\omega)_{\text{eff}} = 1/(T'_2)_{\text{eff}} = (T'_2)^{-1} (\pi/2\alpha_0 L)^{1/2}$ is the mathematically derived effective bandwidth of the input radiation which interacts with the gain profile of the high-gain system. This gain-narrowing effect can be explained physically by noting that in the early stages of growth, a high-gain system preferentially amplifies the central portion of the frequency profile.

Inserting Eq. (31) into (26), we obtain B_1 , and if Δx is chosen such that $\alpha_0 \Delta x \approx 1$ (as in the case of our computer program), Eq. (24) becomes¹⁵

$$\begin{aligned} \Lambda_p(x, T, \nu, M) &= \left(\frac{4\Delta T}{T'_2} \frac{\Delta x}{L} \frac{n_2 \Delta L}{(2\pi\alpha_0 L)^{1/2}} \right)^{1/2} \left(\frac{\mu_p}{\Lambda} \right) \\ &\times \sum_j \sum_i \sum_k \delta(x - x_j) \delta(T - T_i) \delta(\nu - \nu_k) e^{i\phi_{ijk}}. \end{aligned} \quad (33)$$

Note that Λ_p is proportional to μ_p and depends on the total number of excited molecules $n_2 \Delta x \Delta T$ associated with one point in the space-time grid; the square-root dependence occurs because the radiation from independent spontaneous-emission events adds incoherently.

D. Blackbody radiation and "equivalent input field"

In the computer model background thermal radiation is simulated by an input field of randomly fluctuating phase, the intensity of which depends on the bandwidth and the solid angle of the input radiation which interacts with the system. The result of Appendix B can be used to convert the blackbody power per mode $I_{\text{bb}}(x=0) = \hbar\omega/(e^{\hbar\omega/kT} - 1)$ to the plane-wave blackbody power per unit frequency interval $I(\omega, x=0) = (\hbar\omega/4\pi)/(e^{\hbar\omega/kT} - 1)$. As described above, the effective bandwidth of radiation which interacts with a high-gain system is $\Delta\omega_{\text{eff}} = (\pi/2\alpha_0 L)^{1/2}/T'_2$ (see Appendix C), so that the total input power which must be used in order to correctly apply Eq. (25) to this case is

$$\frac{cA}{8\pi} |\mathcal{E}(x=0, T)|^2 = \frac{\hbar\omega_0}{4\pi} \frac{\Delta\omega_{\text{eff}}}{e^{\hbar\omega_0/kT} - 1} \quad (34)$$

or, equivalently,

$$\begin{aligned} \frac{|\mathcal{E}|^2}{8\pi} &= \frac{\hbar\omega_0}{e^{\hbar\omega_0/kT} - 1} \frac{2\pi(\omega_0/2\pi)^2}{c^3} \\ &\times \frac{\lambda^2}{4\pi A} \frac{k\mu_p}{2\pi(2\alpha_0 L/\pi)^{1/2}}. \end{aligned} \quad (35)$$

The factors on the right-hand side of Eq. (35) are, respectively, the background thermal radiation energy per mode, the number of modes of one polarization per unit value per frequency interval $\Delta\nu$, the solid angle factor f , and the gain-dependent effective bandwidth (in units of $\Delta\nu$). Using this value of $|\mathcal{E}(x=0, T)|$ as an input boundary condition, and using Eq. (33) for Λ_p , Eqs. (11) can be numerically integrated to obtain the output radiation intensity. Examples of these computer results are given in Figs. 3 and 5.

Alternatively, spontaneous emission in a high-gain system can be described by replacing the distributed polarization source by an "equivalent"

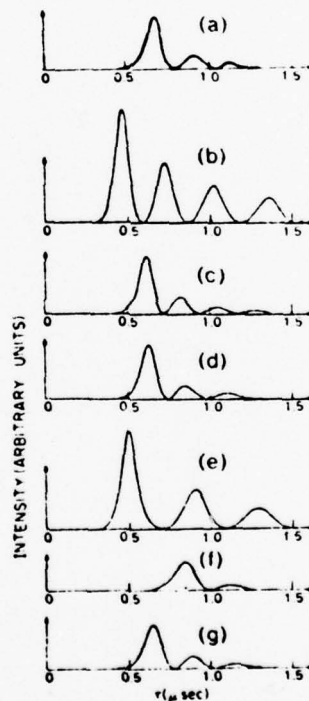


FIG. 5. Computer results showing the influence of parameters on output intensity. The same intensity scale is used throughout. (a) A theoretical fit with parameters $T_R = 6.1$ nsec, $T'_2 = 330$ nsec, $T_2 = 5.4$ μsec, $\kappa L = 2.5$, $J_{\text{lower}} = 2$. All parameters have the same values as in this curve except when stated otherwise. (b) No level degeneracy, $T_2 = T'_2 = \infty$, $\kappa L = 0$. (c) $T_2 = \infty$. (d) $T'_2 = \infty$. (e) $\kappa L = 0$. (f) $\kappa L = 5$. (g) No level degeneracy.

input electric field. The input field (of constant amplitude) which would produce the same output intensity as the distributed source (see Appendix C) for a high-gain system, which combines the contributions of blackbody radiation [Eq. (34)] and spontaneous emission, is⁵⁹

$$\begin{aligned} \frac{cA}{8\pi} |\mathcal{E}_{\text{eff}}(x=0, T)|^2 \\ = \frac{\hbar\omega_0}{4\pi} \frac{k\mu_1}{(2\alpha_0 L/\pi)^{1/2}} \left(\frac{n_2}{n_2 - n_1} + (e^{\hbar\omega_0/kT} - 1)^{-1} \right) \\ = \frac{\hbar\omega_0}{2T_R\sqrt{\pi}} \frac{1}{(2\alpha_0 L)^{1/2}} \left(\frac{n_2}{n_2 - n_1} + (e^{\hbar\omega_0/kT} - 1)^{-1} \right) \end{aligned} \quad (36)$$

The validity of the "equivalent-input" approximation can be understood by noting that in a high-gain system the spontaneous emission which occurs near the input face is most important in initiating the superradiant evolution process. Although all of the output radiation curves in this paper (and in Ref. 15) were fitted using the distributed-polarization-source model, essentially identical computer curves are obtained using the equivalent-input-field approximation. This finding strongly supports the validity of the equivalent-field approach and confirms the interpretation and analysis of Ref. 6.

Since the distributed source can be replaced by an effective input field and since phase fluctuations in the input field do not significantly affect the computer curves (as explained in Sec. IV A and verified by the computer results of Sec. V below), the results of the area theorem [Eq. (19)] may be used for a qualitative understanding of the behavior of the system.⁶⁰ This makes it possible to derive an effective input area θ_0 , which can be used in the area theorem and for obtaining simple analytical expressions for the delay time, pulse width, and peak intensity (Sec. VI). Owing to the exponential nature of the growth of the area [Eq. (19)], the parameter which enters into these expressions is a logarithmic function of θ_0 . Because $|\ln \theta_0| \gg 1$, the expressions are insensitive to the exact numerical coefficient of θ_0 .

As stated earlier, the influence of the effective input field on the evolution of the superradiant state is only significant for a short time after the system is pumped into excitation, and since the output field more than doubles in a time T_R after excitation [Eq. (47)], the input field can be ignored after a time T_R . Therefore, to a good approximation,

$$\theta_0 \approx \mu \mathcal{E}_{\text{eff}} T_R / \hbar \quad (37)$$

an be chosen to be the area of the effective input

pulse. Combining Eqs. (3), (4), and (36) with this expression yields⁵⁹

$$\theta_0^2 = \frac{N_2^{-1}}{\sqrt{2\pi}} (\alpha_0 L)^{-1/2} \left(\frac{n_2}{n_2 - n_1} + \frac{1}{e^{\hbar\omega_0/kT} - 1} \right). \quad (38)$$

For our system, $\theta_0 \sim 10^{-8}$, and in order for the output to evolve to a pulse of area $\sim \pi$, $\alpha_0 L$ [Eq. (19)] must be < 20 . This is readily achieved in the experiments.

V. NUMERICAL RESULTS

The coupled Maxwell-Schrödinger equations [Eqs. (11)] have been integrated by computer, with level degeneracy taken into account in pump and superradiant transitions. Computer-generated curves obtained using input conditions appropriate for the HF case^{14,15} are in good agreement with experimental results. For example, decreasing the sample cell pressure or pump intensity reduces the output intensity and increases the delay time and the width of the output pulse. A detailed comparison of theory and experiment can be found in Ref. 15.

The following general features are evident from the numerical results, and confirm the qualitative statements of Secs. III and IV:

(i) The effects of relaxation are unimportant as long as the homogeneous relaxation time T_2 exceeds the pulse delay T_D . When T_2 becomes comparable to T_D the pulses are reduced in size and the ringing is cut down. At the mTorr pressures of the experiments T_2 , determined by collisions, is always much longer than T_D .

(ii) The influence of the polarization source Λ , is limited to the first few T_R 's. In addition, the output is unchanged when the polarization source [Eq. (33)] is replaced by an input field whose amplitude is given by Eq. (36). This verifies the effective input-field approximation presented in Sec. IVD and the value of \mathcal{E}_{eff} given by Eq. (36).

(iii) The effect of a weak input field (to simulate blackbody radiation) is limited to the first few T_R 's. The output is insensitive to the exact shape and phase of the input field. Delta function, step function, Gaussian pulses, and pulse trains of varying phase all give output pulses of about the same shape and size, as long as their input areas are equal. Also, the presence of random jumps in the phase of the input field has no significant effect on the output pulses.

(iv) The area of the output pulse is determined by the gain $\alpha_0 L$ and the size of the input pulse θ_0 , in accordance with the area theorem [Eq. (19)]. Since in our case $\theta_0 \sim 10^{-8}$, $\alpha_0 L < 20$ is needed for appreciable pulse buildup. Such gains are available in HF at mTorr pressure.

(v) The time scale of the pulse evolution process (i.e., delays, pulse shapes) is almost completely determined by T_R and θ_0 , as long as $\alpha_0 L \gg 1$.

(vi) The output pulses are insensitive to the specific time dependence of the population excitation. This is true for excitation pulses of duration approaching the superradiant pulse delay. (Effects of longer excitation pulses are discussed in Ref. 26.)

(vii) Two forms of the loss coefficient κ [Eq. (11a)] might be important under different experimental conditions: the case of linear (constant) κ , as was used in Ref. 24 and our previous work¹¹; and the case of diffraction loss, where the plane-wave δ field can be modeled as a Gaussian beam, in which case $\kappa = x/(x^2 + L_0^2)$, with $L_0 = A/\lambda$.⁶¹ For the same value of the total loss (κL in the linear-loss case; $\int \kappa dx = \frac{1}{2} \ln[1 + (\lambda L/A)^2]$ in the Gaussian-beam case), the two models give virtually identical output pulses.

(viii) Replacing each of the different matrix elements $(\mu_x)_q$ in a degenerate system by the average value μ_x defined by Eq. (7) does not significantly affect the behavior of the output pulse; i.e., the effects of level degeneracy are negligible.

(ix) The output intensity at a given superradiant transition depends on the pump transition branch used (P or R), in agreement with the experiments. This dependence is due to the different matrix elements and widely different populations of the ground-state levels selected.

In summary, as long as $\alpha_0 L \gg 1$, for a given T_R homogeneous and inhomogeneous broadening, level degeneracy, and moderate variations in the value of κL change the results in only minor ways. The weak influence of these effects on the output pulse can be seen in Fig. 5, which shows the changes in the pulse shape and delay caused by varying these parameters. The simple results obtainable by setting $1/T_2 = 1/T_2^* = \kappa = 0$ and neglecting level degeneracy may be used for a qualitative understanding of the behavior.⁶⁰ This simplified model gives the normalized emission curve of Fig. 4. (Other effects which occur in very long samples, but which are not relevant to the HF experiments, are discussed in Ref. 26.)

VI. SIMPLIFIED THEORY

As indicated by the computer analysis of Sec. V, most of the parameters of the system have very little effect on the superradiant output pulses (Fig. 5). If we set $\gamma = \kappa = \Lambda = \Lambda_p = \kappa = 0$ in Eqs. (11) and ignore the effects of level degeneracy, a set of simplified equations is obtained:

$$\frac{\partial \delta}{\partial x} = -2\pi k S, \quad (39)$$

$$\frac{\partial S}{\partial T} = -\frac{\mu_x^2 n \delta}{h}, \quad (40)$$

$$\frac{\partial n}{\partial T} = \frac{\delta S}{h}. \quad (41)$$

Here, $S = -\delta^*$ and n , S , and S are all real. Note that in this simplified model, in which $\Lambda_p = 0$, the effect of spontaneous emission (which initiates the superradiant evolution process in an initially inverted system) can be included by means of the effective-input-field approximation. In the discussions of this section, an effective input pulse [as given by Eq. (36)] will be used as an initial condition.

Equations (40) and (41) have the solution

$$n = n_0 \cos \psi, \quad (42)$$

$$S = -\mu_x n_0 \sin \psi, \quad (43)$$

$$\frac{\partial \psi}{\partial T} = \frac{\mu_x \delta}{h}. \quad (44)$$

where

$$\psi(x, T) = \int_{-\infty}^T (\mu_x/h) \delta(x, T') dT' \quad (45)$$

is the "partial area" of the pulse, so that $\psi(x, T = \infty) = \theta(x)$. From Eqs. (42) and (43), it can be seen that ψ may also be interpreted in the geometrical representation⁶² as the "tipping angle" of a Bloch vector³⁹ of length n_0 which evolves in the z - y [$n - (S/\mu_x)$] plane. Note [Sec. III] that an extended medium must be represented as a distribution of Bloch vectors whose spatial variations are determined by Eq. (39). The initially inverted system, corresponding to the Bloch vectors all standing on end ($n = n_0, S = 0$), gradually evolves into a superradiant state ($n = 0, S/\mu_x = -n_0$); the evolution of the individual Bloch vector at any point in space is described by Eqs. (42) and (43).

Combining Eqs. (39) and (44) gives an equation for $\psi(x, T)$ ^{22,63}:

$$\frac{\partial^2 \psi}{\partial x \partial (T/T_R)} = \frac{\sin \psi}{L}. \quad (46)$$

This equation was studied for the case of an absorber by Burnham and Chiao⁶³ and others,^{13,45} who showed that for a δ -function input field, the time dependence of $\psi(x, T)$ and therefore [Eq. (44)] of $T_R \delta(x, T)$ was a function of T/T_R only. Our case is that of an amplifier, and the time dependence of the δ -function response is again a function of T/T_R only, from which follows the scaling property of the normalized emission curve of Fig. 4.⁶³ Furthermore, since the effective input field is only important during the first T_R , any input pulse of small effective area θ_0 gives the same response as a δ -function input pulse of the same area. [A more

formal statement of the scaling properties of Fig. 4 is that the transformation $T \rightarrow T/T_R$, $\mathcal{S} \rightarrow T_R \mathcal{S}$ in Eqs. (39)–(41) leaves these equations unchanged and does not affect the area of the input pulse (the boundary condition).] This simple scaling property holds for "end-excited" systems in which the system is excited by a pulse propagating through the medium at velocity c , so that all molecules are excited at the same *retarded* time. It also holds for "side-excited" systems (in which all molecules are excited simultaneously) unless the transit time $L/c \approx 2(T_R/4)[\ln(\theta_0/2\pi)]^2$.²⁶ In the latter case, spontaneous emission in different parts of the medium causes the sample to break into a number of independently superradiating segments as described by Arecchi and Courtens¹³ (see Ref. 26 for further discussion).

The computer results also exhibit these scaling properties, even when all of the refinements of the theory are included (Fig. 5). The main requirement for the validity of the normalized emission curve is that T_R be much shorter than all other times associated with the system ($T_R \ll T_2$), so that superradiant emission can occur before dephasing or relaxation processes set in. It immediately follows from Eq. (22) that this condition is equivalent to $\alpha_0 L \gg 1$, so that any sufficiently high-gain system will undergo superradiant emission when suitably excited.

As a consequence of the long delay times which result from small effective input pulses, ψ remains small for almost all of the pulse evolution time. Accordingly, in the expression for $\mathcal{S}(x, T)$ the small-angle approximation ($\sin \psi \approx \psi$) can be used. (In the final stages of pulse evolution, ψ approaches π and this approximation breaks down.) Also, since the exact form of the effective input field does not matter (Sec. V), a step function can be chosen. A number of useful results can be derived from this model.

Consider first the delay T_D from the time at which the sample is inverted to the time of the first peak of the emitted radiation.⁶⁴ In the small-angle limit a solution of Eq. (46) can be found using the transformation $w = 2(xT)^{1/2}$, which gives Bessel's equation in w . For the initial condition of a small step-function input electric field with envelope $\mathcal{S}(x=0, T>0) = \mathcal{S}_0$, which corresponds to $\mathcal{S}(w=0) = \mathcal{S}_0$, the output field at $x=L$ is of the form

$$\mathcal{S}(L, T) = \mathcal{S}_0 I_n(u), \quad (47)$$

where $I_n(u)$ is the modified Bessel function of order n , and $u = 2(T/T_R)^{1/2}$. Then $\Phi(T) = \psi(x=L, T)$, the partial area at $x=L$, is given by

$$\Phi(T) = \int_0^T (\mu_s/\hbar) \mathcal{S}(L, T') dT' = \theta_0 u I_1(u), \quad (48)$$

where $\theta_0 = \mu_s \mathcal{S}_0 T_R/\hbar$. A property of solutions of Eq. (46) is that for $\theta_0 \ll 1$, $\Phi(T_D) \approx \pi$.⁶⁵ Setting $\Phi(T_D = \pi)$ in Eq. (48) and solving for T_D in the limit $T_D \gg T_R$, one obtains⁶⁶

$$T_D \approx (T_R/4)[\ln(\theta_0/2\pi)]^2. \quad (49)$$

Note that Eq. (49) was derived under the condition of small θ_0 . However, since Φ only deviates from Eq. (48) during the last few T_R before $T = T_D$, only a small error in calculating T_D is made by using Eq. (48) to approximate $\Phi(T_D)$.

In the experimental system, $\theta_0 \sim 10^{-6}$, so $|\ln(\theta_0/2\pi)| \sim 20$ and T_D is insensitive to changes in θ_0 . Therefore $T_D \sim 100 T_R$ is a convenient estimate of the time required for the superradiant state to evolve. Since T_D is proportional to T_R , T_D should be inversely proportional to the excitation density, and therefore, the pressure, in the sample cell. This inverse proportionality and the estimate of T_D , Eq. (49), agree with experimental results.¹⁵

An estimate of the width T_w of the first lobe of the radiation pulse can be obtained from the $1/e$ width of $\Phi(T)$ at $T = T_D$, i.e., by solving the equation $\Phi(T_D - T_w/2) = \Phi(T_D)/e$ for T_w :

$$T_w \sim T_R |\ln(\theta_0/2\pi)|, \quad (50)$$

since $T_w \ll T_D$. Equation (50) predicts a pulse width $\sim 20 T_R$ for our system, which is somewhat smaller than the observed pulse widths of $\sim (20-40) T_R$.¹⁵ This is expected, since the growth of $\Phi(T)$ near T_D is actually slower than that given by Eq. (48).

It was explained above that because the sample is optically thick (i.e., $\alpha_0 L \gg 1$) the polarization envelope $\mathcal{P}(z, T)$ varies over the medium and undergoes changes in sign [Fig. 3(a)]. Since $\mathcal{S} = 2\pi k \int \mathcal{P} dx$, regions of \mathcal{P} of opposite sign tend to cancel and the output radiation at a particular time can be considered to originate from a single spatial region, of width L'_{eff} . Accordingly, L'_{eff} and T_w , the duration of one lobe of the superradiant output, are related; T_w is the "effective" T_R of a sample of length L'_{eff} , $T_w = T_R(L = L'_{\text{eff}}) = 8\pi T_R/\hbar \lambda^2 L'_{\text{eff}}$, from which $L'_{\text{eff}} \approx L/|\ln(\theta_0/2\pi)|$. Comparison with computer plots of $\mathcal{P}(x, T)$ [Fig. 3(a)] shows that L'_{eff} is approximately the half-width at half-maximum of a spatial region. The total extent of a region of polarization (between points of $\mathcal{P} = 0$) is several times larger. We define

$$L_{\text{eff}} = 4L'_{\text{eff}} \approx \frac{4L}{|\ln(\theta_0/2\pi)|} = \frac{4T_R L}{T_w}. \quad (51)$$

Although both L_{eff} and L'_{eff} have the correct functional dependence, the choice of L_{eff} leads to much better agreement between Eq. (54), below, and

computer results.

Equation (51) indicates that a fraction $-4/|\ln(\theta_0/2\pi)|$ of the medium contributes to each lobe of ringing in the superradiant bursts. This suggests that the normalized emission curve should contain $-|\ln(\theta_0/2\pi)|/4$ lobes. This is confirmed by computer results, which give this number of lobes (up to the $1/e$ point) for various values of θ_0 . Systems with finite T_2 will have fewer lobes.

The total energy of the first lobe E_p is

$$E_p = h\omega_0 nAL_{\text{eff}} = \frac{4h\omega_0 nAL}{|\ln(\theta_0/2\pi)|}, \quad (52)$$

and the total peak radiation intensity I_p is approximately the total energy of the first lobe E_p divided by the width of the first lobe T_p ,

$$I_p = \frac{E_p}{T_p} = \frac{h\omega_0 nAL_{\text{eff}}}{T_p} = \frac{4Nh\omega_0/T_R}{|\ln(\theta_0/2\pi)|^2} = \frac{4}{|\ln(\theta_0/2\pi)|^2} \frac{h\omega_0 An^2 \lambda^2 L^2}{8\pi T_R}, \quad (54)$$

and is proportional to L^2 (Fig. 4). As anticipated in the qualitative discussion of Sec. III, the peak radiation rate is enhanced from $Nh\omega_0/T_R$ by a factor proportional to T_p/T_R . Note that in terms of the peak value of the electric field, \mathcal{E}_p , Eq. (54) gives

$$(\mu\mathcal{E}_p/h)(T_p/4) = 1, \quad (55)$$

which shows that the ringing of the superradiant output can be viewed as a form of Rabi nutation.⁶⁷

The formulas for I_p [Eq. (54)], T_p [Eq. (49)], and T_w [Eq. (50)] agree well with experimental data,¹⁵ computer predictions, and the normalized emission curve (Fig. 4). For extremely long samples (in the HF case, ≈ 10 m), the considerations of Ref. 26 must be taken into account.

VII. CONNECTIONS WITH OTHER WORK

Some previous treatments^{11,12,17} of superradiance are based on equations of motion written in terms of the variables $I(t)$ and $n(t)$, the time-dependent intensity and inversion density. To compare the present work with these treatments, consider the approximation in which Eqs. (11) can be rewritten in these two variables, rather than the five real quantities \mathcal{E} , \mathcal{E}' , and n .

An equation for dI/dx can be obtained by multiplying Eq. (11a) by $(cA\mathcal{E}^*/8\pi)$:

$$\frac{\partial I}{\partial x} = -2\kappa I + (\omega_0 A/2) \text{Re}[\mathcal{E}^* \langle \mathcal{E}' \rangle_v], \quad (56)$$

which is a statement of energy balance. An expression for $\partial n/\partial t$ can be obtained by integrating Eq. (11c) over velocity:

$$\begin{aligned} \frac{\partial}{\partial t} \langle n \rangle_v &= -\frac{1}{T_2} \langle (n - T_2 \Lambda) \rangle_v = -\frac{1}{\hbar} \text{Re}[\mathcal{S} \langle \mathcal{E}' \rangle_v] \\ &= -\frac{2}{\hbar \omega_0 A} \left(\frac{\partial I}{\partial x} + 2\kappa I \right), \end{aligned} \quad (57)$$

using Eq. (56). An expression for the total population difference $N = \int n A dx$ is then readily obtained⁶⁸:

$$\begin{aligned} \frac{d}{dt} \langle N \rangle_v &= -\frac{1}{T_2} \langle (N - T_2 \Lambda AL) \rangle_v \\ &= -\frac{2}{\hbar \omega_0} \left(I(L) - I(0) + 2 \int_0^L \kappa I dx \right), \end{aligned} \quad (58)$$

which has an obvious interpretation in terms of number conservation.

Equations (56) and (59) are exact. To simplify Eq. (56), we set $\kappa = 0$, neglect Doppler broadening and level degeneracy, and assume that \mathcal{S} and \mathcal{E}' have a constant phase.^{69,70} Differentiating Eq. (56) with respect to T then gives

$$\begin{aligned} \frac{2}{\omega_0 A} \frac{\partial^2 I}{\partial x \partial T} &= \frac{\partial \mathcal{S}}{\partial T} \mathcal{E}'^* + \mathcal{S} \frac{\partial \mathcal{E}'^*}{\partial T} \\ &= \frac{1}{2I} \frac{\partial I}{\partial T} \mathcal{S} \mathcal{E}'^* - \frac{\mathcal{S} \mathcal{E}'^*}{T_2} + \frac{\mu^2}{\hbar} n |\mathcal{S}|^2 - \mathcal{S} \Lambda_p, \end{aligned} \quad (60)$$

using Eq. (11b). Then, using Eq. (56),

$$\frac{\partial^2 I}{\partial x \partial T} = \frac{1}{2I} \frac{\partial I}{\partial T} \frac{\partial I}{\partial x} - \frac{1}{T_2} \left(\frac{\partial I}{\partial x} - \frac{2nIT_2}{n_0 L T_R} - 2\alpha_0 K_0 \right), \quad (62)$$

The last term in Eq. (62) is obtained by replacing the source term $\mathcal{S} \Lambda_p$ of Eq. (61) by $4\alpha_0 K_0/\omega_0 A T_2$, where the form of K_0 depends on the gain of the system [Eq. (31) or Ref. 61]. This substitution is consistent with the averaging procedure used in Sec. IV in deriving the polarization source. Note that in the equilibrium limit, where $\partial I/\partial t = 0$, Eq. (62) reduces to the usual expression for intensity gain [Eq. (A13)],

$$\frac{dI}{dx} = 2 \left(\frac{nT_2}{n_0 L T_R} \right) I + 2\alpha_0 K_0, \quad (63)$$

the term in parentheses being α_0 .

Equation (62) is exact, subject to the stated assumptions. A system which satisfies these conditions can be described by two real equations, Eqs. (58) [or (59)] and (62), in two unknowns (n and I), rather than by Eqs. (11). Note that the influence of spontaneous emission is included in these equations. In general, they must be solved subject to appropriate initial conditions on I and

n . For simplicity, in the following discussions we will assume that the input field is negligible.

Equations (59) and (62) are a useful starting point to connect the present analysis with some previous treatments^{11,12,17} which developed equations appropriate to a regime which we would like to call "limited superradiance." This regime is characterized by the conditions

$$T_R \ll T_{sp}, \quad (64a)$$

but

$$\alpha_0 L \ll 1, \quad (64b)$$

i.e.,

$$T_2' \ll T_R \ll T_{sp}. \quad (64c)$$

In this limit, spatial variations in ϕ and n are negligible throughout the sample,¹¹ and Eq. (62) can be integrated to obtain

$$\frac{dI}{dt} = -\frac{2I}{T_2} + \frac{4IN}{3T_R N_0} + \frac{\hbar\omega_0}{\pi T_2 T_R}, \quad (65a)$$

where, henceforth, $I = I(L, t)$. Similarly, Eq. (59) becomes

$$\frac{dN}{dt} = -\frac{1}{T_2}(N - T_2 \Lambda AL) - \frac{2I}{\hbar\omega_0}. \quad (65b)$$

As will be seen below, solutions of these equations are very different from those obtained in the high-gain case and from the experimental results (different delay times, no ringing, etc.).

Equations (65) are almost identical to the superradiant rate equations of Bonifacio, Schwendemann, and Haake,¹² which in our notation become

$$\frac{dI}{dt} = -\frac{2I}{T_2} + \frac{4IN}{T_R N_0} - \frac{4I}{T_R N_0}, \quad (66a)$$

$$\frac{dN}{dt} = -\frac{1}{T_1}(N - T_1 \Lambda AL) - \frac{2I}{\hbar\omega_0}. \quad (66b)$$

(They did not assume $T_1 = T_2$.)

Equations (4.10) and (4.11) of Rehler and Eberly¹¹ can be differentiated to obtain equations similar to ours (they assume $T_1^{-1} = 0$):

$$\frac{dI}{dt} = -\frac{2I}{T_2} + \frac{4IN}{T_R N_0}, \quad (67a)$$

$$\frac{dN}{dt} = -\frac{2I}{\hbar\omega_0}. \quad (67b)$$

Similar equations obtained by Ressayre and Tallet¹⁷ include finite Doppler broadening:

$$\frac{dI}{dt} = -\left(\frac{1}{T_2} + \frac{1}{T_2'}\right)I - \frac{IN}{T_R N_0} \exp\left(-\frac{t}{T_2}\right), \quad (68a)$$

$$\frac{dN}{dt} = -\frac{N - T_2 \Lambda AL}{T_2} - \frac{2I}{\hbar\omega_0}. \quad (68b)$$

In the limit of $T_2' \rightarrow \infty$, these equations are of the same form as the others.¹²

These three sets of equations [(66), (67), and (68)] essentially agree with Eqs. (65), which are derived in the thin-sample limit and do not apply to $\alpha_0 L \gg 1$.

In Refs. 11, 12, and 17, these equations are solved in the limit where $2I/T_2$ is negligible compared to $4IN/3T_R N_0$. The solutions for I are then hyperbolic-secant-squared functions of time. However, the ratio of the first term to the second term in Eq. (65a) is

$$\frac{2I/T_2}{4IN/3T_R N_0} = \frac{3}{2\alpha_0 L} \frac{N_0}{N}. \quad (69)$$

In the thin-sample limit, in which Eqs. (65) are valid, $\alpha_0 L = T_2/T_R \ll 1$, and since $|N| \leq N_0$ always, the magnitude of this ratio will always be much greater than 1. As a result, the $2I/T_2$ term may not be neglected, but the term $4IN/3T_R N_0$ is negligible and may be ignored. Therefore, the hyperbolic-secant-squared intensity solutions of Refs. 11, 12, and 17 are incorrect.

The approximate solution of Eqs. (65) may be obtained by neglecting the second term of Eq. (65a):

$$I(L, t) = I(L, t=0) e^{-2t/T_2} + (\hbar\omega_0/4\pi T_R) (1 - e^{-2t/T_2}), \quad (70a)$$

$$N = \frac{2I(L, t=0)}{\hbar\omega_0} (e^{-2t/T_2} - e^{-t/T_2}) + N(t=0) e^{-t/T_2} + T_2 \Lambda AL (1 - e^{-t/T_2}), \quad (70b)$$

where $N(t=0)$ is the initial population inversion and $I(L, t=0)$ is the initial output intensity,¹³ produced by the population existing at $t=0$ in a medium having initial conditions $n(t=0) = n_0 \cos \phi$ and $\phi(t=0) = \mu_B n_0 \sin \phi$ (corresponding to an initial tipping angle ϕ of the Bloch vector):

$$I(L, t=0) = (cA/8\pi) (2\pi k L \mu_B n_0 \sin \phi)^2 = (N \hbar\omega_0/4T_R) \sin^2 \phi. \quad (71)$$

The second term in Eq. (70a), which is due to the source term of Eq. (65a), is only important when $I(L, t=0)$ is negligible ($\propto \hbar\omega_0/4\pi T_R$). In this case incoherent processes initiate the evolution of the system, and Eq. (70a) becomes

$$I = \frac{\hbar\omega_0}{4\pi T_R} (1 - e^{-2t/T_2}) = \frac{N_0 \hbar\omega_0}{T_{sp}} \frac{\lambda^2}{32\pi^2 A} (1 - e^{-2t/T_2}). \quad (72)$$

Here $I(t)$ is proportional to n_0 and decays exponentially in the usual fashion.

The first term in Eq. (70a) is the free-induction decay of $I(L, t=0)$. For $I(L, t=0) \gg \hbar\omega_0/4\pi T_R$, the

second term in Eq. (70a) is negligible, and $I(t)$ is proportional to n_0^2 (coherent emission). This solution is a decaying exponential with decay time $T_2/2 = \alpha_0 L T_R/2 \ll T_R$, rather than the hyperbolic-secant-squared solution of width $\sim T_R$ of Refs. 11 and 12. Therefore, collective radiation occurs for a time much shorter than T_R , after which the excited-state population will have decayed. Integrating $I(t) = (N\hbar\omega_0/4T_R)e^{-2t/T_2}\sin^2\phi$ over time, the total energy radiated coherently is at most $(N\hbar\omega_0/8)(T_2/T_R)$, so that only a small fraction $T_2/8T_R = \alpha_0 L/8 \ll 1$ of the energy is radiated coherently. The decay of the system is determined by ordinary incoherent processes.

Experimental techniques such as free-induction decay and photon echos,¹ which study the collective radiative decay of a system in the limited superradiance regime, are useful for measuring incoherent relaxation processes. In fact, these experiments must be performed in the thin sample ($\alpha_0 L \ll 1$) so that coherent emission does not affect the decay rate. In the regime of limited superradiance, the coherent emission acts as a probe of the state of the system, without significantly affecting its state.

Although limited superradiance can be considered superradiance in the sense that $T_R \ll T_D$, so that collective effects are important [as is seen in the n_0^2 dependence of Eq. (71)], only a very small fraction of the energy is radiated coherently since $T_2 \ll T_R$. This is in sharp contrast to the regime of strong superradiance studied in the HF experiments, which is characterized by the conditions

$$T_R \ll T_D \quad (73a)$$

and

$$\alpha_0 L \gg 1, \quad (73b)$$

i.e.,

$$T_2' \gg T_R. \quad (73c)$$

The latter condition implies that the sample can superradiate before decay processes set in. Accordingly, in the strong superradiant regime essentially all of the energy stored in the sample can be emitted coherently. [The condition of Eq. (73b) for strong superradiance can be made more precise in some cases.⁷⁴]

The long delays preceding the observed output pulses deserve further discussion, in light of the fact that the conditions for strong superradiance [Eqs. (7)] only require $T_2' \gg T_R$, not $T_2' > T_D$. (However, $T_2 > T_D$ is necessary.) For example, typically $T_D \sim 100T_R$, whereas $T_2' \sim 50T_R$, so that $T_D > 2T_2'$. It is remarkable that fully developed pulses with ringing can evolve over such long times, despite the presence of dephasing processes. This be-

havior is unique to high-gain amplifiers, where the high gain can overcome dephasing during the early stages of pulse evolution. The system eventually dephases, but the effective dephasing time is increased to $\alpha_0 L T_2'$, as can be established by considering the response of a high-gain inhomogeneously broadened amplifying medium to a short input pulse of small area θ_0 . (A small step-function input pulse gives similar results.) Analytical expressions have been given by Crisp.⁷⁵ For a Lorentzian line shape the output \mathcal{S} field is of the form

$$\mathcal{S}(x \approx L, T) \approx \frac{\mathcal{S}_0}{2\sqrt{\pi}} \left(\frac{T}{T_R} \right)^{-3/4} \times \exp \left[2 \left(\frac{T}{T_R} \right)^{1/2} - \frac{T}{T_R \alpha_0 L} \right], \quad (74)$$

for an input pulse of small area $\theta_0 = \mu \mathcal{S}_0 T_R / \hbar$. Initially the square-root term in the exponential dominates and \mathcal{S} increases. Its maximum value is reached at $T \approx T_2' \alpha_0 L$, after which exponential decay due to dephasing sets in. Therefore, the effective dephasing time is

$$(T_2')_{\text{eff}} \approx T_2' \alpha_0 L. \quad (75)$$

When this expression is compared with Eq. (49) for the delay time, one finds that

$$\frac{T_D}{(T_2')_{\text{eff}}} \approx \left(\frac{\ln(\theta_0/2\pi)}{2\alpha_0 L} \right)^2, \quad (76)$$

which is always smaller than unity for a high-gain system (where $\alpha_0 L \gg 1$). Therefore, an inhomogeneously broadened system of sufficiently high gain will always superradiate before it can dephase.⁷⁶

In a recent series of papers, Bonifacio and Banfi¹⁸ and Bonifacio and Lugiatto^{19,20} have developed equations in terms of \mathcal{S} , \mathcal{S}' , and n (rather than I and N) for the cooperative radiation from an initially inverted two-level system, which they call superfluorescence. In our notation, the semi-classical equations which they obtain⁷⁷ can be written in the form

$$\begin{aligned} & \left[\frac{1}{c} \left(\frac{\partial}{\partial t} \right)_x + \left(\frac{\partial}{\partial x} \right)_t + \frac{1}{2L} \right] \mathcal{S}(x, t) \\ &= \left[\left(\frac{\partial}{\partial x} \right)_x + \frac{1}{2L} \right] \mathcal{S}(x, T) \\ &= \frac{2\pi\omega_0}{c} \mathcal{P}(x, T) \exp \left(-\frac{t}{2T_2'} \right), \end{aligned} \quad (77a)$$

$$\frac{\partial}{\partial T} \mathcal{P}(x, T) = \frac{\mu^2}{\hbar} n \mathcal{S} \exp \left(-\frac{t}{2T_2'} \right), \quad (77b)$$

$$\frac{\partial}{\partial T} n(x, T) = -\frac{1}{h} \text{Re}(\delta \cdot \phi) \exp\left(-\frac{t}{2T_2}\right), \quad (77c)$$

where $T = t - x/c$. Although these equations are similar to Eqs. (11) above, they contain two major differences: (i) The term $(1/2L)$ in Eq. (77a) has been included to account for "the irreversible escape (propagation) of the total Maxwell field from the active volume to the outside."¹⁹ However, wave propagation is built into Maxwell's equations (the $\partial/\partial x$ terms) so that the $1/2L$ term appears to be incorrect and was added unnecessarily. (ii) To account for inhomogeneous broadening, in Eqs. (77) the factor $\exp(-t/2T_2)$ is included. This factor arises from the assumption¹⁹ that there is no correlation between frequency and position during the evolution of the superradiant pulse, an assumption which we believe is incorrect. Henceforth, we restrict ourselves to the case $T_2 = \infty$, in which case Eq. (77) agrees with Eq. (59).

In Ref. 19, Eqs. (77) are solved by neglecting the $(\partial/\partial x)_t$ term. This incorrect approximation is justified¹⁹ by the argument that in the case of "uniform excitation" (side pumping), Eqs. (77) are spatially invariant for all time. However, since the inverted medium is finite in length, this is not the case—the initial condition is spatially constant only over a finite region of space. Therefore, after a time of order L/c spatial variations will have developed throughout the sample. Computer solutions also substantiate this point.

In summary, we doubt that any optically thick ($\alpha_0 L \gg 1$) superradiant system can accurately be described by any set of differential equations which ignores spatial variations. We also doubt that the pendulum equation of Ref. 19 [Eq. (11.12)] applies to strong superradiance.^{77a}

Another recent paper by Bonifacio, Hopf, Mevstretre, and Scully⁷⁹ deals with the evolution of steady-state pulses. This work is an extension of and in the same spirit as discussions of this subject in Refs. 22 and 24. This work with steady-state pulses is applicable to a system in which the loss coefficient κ is sufficiently high so as to suppress ringing [the decrease in ringing for large κ can be seen in the $\kappa L = 5$ curve in Fig. 5].

VIII. CONCLUSION

This paper has developed a semiclassical description of the evolution of an initially inverted system into a superradiant state, and shown that the inclusion of a properly constructed fluctuating polarization source in the coupled Maxwell-Schrödinger equations gives rise to output pulses which quantitatively agree with experimental results and have all the features expected of a superradiant system. The success of this model makes

clear the simple nature of the superradiant process and places it in perspective with other coherent phenomena.

As shown in this paper, in the optical region spontaneous emission initiates the pulse evolution process and greatly influences the time delay and other experimentally observable features of the output radiation. The quantitative agreement of the semiclassical treatments with experiment is largely due to the fact that in a high-gain system the effects of spontaneous emission can be combined into a single parameter θ_0 which enters the equations logarithmically, so that the exact details of the spontaneous-emission process become unimportant. Nevertheless, the need still exists for a quantized-field treatment to substantiate the semiclassical results and to explore quantum-mechanical features of superradiance such as fluctuations. Since it is now generally recognized that a semiclassical description is adequate once the pulse evolution process is under way, the quantized-field-theory treatment can be restricted to the small-signal regime, where important simplifications occur. Several recent papers⁷⁹ have made useful advances along these lines. It is our hope that the present work will stimulate further research in this direction.

ACKNOWLEDGMENTS

At numerous times during the course of this work we have benefited from discussions and constructive comments from many colleagues, including Rodolpho Bonifacio, Robin Bullough, Barry Feldman, Dick Friedberg, Sven Hartmann, Irving Herman, Ping-Tong Ho, Ali Javan, Sylvan Liberman, Dick Picard, Nick Skribanowitz, Woodie Strandberg, and Chuck Willis. We particularly thank Norman Kurnit for many helpful remarks and for his enthusiasm.

APPENDIX A: DERIVATION OF INTENSITY GAIN EQUATION FROM COUPLED MAXWELL-SCHRÖDINGER EQUATIONS FOR A SYSTEM NEAR THERMAL EQUILIBRIUM

We consider a linear steady-state system. Schrödinger's equation [Eq. (11b)] can be rewritten in the form

$$\left(\frac{\partial}{\partial T}\right) [\phi e^{T(\gamma - i\Gamma)}] = \left(\frac{\mu_z^2}{h}\right) n \delta e^{T(\gamma - i\Gamma)} + \Lambda_p e^{T(\gamma - i\Gamma)}, \quad (A1)$$

where $\Gamma = kv$ and Λ_p , which includes level degeneracy and velocity dependence, is given by Eq. (24),

$$\Lambda_p(x, T, v, M) = B_1 [n_2(x, T, v, M)]^{1/2} \times \sum_{j=1}^{j'} \delta(x - x_j) \sum_{l=-\infty}^{\infty} \delta(T - T_l) \times \sum_{k=1}^{k'} \delta(v - v_k) e^{i\phi_{jlkM}}, \quad (A2)$$

where $x_j = (j - \frac{1}{2})\Delta x$, $\Delta x = L/j'$, $T_l = l\Delta T$, and the v_k are k' discrete velocities. Then integrating Eq. (A1) over T from $-\infty$ to T gives

$$\phi(T) e^{T(T-i\Gamma)} = \frac{\mu_s^2}{\hbar} \int_{-\infty}^T n \delta e^{T'(T-i\Gamma)} dT' + B_1 \sum_j \sum_l \sum_k e^{i\phi_{jlkM}} \delta(x - x_j) \delta(v - v_k) \times \int_{-\infty}^T \delta(T' - T_l) (n_2)^{1/2} \times e^{(T'/T_2 - i\Gamma T')} dT'. \quad (A3)$$

In the case where n and δ are very slowly varying in time and n is approximately constant, we can replace the populations $n(x, T, v, M)$ by their equilibrium values n_0 , and Eq. (A3) becomes

$$\phi(T) = \frac{\mu_s^2}{\hbar} \frac{n_0 \delta}{1/T_2 - i\Gamma} + B_1 (n_2)^{1/2} \sum_j \sum_l \sum_k e^{i\phi_{jlkM}} u(T - T_l) \delta(x - x_j) \times \delta(v - v_k) e^{-(T - T_l)/T_2}, \quad (A4)$$

where $u(t)$ is the unit step function, and n_2 is the equilibrium value of n_2 .

Substituting this result into Maxwell's equation

$$\delta(L, T) = \delta(0, T) e^{\alpha_0 L} + \sum_j \sum_l \sum_k B_2 \sum_{j'=1}^{j'} e^{\alpha_0(j-1/2)\Delta x} u(T - T_l) e^{-(T - T_l)/T_2} e^{i\phi_{jlkM}} \quad (A9)$$

and

$$I(L, T) = |\delta(L, T)|^2 \frac{cA}{8\pi} = |\delta(0, T)|^2 e^{2\alpha_0 L} \frac{cA}{8\pi} + \frac{cA}{8\pi} \sum_j \sum_l \sum_k \sum_{j'} |B_2|^2 e^{(2j-1)\alpha_0 \Delta x} u(T - T_l) e^{-2(T - T_l)/T_2} + (\text{terms containing random phases}). \quad (A10)$$

For $\alpha_0 \Delta x \leq 1$ and $\Delta T/T_2 \leq 1$, no single terms dominate the sum of random-phase terms, and the sum of these terms (which individually average to zero) will be negligible compared to the other two terms

[Eq. (11a)] in the case of no linear loss (which is the case of interest), we obtain

$$\frac{\partial \delta}{\partial x} = \left[\frac{2\pi k \mu_s^2}{\hbar} \left\langle \frac{n_0}{1/T_2 - i\Gamma} \right\rangle_{v, M} \right] \delta = 2\pi k \sum_j \sum_l e^{-(T - T_l)/T_2} u(T - T_l) \delta(x - x_j) \times \left\langle B_1 [n_2(x, T, v, M)]^{1/2} \sum_k \delta(v - v_k) e^{i\phi_{jlkM}} \right\rangle_{v, M} \quad (A5) = 2\pi k \sum_j \sum_l \sum_k \sum_{j'=1}^{j'} e^{-(T - T_l)/T_2} u(T - T_l) \delta(x - x_j) \times B_1 [n_2(x, T, v_k, M)]^{1/2} e^{i\phi_{jlkM}}. \quad (A6)$$

Since the imaginary part of the coefficient of δ in Eq. (A5) vanishes when integrated over velocity, and the real part is the gain at line center α_0 , Eq. (A6) becomes

$$e^{\alpha_0 x} \frac{\partial}{\partial x} [\delta e^{-\alpha_0 x}] = \sum_j \sum_l \sum_k \sum_{j'=1}^{j'} e^{-(T - T_l)/T_2} u(T - T_l) \times \delta(x - x_j) B_2 e^{i\phi_{jlkM}}, \quad (A7)$$

where $B_2(v_k, M) = 2\pi k B_1 [n_2(v_k, M)]^{1/2}$. Integrating along a path of constant T from $x = (j - 1)\Delta x$ to $x = j\Delta x$ gives

$$\delta(j\Delta x) = \delta((j - 1)\Delta x) e^{\alpha_0 \Delta x} + \sum_k \sum_l \sum_{j'=1}^{j'} e^{-(T - T_l)/T_2} u(T - T_l) \times B_2 e^{\alpha_0 \Delta x / 2} e^{i\phi_{jlkM}} \quad (A8)$$

for $j = 1, 2, 3, \dots, j'$. Simultaneous solution gives

in Eq. (A10). Then Eq. (A10) can be written as the intensity gain equation of the text [Eq. (25)],

$$I(x, T) = I(0, T) e^{2\alpha_0 x} + K_0 (e^{2\alpha_0 x} - 1), \quad (A11)$$

where

$$K_0 = \frac{\pi}{2} \frac{\omega_0^2}{c} \frac{AT_2}{2\Delta T} (1 - e^{-2\alpha_0 \Delta x})^{-1} B_1^2 \times \sum_k \sum_M n_{20}(v_k, M). \quad (A12)$$

[Note that Eq. (A11) is the solution of the differential equation

$$\frac{dI}{dx} - 2\alpha_0 I + 2\alpha_0 K_0, \quad (A13)$$

which is therefore an equivalent intensity gain equation.] Examination of Eq. (A12) shows that if the effects of level degeneracy and velocity dependence were eliminated by choosing one velocity and by assuming $M = 0$ for all molecules, we would obtain the same result,

$$K_0 = \frac{\pi}{2} \frac{\omega_0^2}{c} \frac{AT_2}{2\Delta T} (1 - e^{-2\alpha_0 \Delta x})^{-1} B_1^2 n_{20}(x, T), \quad (A14)$$

that would be obtained by summing $n_{20}(v_k, M)$ over k and M . [Here $n_{20}(x, T) = \sum_k \sum_M n_{20}(v_k, M)$.]

APPENDIX B. CONVERSION OF INTENSITY PER MODE TO PLANE WAVE INTENSITY PER UNIT BANDWIDTH

The Einstein intensity equation⁴⁶ [Eq. (27)]

$$\frac{dI_\omega(x)}{dx} = 2\alpha(\omega) \left(I_\omega(x) + \frac{\hbar\omega n_2}{n_2 - n_1} \right) \quad (B1)$$

gives the total energy $I(x)$ per mode in the active region of any linear-gain medium. To convert $I_\omega(x)$ into an intensity $I(\omega, x)$ per unit bandwidth in the plane-wave direction, we note that the total power $I(x)$ in the plane-wave direction is

$$I(x) = \int_0^\infty \left(\frac{2\pi\nu^2 d\nu}{c^3} cA \right) \left(\frac{\lambda^2}{4\pi A} \right) I_\omega(x), \quad (B2)$$

where the first factor is the number of modes of one polarization⁴¹ in the active region in a frequency interval $d\nu = d\omega/2\pi$ and the second factor is that fraction f of the sphere over which plane waves contribute coherently. In the plane-wave limit, valid for a system with large Fresnel number (a "disk"), $f = \Delta\Omega/4\pi = \lambda^2/4\pi A$ [Eq. (1)]. If we define $I(\omega, x)$ by $I(x) = \int I(\omega, x) d\omega$, then $I(\omega, x) = (1/4\pi) I_\omega(x)$, and Eq. (B1) becomes [Eq. (28)]

$$\frac{\partial I(\omega, x)}{\partial x} = 2\alpha(\omega) \left(I(\omega, x) + \frac{\hbar\omega}{4\pi} \frac{n_2}{n_2 - n_1} \right). \quad (B3)$$

APPENDIX C. BANDWIDTH NARROWING IN LINEAR HIGH-GAIN SYSTEM (REFS. 31 AND 39)

The intensity gain equation for the plane-wave intensity $I(\omega, x)$ per unit bandwidth is [Eq. (26) or

(B3)]

$$\frac{\partial I(\omega, x)}{\partial x} = 2\alpha(\omega) \left(I(\omega, x) + \frac{\hbar\omega}{4\pi} \frac{n_2}{n_2 - n_1} \right). \quad (C1)$$

Integrating Eq. (C1) over x gives

$$I(\omega, x) = (e^{2\alpha(\omega)x} - 1) I_x(\omega) + I(\omega, x=0), \quad (C2)$$

where

$$I_x(\omega) = I(\omega, x=0) + \frac{\hbar\omega}{4\pi} \frac{n_2}{n_2 - n_1}. \quad (C3)$$

The total power at $x = L$ can then be obtained by integrating over ω :

$$I(x=L) = \int_0^\infty I(\omega, x=0) d\omega + \int_0^\infty d\omega I_x(\omega) (e^{2\alpha(\omega)L} - 1). \quad (C4)$$

For a high-gain system [$\alpha(\omega = \omega_0)L \gg 20$], the exponential factor in Eq. (C4) is very sharply peaked near $\omega = \omega_0$, so that $I_x(\omega)$ can be replaced by $I_x(\omega_0)$ and removed from the integral. Also for a high-gain system, the first integral can be neglected, being much smaller than the second integral. Equation (C4) becomes

$$I(L) \approx I_x(\omega_0) \int_0^\infty d\omega (e^{2\alpha(\omega)L} - 1). \quad (C5)$$

To find $I(L)$, an integral of the form

$$I_1 = \int_0^\infty d\omega [e^{2\alpha_0 L G(\omega)} - 1] \approx \int_{-\infty}^\infty d\omega (e^{2\alpha_0 L G(\omega)} - 1), \quad (C6)$$

where $\alpha_0 = \alpha(\omega = 0)$ and $G(\omega) = \alpha(\omega)/\alpha_0$, must be solved. Expanding the exponential in a power series and interchanging integration and summation gives

$$I_1 = \sum_{J=1}^\infty \frac{(2\alpha_0 L)^J}{J!} \int_{-\infty}^\infty [G(\omega)]^J d\omega. \quad (C7)$$

For $G(\omega)$ that occur in slowly varying physical systems, such as Lorentzians and Gaussians, $[G(\omega)]^J d\omega \approx [G(\omega)]^{J-1} d\omega$ for $J \gg 1$, so that the ratio of term J to term $J-1$ of Eq. (C7) is approximately $2\alpha_0 L/J$. Therefore, for $\alpha_0 L \gg 1$ (high-gain system), the terms which contribute most to the sum will be those for which $J \approx 2\alpha_0 L$. We can therefore approximate the factor $\int [G(\omega)]^J d\omega$ appearing in Eq. (C7) by $\int [G(\omega)]^{2\alpha_0 L} d\omega$ to obtain

$$I_1 \approx \sum_{J=1}^\infty \frac{(2\alpha_0 L)^J}{J!} \int_{-\infty}^\infty [G(\omega)]^{2\alpha_0 L} d\omega = e^{2\alpha_0 L} \int_{-\infty}^\infty [G(\omega)]^{2\alpha_0 L} d\omega. \quad (C8)$$

For our system, the gain profile is Lorentzian

[see discussion above Eq. (15)], with $G(\omega) = (ku_1)^2 / [(\omega - \omega_0)^2 + (ku_1)^2]$.⁸² Then,

$$I_1 = (\pi/2\alpha_0 L)^{1/2} k u_1 e^{2\alpha_0 L}, \quad (C9)$$

and we obtain the result of Eq. (29),

$$I(L) = \left(I(\omega_0, x=0) + \frac{\hbar\omega_0}{4\pi} \frac{n_2}{n_2 - n_1} \right) e^{2\alpha_0 L} (\Delta\omega)_{\text{eff}}^{-1}, \quad (C10)$$

where $(\Delta\omega)_{\text{eff}}^{-1} = T_1^2 (\pi/2\alpha_0 L)^{1/2}$, as in the text.

Examination of the form of $I_1(\omega)$ [Eq. (C3)] or of $I(L)$ [Eq. (C10)] shows that in a high-gain system, a distributed source can be replaced by an "equivalent" intensity source at the input face which will give the same output intensity. In other

words, a high-gain system described by the intensity gain equation

$$\frac{dI(x)}{dx} = 2\alpha_0 I(x) \quad (C11)$$

and an input intensity

$$I(x=0) = \frac{\hbar\omega_0}{4\pi} \left(\frac{n_2}{n_2 - n_1} + \frac{1}{e^{\hbar\omega_0/kT} - 1} \right) (\Delta\omega)_{\text{eff}} \quad (C12)$$

would give the same output intensity $I(L)$ which we derived [Eq. (C10)] using our distributed-source model. In a high-gain system, therefore, the distributed source of Eq. (C1) can be replaced by an equivalent input field.

*Work supported in part by National Science Foundation, Research Corporation, and U. S. Army Research Office (Durham).

†Alfred P. Sloan Fellow.

¹R. H. Dicke, Phys. Rev. **93**, 99 (1954).

²E. L. Hahn, Phys. Rev. **80**, 580 (1950).

³Feld: R. G. Brewer and R. L. Shoemaker, Phys. Rev. **A 6**, 2001 (1972); R. L. Shoemaker and R. G. Brewer, Bull. Am. Phys. Soc. **17**, 66 (1972). Echoes: N. A. Kurnit, I. D. Abella, and S. R. Hartmann, Phys. Rev. Lett. **13**, 567 (1964); I. D. Abella, N. A. Kurnit, and S. R. Hartmann, Phys. Rev. **141**, 391 (1966); C. K. N. Patel and R. E. Slusher, Phys. Rev. Lett. **20**, 1087 (1968); J. P. Gordon, C. H. Wang, C. K. N. Patel, R. E. Slusher, and W. J. Tomlinson, Phys. Rev. **179**, 294 (1969); B. Bölgner and J. C. Diels, Phys. Lett. **29A**, 401 (1968); R. G. Brewer and R. L. Shoemaker, Phys. Rev. Lett. **27**, 631 (1971). Other cooperative emission effects: R. L. Shoemaker and R. G. Brewer, Phys. Rev. Lett. **28**, 1430 (1972); N. Tan-no, K. Kan-no, K. Yokoto, and H. Inaba, IEEE J. Quantum Electron. **QE-9**, 423 (1973).

⁴A. Abragam, *The Principles of Nuclear Magnetism* (Oxford U. P., London, 1961); R. M. Hill, D. E. Laplan, G. F. Herrmann, and S. K. Ichiki, Phys. Rev. Lett. **18**, 105 (1967). Other references are given in J. C. MacGurk, T. G. Schmalz, and W. H. Flygare, Adv. Chem. Phys. **25**, 1 (1974).

⁵Other cooperative effects, including optical nutation, self-induced transparency, and coherent pulse propagation in absorbers, have also been studied experimentally. These effects are not primarily processes for releasing stored energy; i.e., they are not primarily emissive as are the effects mentioned in the text.

⁶N. Skribanowitz, I. P. Herman, J. C. MacGillivray, and M. S. Feld, Phys. Rev. Lett. **30**, 309 (1973).

⁷V. Ernst and P. Stehle, Phys. Rev. **176**, 1456 (1968).

⁸G. S. Agarwal, Phys. Rev. **A 2**, 2038 (1970).

⁹R. H. Lemberg, Phys. Rev. **A 2**, 883 (1970); **2**, 889 (1970).

¹⁰D. Dialettis, Phys. Rev. **A 2**, 599 (1970).

¹¹N. E. Rehler and J. H. Eberly, Phys. Rev. **A 3**, 1735

(1971).

¹²R. Bonifacio, P. Schwendimann, and F. Haake, Phys. Rev. **A 4**, 302 (1971); **4**, 854 (1971).

¹³F. T. Arecchi and E. Courtens, Phys. Rev. **A 2**, 1730 (1970).

¹⁴I. P. Herman, J. C. MacGillivray, N. Skribanowitz, and M. S. Feld, in *Laser Spectroscopy*, edited by R. G. Brewer and A. Mooradian (Plenum, New York, 1974).

¹⁵P. T. Ho, J. C. MacGillivray, S. Liberman, and M. S. Feld (unpublished).

¹⁶We have recently learned of a new observation of near-infrared superradiant emission in sodium by M. Gross, C. Fabre, P. Pillet, and S. Haroche, Phys. Rev. Lett. **36**, 1035 (1976).

¹⁷E. Ressayre and A. Tallet, Phys. Rev. Lett. **30**, 1239 (1973).

¹⁸G. Banfi and R. Bonifacio, Phys. Rev. Lett. **33**, 1259 (1975).

¹⁹R. Bonifacio and L. A. Lugiato, Phys. Rev. **A 11**, 1507 (1975).

²⁰R. Bonifacio and L. A. Lugiato, Phys. Rev. **A 12**, 587 (1975).

²¹R. H. Dicke, in *Proceedings of the Third International Conference on Quantum Electronics, Paris, 1963*, edited by P. Grivet and N. Bloembergen (Columbia U. P., New York, 1964), p. 35.

²²F. T. Arecchi and R. Bonifacio, IEEE J. Quantum Electron. **QE-1**, 169 (1965).

²³F. A. Hopf and M. O. Scully, Phys. Rev. **179**, 389 (1969).

²⁴A. Isevgi and W. E. Lamb, Jr., Phys. Rev. **145**, 517 (1969).

²⁵R. Friedberg and S. R. Hartmann, Phys. Lett. **38A**, 227 (1972).

²⁶The limits of superradiance as a process for producing ultrashort pulses of large intensity are discussed by J. C. MacGillivray and M. S. Feld (unpublished).

²⁷See, for example, F. A. Hopf, P. Meystre, M. O. Scully, and J. F. Seely, Phys. Rev. Lett. **35**, 511 (1975), and references contained therein.

²⁸W. J. Brya and P. E. Wagner, Phys. Rev. **157**, 400 (1967).

²⁹C. Leonardi, J. C. MacGillivray, S. Liberman, and

- M. S. Feld, Phys. Rev. B **11**, 3298 (1975).
- ³⁰L. W. Casperson and A. Yariv, IEEE J. Quantum Electron. QE-8, 80 (1972).
- ³¹J. H. Parks, in *Fundamental and Applied Laser Physics: Proceedings of the Estahan Symposium*, edited by M. S. Feld, N. A. Kurnit, and A. Javan, (Wiley, New York, 1973), and references contained therein.
- ³²G. I. Peters and L. Allen, J. Phys. A **4**, 238 (1971).
- ³³L. Allen and G. I. Peters, J. Phys. A **4**, 564 (1971).
- ³⁴D. A. Leonard, Appl. Phys. Lett. **7**, 4 (1965).
- ³⁵A. Yariv and R. C. C. Leite, J. Appl. Phys. **34**, 3410 (1963).
- ³⁶The connection between Dicke's formalism and the semiclassical approach has been discussed by F. T. Arecchi, E. Courtens, R. Gilmore, and H. Thomas, in *Fundamental and Applied Laser Physics: Proceedings of the Estahan Symposium*, edited by M. S. Feld, N. A. Kurnit, and A. Javan (Wiley, New York, 1973).
- ³⁷A more detailed description of Dicke's work as it relates to both a point sample and an extended medium is given in Ref. 15.
- ³⁸Various definitions of collective damping times are discussed by R. Friedberg and S. R. Hartmann, Phys. Rev. A **13**, 495 (1976).
- ³⁹C. H. Townes and A. L. Schawlow, *Microwave Spectroscopy* (McGraw-Hill, New York, 1955), Eq. (1-76).
- ⁴⁰F. Bloch, Phys. Rev. **70**, 460 (1946).
- ⁴¹The double peaks in $\phi''(\omega)$ of Fig. 3(a) can be explained as follows: Combining Eqs. (42) and (43) gives that $(S/\mu_e)^2 \cdot n^2$ is constant over space. The dip between the double peaks in $\phi''(\omega)$ then corresponds to a region where the ringing is large enough so that $n(\omega)$ crosses $n = 0$ [Fig. 4]. When the ringing becomes sufficiently damped so that n can no longer become positive, the dip disappears and the double peak becomes a single peak.
- ⁴²Accordingly, in the preceding discussion the length of the dipole array could be considered to be the length $L_{\text{eff}} (\ll L)$ over which the polarization envelope is approximately constant. See Eq. (51) below.
- ⁴³See, for example, Ref. 24.
- ⁴⁴In the far infrared, the background thermal radiation intensity exceeds that due to spontaneous emission and becomes the primary mechanism for initiating the superradiant process [see Eq. (36)].
- ⁴⁵S. L. McCall and E. L. Hahn, Phys. Rev. **183**, 457 (1969); Phys. Rev. Lett. **18**, 908 (1967).
- ⁴⁶For a comprehensive list of references, see G. L. Lamb, Jr., Rev. Mod. Phys. **43**, 99 (1971).
- ⁴⁷Distinguishing between T_1 and T_2 is of no consequence here since the superradiant decay rate is much less than γ .
- ⁴⁸This formula is a consequence of the optical pumping process and is not basic to the superradiant pulse evolution process.
- ⁴⁹If the system is pumped by a P branch line, n_{r0} must be multiplied by $(2J+3)/(2J+5)$.
- ⁵⁰R. Friedberg and S. R. Hartmann, Phys. Lett. **37A**, 285 (1971).
- ⁵¹C. K. Rhodes, A. Szöke, and A. Javan, Phys. Rev. Lett. **21**, 1151 (1968).
- ⁵²It is convenient to assume a constant amplitude for A_p (other than the n_2 dependence) because when contributions to ϕ' from A_p in different regions are added, the summation of random phases will be more important than small amplitude variations in the individual contributions.
- ⁵³A similar expression for A_p without spatial dependence was used by J. A. Fleck, Jr. [Phys. Rev. B **1**, 84 (1970)]. In the present case, spatial dependence of A_p must be included, since in a high-gain system spatial variations are essential to superradiant behavior.
- ⁵⁴The discrete velocities should be chosen to optimize the convergence of Eqs. (11). See Ref. 24.
- ⁵⁵"Very slowly varying" should not be confused with "slowly varying" ($\partial/\partial t \ll \omega_0$, $\partial/\partial z \ll \omega_0/c$), which has already been assumed in the derivation of Eqs. (11a) and (11b). Note that δ is not necessarily very slowly varying in space, even near thermal equilibrium; i.e., we do not require $\partial\delta/\partial z \ll \gamma\delta/c$.
- ⁵⁶These conditions hold, for example, near thermal equilibrium. Note that the presence of delta functions in A_p is not inconsistent with very slowly varying n and δ ; although A_p has delta functions, the source terms for n and δ do not.
- ⁵⁷A. Einstein, Phys. Z. **18**, 121 (1917); Verh. Dtsch. Phys. Ges. No. 13/14 (1916).
- ⁵⁸M. W. P. Strandberg, Phys. Rev. **106**, 617 (1957).
- ⁵⁹For systems which are not high gain, the gain-dependent factor $(\pi/2\alpha_0 L)^{1/2}$ would be replaced by 1, so that $K_0 = [n_2/(n_2 - n_1)]h\omega_0/4\pi T_2$.
- ⁶⁰There are some errors in the numerical factors in the corresponding equations in Ref. 14.
- ⁶¹The derivation (Ref. 44) of the area theorem assumes a zero-phase external field incident upon a nondegenerate medium with no distributed sources.
- ⁶²This follows from the expression for the cross section of a divergent Gaussian beam. See, for example, M. Sargent III et al., *Laser Physics* (Addison-Wesley, Reading, Mass., 1974), p. 369.
- ⁶³R. P. Feynman, F. L. Vernon, Jr., and R. W. Hellwarth, J. Appl. Phys. **28**, 49 (1957).
- ⁶⁴D. C. Burnham and R. Y. Chiao, Phys. Rev. **188**, 667 (1969); see also G. L. Lamb, Jr., Phys. Lett. **29A**, 507 (1969); Ref. 45; and F. T. Arecchi and E. Courtens (Ref. 13).
- ⁶⁵Note added in proof. The normalized emission curve is obtained from Eq. (46) using the substitution $w = 2(xT)^{1/2}$, as in Ref. 63. One obtains $d^2\psi/du^2 + (1/u)d\psi/du = \sin\psi/LT_R$, which for the initial condition $\psi(w=0) \ll 1$ gives the normalized emission curve. This initial condition is equivalent to a δ -function input δ field, which is approximately equivalent (Sec. V) to any other input pulse of equal small effective area.
- ⁶⁶If the population excitation time is appreciable, T_0 should be measured from the central part of the excitation pulse. See Ref. 26.
- ⁶⁷This can be seen from the figures of D. C. Burnham and R. Y. Chiao (Ref. 63).
- ⁶⁸In the derivation of Eq. (49), the argument of the logarithm depends on T_0 and is of order θ_0/π ; the chosen numerical factor provides a very accurate fit to the numerical results of Sec. V.
- ⁶⁹From these approximate expressions a picture emerges in which the normalized output emission curve is similar to a damped sine-squared curve, $I(T) = I_0 e^{-(T-T_0)/\tau} \cos^2[\mu\delta_p(T-T_0)/4\hbar]$, of frequency $(\mu\delta_p/4\hbar)^{-1} [=T_R/\ln(\theta_0/2\pi) - T_0]$ and decay constant τ

$= (\pi/16) T_R [\ln(\theta_0/2\pi)]^2$. This equation gives a qualitative fit to the normalized output curve, and as such illustrates the interpretation of superradiance as a damped oscillatory process, where damping is due to the release of coherent radiation from the sample. Behavior of this type can be derived from a differential equation obtained by considering the fraction of the energy radiated in one lobe of radiation and the time between the first two output peaks. Combining this differential equation with Eq. (55) gives $I(T)$ as above except for a factor of 4 in τ , a difference attributable to the fact that the true decay of energy slows temporarily each time δ passes through zero.

⁶²To simplify intermediate calculations we have assumed negligible transit time so that $t = T$ in Eqs. (59)–(62).

⁶³These approximations were justified in Sec. IV and are confirmed by the numerical results (Sec. V) which, in particular, show that the phase of ϕ' is reasonably constant throughout the medium and in time.

⁶⁴The constant-phase assumption implies that the carrier frequency is close to resonance ($\nu \sim \omega_0$). This approximation is valid because the spontaneous-emission profile is symmetric about its peak at ω_0 .

⁶⁵In integrating Eq. (62) care must be taken to keep all terms of order $\alpha_0 L$ in order to obtain the correct numerical coefficient of the second term in Eq. (65a). However, as seen below, that numerical factor is unimportant because that term is negligible ($\alpha_0 L \ll 1$).

⁶⁶The solutions of Eqs. (68) obtained in Ref. 17 do not agree at all with the experimental results of Ref. 6, notwithstanding the analysis of Ref. 17. In the fit therein to the experimental results, the time axis has been shifted arbitrarily and the experimentally observed ringing is disregarded. Although Ref. 17 claims that large delays are due to inhomogeneous broadening, their calculations do not give the observed delays. In fact, our results show that for constant T_R , the delay decreases as the inhomogeneously broadened width $1/T_2^*$ increases [Eq. (75)].

⁶⁷Equations (66) do not allow $I(L, t=0) = 0$, because Ref. 12 requires that $I(L, t=0)$ must be at least as large as

a value corresponding to spontaneous emission.

⁶⁸As can be seen from the discussion of $(T_2^*)_{\text{eff}}$ [Eq. (75)], $\alpha_0 L \gtrsim |\ln \theta_0|$ is sufficient if T_2^* is the dominant broadening time, but $\alpha_0 L \gg |\ln \theta_0|$ is necessary if T_2 dominates. This follows from the fact that T_D must be shorter than both the incoherent decay time and the effective dephasing time of the system so that coherent decay will dominate.

⁶⁹M. D. Crisp, Phys. Rev. A **1**, 1604 (1970).

⁷⁰Note that this conclusion applies only to an inhomogeneously broadened system, where deexcitation of the levels is unimportant. The population decay associated with homogeneous broadening cannot be counteracted by high gain.

⁷¹Reference 19, Eqs. (10.12), (10.13), and (10.16)–(10.18). For convenience of comparison with Eqs. (11) we have kept only those terms corresponding to the forward traveling wave; this is consistent with the statements in Sec. III that the forward and backward waves do not interact appreciably.

⁷²Note added in proof. The pendulum equation of Ref. 19, $d^2\psi/dt^2 + [(c/2L) + (1/2T_2^*)] d\psi/dt = (c/2LT_R)e^{-t/T_2^*} \times \sin\psi$, is a function of time only. Note that the pendulum equation obtained from the present treatment (Ref. 63a) is a function of both space and time.

⁷³R. Bonifacio, F. A. Hopf, P. Meystre, and M. O. Scully, Phys. Rev. A **12**, 2568 (1975), and references therein.

⁷⁴R. H. Picard and C. R. Willis, Phys. Rev. A **8**, 1536 (1973), and references therein; R. Saunders, R. K. Bullough, and F. Ahmad, J. Phys. A **8**, 759 (1975); F. A. Hopf and P. Meystre, Phys. Rev. A **12**, 2534 (1975); F. A. Hopf, P. Meystre, and D. W. McLaughlin, Phys. Rev. A **13**, 777 (1976).

⁷⁵The very slowly varying approximation implies that the carrier frequency is close to resonance ($\nu \sim \omega_0$), an approximation discussed in Ref. 70.

⁷⁶The intensities of the two polarizations grow independently, but the one which starts first will dominate.

⁷⁷For a Gaussian $G(\omega) = e^{-(\Delta\omega/\hbar\omega)^2}$, $I_1 = (\pi/2\alpha_0 L)^{1/2} \times \hbar\omega e^{2\alpha_0 L} = [\pi/(2\alpha_0 L)]^{1/2} e^{2\alpha_0 L}/T_2^*$.

Criteria for x-ray superradiance^{a)}

J. C. MacGillivray and M. S. Feld^{b)}

Department of Physics and Spectroscopy Laboratory, Massachusetts Institute of Technology, Cambridge, Massachusetts 02139

(Received 21 February 1977; accepted for publication 2 May 1977)

This paper develops a set of criteria for superradiant emission in x-ray systems. These new criteria, which must be satisfied in order to obtain efficient x-ray emission, are given in the form of simple inequalities in terms of experimental parameters.

PACS numbers: 32.30.Rj, 42.55.Bi

Over the past several years there has been considerable discussion of possible x-ray laser schemes.¹ Due to the short spontaneous lifetimes of the transitions and the lack of suitable mirrors in this regime, a high-gain single-pass system which is excited longitudinally at the speed of light (swept excitation) must be used. The properties of such a system will differ considerably from those of conventional lasers. In a recent paper Hopf, Meystre, Scully, and Seely² noted that the rate-equation approach, used to calculate the gain in many proposed schemes, is incorrect due to "laser lethargy", a reduction in gain due to finite amplifier bandwidth and rapid atomic decay. Alternatively, the x-ray radiation process may be viewed as superradiant emission from an initially inverted system, similar to that recently observed³⁻⁵ and analyzed⁶ in infrared systems. This paper exploits the latter point of view to develop a set of simple inequalities in terms of experimental parameters, which must be met in order to obtain efficient x-ray emission. Such criteria, which have not been given previously, should be of interest to proposers of x-ray laser systems. In fact, several proposed schemes fail to meet these criteria.

Superradiance is the spontaneous radiative decay of an assembly of atoms or molecules in the collective mode. Alternatively, it can be viewed⁶ as the transient form of stimulated emission from a high-gain medium. In this process incoherent spontaneous emission induces a small macroscopic polarization which gives rise to a growing electric field and consequently an increasing polarization in space and time. After a long delay, a highly directional pulse is emitted, often accompanied by ringing. The peak output power is proportional to the square of the number of radiators, N .

(1) The ideal case of superradiance occurs when a two-level system with sufficient gain,⁶

$$\alpha L \lesssim \phi, \quad (1)$$

has been inverted by swept excitation with negligible rise time to a population inversion N . Here αL is the small-signal field gain (half the power gain) at line

center, L is the sample length, and⁶

$$\phi = \ln[N^{1/2}(2\pi)^{5/4}(\alpha L)^{3/4}] \approx \frac{1}{2} \ln N. \quad (2)$$

(For typical x-ray systems, $15 < \phi < 30$.) In this case the properties of the emitted radiation are determined by ϕ and the collective radiative damping time,

$$T_R = T_{sp}(8\pi/n\lambda^2 L), \quad n = N/AL, \quad (3)$$

where T_{sp} is the spontaneous lifetime of a single atom, λ is the wavelength of the emitted radiation, n is the initial inversion density, and A is the cross-sectional area of the sample. Note that⁷ $\alpha L = T'_2/T_R$, where T'_2 is the inverse linewidth.

The output radiation is determined from the Maxwell-Schrödinger equations^{6,8}; the peak output power is

$$I_p \approx 4N\hbar\omega/T_R\phi^2 \propto N^2, \quad (4)$$

the width of the output pulse is

$$T_w \approx T_R\phi \propto N^{-1}, \quad (5)$$

and the energy contained is

$$E_p \approx 4N\hbar\omega/\phi \propto N. \quad (6)$$

The delay time from the inversion to I_p is

$$T_D \approx \frac{1}{4}T_R\phi^2 \propto N^{-1}, \quad (7a)$$

so that $T_D \approx \frac{1}{4}T_w\phi$. This pulse is followed by ringing.

(2) Next, consider the case in which the inversion rise time τ is finite but terminates before the superradiant pulse is emitted. In this case the inversion density which would exist in the absence of stimulated emission,⁹ $n^*(t)$, reaches a constant value which can be used in place of n in Eqs. (1)–(6). The delay time T'_D , measured from the commencement of the inversion process, is greater than T_D :

$$T'_D \approx \frac{1}{4}T_R\phi^2 + \tau f(\tau), \quad [\tau < T'_D], \quad (7b)$$

where $f(T)$ is a numerical factor, $0 < f < 1$, determined by the shape of $n^*(t)$ for $t < T$.¹⁰ [If $n^*(t) = \Lambda t^{\beta-1}$, Λ constant and $\beta > 1$, then $f = 1 - 1/\beta$.]

(3) If the superradiant output occurs before the excitation process terminates ($T'_D < \tau$), $n_{eff} = n^*(t = T'_D)$ must be used in place of n in Eqs. (1)–(6). Equation (7b) is then replaced by

$$[1 - f(T'_D)] T'_D \approx (\frac{1}{4}T_{sp}\phi^2)(8\pi/n_{eff}\lambda^2 L), \quad (7c)$$

which can be solved for T'_D for any given $n^*(t)$.¹¹ The frequently made assumption that the x-ray laser pulse

^(a) Work supported in part by National Science Foundation and U.S. Army Research Office (Durham).

^(b) Alfred P. Sloan Fellow.

occurs at the peak of the n^* curve is particularly erroneous in this case. Similarly, gain calculated using this peak value has no particular significance.

For example, for $t < \tau$ we have $n^*(t) = \Lambda t^{\beta-1}$, $\beta > 1$, then

$$n_{\text{eff}} \approx \Lambda (n_s \tau / \Lambda)^{(1-1/\beta)} \propto \Lambda^{1/\beta} \quad (8)$$

and $T_D' \approx (n_{\text{eff}} / \Lambda)^{(1-1/(\beta-1))} = (n_s \tau / \Lambda)^{1/\beta} \propto \Lambda^{-1/\beta}$, where $n_s = 2\pi T_{sp} \phi^2 \beta / \lambda^2 L \tau$, $(T_D' / \tau = n_s / n_{\text{eff}})$. This value of n_{eff} can be used in Eqs. (1)–(6); for example, $I_p \approx \hbar \omega \Lambda L \Lambda \times (n_s \tau / \Lambda)^{(1-2/\beta)}$. Note that in this case $I_p \propto \Lambda^{2/\beta}$, not Λ^2 , but N^2 radiation still occurs because the effective number of radiators $N = n_{\text{eff}} \Lambda L \propto \Lambda^{1/\beta}$. However, although I_p increases with increasing Λ , the efficiency decreases¹². The energy needed to invert the system $E_{\text{inc}} = \Lambda \tau^{\beta-1} \hbar \omega$, so that $E_p / E_{\text{inc}} = (4/\phi)(T_D' / \tau)^{\beta-1}$, as opposed to the ideal case (1), where $E_p / E_{\text{inc}} = 4/\phi$.

It is sometimes useful to rewrite Eq. (8) as $n_{\text{eff}} = [n^*(\tau)]^{(1-f)} n_s^f$, where $n^*(\tau)$, the peak value of n^* , can be conveniently found from Ref. 1(d). Similarly, $\tau_D' \approx \tau [n_s / n^*(\tau)]^{(1-f)}$ and $I_p \approx [\hbar \omega \Lambda L n^*(\tau) / \tau (1-f)] [n_s / n^*(\tau)]^{(2f-1)}$ [$n_s \leq n^*(\tau)$ always]. Written in this form, these expressions hold for most $n^*(t)$.

When the inversion is produced by a beam which crosses the medium in the transverse direction, as in Ref. 1(c), the transit time of this beam can be comparable to T_D' and must be taken into account when calculating $n^*(t)$.

(4) In addition to condition (1), other criteria which arise from effects which are particularly important in x-ray systems must be met:

(a) The homogeneous decay time T_1 , due to spontaneous emission, collisions, Stark broadening, Auger transitions, etc., must satisfy $T_D \leq T_1$, otherwise incoherent decay becomes the dominant mode of deexcitation, preventing superradiance.¹³ This condition gives $\alpha L \geq (\frac{1}{4} \phi^2) (T_2' / T_1)$, or equivalently,

$$nL \geq (2\pi \phi^2 / \lambda^2) (T_{sp} / T_1) \propto \lambda^{-2}, \quad (9)$$

so that with decreasing wavelength the minimum value of nL [or $(nL)_{\text{eff}}$] increases. Combining Eqs. (9) and (4) gives $I_p \geq (\hbar \omega / T_{sp}) (2\pi A \phi^2 / \lambda^2) (T_{sp} / T_1)^2 = \hbar \omega / T_1$.

With decreasing wavelength T_{sp} often becomes the dominant mechanism for T_1 ($T_1 \approx T_{sp}$), so that at threshold ($I_p = \hbar \omega / T_{sp}$) the peak power coherently emitted (into a small solid angle) equals the power that would have been incoherently radiated via spontaneous emission (in all directions).

(b) Excessive loss can inhibit superradiant emission. In x-ray systems loss may be due to photoionization, inverse bremsstrahlung or nonresonant absorption, and the ϵ -field loss coefficient, $\kappa = (1/\epsilon)(\partial \epsilon / \partial x)_{\text{loss}}$, is independent of x . Due to loss, more gain is needed to achieve superradiant output. Equation (1) becomes¹⁴

$$(\alpha - \kappa)L \geq \phi. \quad (10)$$

No matter how large the gain, for $\kappa L \geq \frac{1}{4} \phi$, the pulse stops narrowing and the intensity no longer increases with length,¹⁴ giving rise to a steady-state pulse¹⁵ described by Isevgi and Lamb,¹⁶ Bonifacio *et al.*,¹⁷ and

others. In this regime $n' = n\phi / 4\kappa L$ must be used in place of n in Eqs. (3)–(7), so that $I_p \approx (\hbar \omega A / 32\pi T_{sp}) \times (n\lambda / \kappa)^2$ and $T_w \approx \kappa T_{sp} / n\lambda^2$ no longer depend on L . This sets an upper limit on the useful length of a superradiant system with loss, regardless of its gain. Longer lengths reduce efficiency but not I_p .

(c) In the case of uniform excitation (all atoms excited simultaneously, in contrast to swept excitation), a sample longer than cT_D will break up into independently radiating segments (in a manner described by Arecchi and Courtens¹⁸), resulting in loss of efficiency. This gives rise to a maximum "cooperation length" $L_c = (cT_{sp} \phi^2 / 2n\lambda^2)^{1/2}$, the length for which $T_D = L/c$. The peak output power for $L = L_c$ is [Eq. (4)] $I_p \approx n\hbar \omega A c = N\hbar \omega (c/L)$; for $L > L_c$ the maximum power I_p remains approximately constant. This will be a problem in small samples such as that of Ref. 1(b) in which the entire sample is excited simultaneously.

In summary, in order to achieve superradiant output, n (or n_{eff} or n') and L must satisfy Eqs. (9) and (10). Efficient superradiant emission also requires $\kappa L \leq \frac{1}{4} \phi$ and $L < L_c$, and, in systems for which $\tau > T_D'$ (most x-ray systems), T_D' / τ as large as possible.

To illustrate how these criteria apply, consider the scheme proposed by Duguay and Rentzepis,^{1(a)} in which $2p$ electrons of sodium vapor are to be photoionized to create a population inversion at 372 Å. In this system $p = 0.02$ Torr, $T_1 = T_{sp} = 400$ psec, $T_2' \approx 17$ psec, $L = 500$ cm, $\kappa = 3 \times 10^{-5}$ cm⁻¹, and the degeneracy ratio of the upper to lower states is 3. The pump power (centered at 50 eV) increases linearly with time ($\beta = 3$) at a rate $R = 4$ GWnsec⁻¹ cm⁻³, and 0.3% of the pump energy is absorbed by the medium. (Hence $\Lambda = 0.003R / 2\hbar \omega_{\text{pump}}$ for $t < T_{sp}$.) Equation (7c) applies here and gives $n_{\text{eff}} = 6 \times 10^{12}$ cm⁻³. Since this value satisfies Eqs. (9) and (10), superradiance will occur; then $\phi \approx 23$, $T_D' \approx 100$ psec, $T_w \approx 5$ psec, and $I_p \approx 600$ MW. Computer solution⁵ of the Maxwell-Schrödinger equations for such a system gives $I_p = 600$ MW, $T_D' = 80$ psec, and $T_w = 4$ psec, in

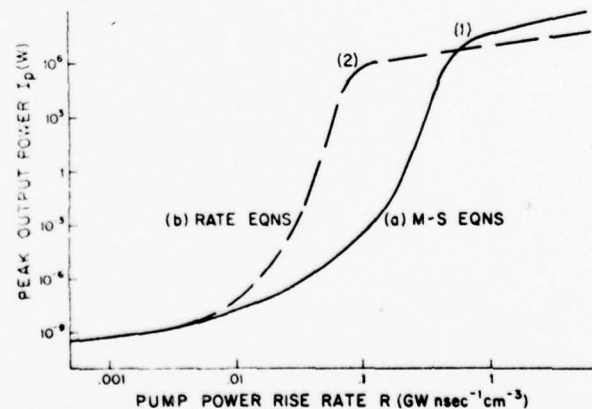


FIG. 1. I_p versus R , for a system identical to that of Duguay and Rentzepis [Ref. 1(a), described in text], except that R is varied and $T_2' = \infty$. At $R = 4$ GWnsec⁻¹ cm⁻³, $n_{\text{eff}} L = 3 \times 10^{15}$ cm⁻². (1,2) Threshold values of I_p and R , obtained from Maxwell-Schrödinger equations [curve (1)] and rate equations [curve (2)] (see Ref. 19).

close agreement with the estimates. These results are markedly different from those obtained from rate equation analysis,¹⁹ which predict I_p about 10 times smaller and T_w about 10 times longer.

Actually, this value of R is almost an order of magnitude larger than that necessary to achieve superradiance. The minimum value, obtained from Eqs. (9) and (10), is $0.8 \text{ GWsec}^{-1} \text{ cm}^{-3}$, giving $I_p \approx 100 \text{ MW}$ and $T_w \approx 11 \text{ psec}$. Computer analysis confirms these results.

To further contrast the predictions of Maxwell-Schrödinger and rate equations, consider the computer curves (Fig. 1) relating I_p and R for a system identical to that described above but with (for simplicity) no Doppler broadening ($T_2^* \rightarrow \infty$). The peak intensity obtained from the Maxwell-Schrödinger equations (a) exceeds that of the rate equations (b) by a factor of 10 in the superradiant regime, and about 10 times as much pump power is necessary to achieve superradiant output.²⁰ This increase in threshold occurs because polarization P cannot be created instantaneously.²¹ For $\alpha L \lesssim \phi$, P evolves slowly, giving rise to a time delay during which P can decay.²² For $\alpha L \gtrsim \phi$, however, P builds up more rapidly, and to a larger value than that predicted by rate equations, giving rise to smaller delays and shorter pulses of larger intensity.

Observing directional anisotropy in the output radiation may be a useful experimental step towards achieving superradiance, since as the experimental parameters approach the threshold of coherent emission, the output radiation becomes redirected into a small angle along the axis. The output intensity from a system with gain of order unity is approximately twice as large in the forward direction as in lateral directions. For example, in the Na scheme of Ref. 1(a), the pump power required for observation of anisotropy is almost three orders of magnitude less than that for superradiance.

We wish to thank Norman Kurnit for useful discussions.

¹See, for example, (a) M.A. Duguay and P.M. Rentzepis, Appl. Phys. Lett. 10, 350 (1967); (b) B. Lax and A.H. Guenther, Appl. Phys. Lett. 21, 361 (1972); (c) R.A. McCorkle, Phys. Rev. Lett. 29, 982 (1972); (d) R.C. Elton, R.W. Waynant, R.A. Andrews, and M.H. Reilly, Naval Research Laboratory Report No. 7412, 1972 (unpublished), and

references therein; (e) P.J. Mallozzi, H.M. Epstein, R.G. Jung, D.C. Applebaum, B.P. Fairand, W.J. Gallagher, R.L. Uecker, and M.C. Muckerheide, J. Appl. Phys. 45, 1891 (1974).

²F.A. Hopf, P. Meystre, M.O. Scully, and J.F. Seely, Phys. Rev. Lett. 35, 511 (1975).

³N. Skribanowitz, I.P. Herman, J.C. MacGillivray, and M.S. Feld, Phys. Rev. Lett. 30, 309 (1973).

⁴I.P. Herman, J.C. MacGillivray, N. Skribanowitz, and M.S. Feld, in *Laser Spectroscopy*, edited by R.G. Brewer and A. Mooradian (Plenum, New York, 1974).

⁵M. Gross, C. Fabre, P. Pillet, and S. Haroche, Phys. Rev. Lett. 36, 1035 (1976).

⁶J.C. MacGillivray and M.S. Feld, Phys. Rev. A 14, 1169 (1976).

⁷R. Friedberg and S.R. Hartmann, Phys. Rev. Lett. A 37, 285 (1971).

⁸When the upper- and lower-level populations decay at different rates, Eq. (11c) of Ref. 6 must be replaced by separate equations for n_{upper} and n_{lower} .

⁹Curves of $n^*(t)$ are easily obtained from rate-equation analyses, such as those of Ref. 1 (d). As in Ref. 1 (d), degenerate levels must be taken into account.

¹⁰In general, $f(T) = \int_0^T n^*(t) dt / [T n^*(T)]$. Usually, f is essentially independent of T .

¹¹Equation (7c) can be solved graphically using $n^*(t)$ curves such as those of Ref. 1 (d). The exact shape of $n(t)$ has little effect on the observed output, for reasons discussed in Ref. 6.

¹²This condition $\tau \leq T_D^*$ for no loss of efficiency is more stringent than the $\tau \leq T_{sp}$ condition of Ref. 1 (d), since $T_D^* < T_{sp}$ always [see text above Eq. (9)].

¹³The effective dephasing time $\alpha L T_2^*$ should also be $\geq T_D^*$, but this does not introduce a new condition, as is shown in Ref. 14.

¹⁴J.C. MacGillivray and M.S. Feld, Phys. Rev. (to be published).

¹⁵The pulse is steady state in retarded time, i.e., its waveform does not change as it propagates.

¹⁶A. Iosevigi and W.E. Lamb, Jr., Phys. Rev. 185, 517 (1969).

¹⁷R. Bonifacio, F.A. Hopf, P. Meystre, and M.O. Scully, Phys. Rev. A 12, 2568 (1975).

¹⁸F.T. Arecchi and E. Courtens, Phys. Rev. A 2, 1730 (1970).

¹⁹The rate equations used are Eqs. (58) and (63) of Ref. 6, with $\kappa \neq 0$, modified as indicated in Ref. 8.

²⁰The equation relating I_p and R for the rate-equation case [Fig. 1 (b)] is $\ln(I/I_0) + T_2^* T_1 \lambda^2 (I - I_0) / 2\pi\hbar\omega A T_{sp} - 2\alpha L$, where $I_0 = \hbar\omega(\pi/2\alpha L)^{1/2} / 4\pi T_1$ (Ref. 6) with α obtained from R . The threshold occurs at $I \sim 2\pi\hbar\omega A T_{sp} / T_2^* T_1 \lambda^2$.

²¹In the rate-equation picture this buildup of P is instantaneous. Note that the rate equations can be obtained from the Maxwell-Schrödinger equations of Ref. 6 by setting $\partial P / \partial T = 0$.

²²Reference 2 describes the smaller output (compared to rate equations) as a spatial delay in the growth of the gain (laser lethargy).

III. Laser Saturation Spectroscopy

Observation of adiabatic rapid passage utilizing narrow infrared saturation resonances*

S. M. Hamadani, A. T. Mattick, N. A. Kurnit, and A. Javan

Physics Department, Massachusetts Institute of Technology, Cambridge, Massachusetts 02139
(Received 17 March 1975)

Population inversion by adiabatic rapid passage (ARP) utilizing narrow saturation resonances is observed for an infrared transition of NH_3 . The population change produced by sweeping the frequency of a strong saturating laser field through the center of a Doppler-broadened absorption line is probed by a weak counterpropagating field as in a Lamb-dip experiment. When the ARP conditions are satisfied, inversion of population is detected as amplification of the probe wave near the line center.

PACS numbers: 32.20.K, 32.20.D

Population inversion by adiabatic rapid passage (ARP) has long been used in NMR to study relaxation effects of spin systems.¹ Recently, this method has been applied in the optical region by Stark tuning an infrared transition in NH_3 through resonance with an intense laser field.² The relaxation of the entire Doppler-broadened line was monitored by a second passage.

In this letter we report the observation of population inversion by ARP for molecules of a specific velocity group by observing the narrow saturation resonance appearing at the center of a Doppler-broadened absorption line (Lamb dip) as a strong saturating wave and a weak counterpropagating wave of the same frequency are rapidly tuned through line center.³ The method has the advantage of easing the conditions required for ARP, in that the frequency sweep need only be of the order of the homogeneously broadened width of the resonance, much narrower than the Doppler width. Furthermore, since molecules in neighboring velocity groups are probed before, during, and immediately after the ARP, fast relaxation processes can be investigated with relatively slow sweep rates. This in turn reduces the requirements on laser power. In addition, for the two

counterpropagating waves having different frequencies, as in a recent slow passage experiment,⁴ relaxation can be studied as a function of molecular velocity.

Let us consider the interaction of a Doppler-broadened transition centered at ω_0 with a strong saturating traveling wave $\mathbf{E}_s \exp[i(\omega t - kz)]$ traveling in the positive z direction and a weak counterpropagating probe wave $\mathbf{E}_p \exp[i(\omega t + kz)]$. For sufficiently slow sweep (as in a conventional Lamb-dip experiment), the strong field selectively saturates those molecules with z component of velocity, v_z , satisfying the condition $|\omega - \omega_0 - kv_z| \leq \gamma_s = (\gamma^2 + \beta^2)^{1/2}$, where γ is the collision-broadening rate and $\beta = \mu E_s / \hbar$. At the same time, the probe field will interact with molecules with v_z satisfying $|\omega - \omega_0 + kv_z| \leq \gamma$. As ω is swept through line center, both fields interact with the same set of molecules ($v_z \approx 0$), and the probe absorption will exhibit the well-known saturation dip, with a symmetrical line shape centered at $\omega = \omega_0$ and a full width of approximately γ_s . In the limit of large saturating field strength ($\beta \gg \gamma$), the absorption of the weak probe field at $\omega = \omega_0$ does not generally approach zero,⁵ as might be expected from complete saturation of the population by the strong saturating

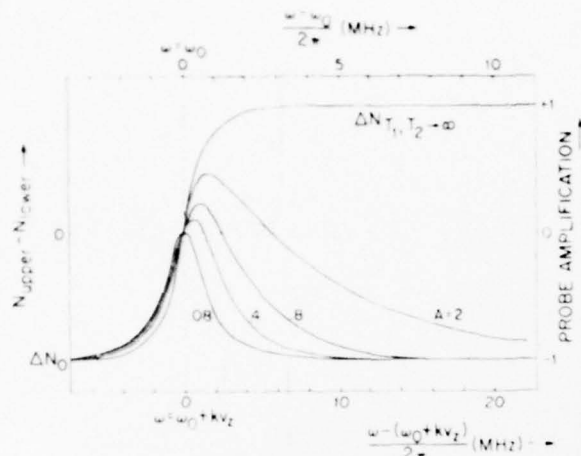


FIG. 1. Computer calculations of population difference $\Delta N(v_z)$ (left and bottom scales) and probe field absorption (right and top scales) as a function of frequency detuning for different sweep rates A (in MHz/μsec) with $\beta = 10^7 \text{ sec}^{-1}$, $T_1 = T_2 = 4.5 \text{ μsec}$. Since the probe frequency is swept, the frequency scale for absorption is expanded by a factor of 2 with respect to that for population difference. The right-hand scale is normalized to the unsaturated absorption coefficient. Also shown is population change in absence of relaxation.

field. This residual absorption results from parametric coupling between the two waves produced by the nonlinear induced polarization and is dependent on the ratio of population decay rate $1/T_1$ to the homogeneous width $\gamma = 1/T_2$. As shown in Ref. 5, the residual absorption can be as much as $\frac{1}{2}$ of the unsaturated absorption and approaches zero only for $T_2 \ll T_1$.

The condition for slow sweep is satisfied when the population change induced by the saturating field can reach equilibrium before ω is detuned by an amount comparable to γ . For adiabatic rapid passage, this condition is reversed. In this case the field must be swept through the power-broadened width of the resonance in a time shorter than the collisional relaxation

time:

$$\frac{d\omega}{dt} \gg \frac{2\beta}{T_2} \quad (1)$$

In addition, a second condition is necessary if the passage is to be adiabatic^{1,2,6}:

$$\frac{d\omega}{dt} \ll \beta^2 \quad (2)$$

If these two conditions are met, the strong saturating wave will completely invert each molecular velocity group as it passes through resonance. A weak counter-propagating probe wave will see absorption on one side of the Doppler-broadened line, but once ω has been swept through ω_0 , the probe will interact with molecules which have already been inverted, and hence will exhibit amplification. As the inverted population relaxes to equilibrium, the amplification decays back to the unsaturated absorption with a time constant determined by T_1 . This will manifest itself as a nonsymmetrical ARP saturation resonance line shape. Thus, as the sweep rate is increased from a low value, the Lamb dip will become deeper, passing over into amplification and becoming increasingly asymmetrical at higher sweep rates (cf. Figs. 1 and 2, which are discussed below).

In formulating the effect, the customary Bloch equations⁷ can be written for the saturating field interacting with the ensemble of molecules having a given velocity component v_z . For these molecules the saturating field appears at the Doppler-shifted frequency $\omega - kv_z$. As this Doppler-shifted frequency is swept through ω_0 , neglecting the relaxation effects, and with ARP conditions (1) and (2) satisfied, the population difference as a function of the time-varying ω will be given by^{6,8}

$$\Delta N_{T_1, T_2}(\omega - kv_z) = -\Delta\omega [(\Delta\omega)^2 + \beta^2]^{-1/2} \Delta N_0(v_z) \quad (3)$$

where $\Delta\omega = \omega - (\omega_0 + kv_z)$ and $\Delta N_0(v_z)$ is the population difference in the absence of the saturating field. In this equation, it is assumed that ω is swept starting at a value well below $\omega_0 + kv_z$. Note that after ω has swept

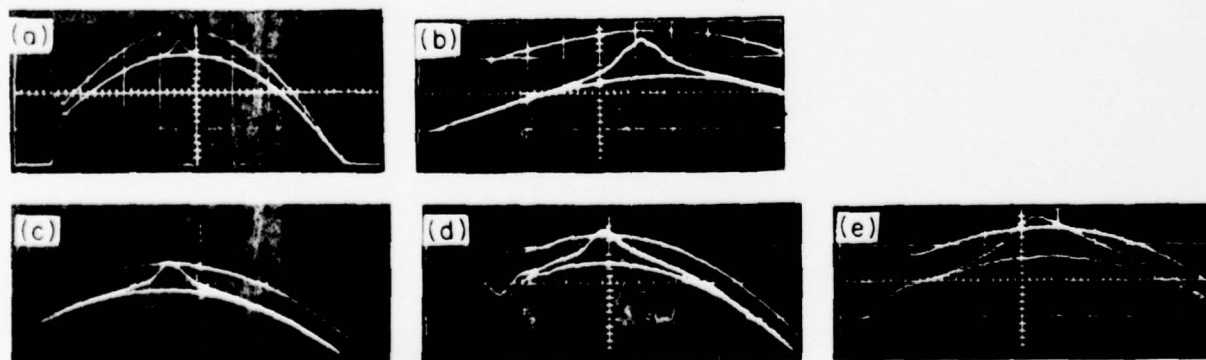


FIG. 2. Evolution of a typical Lamb-dip signal crossing into amplification as the frequency sweep rate is increased to satisfy the ARP conditions. Upper traces show the probe field signal with zero pressure as the laser is swept through resonance. Middle and lower traces show the same signal with and without the saturating field, respectively, for NH_3 pressure of 3 mTorr in (a) and 1.5 mTorr in (b)–(e). Vertical gain in (b) is twice that in (c)–(e). (b) Entire gain profile of N_2O laser is shown. 7 MHz/div, sweep rate $A = 0.08 \text{ MHz/μsec}$. (b) Relevant part of laser signal with increased vertical gain (base line suppressed) (Ref. 11). 1.6 MHz/div, $A = 0.08 \text{ MHz/μsec}$. (c)–(e) 4 MHz/div, increasing sweep rates of 0.4, 0.8, and 2.0 MHz/μsec, respectively.

through $\omega_0 + kv_z$, $\Delta\omega$ in Eq. (3) changes sign, indicating inversion of population by ARP for molecules of velocity v_z .

In the presence of molecular relaxations, the Bloch equations including relaxation terms may be solved numerically to obtain the time-dependent population. Figure 1 shows the population $\Delta N(v_z)$ as the incident field frequency is swept through $\omega_0 + kv_z$ at different sweep rates, computed for a plane wave assuming a linear frequency sweep $\omega = \omega_0 + 2\pi At$ and, for illustration, taking $T_1 = T_2$. As expected, for slow sweeps the time dependence reflects the Lorentzian shape of a resonance and, for very strong saturating field, gives $\Delta N = 0$ at the same time when $\Delta\omega$ becomes zero. As the sweep rate is increased to satisfy condition (1), population inversion results for $\omega > \omega_0 + kv_z$. The curves become deeper and asymmetry appears due to the finite decay time T_1 . The curves in Fig. 1 would also represent the probe field absorption (neglecting parametric terms²) for a fixed-frequency probe. If the probe frequency is swept together with that of the saturating field, the frequency scale must be expanded by a factor of 2 (upper scale in Fig. 1).

In the experiment, population inversion by ARP was observed for the v_z [$asQ(8, 7)$] transition in ammonia. The output of a 1-m-long N_2O laser operating on the $P(13)$ line, which can be tuned through this resonance,⁹ was split into a strong saturating field and a weak probe field and sent in opposite directions through an 81-cm-long absorption cell. To minimize feedback of the fields into the laser the polarization of the strong field was rotated 90° with respect to the probe field so that feedback from both fields could be eliminated with the use of Brewster-angle reflectors. The frequency was swept by varying the length of the laser resonator using a 2-in.-long tubular PZT driven by a sinusoidal modulating voltage (so that $\omega = \omega_0 + 2\pi\xi \sin 2\pi\nu t$, with $\xi \approx 60$ MHz).¹⁰ The laser's frequency sweep was inferred by observing the fringes of a 6328-Å laser beam in a Michelson interferometer which used the PZT-driven laser mirror in one arm.

Figure 2 shows typical results for signals appearing on the probe field with, for comparison, the probe amplitudes with no absorber and with no saturating field. For slow sweeps [Figs. 2(a) and 2(b)] a limiting saturation value of 80% is observed on the probe field.¹¹ As the modulation frequency ν is increased from 200 Hz to 5 kHz, corresponding to sweep rates ranging from 0.08 to 2 MHz/ μ sec, the height of the dip almost doubles, crossing into gain [Figs. 2(c) and 2(d)] with the amplification seen at the highest sweep rate [Fig. 2(e)] amounting to 35–40% of the unsaturated absorption. In these pictures the over-all curvature of the traces reflects the variation of laser intensity as it is tuned across the gain profile of its amplifying transition. For this set of data the peak saturating field intensity was 5 W/cm². The full width at half-maximum for the slow-sweep Lamb dip observed at 1.5 mTorr [Fig. 2(b)] is due to power broadening and is ~ 2 MHz. The known collision broadening parameter⁴ gives for this pressure a FWHM of 35 kHz corresponding to a T_2 of 4.5 μ sec.

In order to calculate the gain expected on the probe wave under our experimental conditions, it is necessary to consider the effect of level degeneracy, which is of importance because the various degenerate M_J transitions have different matrix elements: For a sweep rate consistent with condition (1), smaller matrix elements require higher power for condition (2) to be met. Hence, for a given power and sweep rate, the ARP conditions (1) and (2) may be satisfied to varying degrees for different matrix elements. Computer calculations including level degeneracy, for a probe field having polarization perpendicular to the saturating field,¹² indicate that a value of T_1 twice $T_2 = 4.5$ μ sec is in reasonable agreement with the experimental observations. It should be noted, however, that with the beam radius of 2.5 mm (1/e intensity) employed in these experiments, the molecular transit time through the laser field (≈ 5 μ sec) contributes to these relaxation effects. These results are thus not inconsistent with Loy's measurement of a collisionally induced population decay 5 times slower than T_2 in another transition in NH_3 .^{2,13}

Detailed studies of the pressure dependence of the observed relaxation effects and the extension to the study of the velocity dependence of T_1 using probe and saturating fields of different frequencies are currently in progress.

The authors wish to thank M. Ducloy, M.S. Feld, R.D. Sharma, and A. Szöke for useful discussions.

*Work supported by National Science Foundation, Air Force Cambridge Research Laboratories, Office of Naval Research, and Army Research Office, Durham.

¹A. Abragam, *The Principles of Nuclear Magnetism* (Oxford U.P., London, 1961).

²M.M.T. Loy, *Phys. Rev. Lett.* **32**, 814 (1974). An earlier attempt to observe optical ARP using laser frequency sweep is described in E.B. Treacy and A.J. DeMaria, *Phys. Lett. A* **29**, 369 (1969) and E.B. Treacy, *Ann. N.Y. Acad. Sci.* **168**, 400 (1970). These investigations were inconclusive as discussed in Ref. 2 of M.M.T. Loy's paper.

³S.M. Hamadani, A.T. Mattick, N.A. Kurnit, and A. Javan, *Bull. Am. Phys. Soc.* **19**, 1088 (1974).

⁴A.T. Mattick, A. Sanchez, N.A. Kurnit, and A. Javan, *Appl. Phys. Lett.* **23**, 675 (1973).

⁵E.V. Baklanov and V.P. Chebotayev, *Sov. Phys.-JETP* **33**, 300 (1971); S. Haroche and F. Hartmann, *Phys. Rev. A* **6**, 1280 (1972).

⁶Equations 1–3 follow from the requirement that the Bloch vector (see Ref. 7) be able to precess in a small cone which follows the direction of the instantaneous effective field $(\beta, 0, \Delta\omega)\hbar/\mu$.

⁷R.P. Feynman, F.L. Vernon, and R.W. Hellwarth, *J. Appl. Phys.* **28**, 49 (1957); I.D. Abella, N.A. Kurnit, and S.R. Hartmann, *Phys. Rev.* **141**, 391 (1966).

⁸D. Grischkowsky, in *Laser Applications to Optics and Spectroscopy*, edited by S.F. Jacobs, M. Sargent III, J.F. Scott, and M.O. Scully (Addison-Wesley, Reading, Mass., to be published). See also Refs. 1 and 2.

⁹F. Shimizu, *J. Chem. Phys.* **52**, 3572 (1970); *Appl. Phys. Lett.* **16**, 368 (1970); T. Shimizu and T. Oka, *Phys. Rev. A* **2**, 1177 (1970).

¹⁰The PZT was driven by a resonant LC circuit (utilizing also its mechanical resonances at higher frequencies) with drive voltage chopped at 20% duty cycle to prevent excessive heating. A laser with a shorter cavity would be more suitable for this application. Note that for this repetitive sweep, the

modulation period T must be kept much larger than the relaxation time T_1 in order to observe ARP.

¹¹The structure observed on the side of the resonance in Fig. 2(b) is due to hyperfine splitting and will be discussed elsewhere.

¹²For an axis of quantization chosen along the direction of polarization of the saturating field, this field causes $\Delta M = 0$ transitions, with $\beta_M = M \times 3.4 \times 10^6 \text{ sec}^{-1}$. Since the probe interacts most strongly with the $M = 0$ sublevel, which is not affected by the saturating field, the gain of the probe is at

most 91% of the unsaturated absorption even when conditions (1) and (2) are satisfied for $M = 1$ to 8.

¹³ T_1 -type relaxation dominantly arises from collision-induced decays into the various rotation-inversion levels in each vibrational state, and from elastic collisions appreciably changing v_z . Since collisional coupling is strongest to the inversion level of the same rotational state, more than one relaxation time may be necessary to characterize the decay of the population difference.

Measurement of Molecular-Alignment Relaxation Rate in NH_3 Using Non-Lorentzian Laser-Induced Saturation Resonances

J. R. R. Leite,^(a) M. Ducloy,^(b) A. Sanchez, D. Seligson, and M. S. Feld

*Department of Physics and Spectroscopy Laboratory, Massachusetts Institute of Technology,
Cambridge, Massachusetts 02139*

(Received 2 May 1977)

A general technique is presented in which narrow non-Lorentzian laser-induced resonances are used to study molecular reorientation. The experiments, which study the ν_2 as $Q(8, 7)$ NH_3 transition, yield a value of 6 ± 1 MHz/Torr for the excited-state alignment relaxation rate, 50% larger than the corresponding population relaxation rate.

The technique of laser-induced line narrowing in coupled three-level systems has been the subject of much recent work.^{1,2} Theoretical studies^{3,4} have shown that the shape of the narrow resonance is a sensitive function of the relaxation processes, and non-Lorentzian line shapes⁵ have been observed in neon.⁶ This Letter reports the

first application of this technique to study M -changing collisions in an infrared molecular transition.⁷⁻⁹ The non-Lorentzian line shapes thus observed are used to extract Zeeman-coherence (alignment) relaxation rates. Thus, the present technique complements the well-established technique of level crossing (Hanle effect) in optical

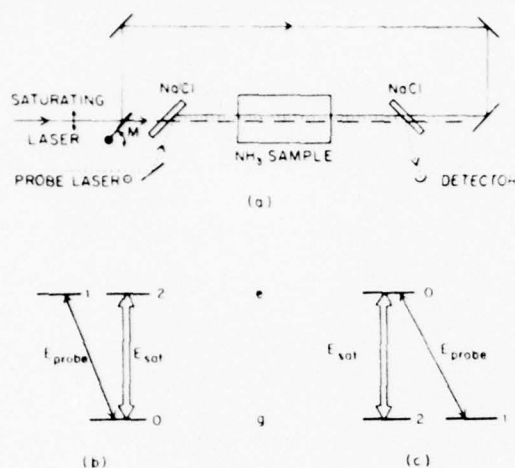


FIG. 1. (a) Experimental setup. (b), (c) Three-level system for common level in ground (b) and excited (c) states.

pumping experiments,¹⁰ and, as such, should be particularly useful for relaxation studies in systems where Stark and Zeeman effects are absent or fluorescence is difficult to observe.

In our experiments the $\nu_{2ASQ}(8,7)$ transition of NH_3 is saturated and probed using two cw N_2O lasers oscillating on the $P(13)$ $10.7\text{-}\mu\text{m}$ line, which falls within the NH_3 Doppler profile¹¹ [Fig. 1(a)]. The two beams overlap and can be adjusted to be copropagating or counterpropagating. Three-level systems are created using crossed linearly polarized fields for probe and saturating beams. The saturating field can be considered to induce $\Delta M = 0$ transitions, and the weak field then probes $\Delta M = \pm 1$ transitions. For weak saturation, in the

absence of M -changing collisions, the system decomposes into two groups of coupled three-level systems, having the common level in the NH_3 ground (g) and excited (e) states, respectively [Figs. 1(b) and 1(c)]. For each three-level system the intense field selectively saturates the $0 \rightarrow 2$ transition ($\Delta M = 0$) over a narrow range of molecular velocities. This produces a sharp change in transmission over a narrow frequency range as the probe field is tuned through the coupled $0 \rightarrow 1$ transition ($\Delta M = 1$). This change signal is composed of contributions due to saturation of the population of the common level (level 0), and to two quantum Raman-type² processes. As is well known, because of interference among components from different molecular velocity groups, the Raman-type processes are negligible in the counterpropagating case, and so probing in the "backward" direction gives rise to a simple Lorentzian line shape, as expected from population considerations. In contrast, in the forward direction (copropagating case) the contribution from Raman-type processes is large and gives rise to an additional line-shape feature in the form of a narrower Lorentzian superimposed on the population contribution.¹

When M -changing collisions occur the theoretical formalism is more complex, since such collisions couple together the independent three-level systems. The full degeneracy of the energy levels must then be included, and allowance made for the different relaxation rates of the various multipole moments of each level. With use of the tensorial formalism¹⁰ to describe these features, the following expression for the change-signal line shapes in the weak saturation limit can be derived:

$$g(\epsilon) = \text{Re} \mathcal{L}(2\Gamma) \sum_{\alpha, e, k} \{ 96/\gamma_{\alpha}^0 - 38/\gamma_{\alpha}^2 + \delta_{e,1} [57\mathcal{L}(\gamma_{\alpha}^2) + \mathcal{L}(\gamma_{\alpha}^1)] \}. \quad (1)$$

In Eq. (1) $\mathcal{L}(x) = (x + i\Delta)^{-1}$, where Δ is the detuning of the probe field from the center of the $\epsilon = \pm 1$ (± 1 forward, -1 backward) resonances. Γ is the relaxation rate of the optical (dipole) polarization and γ_{α}^k the K th-order multipole decay rate in level α (e, g): $K=0$, population; 1 , orientation; 2 , alignment. As seen in Eq. (1), the backward signal is still a single Lorentzian of width 2Γ while the forward signal is composed of various Lorentzian contributions. In the present experiments, the narrow feature of the forward signal is primarily determined by alignment relaxation processes (width γ_{α}^2).

Two features of Eq. (1) are exploited in analyzing

the data: (1) Forward and backward signals have equal areas¹²:

$$\int g(+)d\Delta = \int g(-)d\Delta. \quad (2)$$

(2) The ratio of the peak amplitudes of forward and backward signals is

$$\left[\frac{g(+)}{g(-)} \right]_{\Delta=0} = 1 + \frac{57\tau(2) + \tau(1)}{96\tau(0) - 38\tau(2)}, \quad (3)$$

where $\tau(K) = 1/\gamma_e^K + 1/\gamma_g^K$.

In the experimental setup [Fig. 1(a)] the two grating-tuned N_2O lasers, linearly polarized at right angles, were incident on a 10-cm NH_3 cell

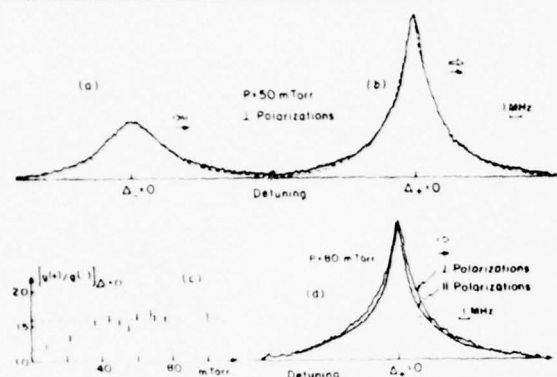


FIG. 2. (a), (b) Observed change signals, laser polarizations oriented at right angles. The dashed curves are calculated from Eq. (1) using the measured relaxation rates. (c) Ratio between peak height of forward and backward signals. The high-pressure limit gives $\gamma_e^2 = 6.0 \pm 1$ MHz/Torr. (d) Comparison of forward change signals using perpendicular and parallel polarizations.

having NaCl windows. A flip mirror (M) was used to reverse the direction of the saturating beam, and thereby select forward or backward configurations. Brewster-angle NaCl beam splitters were used to overlap the beams before the cell and separate them afterwards. The probe beam was monitored using a He-cooled Cu-Ge detector. The Doppler background was eliminated by chopping the saturating beam at 1.2 kHz and using phase-sensitive detection. The short-term (≈ 0.1 sec) frequency jitter of both lasers was less than 100 kHz, and amplitude fluctuations were less than $\frac{1}{2}\%$. Care was taken to insure that both lasers were operating in the TEM₀₀ mode.

In the experiments the frequency of the saturating laser was set close to its line center, and the probe laser was tuned over a ± 35 -MHz range by means of a calibrated piezoelectric transducer (error $< 5\%$). To avoid saturation broadening, the powers of saturating and probe lasers were kept below 15 and 3 mW, respectively. Beam radii of both lasers were 3 mm. Typical experimental traces are shown in Figs. 2(a) and 2(b).

Although all of the relevant rates can be obtained from analysis of our data, several of these have already been established for the $asQ(8,7)$ transition. The backward signal is Lorentzian and its linewidth yields $\Gamma = 24 \pm 1$ MHz/Torr, in agreement with earlier Lamb-dip measurements.¹³ For the population decay, $\gamma_e^0 = 24 \pm 1$ MHz/Torr for the ground state¹⁴ and $\gamma_e^0 = 3.0 \pm 0.8$ MHz/Torr for the excited state.¹⁵ As explained below, these values, which our data confirm, are used in our

analysis to measure γ_e^2 , the excited-state alignment decay rate, which has not previously been determined. As pointed out by Loy,¹⁶ the much larger value of γ_e^0 as compared to that of γ_e^2 is due to the dominance of dipole-dipole inelastic collisions when both collision partners are in the NH₃ ground state (inversion splitting ~ 0.8 cm⁻¹), where the dipole moment does not invert during a collision, as opposed to the case when one of the collision partners is in the excited state (inversion splitting ~ 35 cm⁻¹), where rapid inversion reduces the dipole-dipole interaction probability. Thus, we can expect that in the NH₃ ground state, inelastic collisions dominate, and all the relaxation rates are equal. This is confirmed in the experiments of Ref. 12, in which it was found that in an NH₃ ground-state microwave transition $T_1 = T_2$. Accordingly, in our analysis we set $\gamma_e^2 = \gamma_e^0$.

With these choices for the decay parameters the change-signal expressions $g(\pm)$ become functions of the single unknown parameter γ_e^2 , if we neglect the small contribution from orientation. In fact, it should be possible to obtain γ_e^2 directly from the observed forward-backward peak-height ratio, Eq. (3), without the need of a complete line-shape analysis.

However, in the data the change-signal areas are not equal because the observed resonances are proportional to the effective intensity of the saturating field, which differs in forward and backward directions because of differences in misalignment and attenuation of the saturating beam intensity. Accordingly, in analyzing the data the amplitude scales are chosen such that the areas of the forward and backward change signal are equal, as required by Eq. (2). The resulting peak height ratio of 1.58 ± 0.10 [Fig. 2(c)] gives $\gamma_e^2 = 6.0 \pm 1.0$ MHz/Torr. Using this value, along with the other decay rates in Eq. (1), we obtain theoretical line shapes which are in excellent agreement with the experiment [dashed line of Figs. 2(a) and 2(b)]. The experimentally measured peak-height ratio [Fig. 2(c)] is pressure independent only above 30 mTorr. Below this value pressure-independent mechanisms (transit time, geometrical broadening, and laser frequency fluctuations), as well as velocity-changing collisions,¹³ are expected to influence dramatically the width of the narrow component. Their net effect is to broaden the width and reduce the amplitude of the narrow signal, relative to the broad one. This causes the height ratio to decrease [Fig. 2(c)].

In the foregoing experiments the non-Lorentzian forward change signal was produced using applied fields having crossed polarizations. To demonstrate the inherent polarization dependence of the line shape, similar experiments were done in which the probe-field polarization was oriented parallel to that of the saturating field by inserting a half-wave plate in the path of the saturating beam. A small misalignment¹⁷ was introduced to separate the beams. Figure 2(d) compares the resulting line shape to that of the crossed-field

case, normalized such that the peak heights of the two signals are equal.

Since two electromagnetic waves of the same polarization and same propagation vector are equivalent to an amplitude-modulated excitation, a new type of contribution now occurs, originating in the coherent modulation of the populations at the frequency difference between pump and probe fields. This effect causes additional narrowing of the forward signal if $\gamma_e^0 < \gamma_e^2$. With the use of the tensorial formalism,¹⁰ the change-signal line shape is now given by

$$g_{\parallel}(\epsilon) = \text{Re} \mathcal{L}(2\Gamma) \sum_{\alpha=\pm,0} \{ 96/\gamma_{\alpha}^0 + 76/\gamma_{\alpha}^2 + \delta_{\epsilon,1} [96\mathcal{L}(\gamma_{\alpha}^0) + 76\mathcal{L}(\gamma_{\alpha}^2)] \}. \quad (4)$$

In this case for $p > 30$ mTorr the measured forward-backward peak-height ratio is 1.9 ± 0.15 , in excellent agreement with the value of 2 predicted by Eq. (4). This represents a good check of our normalization procedure. The observed narrowing of the line shape for parallel polarization [Fig. 2(d)] is another clear evidence of M -changing collisions, since for $\gamma_{\alpha}^K = \gamma_{\alpha}^0$ Eqs. (1) and (4) predict the same line shape, contrary to the experimental results. A computer fit of the signal line shape using Eq. (4) confirms the value used for γ_e^0 (3.9 MHz/Torr). We also observe that, as predicted by (1) and (4), the backward signal is independent of the relative polarizations, and yields the same value for Γ .

The good agreement obtained here between experimental and theoretical line shapes demonstrates the usefulness of laser-induced line narrowing as a novel technique for studying M -changing collisions. The success of the model adopted, which does not include velocity-changing collisions, indicates that contributions from such collisions are negligible in NH_3 above 30 mTorr. The measured value for γ_e^2 (6 MHz/Torr) shows that in the NH_3 excited state, alignment-destroying collisions are 50% more probable than are inelastic collisions (4 MHz/Torr). The excess, 2 MHz/Torr, corresponds to the elastic M -changing collisions which are induced by the anisotropic part of the $\text{NH}_3(g)$ - $\text{NH}_3(c)$ interaction potential. The interpretation of the above result, which necessitates the knowledge of the various contributions to the interaction potential (such as dipole-quadrupole, quadrupole-quadrupole, etc.), is under way. Finally, we note the complementarity of our work to the ones by Ouhayoun,⁷ Shoemaker, Stenholm, and Brewer⁸ and Johns *et al.*,⁹ where M -changing collisions have been analyzed by observing narrow change signals in Stark-split

sublevel transitions. The originality of our technique is that it does not need any external (Stark or Zeeman) field, and that it gives a straightforward interpretation in terms of tensorial relaxation rates.

The authors thank P. Berman, M. Gorlicki, and H. Fetterman for useful comments and L. W. Ryan, Jr., for expert technical assistance. This work was supported in part by the National Science Foundation and the U. S. Army Research Office (Durham). The work of one of us (J.R.R.L.) was partially supported by the Conselho Nacional de Pesquisas. Another of us (M.S.F.) is in receipt of an Alfred P. Sloan Foundation Fellowship.

^(a) Present address: Universidade Federal de Pernambuco, Recife, Brazil.

^(b) Present address: Laboratoire de Physique des Lasers, Université Paris-Nord, 93430 Villetaneuse, France.

¹ V. P. Chebotaev, in *Topics in Applied Physics*, edited by K. Shimoda (Springer, Berlin, 1976), Vol. 13, p. 201.

² M. S. Feld, in *Fundamental and Applied Laser Physics*, edited by M. S. Feld, A. Javan, and N. A. Kurnit (Wiley, New York, 1973), p. 369.

³ S. G. Rautian, G. I. Smirnov, and A. M. Shalagin, *Zh. Eksp. Teor. Fiz.* **62**, 2097 (1972) [*Sov. Phys. JETP* **35**, 1095 (1972)]; A. I. Burshtein, E. G. Saprykin, and G. I. Smirnov, *Zh. Eksp. Teor. Fiz.* **66**, 1570 (1974) [*Sov. Phys. JETP* **39**, 769 (1974)].

⁴ P. R. Berman, *Phys. Rev.* **13**, 2191 (1976).

⁵ Im Thek-de, S. G. Rautian, E. G. Saprykin, G. I. Smirnov, and A. M. Shalagin, *Zh. Eksp. Teor. Fiz.* **62**, 1666 (1972) [*Sov. Phys. JETP* **35**, 865 (1972)]; Yu. A. Vdovin, V. M. Ermachenko, A. I. Popov, and E. D. Protchenko *Pis'ma Zh. Eksp. Teor. Fiz.* **15**, 401 (1972) [*JETP Lett.* **15**, 282 (1972)]; C. V. Shank and S. E. Schwartz, *Appl. Phys. Lett.* **13**, 113 (1968).

⁹W. J. Tomlinson and R. L. Fork [Phys. Rev. Lett. **20**, 647 (1968)] have measured such relaxation rates by studying the output behavior of a Zeeman-tuned He-Ne laser.

¹⁰Using Stark splitting, M -changing collision effects have been observed in NH_3 by M. Ouhayoun, Colloq. Int. C.N.R.S. **217**, 155 (1974). For other detailed studies see R. L. Shoemaker, S. S. Stenholm, and R. G. Brewer, Phys. Rev. A **10**, 2037 (1974); J. W. C. Johns, A. R. W. McKellar, T. Oka, and M. Römhild, J. Chem. Phys. **62**, 1488 (1975).

¹¹Shoemaker, Stenholm, and Brewer, Ref. 7.

¹²Johns, McKellar, Oka, and Römhild, Ref. 7.

¹³See, for instance, B. Decomps, M. Dumont, and M. Ducloy, in *Laser Spectroscopy of Atoms and Molecules*, edited by H. Walther (Springer, Berlin, 1976), p. 283.

¹⁴T. Shimizu and T. Oka, Phys. Rev. A **2**, 1177 (1970).

¹⁵B. J. Feldman and M. S. Feld, Phys. Rev. A **12**, 1013, (1975).

¹⁶A. T. Mattick, N. A. Kurnit, and A. Javan, Chem. Phys. Lett. **38**, 176 (1976).

¹⁷G. M. Dobbs, R. H. Mischeels, J. Steinfeld, J. H. S. Wang, and J. M. Levy, J. Chem. Phys. **63**, 1904 (1975).

¹⁸S. M. Hamadani, A. T. Mattick, N. A. Kurnit, and A. Javan, Appl. Phys. Lett. **27**, 21 (1975); S. M. Hamadani, Ph.D. thesis, Massachusetts Institute of Technology, 1976 (unpublished).

¹⁹M. M. T. Loy, Phys. Rev. Lett. **32**, 814 (1974).

²⁰The linewidth contribution from transit time and misalignment is $\Delta\gamma \approx (1 + \psi a/\lambda)u/a$, where ψ is the misalignment angle, a is the beam diameter, and u is the thermal velocity. Since the resolution of the two beams (at the detector) requires $\psi \ll \lambda/a$, the geometrical contribution is necessarily greater than that due to transit time. In our experiment $\gamma \approx 10$ mrad, so that $\Delta\gamma \approx 250$ kHz.

ENERGY ABSORPTION AND VIBRATIONAL EXCITATION BY
INTENSE LASER PULSES

R. E. McNair,^{*} R. Forber, S. F. Fulghum, G. W. Flynn,[#] M. S. Feld

Department of Physics and Spectroscopy Laboratory

Massachusetts Institute of Technology

Cambridge, Massachusetts 02139

B. J. Feldman

Los Alamos Scientific Laboratory

Los Alamos, New Mexico 87545

ABSTRACT

Theoretical and experimental studies are made of the energy flow into and among the vibrational degrees of freedom of polyatomic molecules due to V-V collisions following intense laser excitation. Simple ~~closed~~ ^{some} ~~form~~ expressions are derived for predicting the energy extracted by diatomic and polyatomic molecules from a saturating laser pulse. A new method for measuring the energy stored in the vibrational degrees of freedom is introduced and a model for predicting the steady state partitioning of energy in polyatomics is applied to CH₃F.

^{*}Present address: Hughes Research Laboratories, Malibu, California 90265

[#]Present address: Department of Chemistry, Columbia University, New York, NY

I. INTRODUCTION

The interaction of intense laser fields with molecular systems and the subsequent inter-molecular processes is an area of great interest among physicists and chemists. The laser has become an excellent tool for probing the flow of energy within the internal degrees of freedom of a molecule, and it provides a powerful method for obtaining high levels of excitation. Conversely, the increased knowledge of energy absorption, transfer, and relaxation processes in molecules has led to new and improved lasers, with many more possibilities ahead.

Very little is known about the detailed kinetics involved in the energy absorption process in molecules, nor has the redistribution of absorbed energy among the vibrational degrees of freedom of polyatomics been fully understood. Because of the spectroscopic complexities and the lack of information on interaction potentials, collisional rate constants and energy flow mechanisms, polyatomic molecules have not been investigated as thoroughly as some diatomics.

This paper presents a detailed theoretical and experimental study of energy absorption and transfer in a polyatomic molecule from intense resonant laser pulses in the regime where the energy flow is determined by V-V collisions. This is different from the studies of Letokhov and others, ()

which are concerned with collisionless cascade excitations characteristic of shorter, more intense laser pulses.

The theoretical work investigates both a single mode oscillator and one with two collisionally-coupled modes. We use the collisional rate equations for vibrational energy transfer, as in the works of Shuler and others,^() with the addition of two important features: (1) a laser pumping term, and (2) the assumption of a quasi-equilibrium among the vibrational levels not directly connected to the laser field, which provides a relationship between the populations of all the levels. In the case of a single mode oscillator, simple expressions are derived for predicting the energy absorbed during the laser excitation. The addition of one other vibrational mode, collisionally coupled to the first, is considered in some detail. A general formula is derived and discussed in relation to the one mode case; it is found that the influence of the second mode on the absorption process dramatically depends on its energy spacing relative to the spacing on the energy absorbing mode. Numerical solutions of the population rate of change equations are used to justify the quasi-equilibrium assumptions, and the agreement with theory is quite good.

The experimental work studies the absorption of the P(32) line of CO₂ by ¹³CH₃F, and the subsequent energy transfer among the modes of the molecule. Fitting the single mode model to the measured absorption leads to a determination of γ_{VV} , the VV collision rate constant for the ν_3 mode. In addition,

the partitioning of the absorbed energy among the several vibrational modes is determined by means of a technique for measuring the absolute energy stored in a particular mode. This technique, which involves the use of a "cold gas" filter, is described in detail. Knowledge of the partitioning of energy then allows confirmation of a specific flow path for the transfer of energy between the modes of CH_3F .

Interest in laser development, laser induced chemical reactions, and chemical lasers requires a detailed understanding of the molecular processes involved. The rate constants and paths of energy flow during and after excitation govern the gain, power outputs, reaction rates, mode specific excitation, etc. Once the transient mechanisms of energy absorption and transfer are understood, a vast set of applications await them. It is hoped that the present work contributes to that understanding.

Some of the concepts and data presented here are outlined in Reference . A detailed treatment is given here.

II. THEORY

A. Introduction

Consider the interaction of a resonant laser pulse of carrier frequency ω and duration τ_p with a particular rotational-vibrational transition from the ground vibrational state of a

molecule to its first excited vibrational state (Fig. 1a).

The amount of energy the molecule can absorb depends on τ_p .

As τ_p is increased three distinct regimes can be considered.

1) When τ_p is short compared to the rotational relaxation time, τ_{RR} , then only the fractional population Z_J of molecules in the particular rotational state J of the ground vibrational state can be excited. Therefore, if the pulse is intense enough () to saturate the transition then only the energy $\frac{1}{2}Z_J\hbar\omega$ can be absorbed by the molecule on the average.

2) When τ_p is on the order of τ_{RR}/Z_J then the rotational populations of both the upper and lower vibrational states have time to reach a new equilibrium during the laser pulse. In this case the total population in the upper and lower vibrational states can equalize, and the average energy absorbed by the molecule is $\frac{1}{2}\hbar\omega$.

3) When τ_p is longer than the characteristic time for vibrational-vibrational energy exchanging collisions, τ_{VV} , and both times are longer than τ_{RR}/Z_J then additional energy can be absorbed and stored by the molecule as vibrational energy. () When this condition is satisfied the rotational structure becomes unimportant and the system reduces to that of a simple vibrational oscillator. This last regime is the subject

of this work.

For example consider the process in which two molecules in the $v = 1$ state collide and exchange energy, producing one molecule in the $v = 2$ state and one of the $v = 0$ state. The result is that energy has been carried up the vibrational ladder and a molecule has been returned to the ground state where it can again absorb energy from the laser. Energy will continue to be absorbed through processes of this kind, until the laser pulse length becomes comparable to τ_{VT} , the characteristic time for translational energy transfer. Thus, under appropriate conditions many quanta can be stored as vibrational energy.

This process is analyzed theoretically in the following sections. Section II.B. treats the case of a molecule with only one vibrational mode, as in a diatomic molecule. In Section II.C. the addition of another vibrational mode is considered, in an attempt to obtain an understanding of the vibrational energy absorption process in a polyatomic molecule such as CH_3F . Computer results will be used throughout to verify the analytical results and check the assumptions. A treatment of the conditions necessary for ignoring the rotational structure is given in the Appendix.

B. One Mode Model

If we denote P_v as the probability of a molecule being in state v , where the density in state v is $N_v = P_v N$ (N is the

total number density of molecules in the system), the rate equations describing the interaction of the laser with the oscillator system may be written as

$$\begin{aligned} \frac{dP_0}{dt} &= \left. \frac{\partial P_0}{\partial t} \right|_c - \gamma_p (P_0 - P_1) \\ \frac{dP_1}{dt} &= \left. \frac{\partial P_1}{\partial t} \right|_c + \gamma_p (P_0 - P_1) \\ \frac{dP_v}{dt} &= \left. \frac{\partial P_v}{\partial t} \right|_c \quad v \geq 2 \end{aligned} \quad (1)$$

where $\partial P_v / \partial t|_c$ is the contribution due to V-V collisions and γ_p is the effective rate constant describing the energy flow into the system due to stimulated emission and collisions. [The expression for γ_p is given in Eq. (A-15) of the Appendix.] This expression assumes that the laser pulse duration is sufficient so that the rotational structure can be ignored (the conditions are given in the Appendix), and that the laser intensity is such as to only couple to the $v = 0 \rightarrow 1$ vibrational transition, collisionless multiple photon absorption processes being negligible. Relaxation due to VT processes is also assumed to be unimportant, as in the case when $\tau_p \ll \tau_{VT}$. The treatment will be generalized to include VT processes below.

If we assume resonant binary V V processes, and dipole-dipole collisions in the harmonic oscillator approximation, the process has a probability rate

Therefore, the collision part of the coupled rate equations can be written as ()

$$\left. \frac{\partial P_v}{\partial t} \right|_c = \frac{\gamma_{vv}}{2} \sum_{v'=0}^{\infty} \left\{ (v+1)v' [P_{v+1} P_{v'-1} - P_v P_{v'}] + (v'+1)v [P_{v-1} P_{v'+1} - P_v P_{v'}] \right\} \quad (2)$$

Here γ_{VV} is defined such that for an isolated three level system ($v = 0, 1, 2$),

$$\frac{dP_v}{dt} = \frac{\partial P_v}{\partial t} \Big|_c = 2\gamma_{vv} (P_2 P_0 - P_1 P_1) \quad ,$$

where γ_{VV} is the characteristic "up the ladder" collision rate. () Equation (2) may be simplified by using the condition of number conservation

$$\sum_{v=0}^{\infty} P_v = 1 \quad , \quad (3)$$

and noting that the mean number of quanta stored in an oscillator is given by

$$\epsilon = \sum_{v=0}^{\infty} v P_v = \frac{\text{vibrational energy} / \hbar \omega}{\text{molecule}} \quad . \quad (4)$$

Thus,

$$\frac{\partial P_v}{\partial t} \Big|_c = \frac{\gamma_{vv}}{2} \left\{ -[(2v+1)\epsilon + v] P_v + v\epsilon P_{v-1} + (v+1)(\epsilon+1) P_{v+1} \right\} \quad . \quad (5)$$

We now wish to examine the problem in the limit in which the laser saturates the $v = 0 \rightarrow 1$ transition () such that

$$\frac{dP_0}{dt} \approx \frac{dP_1}{dt} \quad (6)$$

That is, the time rate of change of levels 0 and 1 are locked together, so that if one changes the other follows. Therefore, using Eqs. (1)

$$P_0 - P_1 = \frac{1}{2\gamma_p} \left[\left. \frac{\partial P_0}{\partial t} \right|_c - \left. \frac{\partial P_1}{\partial t} \right|_c \right]$$

Thus, it can be seen from Eq. (5) that $P_0 - P_1$ is at most of order $\gamma_{VV}/2\gamma_p$. So, if

$$\gamma_{VV} \ll 2\gamma_p, \quad (7)$$

then

$$P_0 \approx P_1 \quad (8)$$

Accordingly, (7) is a sufficient condition for equalizing the populations of the $v = 0$ and $v = 1$ levels for all time, and thus insures (8) and (6). Note, however, that we must allow the product $\gamma_p(P_0 - P_1)$ to be non-zero, but as yet unspecified.

Let us now find an expression for the time rate of change of vibrational energy per molecule. Taking the derivative of Eq. (4) and using Eqs. (1)

$$\dot{E} = \sum_{v=0}^{\infty} v \frac{dP_v}{dt} = \sum_{v=0}^{\infty} v \left. \frac{\partial P_v}{\partial t} \right|_c + \gamma_p(P_0 - P_1)$$

Substituting Eq. (5) one obtains $\sum_{v=0}^{\infty} v \left. \frac{\partial P_v}{\partial t} \right|_c \equiv 0$, as expected, since energy is conserved in the collisions in this model.

Thus,

$$\dot{\epsilon} = \gamma_p (P_0 - P_1) , \quad (9)$$

and the rate equations become

$$\dot{P}_0 = \left. \frac{\partial P_0}{\partial t} \right|_c - \dot{\epsilon} , \quad (10a)$$

$$\dot{P}_1 = \left. \frac{\partial P_1}{\partial t} \right|_c + \dot{\epsilon} , \quad (10b)$$

$$\dot{P}_v = \left. \frac{\partial P_v}{\partial t} \right|_c \quad v \geq 2 . \quad (10c)$$

The $\dot{\epsilon}$ term may be considered as a perturbation, not necessarily small, on the usual collisional relaxation. The VV processes attempt to drive all the populations to a Boltzmann equilibrium, () but the $\dot{\epsilon}$ term offsets the process by maintaining nearly equal populations in $v = 0$ and $v = 1$. As a result, VV collisions pump molecules to higher vibrational levels, with the laser supplying the necessary energy.

Using Eqs. (5) and (10) with $P_0 = P_1$ and $\dot{P}_0 = \dot{P}_1$

$$\dot{\epsilon} = \frac{\gamma_{vw}}{2} P_1 - \dot{P}_1 . \quad (11)$$

This equation gives ϵ once $P_1(t)$ is known. Conversely, $P_1(t)$ can be found once ϵ is specified as a function of t or P_1 . The fact is, $\dot{\epsilon} = \gamma_p (P_0 - P_1)$ is an unspecified parameter other than the requirement $P_0(t) \approx P_1(t)$.

This difficulty can be overcome by taking advantage of the fact that the vibrational levels $v \geq 2$ are all in

equilibrium with respect to the $v = 1$ level. This can be understood in the following way. With $P_0 = P_1$ the tendency of the collision terms in Eqs. (10a) and (10b) is to increase P_0 and decrease P_1 [cf. Eq. (2)]. However, the $\dot{\epsilon}$ terms in these two expressions oppose these changes and sufficiently retards the relaxation of these two levels so that they can be considered slowly varying on the VV time scale.^() The remainder of the levels then come into equilibrium with the $v = 1$ level in a time $1/\gamma_{vv}$. Thus, the vibrational populations can be described by an effective temperature in the form

$$\begin{aligned} P_0 &= P_1 \equiv P \\ P_v &= P e^{-(v-1)\theta} \end{aligned} \quad (12)$$

where $\theta = \hbar\omega/kT_v$, with T_v being the time-dependent effective vibrational temperature of the $v = 1 \rightarrow \infty$ vibrational levels relative to the $v = 1$ level. This assumed time dependent quasi-equilibrium distribution is verified by computer solutions of Eqs. (1) and (2). Figure compares the distribution of Eq. (12) with the rate equation predictions for a value of $\gamma_p/\gamma_{vv} \approx 100$. As can be seen, the overall agreement is excellent. The small discrepancies are inconsequential, since $\epsilon(t)$ is determined by a sum over the P_v 's and is not very sensitive to individual values.

Substituting (12) into (3) and (4), and solving for ϵ in terms of P

$$\epsilon = (1-P)^2/P \quad (13)$$

and

$$\dot{\epsilon} = - \frac{1-P^2}{P^2} \dot{P} \quad (14)$$

This gives an independent expression for $\dot{\epsilon}(P)$, as desired. Equating the two expressions for $\dot{\epsilon}$, (11) and (14), one obtains a differential equation for P

$$\dot{P} \left[2 - \frac{1}{P^2} \right] = \frac{\gamma_{VV}}{2} P \quad (15)$$

which can be easily integrated subject to the relevant boundary conditions. Since the laser saturates the $v = 0 \rightarrow 1$ transition on a time scale substantially shorter than the characteristic VV time [see Eq. (7)], the appropriate boundary conditions are

$$P(t=0) = P_i(t=0) = P_o(t=0) = \frac{1}{2} \quad (16)$$

Thus

$$\frac{1}{P^2} + 4 \ln 2P = \gamma_{VV} \tau_p + 4 \quad (17)$$

This simple expression, together with Eq. (13), determines the number of quanta per molecule absorbed. Note that ϵ is entirely determined by the product of the VV rate constant and the laser pulse duration, which is roughly the number of V-V collisions occurring during the laser pulse. Neither the laser intensity

nor any other parameters enter in. Values of $\epsilon(t)$ predicted by Eqs. (17) and (13) are in precise agreement with computer solutions of the coupled rate equations (1,2) (Fig.).

This solution has interesting forms for the limiting values of $\gamma_{VV}\tau_p$. For $\gamma_{VV}\tau_p \ll 1$, $P(\gamma_{VV}\tau_p)$ doesn't change much from its initial value and

$$\epsilon \approx \frac{1}{2} + \frac{3}{8} \gamma_{VV} \tau_p \quad . \quad (18a)$$

Thus, in the initial part of the pulse the energy stored increases linearly with time. In the other extreme, when $\gamma_{VV}\tau_p \gg 1$, $P(\gamma_{VV}\tau_p) \ll 1$ and consequently

$$\epsilon \approx \sqrt{\gamma_{VV} \tau_p} \quad (18b)$$

This expresses the fact that the energy absorption becomes more like a random walk ($\gamma_{VV}\tau_p$ = number of VV collisions), since higher states are populated and energy can flow down the vibrational ladder, as well as up. Furthermore, in these two limits

$$\dot{P}_0 \approx \dot{P}_1 \approx -\frac{1}{8} \gamma_{VV} \quad , \quad \gamma_{VV} t \ll 1$$

$$\dot{P}_0 \approx \dot{P}_1 \approx -\frac{1}{2(\gamma_{VV} t)^{3/2}} \gamma_{VV} \quad , \quad \gamma_{VV} t \gg 1$$

so that P_0 and P_1 do change at a rate substantially slower than the characteristic VV rate, γ_{VV} , which is consistent with assumption (12).

According to the results so far, any desired amount of

of laser energy can be transferred to the molecule by using a laser pulse of sufficiently long duration. In actuality, vibration-to-translation (VT) relaxation processes place an upper limit on the maximum amount of stored energy. For pulses exceeding τ_{VT} , the VT relaxation time, some of the stored vibrational energy will be converted to translational energy. Thus, for $\tau_p \sim \tau_{VT}$ the amount of stored vibrational energy reaches a limiting value.

To include the influence of VT processes one must include this interaction in the rate equations. For this the term

$$\gamma_{VT} \left[(v+1) (P_{v+1} - \eta P_v) - v (P_v - \eta P_{v-1}) \right]$$

must be added to each of Eqs. (1), where $\gamma_{VT} = \tau_{VT}^{-1}$ is the VT relaxation rate^(*) and η is given by $\eta = e^{-\hbar\omega/kT}$, as is necessary for detailed balancing.^(*) In this case Eq. (9) becomes

$$\dot{\epsilon} + \gamma_{VT} (\epsilon - \eta(\epsilon+1)) = \gamma_p (P_0 - P_1) .$$

using the expression for the laser pumping term in the revised Eqs. (1), with $P_0 = P_1$ and $\dot{P}_0 = \dot{P}_1$, and the expressions for ϵ and $\dot{\epsilon}$ from the temperature assumption [Eqs. (13), (14)], the differential equation for P becomes

* When the system comes into thermal equilibrium (i.e. the vibrational temperature equal to kinetic temperature, T) this choice of η causes $\frac{\partial P_v}{\partial t} \text{ VT Coll} \equiv 0$.

$$\dot{P} \left[2 - \frac{1}{P^2} \right] = \frac{\gamma_{VV}}{2} P - \gamma_{VT} \left[(1-\eta) \frac{1}{P} - (2-\eta) \right]. \quad (19)$$

This can be integrated with the initial condition,

$P(t=0) = 1/2$, as before. For $\eta \ll 1$ and $\gamma_{VV} \gg \gamma_{VT}$

(the usual case) the energy per molecule is

$$\frac{E}{\hbar\omega} = \epsilon(\tau_p) \approx \sqrt{\frac{\gamma_{VV}}{2\gamma_{VT}}} \left(1 - \frac{1}{2} e^{-2\gamma_{VT}\tau_p} \right), \quad (20)$$

valid for $\tau_p \geq \tau_{VT}$. Thus, for laser pulses longer than a few τ_{VT} the number of quanta per molecule reaches the limiting value $\sqrt{\gamma_{VV}/2\gamma_{VT}}$. Thus, VT processes place an upper limit on the amount of laser energy which can be vibrationally stored in the molecule.

Finally, Eqs. (1) with VT interaction but without the laser (after the laser pulse is terminated) have the expected solution for $t > \tau_p$ $\epsilon(t) = \epsilon_0 + [\epsilon(\tau_p) - \epsilon_0] \exp [-(1-\eta)\gamma_{VT}(t-\tau_p)]$ where $\epsilon_0 \equiv \eta/(1-\eta)$ is the energy of the oscillator system at room temperature.

It should be noted that this model becomes inadequate for cases in which the laser induces substantial population into high lying levels in which there is a significant degree of anharmonicity. This is so because an anharmonic oscillator does not evolve toward equilibrium through a continuous series of Boltzmann-like distributions, () hence assumption (12) becomes inadequate. To get an idea of when this effect becomes important assume that the temperature assumption of Eqs. (12) is still approximately valid and notice that Eqs. (3) and (4) for small P lead to

$$P_v \approx P e^{-(v-1)/\epsilon}$$

Thus, if the degree of anharmonicity is not significant up to vibrational level $v = 10$, for instance, then the model remains valid for energy absorption of up to 4 or 5 photons. After that anharmonicity effects such as bottlenecking, Trainor pumping, etc. () may become important.

III. ENERGY ABSORPTION IN METHYL FLUORIDE (CH_3F)

A. Relevant Properties

The energy absorption from an intense laser pulse and subsequent vibrational partitioning, induced by vibrational collisions, have been studied in methyl fluoride. This molecule was chosen because of several features which make it well suited for our studies. The attractive features of methyl fluoride are: (a) A strong $\text{C}^{13}\text{H}_3\text{F}$ absorption resonance coincides with a strong CO_2 laser line⁽³⁾, (b) in methyl fluoride the relaxation processes obey the relations $\tau_{V-T} \ll \tau_{V-V} \ll \tau_{R-R}$ ⁽¹⁹⁾, (c) its energy flow path and kinetics in the low excitation regime has been well established, and (d) fluorescence observed from emission by the vibrational modes make it possible to study partitioning of the vibrational energy after the laser excitation process is completed.

Strong fluorescence from the C-F stretch mode, ν_3 near $9.6 \mu\text{m}$, and the C-H stretch, ν_1 and ν_4 near $3.4 \mu\text{m}$, have been observed.⁽³⁾ Weaker but observable emissions also have been reported from the bending modes, ν_2 and ν_5 , near $6.8 \mu\text{m}$ and the methyl rock mode, ν_6 near $8.8 \mu\text{m}$.⁽⁴⁾ (ν_4, ν_5 , and ν_6 are all doubly degenerate modes.)

These fluorescing modes have provided much information about relaxation processes in methyl fluoride. The rotational relaxation time in methyl fluoride, measured from pressure broadening data, was reported to be 8×10^{-9} sec.⁽¹⁵⁾ τ_{V-V} and τ_{V-T} have been determined from laser induced fluorescence techniques with reported values of $0.83 \mu\text{sec-torr}$ ⁽¹⁹⁾ and 1.69 msec-torr ⁽³⁾, respectively.

B. Experiment

The 2.165 μm P(32) TEA CO_2 laser line falls within 25 MHz of the ν_3 ($V = 0 \rightarrow 1$) R(4,3) transition of $^{13}\text{CH}_3\text{F}$. Laser pulses were typically 2-3 μsec duration with energies ≤ 0.25 Joules, small enough to avoid appreciable absorption by collisionless processes, (16,17) but sufficiently large to ensure complete saturation of the Doppler profile. Single mode output of the grating coupled ^{laser oscillat-} cavity was ensured by placing apertures inside the cavity. Care was taken to avoid mode locking which could produce ambiguities in the data analysis. The long pulses, necessary to insure many V-V collisions during the laser excitation process, were obtained by adjusting the nitrogen content of the laser gas mixture.

The laser output, collimated to a 6 mm spotsize, was passed through an 18 cm glass absorption cell. A KCl beam splitter was placed in front of the cell to sample a portion of the incident beam for monitoring. Both the sample beam and the transmitted beam were scattered off coarse aluminum surfaces to avoid the viewing of hot spots by two Au:Ge detectors whose outputs were integrated by an RC circuit and viewed on a dual beam oscilloscope. A Scientech 362 energy-power meter was used to calibrate the detectors and establish their linearity. Gas samples used were 90% $^{13}\text{CH}_3\text{F}$ and 10% $^{12}\text{CH}_3\text{F}$ from Merk, Sharp, and Dohme of Canada. The appropriate factors for the isotopic purities used were included in all analysis.

The volume of the interaction region was carefully estimated to within 10%. The number of CO_2 quanta absorbed, \bar{Q} , was obtained by measuring the amount of energy absorbed from the laser beam and

dividing by the number of molecules in the interaction region.

The data points of Figure ^{SF2} 4a give the measured number of CO₂ quanta absorbed vs ¹³CH₃F pressure. As can be seen, \bar{q} rises monotonically up to a value of 2.6 quanta absorbed at 6.0 torr, at which point it starts to decrease. This decline is due to absorption of the laser pulse as it transverses the gas sample. As explained in the previous section, the condition, $I > (500 \sigma_{\text{abs}}) \gamma_{\text{V-V}} \tau_p$ must be satisfied in order for efficient vibrational heating to occur. At higher pressure, however, sufficient attenuation occurs so that the laser intensity is reduced below this value before the end of the sample cell, leading to a reduction in V-V heating efficiency. ⁽⁵⁾ The use of a shorter cell would not have permitted sufficient observable absorption for accurate measurements below 3.0 torr.

The data was analyzed using the model discussed in Section III. The assumptions made in the derivation,

$$\tau_{\text{RR}} < \tau_{\text{V-V}} < \tau_p < \tau_{\text{V-T}},$$

are all satisfied in CH₃F. As explained in Section II, analytical result of eq. 15 should be accurate to within 20%; accordingly, this simple expression was used. Taking the experimental value of laser pulse duration, $\tau_p \approx 3$ psec, eq. 15 was fit to the data points of figure ^{SF2} 4a by varying the single parameter $\gamma_{\text{V-V}}$. The best fit (solid curve of figure ^{SF2} 4a) resulted in a value of $\gamma_{\text{V-V}} = 0.8 \pm 0.2 \text{ psec}^{-1} \text{ torr}^{-1}$. No significant improvement in fit could be gained by using the two mode computer model of Section II. The principle sources of error in the quoted value are uncertainty in the beam volume and fluctuations of the laser pulse amplitude.

This value is within experimental error of the Earl and Ronn⁽¹⁹⁾ value of $1.2 \pm 0.3 \text{ psec}^{-1} \text{ torr}^{-1}$ measured using laser induced fluorescence techniques.

As explained earlier, efficient VV heating can only occur in the absence of a rotational bottleneck. The necessary condition, derived in the Appendix, is $\tau_B = \frac{\tau_R}{Z_A} \ll \tau_{V-V}$.

However, if this inequality is not satisfied by the pure absorbing gas, a buffer gas can be added to decrease τ_R , hence, τ_B . To test for the presence of a bottleneck, energy absorption experiments were performed at a fixed CH_3F pressure, 5.0 torr, while different amounts of argon was added up to 500 torr. Argon was chosen because this heavy inert atom should leave the V-V rate unaffected but should increase the rotational collision rate, τ_R , without appreciably deactivating the level populations via V-T processes.

The pressure broadening of CH_3F by argon was estimated to be $\approx 3 \text{ MHz/torr}$, by comparison of pressure broadening data in references [20, 21, 29, 30]. The CH_3F self broadening is 40 MHz/torr,⁽¹⁵⁾ thus, 500 torr of argon would broaden the 200 MHz CH_3F lines to 1400 MHz. This represents a factor seven increase in the rotational collision time given by

$$\tau_{R-R} = 1/\pi \Delta\nu$$

where $\Delta\nu$ is the linewidth (FWHM). This gives $\tau_{R-R} \approx 0.23^{18} \text{ nsec}$ at 500 torr argon, more than sufficient to remove any potential bottleneck. However, the transmitted intensity vs. argon pressure indicates no detectable increase in the energy absorbed as argon was added.

← We could then conclude that in pure CH_3F , no rotational bottleneck is present under our experimental conditions. These results also suggest the absence of multiple photon or other non $v=2 \rightarrow 1$ absorption of CH_3F . The condition for efficient laser pumping is by equation (1).

$$\tau_B = \tau_{R-R} / Z_{JK} \ll \tau_{V-V}$$

where τ_B is the Rotational bottleneck time and Z_{JK} the fraction of molecules in any (J,K) state. Using $\tau_{R-R} = 8 \text{ nsec}$ ^{at 1.0 Torr} and $Z_{JK} = .0073$ for the R(4,3) transition, we find $\tau_B = 1.1 \text{ usec}$ or $\tau_B \approx \tau_{V-V}$ and, therefore, the existence of a bottleneck. This conflict with experimental observations suggest that maybe τ_{R-R} is inaccurate due to the J-dependence of the pressure broadening. Also, the unequal distribution of population among the (J,K) states with a large concentration in the $K = 3, 6, 9 \dots$ states can shorten the number of collisions necessary for transfer of molecules into the (J = 4, K = 3) state for pumping. Nevertheless, experiment establishes the absence of bottleneck effects, and to resolve this discrepancy, requires a more careful examination of the parameter τ_{R-R} and how it is used here *is required*.

AD-A058 441

MASSACHUSETTS INST OF TECH CAMBRIDGE DEPT OF PHYSICS
MEASUREMENT OF FREQUENCY OF LIGHT AND ITS APPLICATION.(U)
AUG 78 A JAVAN, M S FELD

F/G 17/5

DAAG29-75-C-0026

UNCLASSIFIED

ARO-13227.12-P

NL

2 OF 3

AD
A058441



IV. Energy Distribution in CH₃F

To establish that for times $\ll \tau_{vt}$ the absorbed energy resides in the vibrational degrees of freedom, the time evolution of the fluorescence from the 9.6 μm C-F stretch mode (ν_3) was monitored by a Cu:Ge detector. ^{Fig SF3} In the pressure range of the experiments the fluorescence was always in the form of a rapid rise, governed by the duration of the laser pulse, followed by a long (\sim ms) decay, determined by the V-T relaxation processes. The 3.3 μm C-H stretch (ν_1, ν_4) and 6.8 μm bend (ν_2, ν_5) fluorescence bands exhibited the same temporal behavior as ν_3 . ^{Fig SF3} This indicates fast intermode V-V rates and that a vibrational steady state among the modes is reached soon after the laser pulse terminates.

A. Cold Gas Filter Analysis of Mode Temperature

Since the absorbed energy is distributed among all the vibrational modes, it is important to determine how much is stored in each. Absolute measurements of fluorescence intensities from each mode could provide this information but such are difficult and imprecise. A new technique, which utilizes the fact that a steady state is rapidly established among the vibrational modes, was used to measure the energy stored in the ν_3 mode. In this technique the peak fluorescence is first observed after it passes through an empty "cold gas filter" cell to give $I(0)$. Then, methyl fluoride gas at room temperature

is introduced into this cell to remove the $v = 1 \rightarrow v = 0$ component of the fluorescence, giving $I(0) - I_{10}$. This "cold" gas (room temperature) is an ideal filter for the $v = 1 \rightarrow v = 0$ fluorescence since its absorption frequencies match the emission frequencies line for line, and only the vibrational ground state is significantly populated. The small anharmonicity (18 cm^{-1}) is sufficient to prevent the absorption of v_3 fluorescence from higher lying levels.

The ratio $\frac{I(0) - I_{10}}{I(0)}$ is an easily measured quantity which determines the vibrational temperature or energy content of the mode in question. At higher temperatures more of the fluorescence arises from higher lying vibrational states and the ratio tends to unity. At lower temperatures the fluorescence is primarily I_{10} and the ratio tends to zero.

Describing the vibrational level populations of the v_3 mode, vibrational frequency ν_3 , by a Boltzmann distribution at temperature T_3 , the fluorescence intensity arising from a particular vibrational transition is

$$I_{v,v-1} \propto |\mu_{v,v-1}|^2 \cdot e^{-v\beta_3} (1 - e^{-\beta_3}) \quad (1)$$

where $\beta_3 = \frac{h\nu_3}{kT_3}$. $I_{v,v-1}$ is the net fluorescence intensity summed over the individual rotational quantum numbers J, K .

Thus $|\mu_{v,v-1}|^2$ is the vibrational transition moment and the re-

maining factor is proportional to the total population of level v . Assuming harmonic oscillator transition moment matrix elements $|\mu_{v,v-1}^2 - \mu_{1,0}^2|$ the ratio becomes

$$\frac{I(o) - I_{10}}{I(o)} = 1 - (1 - e^{-\beta_3})^2 = 1 - (1 + \epsilon_3)^{-2} \quad (2)$$

where ϵ_3 is the number of vibrational quanta stored in v_3 .

This equation is valid when the I_{10} component is completely removed by the cold gas filter. In practice, however, several problems are incurred in achieving this. The $v = 1$ to $v = 0$ fluorescence is composed of many rotational-vibrational lines. The intense emission lines are absorbed strongly; conversely, the weak emission lines are absorbed weakly. A similar effect occurs because each rotational-vibrational line is Doppler broadened and the wings of its profile are absorbed more slowly than its line center. As a result the curve of transmitted intensity $I(P')$ versus cold gas filter pressure P' is not a single exponential but instead has a long tail.

In principle all of I_{10} can be filtered out by increasing the optical absorption length, proportional to $P'L'$ in the Doppler regime. However, signal is lost to solid angle if L' , the filter cell length, is made too long. Furthermore, if the pressure P' is increased too much, the I_{10} absorption lines may be pressure broadened sufficiently to overlap rotational-

vibrational lines of higher vibrational transitions. To avoid these problems the dependence of I_{10} on $P'L'$ was determined by considering the absorption of each individual rotational-vibrational emission line and summing over J, K .

The spontaneous emission intensity of an individual line ($J, K \rightarrow J', K'$) is determined by the population of its upper state and its matrix element. Both are functions of the rotational quantum numbers. Similarly, its absorption by the cold gas filter is dependent on the matrix element and the population difference between its upper and lower states. Neglecting for the moment the non-zero linewidths of the rotational-vibrational transitions, we have

$$I_{10}(P'L') \propto \sum_{PQR} \sum_{JK} N_{JK} |\mu_{JK-J'K'}|^2 e^{-\alpha_{JK-J'K'} P'L'} \quad (3)$$

with absorption coefficient

$$\alpha_{JK-J'K'} = c' \mu_{JK-J'K'}^2 (N_{JK} - N_{J'K'}) \quad (4)$$

where C' is a known constant. Here N_{JK} and $\frac{N}{g_{J'K'}}$ are the populations in the upper and lower states, respectively (including statistical weighting factors for nuclear spin and K degeneracy) and $|\mu_{JK-J'K'}|^2$ is the matrix element for the branch considered (P, Q, R).⁽²¹⁾ The value for the transition dipole moment, necessary for calculating $\mu_{JK-J'K'}$, was deter-

mined from known absorption coefficients.⁽¹⁵⁾ The effects of Doppler broadening (non-zero linewidth) are included by replacing the single exponential $e^{-\alpha_{JK-J'K'}P'L'}$ in Eq. () by $\sum_{n=0}^{\infty} (-\alpha_{JK-J'K'} P'L')^n / n! \sqrt{n+1}$. This function is readily derived by considering the absorption of a Doppler broadened line by a gas whose absorption coefficient is also Doppler broadened [similar considerations are found in Ref. ()].

This numerical procedure establishes an expression for the transmitted intensity as a function of $P'L'$. To facilitate data analysis this generated curve was approximated by a three exponential fit, $\chi(P'L') = 0.567 \exp(-0.614 P'L') + 0.331 \exp(-0.145 P'L') + 0.102 \exp(-0.019 P'L')$ so that

$$I_{10}(P'L') = I_{10}(0) \chi(P'L') \quad (5)$$

Equation () can thus be modified to include the dependence on $P'L'$.

$$\frac{I(P'L')}{I(0)} = \frac{I(0) - I_{10} + I_{10}(P'L')}{I(0)} = 1 - (1 + \epsilon_3)^{-2} [1 - \chi(P'L')] \quad (6)$$

In the data analysis, the parameter ϵ_3 of Eq. (6) was varied until the resulting theoretical curve matched the experimental data (Fig. 8).

In the experiments (Fig. 8) ^{SF1} a 0.25J CO₂ laser beam, 0.6 cm diameter, was passed through a fluorescence cell de-

signed for viewing emission at right angles to the beam. Noise from laser scatter, most of which is off the exit window, was minimized by locating the exit window far from the side window (Fig. ^{SF1}8). Since $^{13}\text{CH}_3\text{F}$ is a strong absorber, the scattered radiation was completely absorbed in the long optical path between the two windows. To minimize reabsorption of the fluorescence by unexcited gas it is important to keep the laser beam close to the side window. Recessing the side window into the cell reduced this distance to only 2 mm. The 6 mm beam diameter was sufficiently small so that absorption of fluorescence in the excited region was unimportant. The side light emission from this fluorescence cell was passed through an 8 cm cold gas filter. The transmitted intensity was focused onto a Cu:Ge detector whose output was displayed on an oscilloscope.

Figure ^{SF4}9 shows the experimental data and the theoretical fits for various fluorescence cell pressures, P. As can be seen, at higher pressures, P, and thus higher VV rates, the number of quanta found in ν_3 increases as expected. However, this represents only 40-50% of the total energy absorbed by the molecule. The remaining energy is transferred to the other vibrational modes through VV cross-over collisions.

B. Energy Distribution and Flow Paths

The VV cross over collisions which transfer energy from v_3 to the other vibrational modes have rates about 1/10 of the VV rate within the v_3 mode.⁽¹⁹⁾ As explained above, the VT relaxation rate is slow enough to allow all of the modes to reach a vibrational equilibrium, with each mode at a different vibrational temperature.

Measuring the temperatures of modes other than v_3 by the cold gas filter method is generally not practical because of the weaker absorption coefficients characteristic of these modes.

For these modes, I_{10} can only be absorbed out by increasing P'L' to the point where the signal to noise and pressure broadening limitations are significant. A cold gas filter measurement on both (v_1, v_4) and (v_2, v_5) was only able to give an upper bound to the energies (v_1, v_4) which agrees with Fig. 4. Once the temperature of v_3 is established by the CGF method, however, relative fluorescence intensities can be used to determine the temperatures of the other modes.

The fluorescence intensity due to a particular vibrational transition in a mode of frequency ω is

$$I_{v,v-1} \propto \omega^4 \nu \mu_{10}^2 n_0 e^{-v\beta} \quad (7)$$

where n_0 is the population of the vibrational ground state.

The integrated absorption "strengths", α , for each mode, which are tabulated in the literature allow us to replace μ_{10}^2 in the equation since

$$\alpha = \frac{n_0 4\pi^2 \omega}{\hbar c} \mu_{10}^2. \quad (8)$$

Summing over all v yields the total fluorescence intensity for the mode.

$$I \propto \omega^3 \alpha e^{-\beta} (1 - e^{-\beta})^2 \quad (9)$$

Therefore, from measurements of I_B/I_A , the ratio of the fluorescence intensities of two modes, A and B, the vibrational temperature of mode B can be obtained from the known temperature of mode A via

$$e^{-\beta_B} (1 - e^{-\beta_B})^{-2} = \frac{I_B}{I_A} \left(\frac{\omega_A}{\omega_B} \right)^3 \frac{\alpha_A}{\alpha_B} e^{-\beta_A} (1 - e^{-\beta_A})^{-2} \quad (10)$$

Once the temperature is known, of course, the energy stored in the mode ϵ_B is also known [Eq. ()].

This method was applied to the degenerate modes v_2 and v_5 at 6.8 μm and degenerate modes v_1 and v_4 at 3.4 μm . The fluorescence from the v_6 mode at 8.8 μm was too weak to measure. The (v_1, v_4) fluorescence was isolated with an infrasil quartz filter and the v_2, v_5 fluorescence with a wide bandpass dielectric filter. The v_3 fluorescence, which served

as the reference intensity was isolated by a dielectric filter which passed long wavelengths. In establishing the relative vibrational temperatures with Eq. (), the tabulated values of integrated absorption coefficients of Ref. 24 were used. These values agree with the absorption spectra given in Refs. 25,26. In the analysis (ν_2, ν_5) was considered to be triply degenerate since the doubly degenerate ν_5 is only 4 cm^{-1} below ν_2 . Likewise, (ν_1, ν_4) was treated as triply degenerate since doubly degenerate ν_4 is 15 cm^{-1} above ν_1 . Contributions to the $3 \text{ }\mu\text{m}$ fluorescence from the Fermi mixed (ν_2, ν_5) state were neglected because of its relatively weak intensity. (27)

The results of these measurements are shown as data points in Fig. 4. $\epsilon_{2,5}$ and $\epsilon_{1,4}$ are the sums of all the consistent degenerate modes' energies. Although ϵ_6 was not measured, it could be estimated theoretically (as discussed below). Thus, we have experimentally established that for times $\ll VT$, all of the absorbed energy is partitioned among the vibrational degrees of freedom. This result also establishes the internal consistency of the absorption, cold gas filter, and relative fluorescence techniques.

Given a knowledge of the energy flow paths between equilibrating vibrational modes, and the total amount of energy absorbed, the distribution of this energy among the modes can

be circulated theoretically. Since we have measured these energies experimentally we can choose between various possible flow paths on the basis of how well they fit the data. The solid curves, (b), (c), (d) and (e) of Fig. 4 are theoretical fits assuming a model given below.

The path below, Path 1, used to calculate the curves in Fig. 4, has been shown by Flynn and coworkers (23) to be the dominant path in the weak excitation regime.

Path 1

- (1) $(v_3) + (0) \rightleftharpoons (v_6) + (0) - 147 \text{ cm}^{-1}$
- (2) $(v_6) + (0) \rightleftharpoons (v_2, v_5) + (0) - 275 \text{ cm}^{-1}$
- (3) $2(v_2, v_5) \rightleftharpoons (2v_2, 2v_5) + (0) - 68 \text{ cm}^{-1}$
- (4) $(2v_2, 2v_5) + (0) \rightleftharpoons (v_1, v_4) + (0) + 103 \text{ cm}^{-1}$

where, for instance, $(2v_2, 2v_5)$ represents a single molecule with two quanta in mode v_2 and two quanta in mode v_5 and (0) , a molecule in the vibrational ground state.

The temperatures, T_A and T_B , of two different modes in vibrational equilibrium with each other are related by

$$\frac{\omega_A}{T_A} - \frac{\omega_B}{T_B} = \frac{(\omega_A - \omega_B)}{T} \quad (11)$$

where the ω 's are the vibrational frequencies and T is the kinetic temperature. Applying Eq. (), for example, to the two modes v_3 and v_6 held in vibrational equilibrium with each other by reaction (1) in Path 1 we find

$$T_6 = \omega_6 \left[\frac{2\pi c (147 \text{ cm}^{-1})}{300^\circ \text{K}} + \frac{\omega_3}{T_3} \right]^{-1}$$

(12)

which for $T_3 = 2000^\circ \text{ K}$ gives $T_6 = 1180^\circ \text{ K}$. Similarly from this T_6 and reaction (2), $T_{2,5}$ can be calculated and so on. From these temperatures we can relate a particular distribution of energy among the modes to the total vibrational energy of a molecule. Curves (b), (c), (d), and (e) were determined in this fashion from the total energy curve (a) which itself was a theoretical fit to the data assuming a particular γ_{VV} .

The good agreement of these curves with the experimental data in Fig. 4 argues well for the validity of Path 1. A possible alternative path, Path 2 below, was shown not to agree with the experimental results.

Path 2

- (1) $(v_3) + (v_3) \rightleftharpoons (2v_3) + (0) +$
- (2) $(2v_3) + (v_3) \rightleftharpoons (3v_3) + (0) +$
- (3) $(3v_3) + (0) \rightleftharpoons (v_1, v_4) + (0) + 16 \text{ cm}^{-1}$

For example, small energy defect of reaction 3 would indicate $T_{14} = 2000.4^\circ \text{ K}$. or $\epsilon_{14} = .13$ for a T_3 of 2000° K . This is much greater than the measured $\epsilon_{1,4}$.

DRAWINGS
FOR PAPER

HAVE MAILED ALL
FIGURE REFERENCES IN
THESE SECTIONS AS
SF1, SF2, SF3, SF

FIGURE
SF 1

YOU WILL
HAVE TO
ISSUE AN
ABSOLUTE
NUMBER
WHEN YOU
PUT YOUR
FIGURES IN

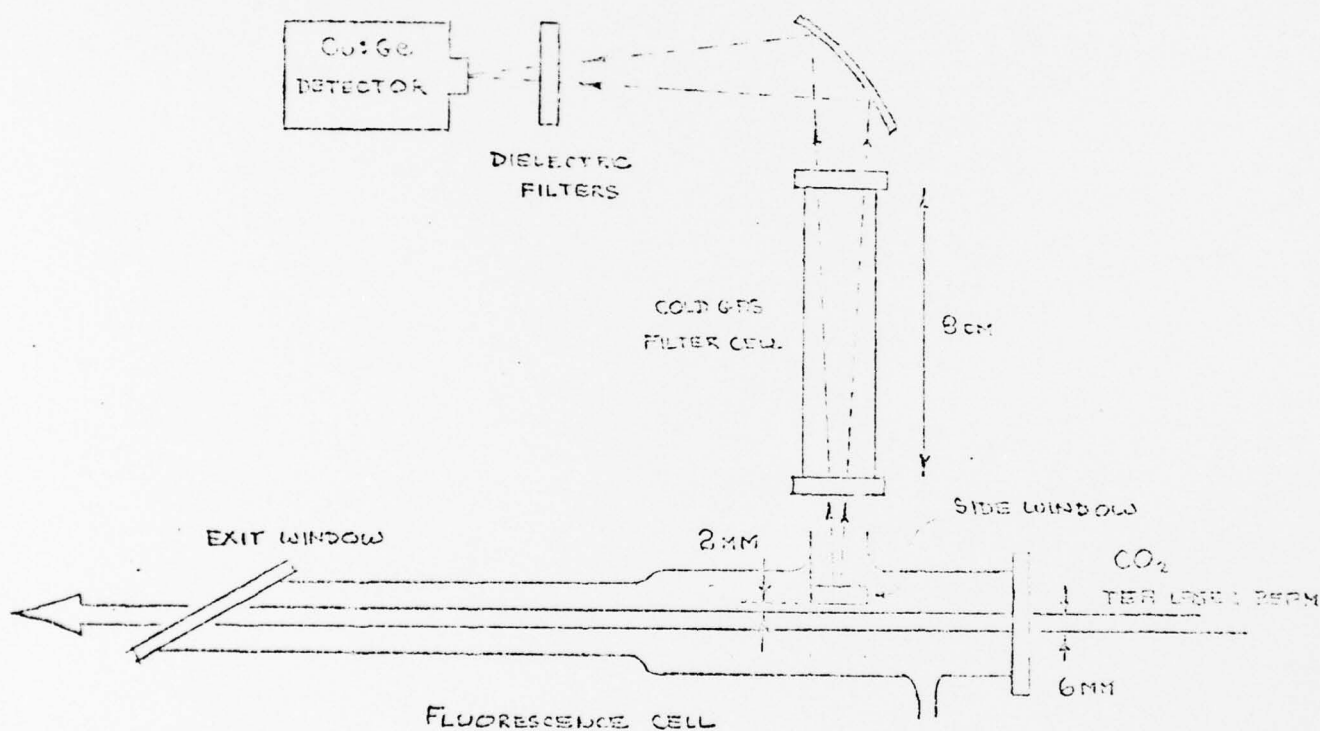
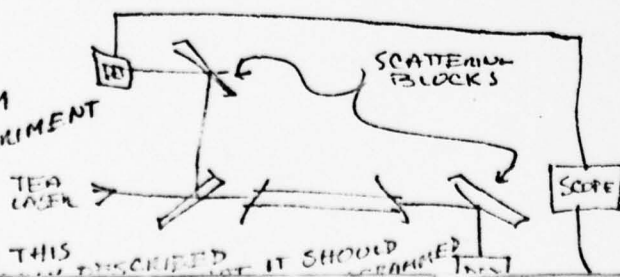


Fig. 6

HERE ARE 5 OF THE 6
DRAWINGS WE CONSIDERED
THE SKTH IS THE DIAGRAM
OF THE ABSORPTION EXPERIMENT



THINK THIS
IT SHOULD
BE ARRANGED

Figure
SF2

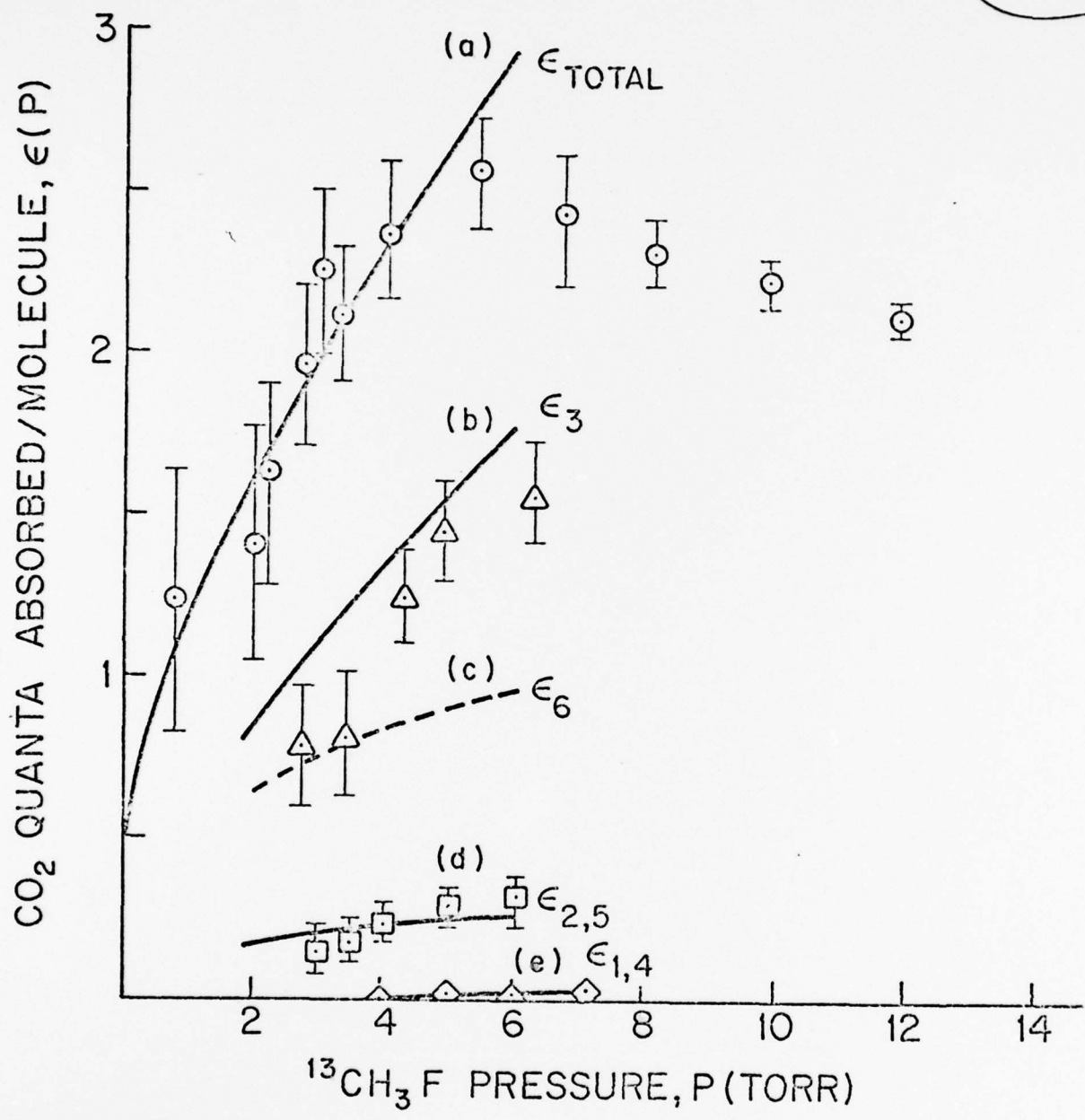
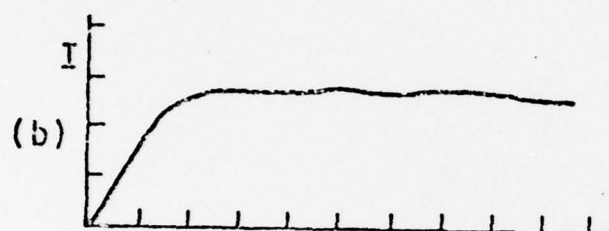


FIGURE
SF3



← DECREASE
SPACES OF
COURSE

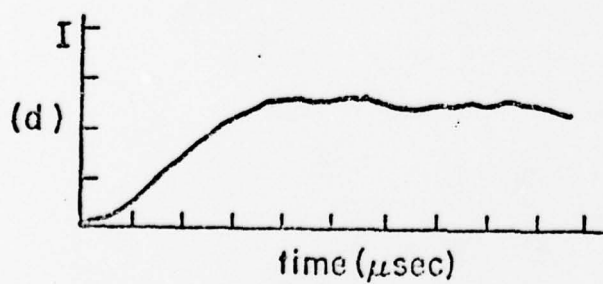
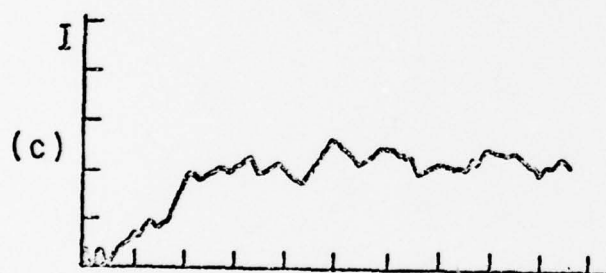
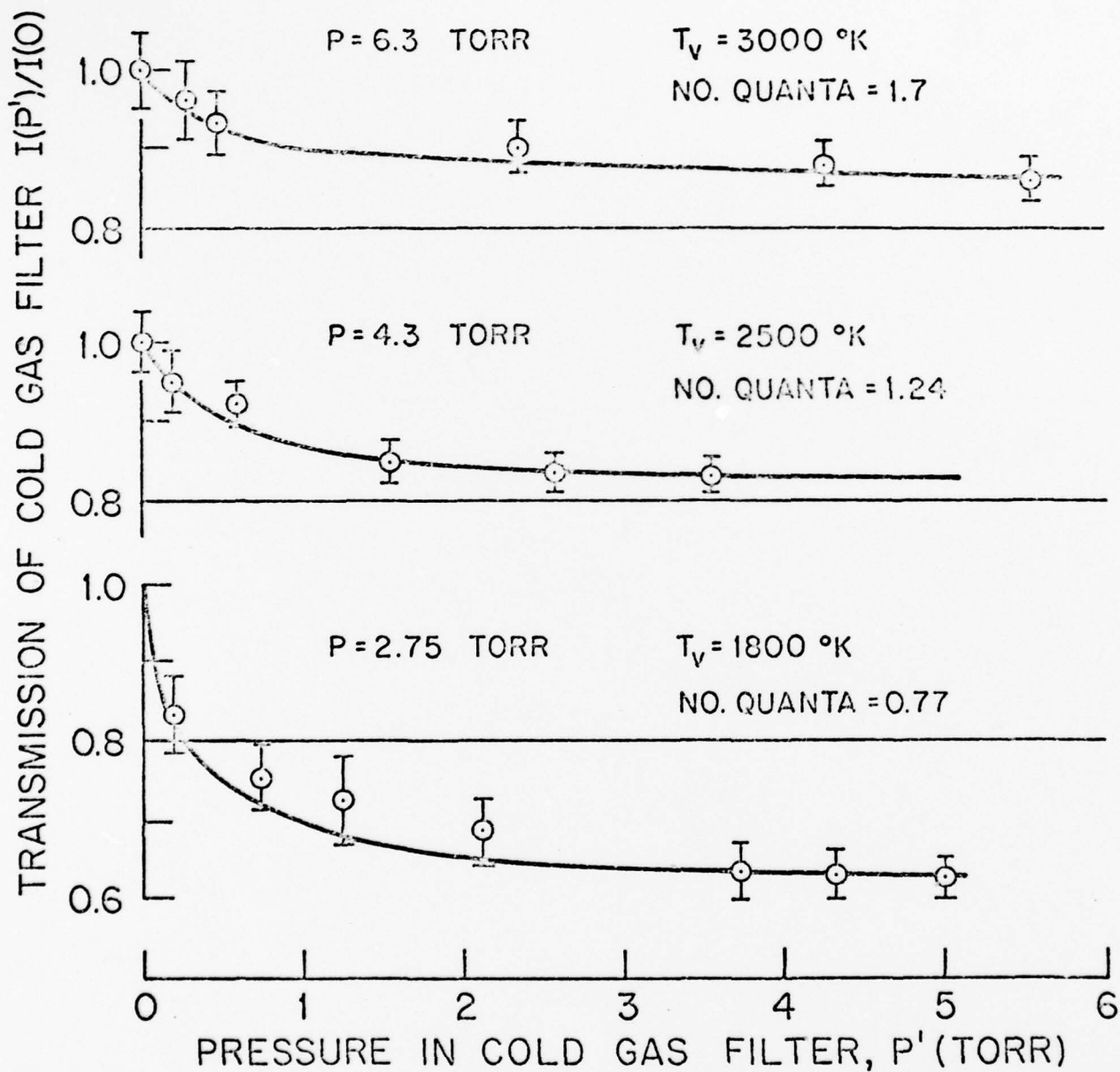


FIGURE
SF4



HAVE A GOOD ONE AT 8.8 TORR
 $T_v = 3200$ °K
1.7 quanta

3.42 TORR
1850 °K
1.71 quanta

SOMETHING
WENT ON HERE
SEE 2.75 TORR

IF WHERE
OF $I(P')/I(0)$
WESSED UP
7.10 - NO 0.8

4.95 TORR
2800 °K
1.43 quanta

CAN TAKE THESE
RIGHT OUT OF THESIS
GIVE TO DRAFTSMAN

LASER SATURATION SPECTROSCOPY
IN THE TIME-DELAYED MODE†

Martial Ducloy*
Laboratoire de Physique des Lasers
Université Paris-Nord
Villetaneuse France 93430

and
Michael S. Felds
Department of Physics and Spectroscopy Laboratory
Massachusetts Institute of Technology
Cambridge, MA 02139

ABSTRACT

This paper describes a new class of techniques, called time-delayed laser saturation spectroscopy, which combine frequency and time-domain methods of laser spectroscopy to provide a way of studying a molecular system as it evolves from an initially-prepared stationary state to a second, final state. The specific example analyzed here is three-level free induction decay, in which the time dependent gain of a Doppler-broadened molecular transition is probed after the sudden termination of an intense field resonating with a coupled transition. The calculated lineshape features expected under different experimental conditions are described, and some of these are demonstrated in NH_3 . The experiments clearly separate the contributions of population saturation and Raman-type processes in the time evolution of the lineshapes, and yield the first measurement of the alignment relaxation rate in the ground electronic state of a molecule.

† Supported in part by NSF and ARO (Durham).

* This work was performed while the author was a Visiting Scientist at MIT.

§ Alfred P. Sloan Research Fellow.

1. Introduction

Over the past decade powerful laser saturation techniques for inducing narrow resonances in Doppler-broadened systems have become a major tool for studying atomic and molecular structure in the frequency domain [1]. On the other hand, the recently developed coherent transient techniques have been very useful in obtaining new information about laser interactions and relaxation processes in the time domain [2]. The purpose of this paper is to show that these two approaches can be merged to form a new class of techniques which yields information in both fre-

quency and time domains and thus extends the range of available information.

As an example, consider a conventional saturated absorption experiment in which the saturation of a Doppler-broadened transition by an intense monochromatic field is observed by studying the narrow resonance induced in the transmission of a tunable probe beam (Fig. 1.).



Fig.1 Example of the time-delayed technique. The configuration shown is that of time-delayed Lamb dip.

Now suppose that the saturating field is suddenly switched off, and the lineshape of the narrow resonance is probed a fixed interval of time later. As the time delay is increased the change signal will become smaller, corresponding to the decay of the saturated molecules and their return to equilibrium. Furthermore, as shown below the *shape* of the resonance may evolve from its steady state form. This information can be combined to form a surface in a coordinate system having axes: probe intensity (z-axis), frequency detuning (x-axis), time delay (y-axis) (Fig. 2).

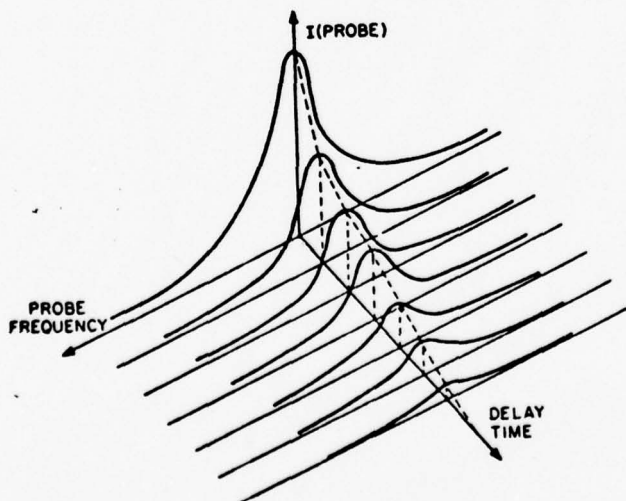


Fig.2 Three dimensional representation of the time-delayed change signals.

Sections parallel to the x-axis give the resonance lineshape at

delayed times. Similarly, sections parallel to the y-axis give the free decay of the system at various values of frequency detuning.

Experiments of this type are inherently different from conventional free induction decay experiments [2], where the probe field does not interact with the molecules and serves only as a local oscillator for heterodyne detection. Thus, in such experiments there is no resonant behavior as the probe field is tuned. For the same reason the new technique is not an analog of pulse Fourier transform spectroscopy [2], and the time-delayed lineshapes may bear no relationship to the corresponding decay times. In fact, different portions of the lineshape may decay at different rates, resulting in a deformation of the overall lineshape. Lineshape evolution of this type becomes particularly important when the physical processes contributing to the change signal decay at different characteristic rates (e.g. T_1 processes vs. T_2 processes), or the lineshape exhibits Ramsey-type fringes due to decay of a phase-coherent contribution. Other features of the time-delayed change signals which occur at high saturation field intensities include power broadening and dephasing, and oscillatory behavior related to the dynamic Stark effect.

The wide range of techniques to which time-delayed saturation spectroscopy can be applied includes free decay, optical nutation and photon echoes in two and three level systems (both cascade and folded), for probe and saturating waves either co- or counter-propagating [3]. In the following we shall concentrate on free decay in Doppler-broadened three level systems.

2. Theory of Free Decay in Three Level Systems [4,5]

When an intense, monochromatic laser field, E_2 , frequency Ω_2 , resonates with one of the transitions (0-2, see Fig. 3) of a Doppler-broadened gas, the populations of levels 0 and 2 are altered over a narrow range of axial velocities centered about v_2 , satisfying the resonance condition $\Omega_2 - k_2 v_2 = \omega_2$ (ω_2 molecular frequency, $k_2 = \Omega_2/c$).

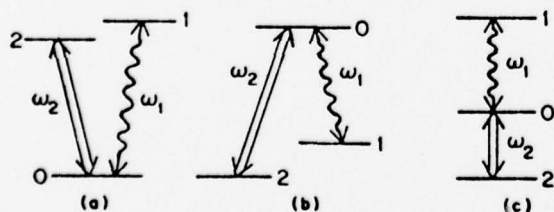


Fig.3 Energy level diagrams.

This resonant change in the velocity distribution can manifest itself in the spectral profile of a Doppler-broadened transition, 0-1, sharing a common level with 0-2. If a weak monochromatic

field, $E_1(\Omega_1)$, colinear with the intense field, probes the 0-1 transition, center frequency ω_1 , a sharp change in transmission will occur when ω_1 is tuned into resonance with the molecules of velocity v_2 :

$$\Omega_1 = \Omega_1(\epsilon) \text{ where } \Omega_1(\epsilon) = \omega_1 + \epsilon k_1(\Omega_2 - \omega_2)/k_2 \quad (1)$$

($\epsilon = +1$ and -1 for co-propagating and counter-propagating waves, respectively). This effect, called laser induced line narrowing, has been the subject of numerous theoretical and the experimental investigations devoted to studying the steady state change signals at the probe transition [1]. It is now well known that the change signal lineshape cannot be accounted for in terms of population considerations alone, and that coherent Raman-type processes such as two-photon transitions play an important role [6]. Thus, for example, the widths of the change signals in the forward ($\epsilon = +1$) and backward ($\epsilon = -1$) directions can differ considerably. This and other lineshape asymmetries have been useful in extracting detailed information about collisional and radiative decay processes.

Our purpose is to analyze the transient behavior of the change signal lineshape when the saturating field is suddenly terminated at time $t = 0$. In the thin sample approximation the probe change signal is proportional to the velocity-integrated value of $\text{Im}(P)$, with $P(\Omega_1)$ the amplitude of the optical polarization induced by the probe field. In the slowly-varying envelope approximation P obeys an oscillator equation of the type [4,5]

$$\partial_t P + LP = i\mu_1^2 E_1 (n_1 - \sigma_{00}) + i\mu_1 \mu_2 E_2 \sigma_{21}, \quad (2)$$

where $L = \gamma_{01} + i(\Omega_1 - \omega_1 - k_1 v)$ and $n = 1$; n_j is the thermal (or background) population of level j ; μ_j is the 0-j dipole moment matrix element; σ_{ij} is the envelope of the i-j density matrix element (σ_{00} , population of level 0 as influenced by E_2 ; σ_{21} , coherence induced by Raman-type transitions) and γ_{ij} is its relaxation rate. As can be seen, P can be excited by both population and Raman-type driving terms.

The solution of (2) in the transient regime ($E_2 = 0$, $t > 0$) is given by

$$P(t) = P_L + P(0)e^{-Lt} - i\mu_1^2 E_1 \int_0^t \Delta n(t') e^{-L(t-t')} dt', \quad (3)$$

where P_L is the linear (unsaturated) polarization, $P(0)$ the initial value ($t = 0$) of the saturated polarization, and

$$\Delta n(t) = [\sigma_{00}(0) - n_0] e^{-\gamma_0 t}, \quad (4)$$

with γ_0 the population decay rate of level 0. The last term in (3) describes the coupling of P with σ_{00} . Since $E_2 = 0$ for $t > 0$, transient Raman processes do not occur (as they would in three level optical nutation). But their influence is contained in the initial polarization, along with that of the saturated population of level 0:

$$P(0) = i[-\mu_1^2 E_1 \Delta n(0) + \mu_1 \mu_2 E_2 \sigma_{21}(0)]/L. \quad (5)$$

The resulting probe lineshapes, obtained by integrating (3) over velocity, depend on the relative direction of the two waves.

In the following the lineshape features will be described for a folded three level system (Figs. 3a,b). In the cascade case (Fig. 3c) the lineshapes are the same, except that the roles of forward and backward signals are interchanged.

2.1 Counter-Propagating Waves ($\epsilon = -1$)

For weakly saturating pump field the lineshape is given by the real part of g ($\epsilon = \pm 1$):

$$g(-) = \frac{e^{-[\Gamma+i\delta(-)]t}}{\Gamma+i\delta(-)} + \frac{e^{-\gamma_0 t} e^{-[\Gamma+i\delta(-)]t}}{\Gamma-\gamma_0+i\delta(-)}, \quad (6)$$

where $\delta(-)$ is the probe field detuning [$\delta(\epsilon) = \Omega_1 - \Omega_1(\epsilon)$], and $\Gamma = \gamma_{01} + k_1 \gamma_{02}/k_2$. The first term in $g(-)$ describes the decay of the initial polarization. Its decay rate, Γ , consists of two terms, the ordinary relaxation rate, γ_{01} , and a Doppler dephasing contribution, $k_1 \gamma_{02}/k_2$. This latter term is due to the velocity spread $\Delta v = \gamma_{02}/k_2$ of the excited molecules, which gives rise to a corresponding spread in the reradiated frequencies.

The second term in (6) comes from the coupling of P with the saturated level population, and decays at characteristic rate γ_0 .

The first term exhibits Ramsey-type fringes and the associated line narrowing, as is characteristic of the time-delayed lineshape resulting from the decay of a phase-coherent polarization. This type of behavior can be observed in $g(-)$ for $\Gamma \leq \gamma_0$. As seen in Fig. 4, for $t \geq 1/\Gamma$ the line narrows below its natural width.

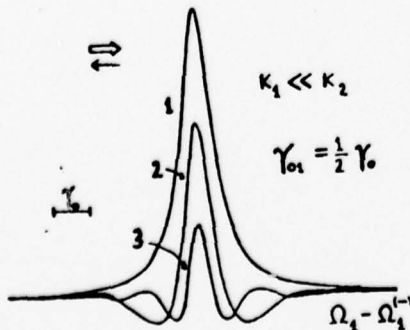


Fig. 4 $g(-)$ change signal for $\Gamma = \gamma_0/2$. Time delays: $t_1 = 0$, $t_2 = 2/\gamma_0$, $t_3 = 4/\gamma_0$.

This extreme narrowing is due to the selection of long-lived molecules by the time-delayed measurement process.

In the case of $\Gamma > \gamma_0$ the polarization contribution is dominated by the population term for $t \geq 1/\Gamma$, leading to a different type of behavior. There are no fringes and the line remains Lorentzian, narrowing from an initial width Γ to an eventual width $\Gamma - \gamma_0$ at $t > 1/\Gamma$.

In contrast, when there are strong phase-changing collisions $[\gamma_{ij} \gg (\gamma_i + \gamma_j)/2]$ the lineshape is not deformed during the transient evolution (Fig. 5b).

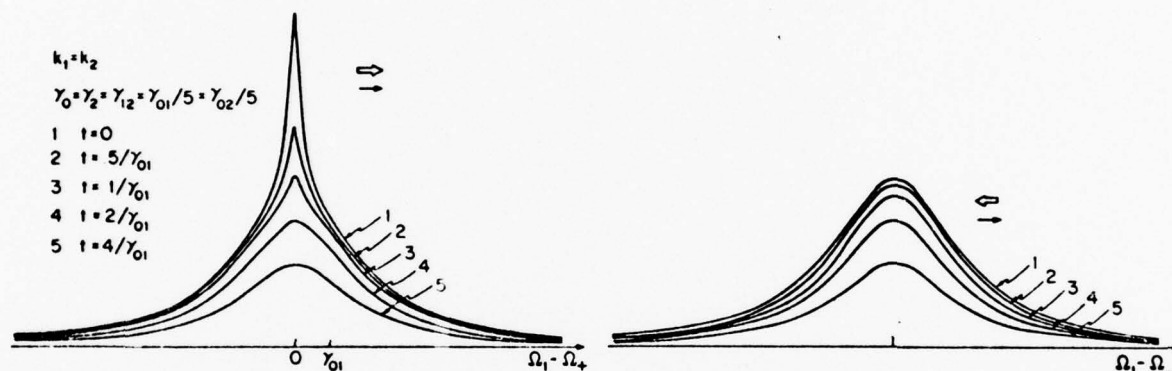


Fig. 5 Forward (a) and backward (b) change signals when phase-changing collisions predominate.

The resonance, a Lorentzian of width Γ , then decays with the population time constant:

$$g(-) \approx e^{-\gamma_0 t} / [\Gamma + i\delta(-)]. \quad (7)$$

Finally, note that in all cases Raman-type contributions are absent in $g(-)$, as can be seen by the absence in (6) of terms containing γ_{12} , the Raman-coherence decay rate. These contributions cancel in the velocity integration because of the destructive interference arising from their strong velocity dependence.

2.2 Co-Propagating Waves ($\epsilon = +1$)

In contrast to 2.1, in the forward direction the change signal is influenced by Raman-type processes, which are not averaged out in the velocity integration. It also depends on whether $k_2 \gtrless k_1$.

For $k_2 < k_1$ and no phase-changing collisions $[\gamma_{ij} = (\gamma_i + \gamma_j)/2]$ the lineshape [4] is a single Lorentzian of width characterized

by Raman-type processes (and therefore narrower than the $\epsilon = -1$ case), which is undistorted during the decay. However, this is not the case when phase changing collisions dominate ($\gamma_{01}, \gamma_{02} \gg \gamma_0, \gamma_{12}$). For example, in the important special case of $k_1 \approx k_2$ the change signal lineshape is given by

$$g(+)\approx \frac{e^{-\gamma_0 t}}{\Gamma+i\delta(+)} + \frac{\gamma_0}{\Gamma} \frac{e^{-\Gamma t}}{\gamma_{12}+i\delta(+)} \quad (8)$$

The first term describes a broad resonance, induced by population saturation, which decays at characteristic rate γ_0 . It is identical to the corresponding $g(-)$ lineshape, (7). The second term is a narrow resonance of width γ_{12} , induced by Raman-type processes, which decays at the much faster rate $\Gamma = \gamma_{01} + \gamma_{02}$, characteristic of the decay of the initial polarization. This leads to the remarkable conclusion that after a time $\sim 1/\Gamma$ the narrow contribution decays away and the forward change signal evolves to a broad Lorentzian identical to that of the backward signal, (6). An example is shown in Fig. 5a.

When $k_2 > k_1$ there is an additional contribution to the change signal, due to the decay of a new velocity group prepared in the steady state ($t \leq 0$). This velocity group, associated with the resonance condition for Raman-type processes, is centered at v_{12} , defined by $\Omega_2 - \Omega_1 - (k_2 - k_1)v_{12} = \omega_2 - \omega_1$. (This is the energy conservation condition for 2+1 two quantum transitions.) This extra term, which exists even when the medium is transparent to the saturating field ($n_2 = n_0 \neq n_1$), is proportional to the real part of

$$g'(+)=\kappa \frac{e^{-[\gamma+i\delta(+)]t/\kappa}}{[\gamma+i\delta(+)]^2} \quad (9)$$

with $\kappa = (k_2 - k_1)/k_2$ and $\gamma = \kappa\gamma_{01} + k_1\gamma_{02}/k_2$. As can be seen in Fig. 6, the corresponding time-delayed lineshape exhibits Ramsey-type fringes, as is characteristic of a pure phase-coherent contribution.

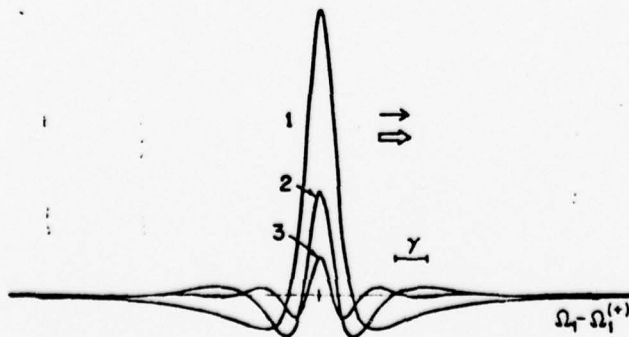


Fig.6 $g(+)$ change signal for $n_2 = n_0 \neq n_1$, $k_2 = 2k_1$, $\gamma_{ij} = \gamma$.
Time delays: $t_1 = 0$, $t_2 = 0.5/\gamma$, $t_3 = 1/\gamma$.

2.3 Saturation Effects

The above results describe the case in which the saturation induced by the intense laser field is small. The additional lineshape effects occurring in the case of strong saturation include power broadening and dephasing, and dynamic Stark splittings exhibiting a novel type of oscillatory decay. A complete discussion of these effects is given in Ref. 5.

3. Experiments in NH_3 [ν_2 asQ(8,7) transition]

3.1 Experimental set-up (Fig. 7)

In the experiments the ν_2 asQ(8,7) transition of NH_3 was saturated and probed using two c.w. N_2O lasers oscillating on the P(13) line ($\lambda = 10.78 \mu\text{m}$), which falls within the NH_3 Doppler profile.

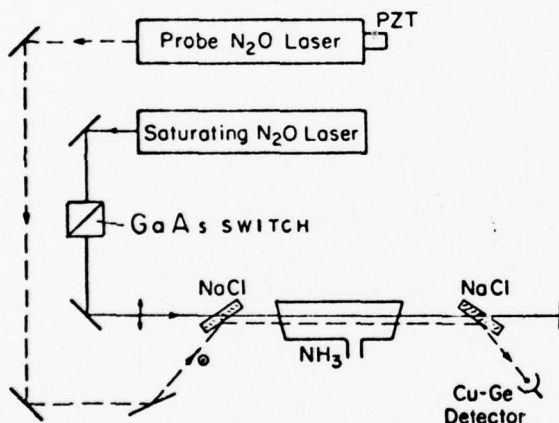


Fig.7 Experimental set-up.
The GaAs switch was absent in the steady-state experiments.

A 10 cm glass sample cell with NaCl end windows was used. Holding the frequency of the saturating N_2O laser fixed, the probe was tuned (tuning range, ± 35 MHz) by means of calibrated PZT. A flip mirror was used to reverse the direction of the saturating beam and thereby select forward or backward configurations. The two laser beams were linearly polarized at right angles, and Brewster angle NaCl beam splitters were used to overlap the beams before the cell and separate them afterwards. The probe beam was monitored using a He-cooled Cu-Ge detector. Steady-state experiments were performed by chopping the saturating beam at a low frequency (~ 1 kHz) and using phase sensitive detection. The transient change signals were observed by turning on and off the saturating beam with an external electro-optic modulator, a GaAs crystal to which high voltage square pulses were applied (rise-

time 30 ns, duration 10 μ s, repetition rate 1 kHz), thus inducing a fast rotation of the polarization of the c.w. saturating beam. A subsequent analyzer, a Brewster angle silicon plate, yielded the square pulses of the saturating beam. Probe signals were analyzed with a Boxcar integrator operated in two different modes: either monitoring the decaying signal at a fixed probe frequency, or scanning the probe frequency at fixed time delays.

3.2 Steady-State Lineshapes [7]

Experimental lineshapes for co- and counter-propagating waves are shown in Figs. 8a,b.

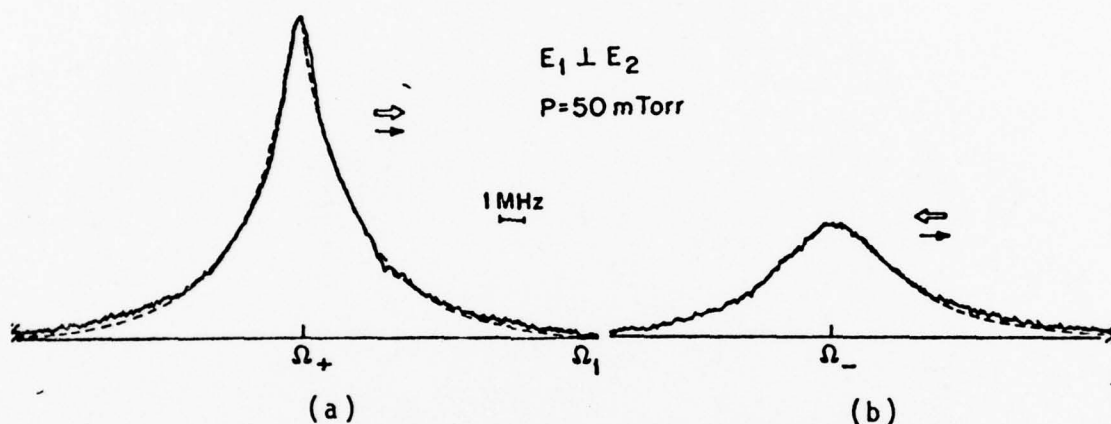


Fig.8 Steady state forward (a) and backward (b) observed change signals. The dashed line shows the theoretical fit.

Since the NH_3 transition is degenerate ($J = 8 \rightarrow 8$) and the two beams have perpendicular linear polarizations, the saturating field can be considered to induce $\Delta M = 0$ transitions, and the weak field then probes $\Delta M = \pm 1$ transitions. In the absence of M-changing collisions the system decomposes into two groups of coupled three-level systems having the common level in the ground (g) and excited (e) states, respectively. The Raman coherence responsible for the forward-backward asymmetry of the signals of Fig. 8 is thus the coherence between adjacent M-sublevels.

As is characteristic of systems with strong phase-changing collisions [(7) and (8)], the backward change signal of Fig. 8 is a single Lorentzian, whereas the forward signal contains an additional narrow feature. However, a quantitative analysis of the experimental results requires further consideration, since in the degenerate NH_3 transition strong M-changing collisions couple together the independent three level systems. As is well known from the symmetry properties of collisional relaxation processes in gases [8], allowance must then be made for different relaxation rates of the various multipole moments of each level.

Using the tensorial formalism [8] to account for these features, the following expression for the change signals can be derived [9]:

$$G(\epsilon) = L(2\gamma_{eg}^1) \sum_{\alpha=e,g} \left\{ \frac{96}{\gamma_{\alpha}^0} - \frac{38}{\gamma_{\alpha}^1} + \frac{\epsilon+1}{2} [57L(\gamma_{\alpha}^2) + L(\gamma_{\alpha}^1)] \right\}, \quad (10)$$

where $L(x) = [x+i\delta(\epsilon)]$. γ_{eg}^1 is the relaxation rate of the optical polarization and γ_{α}^k the decay rate of the k^{th} order multipole in level α : $k = 0$, population; 1, orientation; 2, alignment. Thus, in the presence of M-changing collisions the backward signal is still a single Lorentzian of width $2\gamma_{eg}^1$, but the forward one now consists of several Lorentzian components associated with the various tensorial moments. In the present experiments the width of the narrow Raman-type contribution of the forward signal is primarily determined by alignment relaxation processes (γ_{α}^2).

The observed width of the backward signal gives $\gamma_{eg}^1 = 24 \pm 1$ MHz/torr, consistent with earlier Lamb dip measurements. Previous microwave experiments in the NH_3 ground state have shown that due to the small inversion splitting of 0.8 cm^{-1} , inelastic collisions are the predominant relaxation mechanism (which implies $\gamma_g^k = \gamma_g^0$) and that $\gamma_g^0 = \gamma_{eg}^1$ [10]. This is not true for the excited state, where the inversion splitting is much larger, $\sim 36 \text{ cm}^{-1}$. In the next section we show that transient experiments yield $\gamma_e^0 = 3.5 \pm 0.6$ MHz/torr. The best fit of the experimental forward signal to (10) (dashed curve of Fig. 8) then gives $\gamma_e^2 = 6 \pm 1$ MHz/torr [7].

To demonstrate the inherent polarization dependence of the change signal lineshapes, similar experiments were done in which the probe field polarization was oriented *parallel* to that of the saturating field by inserting a half-wave plate in the path of the saturating beam. A small misalignment was introduced to separate the beams. As seen in Fig. 9, in this case the forward change signal is narrower than that observed for crossed polarizations.

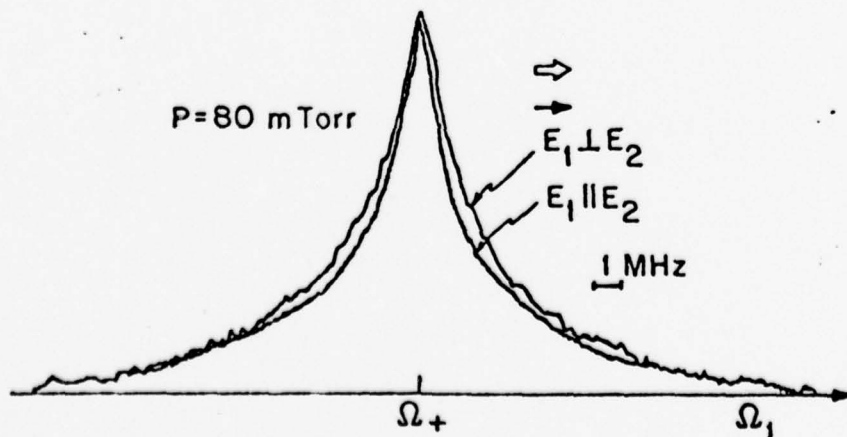


Fig.9 Forward change signal for parallel polarizations of probe (E_1) and saturating (E_2) fields. The corresponding signal for $E_1 \perp E_2$ is shown for comparison, normalized such that the peak heights are equal.

(The change signal linewidths observed in the backward direction are the same, as predicted by (11).) This can be understood as follows: When the polarizations are parallel both fields obey $\Delta M = 0$ selection rules, and so no Raman coherence can be induced. However, since two e.m. fields of the same polarization and propagation vector are equivalent to an amplitude modulated excitation, a new type of contribution now arises, originating in the coherent modulation of the level populations at the frequency difference between pump and probe fields. This effect causes additional narrowing of the forward signal if $\gamma_e < \gamma_g$. Using the tensorial formalism, the change signal lineshape is now given by [9]

$$G_{11}(\epsilon) = L(2\gamma_{eg}) \sum_{\alpha=e,g} \left\{ \frac{96}{\gamma_{\alpha}^0} + \frac{76}{\gamma_{\alpha}^2} + \frac{\epsilon+1}{2} [96L(\gamma_{\alpha}^0) + 76L(\gamma_{\alpha}^2)] \right\}. \quad (11)$$

The observed narrowing of the lineshape for parallel polarization is another clear evidence of M-changing collisions, since for $\gamma_{\alpha}^k = \gamma_{\alpha}^2$ (10) and (11) predict the same lineshape, contrary to the experimental results.

From the above results it follows that in the $asQ(8,7)$ excited state the cross-section for elastic M-changing collisions is about two-thirds as large as that for inelastic collisions. To our knowledge, this is the first measurement of the alignment relaxation rate in the ground electronic state of a molecule. The present experimental technique does not require Stark or Zeeman tuning nor fluorescence detection, and thus compliments the well-established Hanle effect and double resonance techniques of optical pumping [8].

3.3 Time-Delayed Lineshapes

As mentioned above, the experiments have been carried out in two different ways: Either the probe frequency is fixed and the transient signal is observed as a function of time (Fig. 10), or the transient lineshape is studied by tuning the probe frequency at a given delay time after the saturating field has been interrupted (Fig. 11).

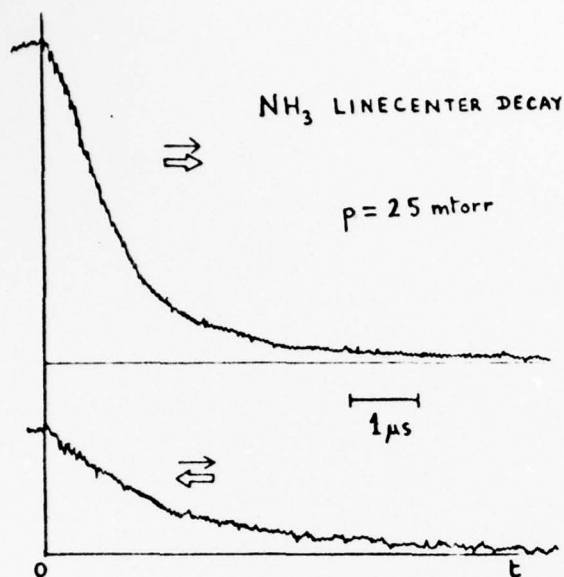


Fig.10 Time domain study of forward (upper trace) and backward (lower trace) change signals. In these traces the probe field is tuned to line center ($\delta = 0$). As can be seen, the backward decay is a single exponential, whereas the forward decay contains fast and slow exponential components.

Figure 10 shows the decay signals at line center and Figs. 11a,b show the transient lineshapes observed at different time delays.

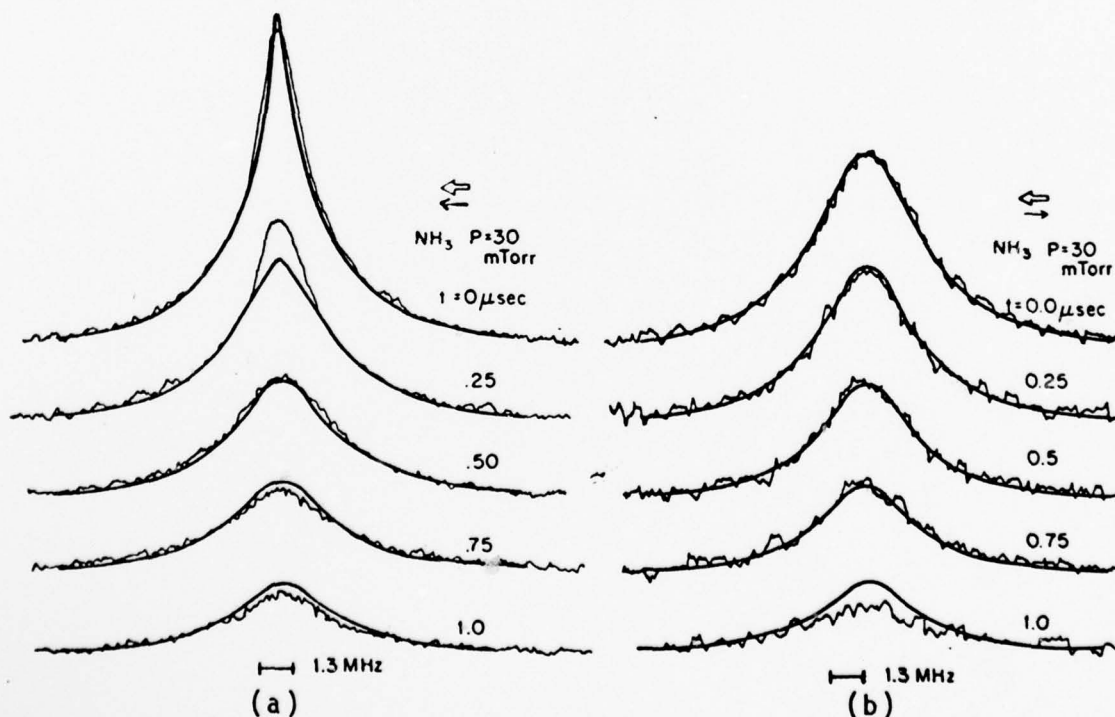


Fig.11 Time delayed lineshapes observed in forward (a) and backward (b) directions. The solid curves give the theoretical fit.

The simple three-level model of Section 2 predicts that forward

and backward signals differ by the narrow Raman-type contribution, and this contribution decays away rapidly, leaving a slowly-decaying population-induced component which is the same in both propagation directions [(7) and (8) and Fig. 5]. These predictions are confirmed by Figs. 10 and 11. However, quantitative comparison of experiment with theory must take into account the level degeneracy, the existence of M-changing collisions, and also the power-broadening induced by the pump field. As explained in the previous section, level degeneracy and re-orienting collisions can be included by means of the tensorial formalism [9]:

(i) In the same way as in the simple theory, Raman-type contributions have a characteristic decay rate $2\gamma_{eg}^1$ ($= 48 \text{ MHz/torr}$). A theoretical study valid for arbitrary intensities of the saturating field [5] shows that this decay rate is shortened by power dephasing. For instance, in Fig. 11 power dephasing (for $I = 70 \text{ mW/cm}^2$ and $p = 30 \text{ mtorr}$) contributes 0.5 MHz to the Γ decay rate.

(ii) Population saturation contributions are the same in both propagation directions and have a Lorentzian lineshape of width $2\gamma_{eg}^1$. A noteworthy feature is that their decay rate is not sensitive to power dephasing [5]. Eq. (10) shows that various multipole moments in excited and ground states contribute to the corresponding components of the change signal amplitudes and thus, there should be several time constants associated with the decay of the backward signal. However, due to the short lifetime of the ground state, the amplitude of its steady-state contribution is very small compared to that of the excited state population. (The ratio is about $58\gamma_e^0/96\gamma_g^0 \approx 9\%$.) In addition, its decay is very fast. On the other hand, in the excited state, (10) shows that the ratio of alignment to population contributions is $38\gamma_e^0/96\gamma_e^2 \approx 23\%$. The excited state population therefore provides the dominant contribution to the decaying change signals, and lasts for the longest time. γ_e^0 can thus be extracted from the slowly-varying component of the curves of Fig. 10. The pressure dependence of this decay rate is shown in Fig. 12.

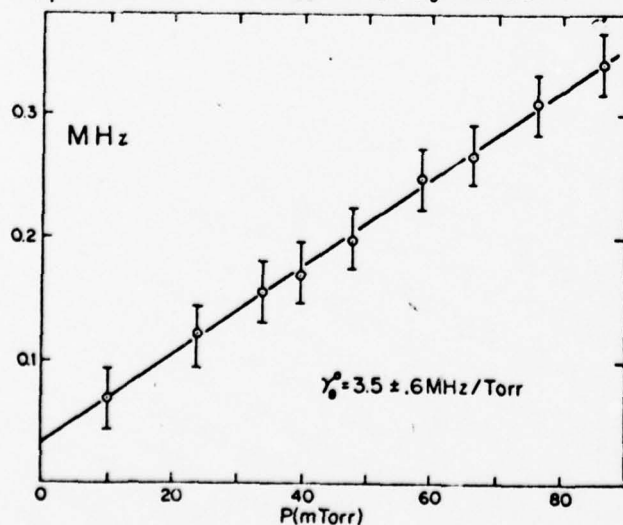


Fig. 12 $(2\pi T_0)^{-1}$ vs. pressure. The data was taken from the slowly-decaying component of the forward change signal (upper trace of Fig. 10).

The zero-pressure value (~ 0.04 MHz) is due to molecular transit time effects.

Since all the parameters are known, the theoretical predictions can be compared with the experimental lineshapes (Fig. 11). The agreement is quite good, except for the short term ($t = 0.25 \mu\text{s}$) behavior of the forward signal, where the time resolution of the electronic detection system was not sufficiently high to follow the fast decay of the narrow component. The success of the model adopted here, which does not include velocity changing collisions, indicates that in the range of pressures observed ($p \geq 30$ mtorr), contributions from such collisions are negligible in NH_3 .

4. Conclusion

These first results demonstrate the power of time-delayed saturation spectroscopy. By combining frequency and time-domain measurements in NH_3 we have obtained a complete set of information which improves our knowledge of the dynamics of the excited vibrational state, providing the first measurement of a molecular alignment relaxation rate in an infrared transition.

We have already pointed out the applicability of time-delayed saturation spectroscopy to optical nutation and photon echoes in multilevel systems. To underscore the generality of the technique, notice that it provides a precise analysis of the dynamics of atomic and molecular systems: Scattering and diffusion mechanisms, thermalization by velocity-changing collisions and radiative transfer, velocity-dependence of such processes can all be studied. Extension to four-level systems, where pump and probe transitions have no common level, should lead to similar information about inelastic collisions. These kinds of experiments in excited neon are now underway at Université Paris-Nord (France).

Acknowledgments

We are grateful to our colleagues José Leite, Antonio Sanchez and Dan Seligson for their contributions to various parts of this work.

References

- 1 See e.g. V.S. Letokhov and V.P. Chebotayev, Nonlinear Laser Spectroscopy, Springer Series in Optical Sciences, Vol. 4, (Springer-Verlag, 1977).
- 2 See the contribution by R.G. Brewer in this volume.
- 3 A time-delayed Lamb dip experiment has been performed using a pulsed dye laser to produce counter-propagating beams: T.W. Hänsch, I.S. Shahin and A.L. Shcawlow, Phys. Rev. Lett. **27**, 707 (1971). It should be noted that pulsed lasers are not

ideal for such studies. The present approach has the advantage that the system can be prepared in a well defined steady state, and the weak c.w. field can precisely probe its decay. The importance of studying both co- and counter-propagating change signals is also emphasized.

- 4 M. Ducloy and M.S. Feld, J. de Phys.-Lettres (Paris) 37, L-173 (1976); M. Ducloy, J. Leite, R. Sheffield and M.S. Feld, Bull. Am. Phys. Soc. 21, 599 (1976).
- 5 M. Ducloy, J.R.R. Leite and M.S. Feld, to be published.
- 6 Both single and double-quantum Raman-type processes can occur in coupled systems of this type having a resonant intermediate state. See, for example, M.S. Feld in Fundamental and Applied Laser Physics, edited by M.S. Feld, N.A. Kurnit and A. Javan (Wiley, New York, 1973), pp. 369-420.
- 7 J.R.R. Leite, M. Ducloy, A. Sanchez, D. Seligson and M.S. Feld, to be published.
- 8 For a general review of tensorial formalism and multipole moments see A. Omont in Progress in Quantum Electronics, Vol. 5, p. 69 (Pergamon Press, Oxford, 1977). For their application in laser spectroscopy see B. Decomps, M. Dumont and M. Ducloy in Laser Spectroscopy of Atoms and Molecules p. 283 (Topics in Applied Physics, Vol. 2, Springer-Verlag, 1976).
- 9 M. Gorlicki and M. Ducloy, to be published.
- 10 G.M. Dobbs, R.H. Mischeels, J. Steinfeld, J.H.S. Wang and J.M. Levy, J. Chem. Phys. 63, 1904 (1975).

Laser Saturation Resonances in NH_3 Observed in the Time-Delayed Mode

J. R. R. Leite,^(a) M. Ducloy,^(b) A. Sanchez,^(c) D. Seligson, and M. S. Feld
*Department of Physics and Spectroscopy Laboratory, Massachusetts Institute of Technology,
 Cambridge, Massachusetts 02139*

(Received 26 August 1977)

A time-delayed technique is used to study the decay of narrow laser saturation resonances induced in the ν_2 as $Q(8,7)$ transition of NH_3 . The experiments dramatically separate the distinct contributions to the line shape due to population saturation and Raman-type processes, and yield a value of 3.5 ± 0.6 MHz/Torr for the excited-state population decay rate.

This Letter reports the first observation of a new category of effects, called time-delayed laser saturation spectroscopy, which combines the high-resolution techniques of laser saturation spectroscopy with those of coherent transients observed in the heterodyne mode to provide a precise way of studying a molecular system as it evolves from an initially prepared stationary state to a second final state. In the experiments a weak, tunable, monochromatic field probes the line shape of the narrow resonance induced in a Doppler-broadened molecular system after the saturating laser field is suddenly turned on or off, or switched in frequency [Fig. 1(a)]. Both two-level and multilevel systems with or without a common level can be studied in either transmission or fluorescence.

Experiments of this type are inherently different from conventional optical-nutation and free-induction-decay experiments,¹ where the probe field does not interact with the molecules and serves only as a local oscillator for heterodyne detection. Thus, in the experiments of Ref. 1

there is no resonant behavior as the probe field is tuned. For the same reason the new technique is not an analog of pulse Fourier-transform spectroscopy.² As seen below, the observed decay time need not be related to the inverse linewidth, and different portions of the line shape may decay

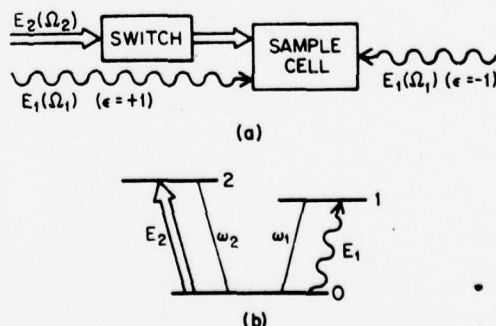


FIG. 1. (a) Simplified setup for observing time-delayed laser saturation resonances. E_2 is the saturating field and E_1 the probe field. The applied fields may be either copropagating ($\epsilon = +1$) or counterpropagating ($\epsilon = -1$). (b) Energy level diagram.

with different characteristic times. Thus, the shape of the change signal can evolve in time. This time-dependent line-shape distortion is utilized in the present experiments to separate dramatically the contributions of level population saturation from those of Raman-type processes.

These first results in time-delayed laser saturation spectroscopy clearly demonstrate the power of the technique. It is illustrated here in a three-level system, where it has allowed us to separate in time the different physical processes contributing to the steady-state, laser-induced line-narrowing change signals. This method can be applied to many other laser phenomena, including observation of Ramsey-type fringes,³ three-level optical nutation, and photon echoes. It also provides a powerful tool for analyzing the dynamical response of atomic and molecular systems: Relaxation mechanisms such as elastic and inelastic scattering, velocity-changing collisions, and radiative trapping can all be studied.

In the example studied here, three-level free decay, an intense field E_2 , of frequency Ω_2 , saturates a Doppler-broadened transition (0-2, center frequency ω_2) as a weak, tunable, monochromatic field, E_1 (Ω_1), probes the coupled 0-1 transition, frequency ω_1 [Fig. 1(b)]. Saturating and probe beams overlap and may be either copropagating ($\epsilon = +1$) or counterpropagating ($\epsilon = -1$). The probe transmission exhibits a sharp resonant change ("change signal") when Ω_1 is tuned such that both fields interact with the same velocity group: $\Omega_1 = \Omega_1^{(\epsilon)} = \omega_1 + \epsilon(\omega_1/\omega_2)(\Omega_2 - \omega_2)$. The narrow steady-state resonances obtained by this technique, known as laser-induced line narrowing, have been extensively studied over the past decade.^{4,5} In the present work frequency and time domains are observed simultaneously by suddenly interrupting the saturating field at $t = 0$ and studying the transient change-signal line shape at later times.

As discussed in an earlier work,⁶ the time behavior of the probe signals provides a unique way of separating the effects of population saturation and Raman-type processes,^{4,7} because of their different characteristic decay times. For instance, for weakly saturating E_2 field and close transition frequencies ($\omega_2 \approx \omega_1$) the change-signal line shape is given by⁶

$$g(\epsilon) = \text{Re} \left[\frac{\exp(-\gamma_0 t)/\gamma_0}{\Gamma + i\delta(\epsilon)} + \frac{\epsilon + 1}{2} \frac{e^{-\Gamma t/\Gamma}}{\gamma_{12} + i\delta(\epsilon)} \right], \quad (1)$$

where $\delta(\epsilon) = \Omega_1 - \Omega_1^{(\epsilon)}$ is the detuning from the center frequency of the narrow resonance and Γ

$= \gamma_{01} + \gamma_{02}$. γ_0 is the relaxation rate of the population of level 0 and γ_{ij} is the decay rate of the i - j coherence, γ_{0j} for the optical polarization, γ_{12} for the coherence induced by 1-2 Raman-type transitions. Equation (1) is obtained in the limit of strong phase-changing collisions: $\gamma_{01}, \gamma_{02} \gg \gamma_0, \gamma_{12}$.⁶

The first term of (1) describes a broad resonance of width $\gamma_{01} + \gamma_{02}$, induced by the population saturation of level 0, and thus decaying at rate γ_0 . This is the only contribution to the decaying backward change signal ($\epsilon = 1$, Lamb-dip-type configuration). Raman-type contributions are absent: Because of their strong velocity dependence they cancel in the integration over the broad molecular velocity distribution leading to (1). In contrast, in the forward direction ($\epsilon = +1$) there is an additional contribution in the form of a narrow resonance of width γ_{12} , induced by Raman-type transitions, which decays at the much faster rate of $\Gamma = \gamma_{01} + \gamma_{02}$. Since $E_2 = 0$ for $t > 0$, transient Raman processes do not occur (as they would in three-level optical nutation). But their influence is contained in the initial polarization induced at the probe frequency, and thus decays with it. The decay rate of this initial polarization contains two terms, the normal γ_{01} rate and a "Doppler dephasing" contribution, γ_{02} . This latter term is due to the velocity spread of the initially excited molecules, which gives rise to a corresponding spread in the reemitted frequencies and leads to destructive interference in a time $t \approx \gamma_{02}^{-1}$.

In the experiments the ν_2 as Q(8, 7) transition of NH_3 was saturated and probed using two linearly polarized cw N_2O lasers oscillating on the $P(13)$ line ($\lambda = 10.78 \mu\text{m}$), which falls within the NH_3 Doppler profile. A 10-cm glass sample cell with NaCl end windows was used. With the frequency of the saturating laser held fixed, the probe was tuned by means of a calibrated piezoelectric transducer. The polarization vectors of the two laser beams were oriented at right angles to one another. NaCl beam splitters were used to overlap the beams before the sample cell and separate them afterwards. A flip mirror was used to reverse the direction of the saturating beam and thereby select forward or backward configurations. The probe transmission was monitored using a He-cooled Cu-Ge detector. The saturating beam was chopped with an external electro-optical modulator, a GaAs crystal to which high-voltage square pulses were applied (rise time 30 ns, duration 10 μs , repetition rate 1 kHz), thus

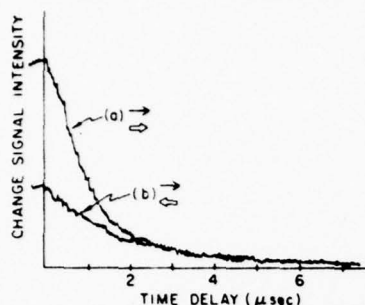


FIG. 2. Time-domain study of (a) forward and (b) backward change signals; $p = 25$ mTorr. In these traces the probe field is tuned to line center ($\delta(\pm) = 0$). The backward decay is a single exponential, whereas the forward decay contains fast and slow exponential components.

inducing a fast rotation of the polarization of the cw saturating beam. A subsequent analyzer, a Brewster-angle silicon plate, yielded the square pulses of the saturating beam. The frequency resolution of the system, determined by laser frequency jitter, transit time, and misalignment of probe and saturating beams, was about 300 kHz.

Transient change signals were analyzed with a boxcar integrator operated in two different modes: either monitoring the decaying signal at a fixed probe frequency (Fig. 2), or scanning the probe frequency at fixed time delays (Fig. 3). The $t = 0$ signals of Fig. 3 correspond to the steady-state regime studied in earlier experiments.⁸

Since the NH_3 transition is degenerate ($J = 8-8$) and the two beams have perpendicular linear polarizations, the saturating field can be considered to induce $\Delta M = 0$ transitions, and the weak field then probes $\Delta M = \pm 1$ transitions. In the absence of M -changing collisions the system decomposes into two groups of coupled three-level systems having the common level in the ground (g) and excited (e) states, respectively. The Raman coherence responsible for the forward-backward asymmetry of the $t = 0$ signals of Fig. 3 is thus the coherence between adjacent M sublevels. The analysis leading to Eq. (1) then predicts that forward and backward signals differ by the narrow Raman-type contribution, and that this contribution decays away rapidly, leaving a slowly decaying population-induced component which is the same for both propagation directions. Figures 2 and 3 give direct experimental evidence for the two distinct physical processes which contribute to the narrow resonances of laser-induced

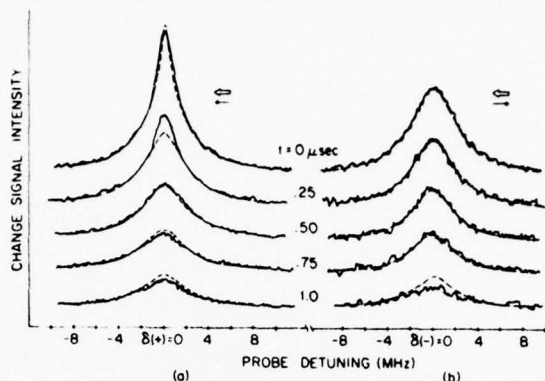


FIG. 3. Time-delayed line shapes observed in (a) forward and (b) backward directions; $p = 30$ mTorr. The dashed curves give the theoretical fit.

line narrowing.

A quantitative analysis of the experiments must take into account the occurrence of M -changing collisions.⁸ This is done by using the tensorial formalism and allowing for different multipole relaxation rates in each level.⁹ A careful study of the steady-state line shapes⁸ shows that the width of the narrow Raman-type contribution arises essentially from the decay of the excited-state alignment, yielding a relaxation rate $\gamma_e^{(2)} = 6 \pm 1$ MHz/Torr. Just as in the simple theory of Eq. (1), this contribution decays at twice the optical dipole relaxation rate $2\gamma_e^{(1)} = 48 \pm 2$ MHz/Torr, as obtained from the linewidth of the backward signal. On the other hand, the tensorial analysis shows that the dominant contribution to the decay of the backward signal comes from the excited-state population. Its line-center decay [Fig. 2(b)] then yields $\gamma_e^{(0)} = 3.5 \pm 0.6$ MHz/Torr (Fig. 4), in agreement with a previous measurement.¹⁰ Finally, microwave experiments¹¹ have shown that the relaxation of the ground state is governed by a single rate, $\gamma_g \approx 24$ MHz/Torr. Since all the parameters are known, one can compare theoretical predictions (dashed curves of Fig. 3) and experimental line shapes.¹² The agreement is quite good, except for the short-term ($t = 0.25$ μs) behavior of the forward signal, where the time resolution of the electronic detection system (0.1 μs) was not high enough to follow the fast decay of the narrow component.

Several recent experiments¹³⁻¹⁶ have investigated the transient behavior of cascade and folded three-level systems when the two-quantum (or Raman) transition is resonant or nearly resonant but the applied fields are detuned from their re-

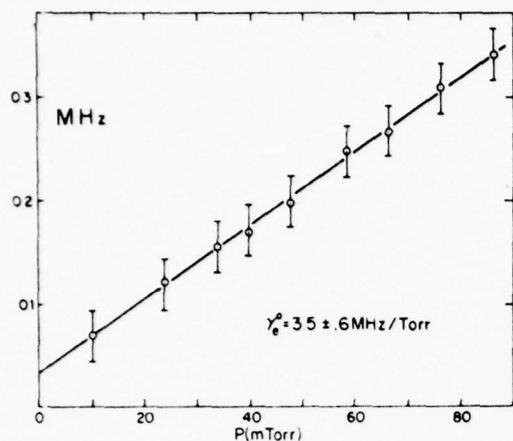


FIG. 4. $\gamma_e^{(0)}$ vs pressure. The data were taken from backward change signals [Fig. 2(b)].

spective single-quantum transitions. Unlike the present studies, in which the intermediate state (level 0) is resonant, in these experiments the buildup of population in the intermediate state is small and there is no interference between single- and double-quantum events. Thus, the form of the change signals simplifies and many of the line-shape details discussed above are absent. Furthermore, the large intermediate-state detuning causes the change-signal contribution coming from the initially prepared polarization to follow adiabatically the saturating field, so that information about the decay of the initial polarization is absent. Further comparison of these two types of experiments is given by Ducloy, Leite, and Feld,³ who also derive the line-shape expressions for the case of fully saturating E_2 . A time-delayed Lamb-dip experiment has also been performed using a pulsed dye laser to produce counterpropagating beams.¹⁷

This work was supported in part by the National Science Foundation and by the U. S. Army Research Office (Durham). One of us (M.S.F.) acknowledges receipt of an Alfred P. Sloan Foundation Fellowship.

^(a) Present address: Universidade Federal de Pernambuco, Recife, Brazil.

^(b) Present address: Laboratoire de Physique des Lasers, Université Paris-Nord, 93430 Villetaneuse, France.

^(c) Present address: Lincoln Laboratory, Lexington, Mass. 02173.

¹R. G. Brewer and R. L. Shoemaker, Phys. Rev. A **6**, 2001 (1972).

²S. B. Grossman, A. Schenzle, and R. G. Brewer, Phys. Rev. Lett. **38**, 275 (1977).

³M. Ducloy, J. R. R. Leite, and M. S. Feld, Phys. Rev. A (to be published).

⁴M. S. Feld, in *Proceedings of the Esfahan Symposium on Fundamental and Applied Laser Physics*, edited by M. S. Feld, N. A. Kurnit, and A. Javan (Wiley, New York, 1973), p. 369.

⁵V. P. Chebotayev, in *High Resolution Laser Spectroscopy*, Topics in Applied Physics, edited by K. Shimoda (Springer, New York, 1976), Vol. 13, p. 201.

⁶M. Ducloy and M. S. Feld, J. Phys. (Paris), Lett. **37**, L-173 (1976).

⁷One example of Raman-type processes in the double-quantum event in which a molecule initially in level 2 undergoes transition to level 1 by exchanging two photons of energies $\hbar\Omega_1$ and $\hbar\Omega_2$ with the applied radiation fields without loss of phase memory. However, the term "Raman-type processes" also includes coherent single-quantum transitions (see Ref. 4).

⁸J. R. R. Leite, M. Ducloy, A. Sanchez, D. Seligson, and M. S. Feld, preceding Letter [Phys. Rev. Lett. **39**, 1465 (1977)].

⁹M. Gorlicki and M. Ducloy, to be published.

¹⁰S. M. Hamada, A. T. Mattick, N. A. Kurnit, and A. Javan, Appl. Phys. Lett. **27**, 21 (1975).

¹¹G. M. Dobbs, R. H. Mischeels, J. Steinfeld, J. H. S. Wang, and J. M. Levy, J. Chem. Phys. **63**, 1904 (1975).

¹²In the theoretical curves of Fig. 3 an average power broadening of 0.5 MHz was included, using the expressions of Ref. 3.

¹³M. Bassini, F. Biraben, B. Cagnac, and G. Grynberg, Opt. Commun. **21**, 263 (1977).

¹⁴D. Grischkowsky, Phys. Rev. A **14**, 802 (1976).

¹⁵P. F. Williams, D. L. Rousseau, and S. H. Dworket-sky, Phys. Rev. Lett. **32**, 196 (1974).

¹⁶J. L. Carlsten and A. Szöke, Phys. Rev. Lett. **36**, 667 (1976), and J. Phys. B **9**, L231 (1976).

¹⁷T. W. Hänsch, I. S. Shahin, and A. L. Schawlow, Phys. Rev. Lett. **27**, 707 (1971). It should be noted that pulsed lasers are not ideal for such studies. The present approach has the advantage that the system can be prepared in a well-defined steady state, and the weak cw field can precisely probe its decay. The importance of studying both copropagating or counterpropagating change signals is also emphasized.

Laser saturation spectroscopy in the time-delayed mode. Theory of optical free induction decay in coupled Doppler-broadened systems

Martial Ducloy*

Laboratoire de Physique des Lasers, Université Paris-Nord, 93430 Villetaneuse, France

José R. R. Leite[†] and Michael S. Feld

Department of Physics and Spectroscopy Laboratory, Massachusetts Institute of Technology, Cambridge, Massachusetts 02139

(Received 4 August 1977)

This paper describes a new class of techniques, called time-delayed laser saturation spectroscopy, which combine frequency- and time-domain methods of laser spectroscopy to provide a way of studying a molecular system as it evolves from an initially prepared stationary state to a second, final state. The specific example analyzed here is three-level free induction decay, in which the time-dependent gain of a Doppler-broadened molecular transition is probed after the sudden termination of an intense field resonating with a coupled transition. The theoretical calculation is based on the coupled density-matrix equations of motion in the slowly-varying envelope approximation. The time-delayed line shapes, which may be studied in either transmission or side fluorescence, exhibit linewidth asymmetries, line-shape deformations, Ramsey-type fringes, power broadening and dephasing, and dynamic Stark splittings and oscillatory decays. The technique provides a unique way of distinguishing the influence of Raman-type processes from that of population saturation and a means to separately measure the associated decay rates. The relationship of the present work to other studies is also discussed.

1. INTRODUCTION

Developments over the past decade of powerful techniques in laser spectroscopy for measuring atomic and molecular structure and collisional dynamics in Doppler-broadened gases can be classified in two major categories. On the one hand, steady-state phenomena such as standing-wave saturation¹⁻³ (Lamb dip) and laser-induced line narrowing⁴⁻⁶ (three-level) techniques have been used to obtain spectroscopic information in the frequency domain with great precision. On the other hand, coherent transient phenomena such as free-induction decay,⁷ optical nutation,⁸ and photon echoes⁹ have been used in obtaining new information about relaxation processes in the time domain. The main point of this paper is to show that by merging the techniques of these two categories one can combine the advantages of transient and steady-state spectroscopy to extend the range of available information.

To illustrate the new class of techniques, consider a conventional high-resolution spectroscopy experiment in which a tunable monochromatic probe is tuned through a Doppler-broadened transition saturated by an intense monochromatic field to obtain a narrow saturation resonance (Fig. 1). Now suppose that the intense field is suddenly turned off, and the line shape of the narrow resonance is probed a fixed interval of time later. As the time delay is increased the change signal will become smaller, corresponding to the decay of the saturated molecules and their return to equilibrium.

Thus, by studying the line shape as a function of delay time a family of curves can be generated. This information can be combined to form a surface in a coordinate system having axes: change-signal intensity (z axis), frequency detuning (x axis), time delay (y axis) (Fig. 2). Sections parallel to the x axis give the change-signal line shape at delayed times. Similarly, sections parallel to the y axis give the free decay of the system at various frequencies. Note that this surface could have equally well been generated from the family of curves obtained from the time decay of the steady-state change signal, holding the probe field fixed at various frequencies.

Studies of this type might well be termed "frequency-time-domain spectroscopy" because both

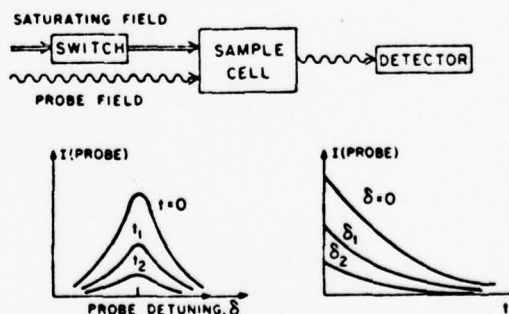


FIG. 1. Simplified setup for time-delayed saturation spectroscopy experiments. The double arrow indicates the saturating field, the wavy arrow the probe field. The saturating field is terminated at time $t = 0$.

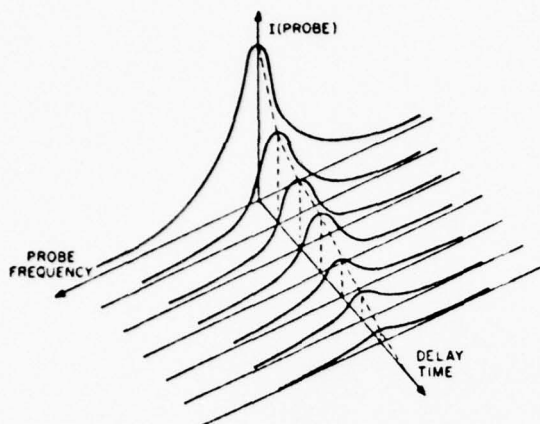


FIG. 2. Three-dimensional representation of the time-delayed change signals.

types of information are obtained simultaneously. As will be seen, such studies extend the possibilities of laser saturation spectroscopy, which only provides information in the frequency domain, as well as those of ordinary coherent transient experiments, which only provide time-domain information.

These time-delayed change signals have some very interesting features. For example, their characteristic decay times may be totally unrelated to the inverse steady-state linewidths. What is more, different portions of the line shape can decay at different rates. Consequently, the *shape* of the narrow resonance can change during the decay process. This behavior occurs because the change signal is composed of contributions arising from different physical processes (population saturation, Raman-type processes, etc.), each of which has a different steady-state linewidth and decays at a different rate. Thus, new physical information not available from the steady-state line shape can be obtained by studying the free decay of the change signal and its line shape as it evolves in time. Other features which can manifest themselves in the time-delayed line shapes include power broadening and dephasing, ac Stark splittings, oscillatory decays, and narrow Ramsey-type resonances.

The time-delayed saturation signals have some features in common with conventional free-induction decay signals observed by means of heterodyne detection using a monochromatic laser field as the local oscillator.⁷ In the new technique the probe field acts as a local oscillator to beat with the transient signals induced when the intense field is terminated. However, in this case the probe field also resonantly interacts with the saturated molecules, which is not the case in the heterodyne de-

tection of ordinary free-induction decay. It is this interaction which gives rise to the observation of narrow spectral line shapes. In contrast, the ordinary free-induction decay signal is the same, independent of the tuning of the heterodyne laser. This distinction will be made more explicit in what follows.

As is evident from the above discussion, the time decay of the change signal is not simply the Fourier transform of the steady-state line shape. Thus, the present technique is not an analog of Fourier transform spectroscopy,¹⁰ where a computer is used to transform free-induction decay signals and thus obtain a frequency spectrum. One might loosely say that in the new technique the molecules themselves take the transform of the free-decay signals, but it is emphasized that the frequency-domain signals so obtained contain physical information not present in the signals of ordinary free-induction decay. This distinction will be elaborated later on.

The experiment above is one example of a class of time-delayed laser-saturation techniques. Similar behavior will also occur when studying the time-delayed probe line shapes after the intense field is suddenly turned on (analog of optical nutation).¹¹ The technique is also applicable to studying echoes and other coherent phenomena. Also note that the effects can be studied both in two-level systems and in coupled three-level systems, either by observing the probe transmission or by detecting the side fluorescence from one of the interacting levels. In all cases there are interesting features which depend on whether the probe is co-propagating or counter-propagating with respect to the intense field.

The present paper presents a theoretical analysis of one aspect of this new class of phenomena, three-level free-induction decay, and discusses the new information available, as compared to that obtainable in the usual free-decay and steady-state three-level experiments. In this type of experiment the intense field saturates one transition and the probe field, which may be co- or counter-propagating, acts on a coupled transition (Fig. 3). Both folded [Figs. 3(a) and 3(b)] and cascade [Fig. 3(c)] systems may be studied. This technique pro-

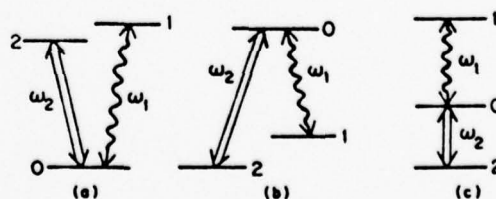


FIG. 3. Energy level diagrams.

vides a novel way of measuring relaxation processes, and a unique means of separating the effects of population saturation from those of Raman-type processes (see below). One application is to describe the transient behavior of optically pumped lasers.

A brief description of the technique and some of the line-shape features of three-level free decay and optical nutation were given in an earlier publication.¹² An experiment which demonstrates the technique in NH_3 will be reported elsewhere.¹³

In this paper, after a discussion of the equations of motion in a three-level system (Sec. II), we calculate the molecular response at the probe frequency for arbitrary intensities of the saturating field (Sec. III) and present a detailed study of the velocity average. The two subsequent sections are devoted to the discussion of the transient response of the probe field in the limits of weak (Sec. IV) and strong (Sec. V) saturating field intensities.

Section VI calculates the time evolution of the side fluorescence and compares the results with those obtained for the probe transmission.

Many different symbols will be used throughout this article. To make it easier to read, a glossary of the main symbols is given in Table I.

Before presenting the theoretical analysis, let us mention some relevant previous studies: coherent Raman beats observed in the response of a single electromagnetic (e.m.) field to the sudden Stark splitting of a degenerate transition,^{14,15} fluorescence quantum beats induced by pulse excitation,¹⁶ transient two-photon absorption^{17,18} and Raman emission,¹⁹ both in the case of a nonresonant intermediate state, and transients in infrared-microwave double resonance.²⁰ An experiment to study the time-delayed Lamb dip in sodium has also been performed.²¹ The connections between some of these works and the present technique will be discussed in the concluding section (Sec. VII).

TABLE I. Glossary of symbols.

	Equation	
$E_1, E_2, \mathcal{E}_1^0, \mathcal{E}_2^0$	(1)	Electromagnetic fields
$g(t), g_0$	(9b), (28a)	Probe gain
$G(\omega)$	(27)	Velocity distribution
k_1, k_2	(1)	Wave vectors
L_1, L_2, L_{12}	(4)	Resonant frequency denominators
L_B, L_N, L_B^0, L_N^0	(88), (91)	Lorentzian resonance line shapes
P_1, \mathcal{P}_1	(8)	Macroscopic polarization
Q	(30)	$\sqrt{1+s}$
s	(19)	Saturation parameter
S	(42b)	High-frequency Stark splitting
u	(27)	Thermal velocity
v_1, v_2, v_{12}^0	(28), (33), (57)	Resonant velocities
$\bar{v}_2, \bar{v}_{12}, \bar{v}_{12}^0$	(29), (A6), (57)	(Complex) resonant velocities
α, β	(5)	Rabi frequencies
γ_{ij}	(6)	Relaxation rate of σ_{ij}
$\gamma_B, \gamma_N, \gamma_B^0, \gamma_N^0$	(36), (37), (50), (51)	Effective decay rates
$\gamma(c)$	(39)	Resonance linewidth
$\bar{\gamma}, \Gamma, \Gamma'$	(42d), (42e), (42c)	Effective decay rates
$\delta_1, \delta_2, \delta_{12}$	(A3)	Frequency detunings
$\delta(c)$	(34)	Probe frequency detuning
$\Delta, \Delta', \Delta_2$	(42a), (42e), (72)	Frequency detunings
$\Delta g'$	(28b)	Gain change
Δn_1	(85)	Population change
$\Delta \sigma_{01}^{(1)}, \Delta \sigma_{11}^{(2)}$	(23), (83)	Density matrix changes
$\zeta(c)$	(92), (93)	Population-change line shape
κ	(42c)	$(k_2 - k_1)/k_2$
Λ	(41b)	
$\xi(c)$	(53), (55)	Gain-change line shape
ρ_{ij}, σ_{ij}	(2)	Density matrix
χ	(A4)	$(ck_2 - k_1)/k_1$
ω_1, ω_2		Molecular frequencies
Ω_1, Ω_2	(1)	Laser frequencies
$\Omega_1^{(c)}$	(35)	Probe peak frequency

II. EQUATIONS OF MOTION

A. Background

When an intense monochromatic field E_2 , frequency Ω_2 , resonantly interacts with one of the transitions, 0-2, of a Doppler-broadened molecular (or atomic) gas, the level populations of the transition are altered over a narrow range of axial velocities centered about velocity v_2 satisfying the resonance condition (in the molecular rest frame) $\Omega_2 - k_2 v_2 = \omega_2$ (ω_2 being the molecular center frequency; $k_2 = \Omega_2/c$). This selective saturation of the level populations alters the spectral properties of a second coupled transition, 0-1, molecular center frequency ω_1 , formed by either of the saturated levels and a third level (Fig. 3). In particular, if a weak monochromatic probe field E_1 , frequency Ω_1 , propagating either parallel (+) or antiparallel (-) to E_2 is tuned through the 0-1 transition, a narrow resonant change in transmission occurs, superimposed upon the broad Doppler profile, when Ω_1 is such that the probe field interacts with molecules of velocity v_1 : $\Omega_1 = \omega_1 \pm k_1 v_1$ ($k_1 = \Omega_1/c$). This effect, called laser-induced line narrowing, has been the subject of numerous theoretical⁴ and experimental⁵ investigations devoted to studying the line shape of the change signal and using the narrow resonances thus obtained in high-resolution spectroscopic studies.⁶ It is now well known that this effect cannot be analyzed in terms of population-saturation considerations alone, and that coherent processes play an important role. For example, via double-quantum processes a molecule initially in level 2 can undergo transition to level 1 by exchanging two photons of energy $\hbar\Omega_1$ and $\hbar\Omega_2$ with the applied radiation fields without loss of phase memory.

Because of the close correspondence with the Raman effect, transitions of this kind are sometimes called Raman-type processes.²² Such processes exhibit very different dependence on molecular velocity, according to whether E_1 and E_2 are co-propagating or counter-propagating. This difference gives rise to a directional anisotropy in the net response, comprised of contributions from molecules of all velocities. Thus, the line shapes observed in co-propagating case (forward change signal) and counter-propagating case (backward change signal) always differ, in some cases dramatically. This directional anisotropy has been used to advantage in the recently introduced high-resolution spectroscopic techniques using Doppler-free two-photon absorption.²³

The aim of this paper is to study the transient response of the molecular medium as observed on the transmission of the probe field after E_2 is abruptly terminated. As will be seen, many of the

features discussed in the introduction will occur. One particularly interesting feature lies in the relative time evolution of population-saturation contributions versus Raman-type processes. As soon as E_2 is terminated Raman-type processes cease to occur, since E_2 is absent and can have no direct influence. However, the initial (steady-state) value of $P_1(t)$, the optical polarization oscillating at Ω_1 , is influenced by the Raman-type processes occurring during the preparative step ($t \leq 0$). The probe change signals are completely determined by $P_1(t)$. Therefore, as $P_1(0)$ decays the directional anisotropy and other features of the change-signal line shapes associated with Raman-type processes will gradually disappear. This effect is particularly striking when the polarization decay rate (" T_2 processes") exceeds that of the level populations (" T_1 processes"), $T_2 \ll T_1$, so that the change signals can persist well beyond the decay of $P_1(0)$. In this case the shape of the forward change signal will evolve in time, as the influence of Raman-type processes decreases, and with increasing time delay the initially different forward and backward change-signal line shapes will eventually become identical. This opens the possibility of uniquely distinguishing the influence of Raman-type processes from that of population saturation and to separately measure the associated decay rates.

B. Coupled equations in the slowly varying envelope approximation

Consider a sample cell of gas molecules irradiated by two e.m. fields, $E_1(\Omega_1)$ and $E_2(\Omega_2)$, propagating along the z axis, having wave vectors k_1 and ϵk_2 , $\epsilon = +1$ or -1 according to whether E_2 propagates parallel or antiparallel to E_1 :

$$\begin{aligned} E_1 &= \delta_1^0 \cos(\Omega_1 t - k_1 z), \\ E_2 &= \delta_2^0 \cos(\Omega_2 t - \epsilon k_2 z). \end{aligned} \quad (1)$$

The molecular energy levels of interest, levels 0, 1, and 2, form a pair of Doppler-broadened transitions with molecular center frequencies ω_1 and ω_2 sharing a common level (Fig. 3). It is assumed that Ω_1 is close to ω_1 and Ω_2 to ω_2 , so that E_1 resonates with the 0-1 transition ($|\Omega_1 - \omega_1| < \text{Doppler width}$). It is further assumed that E_2 cannot resonate with the 0-1 transition, nor E_1 with the 0-2 transition. This can be ensured either by proper choice of the polarizations of the E fields or by having the molecular center frequencies sufficiently separated ($|\omega_1 - \omega_2| > \text{Doppler widths}$). To be specific, the problem will be formulated for the three-level configuration of Fig. 3(a), a folded system with level 0 lying lowest. The equations describing the other level configurations, Figs.

3(b) and 3(c), are more or less the same.^{24(a)}

The system's time evolution can be conveniently described by means of the ensemble-averaged density-matrix formalism, in which $\rho_{ij}(v)$ is the density-matrix element describing the molecules with axial (z-axis) velocity component v . ρ_{jj} is the population of level j , ρ_{0j} ($j=1,2$) is the optical coherence associated with the 0- j transition (it is proportional to the induced polarization oscillating at Ω_j), and ρ_{12} represents the macroscopic molecular coherence induced between levels 1 and 2. The following transformation allows one to go into the rotating frame:

$$\begin{aligned}\rho_{ii} &= \sigma_{ii}, \\ \rho_{0i} &= \sigma_{0i} \exp[i(\Omega_i t - k_1 z)], \\ \rho_{02} &= \sigma_{02} \exp[i(\Omega_2 t - \epsilon k_2 z)], \\ \rho_{12} &= \sigma_{12} \exp\{i[(\Omega_2 - \Omega_1)t - (\epsilon k_2 - k_1)z]\},\end{aligned}\quad (2)$$

where the σ_{ij} are the slowly varying envelopes ($\partial \sigma_{ij}/\partial t \ll \omega \sigma_{ij}$, $\partial \sigma_{ij}/\partial z \ll k \sigma_{ij}$). In the rotating-wave approximation the σ_{ij} obey the following equations of motion^{24b}:

$$\begin{aligned}\dot{\sigma}_{00} + \gamma_0(\sigma_{00} - n_0) &= -\frac{1}{2}i\alpha(\sigma_{01} - \sigma_{01}^*) - \frac{1}{2}i\beta(\sigma_{02} - \sigma_{02}^*), \\ \dot{\sigma}_{11} + \gamma_1(\sigma_{11} - n_1) &= \frac{1}{2}i\alpha(\sigma_{01} - \sigma_{01}^*), \\ \dot{\sigma}_{22} + \gamma_2(\sigma_{22} - n_2) &= \frac{1}{2}i\beta(\sigma_{02} - \sigma_{02}^*), \\ \dot{\sigma}_{12} + L_1 \sigma_{12} &= \frac{1}{2}i\alpha\sigma_{02} - \frac{1}{2}i\beta\sigma_{01}^*, \\ \dot{\sigma}_{01} + L_1 \sigma_{01} &= \frac{1}{2}i\alpha(\sigma_{11} - \sigma_{00}) + \frac{1}{2}i\beta\sigma_{12}^*, \\ \dot{\sigma}_{02} + L_2 \sigma_{02} &= \frac{1}{2}i\beta(\sigma_{22} - \sigma_{00}) + \frac{1}{2}i\alpha\sigma_{12},\end{aligned}\quad (3)$$

where $\dot{\sigma} = d\sigma/dt$,

$$\begin{aligned}L_1 &= \gamma_{01} + i(\Omega_1 - \omega_1 - k_1 v), \\ L_2 &= \gamma_{02} + i(\Omega_2 - \omega_2 - \epsilon k_2 v), \\ L_{12} &= \gamma_{12} + i[\Omega_1 - \Omega_2 - \omega_1 + \omega_2 - (k_1 - \epsilon k_2)v],\end{aligned}\quad (4)$$

and

$$\alpha = \mu_{01} \mathcal{E}_1^0 / \hbar, \quad \beta = \mu_{02} \mathcal{E}_2^0 / \hbar. \quad (5)$$

In Eqs. (3)–(5), μ_{0j} is the dipole-moment matrix element connecting levels 0 and j . The Rabi frequencies α and β can be taken to be real without loss of generality. The background population density of level j (i.e., its population in the absence of the applied laser field) in the narrow interval between v and $v+dv$ is denoted by $n_j(v)dv$,

$$n_j(v) = \bar{n}_j G(v), \quad \int G(v) dv = 1,$$

where \bar{n}_j is the total background population density of level j and $G(v)$ is the normalized velocity distribution. Finally, γ_i and γ_{ij} are the decay rates of the population of level i and the σ_{ij} coherence respectively. In general,

$$\gamma_{ij} \geq \frac{1}{2}(\gamma_i + \gamma_j). \quad (6)$$

The equality in Eq. (6) holds only when phase-changing collisions are absent, for instance in the case of radiative decay or relaxation by inelastic collisions.

The macroscopic polarization associated with the 0- j transition is given by

$$P_j = \text{Re}\{\Phi_j \exp[i(\Omega_j t - k_j z)]\},$$

with

$$\Phi_j = 2\mu_{0j}\langle\sigma_{0j}\rangle,$$

where $\langle \rangle$ denotes velocity integration over $G(v)$. The net field associated with the 0-1 transition is composed of incident and reradiated components,

$$E_1(z, t) = \text{Re}\{(\mathcal{E}_1^0 + \Delta\mathcal{E}_1) \exp[i(\Omega_1 t - k_1 z)]\}. \quad (7)$$

In the experiments of interest the sample is assumed to be optically thin and short (no phase-matching problem¹⁵). In this case the amplitude of the reradiated field will be small compared to the incident field ($|\Delta\mathcal{E}_1| \ll \mathcal{E}_1^0$). At the output face of the sample cell ($z=l$), ΔE_1 is then given by¹⁵

$$\Delta\mathcal{E}_1 = \frac{-2\pi i \Omega_1 l}{c} \Phi_1 = \frac{-4\pi i \Omega_1 l}{c} \mu_{01} \langle\sigma_{01}\rangle. \quad (8)$$

This gives rise to a change in transmitted intensity at the probe frequency:

$$I_1(t) = I_1^0 + \hbar \Omega_1 \alpha l \text{Im}\langle\sigma_{01}(t)\rangle, \quad (9a)$$

with $I_1 = c|\mathcal{E}_1|^2/8\pi$ and I_1^0 the incident intensity of the probe field. The last term of this expression is the heterodyne beat between the incident probe field and the reradiated field. It will exhibit transient behavior when the saturating field is turned on or off.

The gain at the probe transition can be defined by

$$I_1(t) = I_1^0 + g I_1^0.$$

We then have

$$g(t) = (8\pi/c) \Omega_1 l \mu_{01} \text{Im}\langle\sigma_{01}\rangle / \mathcal{E}_1^0. \quad (9b)$$

In transmission studies, and also in studies of spontaneous emission line shapes at the 0-1 transition,⁴ g is the quantity of experimental interest.

In some experiments²³ it may be more convenient to detect the net fluorescence emitted from a transition formed by level 1 and another lower-lying level, level 4, as E_1 is tuned through the 0-1 transition. In this case the net intensity emitted at the 1-4 transition, frequency ω , into solid angle $d\Omega$ is given by^{25,26}

$$I_F = (\omega^4 d\Omega / 2\pi c^3) \mu_{14}^2 \langle\sigma_{11}\rangle, \quad (10)$$

where μ_{14} is the 1-4 transition matrix element.

Note that in experiments of this type one directly monitors the time evolution of the total population of level 1, as opposed to the transmission experiments, which study $\langle \sigma_{01} \rangle$. However, the transient signals observed in the two cases will be similar, since the two quantities are intimately related.

C. General way of solving the equations

When the condition $\alpha \ll \gamma_{ij}$ is fulfilled, the probe field is weak enough so that Eqs. (3) can be solved by using a perturbation expansion of σ_{ij} in α :

$$\sigma_{ij} = \sum_n \sigma_{ij}^{(n)},$$

where $\sigma_{ij}^{(n)}$ is proportional to α^n . This expansion of σ_{ij} , when inserted in Eqs. (3), leads to a set of equations which can be solved for arbitrary intensities of the saturating field, i.e., for arbitrary values of β .

The zeroth-order set of equations corresponds to the case in which the probe field is absent ($\alpha = 0$). In this case the molecular system becomes equivalent to a two-level system:

$$\delta_{00}^{(0)} + \gamma_0(\sigma_{00}^{(0)} - n_0) = -\frac{1}{2}i\beta(\sigma_{02}^{(0)} - \sigma_{02}^{(0)*}), \quad (11a)$$

$$\delta_{22}^{(0)} + \gamma_2(\sigma_{22}^{(0)} - n_2) = \frac{1}{2}i\beta(\sigma_{02}^{(0)} - \sigma_{02}^{(0)*}), \quad (11b)$$

$$\delta_{02}^{(0)} + L_2\sigma_{02}^{(0)} = \frac{1}{2}i\beta(\sigma_{02}^{(0)} - \sigma_{02}^{(0)*}). \quad (11c)$$

There is no coherence between level 1 and levels 0-2,

$$\sigma_{01}^{(0)}(t) = \sigma_{12}^{(0)}(t) = 0, \quad (12)$$

and the population of level 1 is given by its background value,

$$\sigma_{11}^{(0)}(t) = n_1. \quad (13)$$

In the first order in α the E_1 field does not change the level populations, nor the 0-2 optical polarization,

$$\sigma_{11}^{(1)}(t) = \sigma_{02}^{(1)}(t) = 0, \quad (14)$$

but it induces an optical polarization at the 0-1 transition, as well as a coherence between levels 1 and 2. These two quantities satisfy the coupled equations

$$\delta_{01}^{(1)} + L_1\sigma_{01}^{(1)} = \frac{1}{2}i\alpha(n_1 - \sigma_{00}^{(0)}) + \frac{1}{2}i\beta\sigma_{12}^{(1)*}, \quad (15a)$$

$$\delta_{12}^{(1)*} + L_2\sigma_{12}^{(1)*} = -\frac{1}{2}i\alpha\sigma_{02}^{(0)*} + \frac{1}{2}i\beta\sigma_{01}^{(1)}. \quad (15b)$$

The 1-2 coherence results from Raman-type processes in which for example, the molecules undergo transitions from levels 2 to 1 by emitting a photon at Ω_2 and absorbing a photon at Ω_1 .²²

In the case of fluorescence measurements one needs to solve the equations up to the second order in α . The E_1 -induced population change of level 1 is given by

$$\delta_{11}^{(2)} + \gamma_1\sigma_{11}^{(2)} = \frac{1}{2}i\alpha(\sigma_{01}^{(1)} - \sigma_{01}^{(1)*}). \quad (16)$$

As can be seen from Eq. (16), in the *steady-state regime* fluorescence techniques and transmission measurements give equivalent information, since $\gamma_1\sigma_{11}^{(2)} = -\alpha \text{Im}\sigma_{01}^{(1)}$. This is a direct consequence of the energy conservation condition at the 0-1 transition.

Note that Eqs. (11)-(16) are valid regardless of the form of the time variations of β . In the following we shall deal with the free-decay case (constant $\beta \neq 0$ for $t < 0$, $\beta = 0$ for $t \geq 0$).

III. CALCULATION OF THE PROBE FIELD GAIN

A. Response of a molecular velocity group

In the steady-state regime ($t \leq 0$, $\dot{\sigma} = 0$), the solution of the zeroth-order Eqs. (11) is given by

$$\sigma_{02}^{(0)*}(0) = -i \frac{n_2\beta}{2} \frac{L_2}{|L_2(\beta)|^2}, \quad (17a)$$

$$\sigma_{00}^{(0)}(0) = n_0 + \frac{\beta^2}{2} \frac{\gamma_{02}}{\gamma_0} \frac{n_{20}}{|L_2(\beta)|^2}, \quad (17b)$$

where

$$L_2(\beta) = \gamma_{02}(1+s)^{1/2} + i(\Omega_2 - \omega_2 - ck_2v), \quad (18)$$

the saturation parameter s is proportional to the intensity of the E_2 field,

$$s = \beta^2(\gamma_0 + \gamma_2)(2\gamma_0\gamma_2\gamma_{02})^{-1}, \quad (19)$$

and n_{j0} is the 0- j background inversion density,

$$n_{j0} = n_j - n_0. \quad (20)$$

For $t > 0$ ($\beta = 0$) the decay of the population and of the 0-2 macroscopic polarization are straightforwardly given by

$$\sigma_{02}^{(0)*}(t) = \sigma_{02}^{(0)*}(0)e^{-L_2^*t}, \quad (21a)$$

$$\sigma_{00}^{(0)}(t) = n_0 + [\sigma_{00}^{(0)}(0) - n_0]e^{-\gamma_0 t}. \quad (21b)$$

The polarization at the probe frequency is obtained by solving Eqs. (15a) and (15b). The origin of the distinct contributions arising from population-saturation effects and Raman-type processes can be readily seen in the steady-state form of Eq. (15a),

$$L_1\sigma_{01}^{(1)} = \frac{1}{2}i\alpha(n_1 - \sigma_{00}^{(0)}) + \frac{1}{2}i\beta\sigma_{12}^{(1)*}. \quad (22)$$

The two terms on the right-hand side act as source terms to drive σ_{01} . The coupling between σ_{01} and the level populations is evident in the first term, which gives rise to the population-saturation contributions ("stepwise" transitions). The coupling of σ_{12} to the probe polarization appears in the second term, and is responsible for the occurrence of Raman-type contributions.

The expression for the polarization at the probe

frequency follows from Eqs. (15a) and (15b). It may be written in the form

$$\sigma_{01}^{(1)}(t) = \frac{1}{2} i \alpha \frac{n_{10}}{L_1} + \Delta \sigma_{01}^{(1)}(t). \quad (23)$$

The first term on the right-hand side describes the linear response of the probe field. It is independent of β and so does not exhibit transient behavior. After velocity integration it gives rise to the constant Doppler-broadened background gain.

The second term of Eq. (23) describes the influence of the saturating field on the probe polarization. Its value in the steady state may be obtained from the simultaneous solution of Eqs. (15a) and (15b) for $\dot{\sigma}_{ij} = 0$,

$$\Delta \sigma_{01}^{(1)}(0) = \frac{-\frac{1}{2} i \alpha \beta^2}{L_1 L_{12} + \frac{1}{4} \beta^2} \left[\frac{n_{10}}{L_1} + \frac{n_{20}}{|L_2(\beta)|^2} \times \left(L_2 + 2 \frac{\gamma_{02}}{\gamma_0} L_{12} \right) \right]. \quad (24)$$

The transient evolution of $\Delta \sigma_{01}^{(1)}$ is determined by Eq. (15a) with β set equal to zero. This leads to

$$\Delta \dot{\sigma}_{01}^{(1)} + L_1 \Delta \sigma_{01}^{(1)} = \frac{1}{2} i \alpha (n_0 - \sigma_{00}^{(0)}). \quad (25)$$

The solution is obtained with the help of Eqs. (17) and (21),

$$\Delta \sigma_{01}^{(1)}(t) = \Delta \sigma_{01}^{(1)}(0) e^{-L_1 t} + i \frac{\alpha \beta^2}{4} \frac{\gamma_{02}}{\gamma_0} \frac{n_{20}}{|L_2(\beta)|^2} \frac{e^{-L_1 t} - e^{-\gamma_0 t}}{L_1 - \gamma_0}, \quad (26)$$

where $\Delta \sigma_{01}^{(1)}(0)$ is given by Eq. (24). The first term in Eq. (26) represents the decay of the polarization created before $t=0$. The second term comes from the coupling between population and polarization, which still exists after $t=0$. Since the reradiated field is proportional to $\Delta \sigma_{01}^{(1)}(t) e^{-i\omega_1 t}$ [see Eqs. (7), (8)] the decay of $\Delta \sigma_{01}^{(1)}$ ($e^{-L_1 t}$ term) gives rise to emission of radiation at the Doppler-shifted natural frequency, $\omega_1 + k_1 v$, while the change in the population of level 0 ($e^{-\gamma_0 t}$ term) modifies the stimulated emission at the probe frequency, Ω_1 . Also note that since E_2 is absent after $t=0$, $\sigma_{01}^{(1)}$ is not coupled to $\sigma_{12}^{(1)}$, and so transient Raman processes do not show up (as they would in optical nutation). However, Raman-type processes do manifest themselves in the steady-state polarization, $\Delta \sigma_{01}^{(1)}(0)$, and so their influence decays with the characteristic decay time of the 0-1 polarization.

B. Velocity integrated gain

To obtain the expression for the probe gain [Eq. (9b)], one must average the 0-1 polarization over

the molecular velocity distribution. In the following, a Gaussian distribution,

$$G(v) = (1/u\sqrt{\pi}) e^{-v^2/u^2}, \quad (27)$$

will be used, with u the thermal velocity. Using Eqs. (9b) and (23), one finds that the gain at the probe transition is given by

$$g = g_0 + (8\pi k_1 I \mu_{01}^2 / \hbar \alpha) \text{Im} \langle \Delta \sigma_{01}^{(1)}(v, t) \rangle, \quad (28a)$$

with g_0 the linear background gain. In the Doppler-broadened limit ($\gamma_{01} \ll k_1 u$)

$$g_0 = 4\pi I \mu_{01}^2 N_{10} / \hbar,$$

with

$$N_{10} = \pi N_{10} G(v_1), \quad v_1 = (\Omega_1 - \omega_1) / k_1.$$

The probe field change signal may then be defined as

$$\Delta g(t) = (2k_1 g_0 / \alpha N_{10}) \text{Im} \langle \Delta \sigma_{01}^{(1)}(v, t) \rangle. \quad (28b)$$

In the fully Doppler-broadened limit, where the natural widths, γ_{01} , and the power-broadened 0-2 transition linewidth, $\gamma_{02}(1+s)^{1/2}$, are much smaller than the Doppler widths $k_1 u$ and $k_2 u$, $G(v)$ is slowly varying compared to $\Delta \sigma(v, t)$ [Eq. (26)] and can be taken as constant in the velocity integration. This integration can then be performed using contour integration, by considering $\Delta \sigma$ as an analytic function of the complex variable \tilde{v} . The path of integration is the real axis of the complex plane, and the contour can be closed at $+\infty$ and $-\infty$ in the upper half of the complex plane in order that the exponential term $e^{i k_1 \tilde{v} t}$ (coming from $e^{-L_1 t}$) vanishes for infinite values of the imaginary part of \tilde{v} , at $t > 0$. The integration then consists of evaluating $\Delta \sigma(v, t)$ at the poles lying in the upper half of the complex plane.²⁷

In $\Delta \sigma_{01}^{(1)}(v, t)$ the poles corresponding to $L_1 = 0$ and $L_1 - \gamma_0 = 0$ lie in the lower half of the complex plane and do not contribute. Of the two poles coming from $|L_2(\beta)|^2 = 0$, only one brings a nonvanishing contribution. The denominator $(L_1 L_{12} + \frac{1}{4} \beta^2)^{-1}$ is much more complicated: its two poles are analyzed in Appendix A. When $k_1 - \epsilon k_2 \geq 0$, there is no contribution. This condition corresponds to either $\epsilon = -1$ (counter-propagating waves), or $\epsilon = +1$ and $k_1 \geq k_2$. In the remaining case ($\epsilon = 1$; $k_2 > k_1$) one of the poles lies in the upper half of the complex plane and brings an additional contribution to $\langle \Delta \sigma \rangle$.^{24(a)}

1. $k_1 - \epsilon k_2 > 0$

As an example of the velocity integration, we shall discuss this first case in some detail. The pole of $|L_2(\beta)|^{-2}$ lying in the upper half of the complex plane is given by

$$k_2 \tilde{v}_2 = \epsilon(\Omega_2 - \omega_2) + i \gamma_{02} Q, \quad (29)$$

where

$$Q = (1+s)^{1/2}. \quad (30)$$

Using the residue theorem, this pole leads to the following expression for the probe field change signal:

$$\Delta g(\bar{v}_2, t, \epsilon) = -g_0 \left(\frac{k_1}{2k_2} \frac{\beta^2}{\gamma_0^2 Q} \frac{N_{20}}{N_{10}} \right) \text{Re} \gamma_0 \left[\frac{e^{-\gamma_0 t} - e^{-(\gamma_B + i\delta(\epsilon))t}}{\gamma_B - \gamma_0 + i\delta(\epsilon)} + \frac{\gamma_N + \frac{1}{2}\gamma_0(1+\epsilon Q) + i\delta(\epsilon)}{[\gamma_B + i\delta(\epsilon)][\gamma_N + i\delta(\epsilon)] + \frac{1}{4}\beta^2} e^{-(\gamma_B + i\delta(\epsilon))t} \right], \quad (31)$$

where N_{20} is proportional to the 0-2 inversion density for the resonant molecular velocity v_2 ,

$$N_{20} = \pi \bar{n}_{20} G(v_2), \quad (32)$$

$$v_2 = \epsilon(\Omega_2 - \omega_2)k_2^{-1}, \quad (33)$$

and $\delta(\epsilon)$ is the detuning of the probe frequency from the line center of the steady-state saturation resonance, $\Omega_1^{(c)}$,

$$\delta(\epsilon) = \Omega_1 - \Omega_1^{(c)}, \quad (34)$$

$$\Omega_1^{(c)} = \omega_1 + \epsilon(k_1/k_2)(\Omega_2 - \omega_2). \quad (35)$$

Finally, two effective decay rates have been introduced,

$$\gamma_B = \gamma_{01} + (k_1/k_2)\gamma_0 Q, \quad (36)$$

$$\gamma_N = \gamma_{12} + [(k_1 - \epsilon k_2)/k_2]\gamma_{12} Q. \quad (37)$$

The physical interpretation of Eq. (31) is as follows: (i) The last term in brackets describes the decay of the initial polarization induced by the saturating field E_2 before $t=0$. Since this polarization is due to molecules in the velocity band centered at v_2 , the decay occurs at the Doppler-shifted frequency $\omega_1 + k_1 v_2 = \Omega_1^{(c)}$. The corresponding emitted field interferes with the probe field to give a beat at frequency $\delta(\epsilon)$. The decay of this beat consists of two contributions: the γ_{01} term, which is due to the decay of the 0-1 polarization, and a "Doppler dephasing" contribution, $\gamma_{02} Q k_1/k_2$, which is due to the velocity spread of the excited molecules [$\text{Im } \epsilon$, in Eq. (29)] and gives rise to a corresponding spread in the emitted frequencies, leading to destructive interference in a time of the order of $k_2(k_1\gamma_0 Q)^{-1}$. Notice that the latter contribution contains the influence of power broadening in the preparative step. Finally, as expected, for $t=0$, the last term of Eq. (31) gives rise to the well-known line shape of the saturation resonance in a three-level system.⁴

(ii) The first term in brackets is a pure transient contribution (it cancels for both $t=0$ and $t \gg \gamma_0^{-1}$), coming from the coupling of the 0-1 polarization

to the transient population of level 0. Since this term describes the change in stimulated emission resulting from population decay, it contains a contribution ($e^{-\gamma_0 t}$) exhibiting neither Doppler dephasing (hence no dephasing due to power broadening), nor beat frequency.

When there are no dephasing collisions [$\gamma_{12} = \frac{1}{2}(\gamma_1 + \gamma_2)$], Eq. (31) may be simplified to yield

$$\Delta g(\bar{v}_2, t, \epsilon) = -g_0 \left(\frac{k_1}{2k_2} \frac{\beta^2}{\gamma_0^2 Q} \frac{N_{20}}{N_{10}} \right) \text{Re} \frac{\gamma_0^2}{\gamma_B - \gamma_0 + i\delta(\epsilon)} \times \left(\frac{e^{-\gamma_0 t}}{\gamma_0} - \frac{1 - \epsilon Q}{2} \frac{e^{-(\gamma_B + i\delta(\epsilon))t}}{\gamma(\epsilon) + i\delta(\epsilon)} \right), \quad (38)$$

where $\gamma(\epsilon)$ is the width of the Lorentzian line shape observed in the steady-state regime ($t=0$),

$$\gamma(\epsilon) = \frac{1}{2}\gamma_1 + (k_1/k_2)\gamma_{02} Q - \epsilon(\gamma_0/2)Q. \quad (39)$$

Equation (39) straightforwardly shows the well-known result that the change-signal linewidth is narrower for forward scattering ($\epsilon = +1$) than for backward scattering ($\epsilon = -1$). Since the net areas under the gain curves are equal,²⁶ it follows that the peak amplitude of the forward signal is large, than that of the backward signal. This point and others will be discussed in more detail in the following section.

2. $\epsilon = +1$; $k_2 > k_1$

In the case of forward scattering with $k_2 > k_1$ [Ref. 24a] there is an additional contribution to the change-signal gain, coming from the new resonant velocity $\bar{v}_{12} = x_-(\beta)/k_1$, where $x_-(\beta)$ is defined in Eq. (A8). We then have

$$\Delta g(t, +) = \Delta g(\bar{v}_2, t, +) + \Delta g(\bar{v}_{12}, t, +), \quad (40)$$

where $\Delta g(\bar{v}_2, t, +)$ is given by Eq. (31), and

$$\Delta g(\bar{v}_{12}, t, +) = -\frac{1}{2}g_0 S^2 \text{Re} \frac{e^{-(\Gamma' + i\Delta')t/\kappa}}{(\Gamma' + i\Delta')\Lambda}, \quad (41a)$$

with

$$\Lambda^{-1} = \frac{1}{\Gamma' + i\Delta'} + \frac{k_2}{k_1} \frac{N_{20}}{N_{10}} \frac{[\Gamma' - \kappa\gamma_{01} + i(\Delta' - \kappa\delta)] + \kappa(\gamma_{02}/\gamma_0)[(k_1/k_2)\gamma_0 + \bar{\gamma} - \Gamma + i(\delta - \Delta)]}{\kappa^2 \gamma_{02}^2 Q^2 - (k_2/k_1)^2 [\Gamma' - \kappa\gamma_{01} + i(\Delta' - \kappa\delta)]^2}. \quad (41b)$$

In this equation the following notation is used:

$$\Gamma + i\Delta = [(\bar{\gamma} + i\delta)^2 + S^2]^{1/2}, \quad (42a)$$

$$S = \beta[(k_1/k_2)\kappa]^{1/2}, \quad (42b)$$

$$\kappa = (k_2 - k_1)/k_2, \quad (42c)$$

$$\bar{\gamma} = (k_1/k_2)\gamma_{12} + \kappa\gamma_{01}, \quad (42d)$$

$$\Gamma' = \frac{1}{2}(\Gamma + \bar{\gamma}), \quad \Delta' = \frac{1}{2}(\Delta + \delta). \quad (42e)$$

with δ the probe frequency detuning [Eq. (34) with $\epsilon = +1$]. The sign of the complex square root in Eq. (42a) is determined by continuity from $\bar{\gamma} + i\delta$ at $\beta = 0$. The physical interpretation of Eq. (41) is not as simple as that of Eq. (31), and will be elaborated on in the following sections. As shown below, the contribution from the ν_{12} group arises from Raman-type processes. (For small β , $\bar{\nu}_{12}$ is determined by the resonance condition $L_{12} = 0$.) This is the reason why this contribution does not vanish even if the 0-2 transition is transparent to the saturating field ($N_{20} = 0$, $N_{10} \neq 0$). For high intensities we shall see that this contribution exhibits dynamic Stark splitting ["Autler-Townes effect"²⁸]. Finally, note that $\Delta g(\bar{\nu}_{12}, t, +)$ simplifies considerably when there are no phase-changing collisions [$\gamma_{ij} = \frac{1}{2}(\gamma_i + \gamma_j)$] and

$$k_2 = 2k_1, \quad \gamma_0 = \gamma_2.$$

The quantity Λ , Eq. (41b), then reduces to

$$\frac{1}{\Lambda} = \frac{1}{\Gamma' + i\Delta'} - \frac{N_{20}/N_{10}}{\frac{1}{2}\gamma_1 + i\delta}. \quad (43)$$

C. General features of the probe field gain

1. Equal-area property

A very interesting feature of the gain curves is that the area under the forward change signal is equal to that under the backward change signal at any time during the decay. Thus, it can be readily shown by contour integration of Eqs. (31) and (41) that

$$\int \Delta g(\bar{\nu}_2, t, \epsilon) d\delta(\epsilon) = -g_0 \frac{\pi k_1}{2k_2} \frac{\beta^2}{\gamma_0 Q} \frac{N_{20}}{N_{10}} e^{-\gamma_0 t} \quad (44)$$

and

$$\int \Delta g(\bar{\nu}_{12}, t, +) d\delta = 0.$$

We thus obtain the statement of the equal-area property,

$$\int \Delta g(t, +) d\delta(+) = \int \Delta g(t, -) d\delta(-). \quad (45)$$

The equal area property of the steady-state change signals (i.e., at $t=0$) has been discussed before.²⁹ The fact that the areas remain equal during the

decay of the change signals follows from a general result presented in Ref. 26. According to this result, the time behavior of the frequency-integrated gain should follow the decay of $\langle \sigma_{00}(t) \rangle$, the velocity-integrated population of level 0. It is easily seen from Eqs. (17b) and (21b) that

$$\langle \sigma_{00}(t) \rangle = \bar{n}_0 + \frac{\beta^2}{2k_2 \gamma_0 Q} N_{20} e^{-\gamma_0 t}.$$

Thus, using Eq. (44) we can write Eq. (45) in the form

$$\int \Delta g(t, \epsilon) d\delta(\epsilon) = -\frac{4\pi^2 k_1 \mu_{10}^2 t}{\hbar} (\langle \sigma_{00}(t) \rangle - \bar{n}_0), \quad (46)$$

in agreement with the general result.³⁰ It also follows from this result that the net area under the $\Delta g(\bar{\nu}_{12}, t, \epsilon)$ change signal is always zero. Thus, this quantity is either identically zero, as in the $\epsilon = -1$ case, or it exhibits sign changes as the detuning is varied, as in the $\epsilon = +1$ case.

Finally, it should be mentioned that these results hold for any particular velocity group, as can be seen from the frequency integration of Eqs. (24) and (26), which leads to a relation similar to Eq. (46). Thus, Eq. (46) is not restricted to the fully Doppler-broadened limit. It holds for a velocity distribution of arbitrary width, including the case of complete homogeneous broadening [$G(\nu)$ sharp].

The equal-area property will be made use of below in analyzing the frequency behavior of the change-signal curves.

2. Independent-field approximation (IFA)

The independent-field approximation (sometimes referred to as the rate-equation approximation) assumes that E_1 and E_2 interact independently with their respective transitions. The effects of Raman-type processes are neglected, and so coupling only occurs through saturation of the level populations. This limit can be obtained easily from Eqs. (31) and (41) by taking the limit $\gamma_{12} \rightarrow \infty$. As can be seen from Eqs. (3), this has the effect of completely destroying the influence of Raman-type processes. In the limit $\Delta g(\bar{\nu}_{12}, t, +)$ vanishes and one obtains

$$\begin{aligned} \Delta g_{IFA}(t, \epsilon) = & -g_0 \left(\frac{k_1}{2k_2} \frac{\beta^2}{\gamma_0 Q} \frac{N_{20}}{N_{10}} \right) \\ & \times \text{Re} \left\{ \frac{\gamma_0^2}{\gamma_B - \gamma_0 + i\delta(\epsilon)} \right. \\ & \left. \times \left[\frac{e^{-\gamma_0 t}}{\gamma_0} - \frac{e^{-[\gamma_B + i\delta(\epsilon)]t}}{\gamma_B + i\delta(\epsilon)} \right] \right\}. \quad (47) \end{aligned}$$

Therefore, in the IFA there is no directional anisotropy and forward and backward change signals are the same. For weak saturation the change

signals in the IFA limit are identical to that of the $\epsilon = -1$ case [see Eq. (53), below]. However, for $\beta \gg \gamma$ the saturation behavior of the IFA result differs from that of the $\epsilon = -1$ case. This is readily apparent in the case where there are no dephasing collisions, Eq. (38), since the factor $(\gamma_B + i\delta)^{-1}$ appears in the second term in square brackets in Eq. (47) instead of $\frac{1}{2}(1+Q)/[\gamma(-) + i\delta(-)]$. Thus, for $t \ll \gamma_B^{-1}$ the IFA predicts Lorentzian forward and backward change signals of width γ_B rather

than $\gamma(\epsilon)$. However, for $\gamma_0^{-1} > t \gg \gamma_B^{-1}$, when the initial polarization has decayed away, both forward and backward change signals evolve towards the IFA value (see discussion in Sec. V A).

IV. FEATURES OF THE WEAK FIELD RESPONSE

When the saturating field is not intense ($\beta \ll \gamma_{ij}$), the results can be simplified by expanding Eqs. (31) and (41) in orders of β/γ . At the second order we have

$$\Delta g(\bar{\nu}_2, t, \epsilon) = -g_0 \left(\frac{k_1}{2k_2} \frac{\beta^2}{\gamma_0^2} \frac{N_{20}}{N_{10}} \right) \text{Re} \gamma_0 \left[\frac{\exp(-\gamma_0 t) - \exp\{-[\gamma_B^0 + i\delta(\epsilon)]t\}}{\gamma_B^0 - \gamma_0 + i\delta(\epsilon)} + \frac{\gamma_0^0 + \frac{1}{2}\gamma_0(1+\epsilon) + i\delta(\epsilon)}{[\gamma_B^0 + i\delta(\epsilon)][\gamma_0^0 + i\delta(\epsilon)]} \exp\{-[\gamma_B^0 + i\delta(\epsilon)]t\} \right], \quad (48)$$

and

$$\Delta g(\bar{\nu}_{12}, t, +) = -g_0 \left(\frac{k_1}{2k_2} \frac{\beta^2}{\gamma_0^2} \right) \text{Re} \gamma_0^2 \left(\frac{1}{\bar{\gamma} + i\delta} - \frac{N_{20}/N_{10}}{\gamma_{12} - \kappa \gamma_{02} + i\delta} \right) \frac{\exp[-(\bar{\gamma} + i\delta)t/\kappa]}{\bar{\gamma} + i\delta}. \quad (49)$$

In these equations γ_B^0 and γ_0^0 are the values taken by γ_B and γ_0 for $\beta = 0$,

$$\gamma_B^0 = \gamma_{01} + (k_1/k_2)\gamma_{02}, \quad (50)$$

$$\gamma_0^0 = \gamma_{12} + [(k_1 - \epsilon k_2)/k_2]\gamma_{02}. \quad (51)$$

In obtaining Eq. (49), note that for $\beta/\gamma \ll 1$,

$$\Gamma + i\Delta = \Gamma' + i\Delta' = \bar{\gamma} + i\delta. \quad (52)$$

A. Counter-propagating waves

When the saturating and probe fields are propagating antiparallel to each other ($\epsilon = -1$), Δg has a simple form. The term in brackets in Eq. (48), which determines the line shape of the change signal, is equal to

$$\xi(-) = \frac{\exp(-\gamma_0 t) - \exp\{-[\gamma_B^0 + i\delta(-)]t\}}{\gamma_B^0 - \gamma_0 + i\delta(-)} + \frac{\exp\{-[\gamma_B^0 + i\delta(-)]t\}}{\gamma_B^0 + i\delta(-)}. \quad (53)$$

The time-varying gain is proportional to the real part of $\xi(-)$. A first remarkable result is that this expression is independent of γ_{12} . This is related to the fact that for $\epsilon = -1$ the coupling of σ_{12} with σ_{01} cancels after velocity integration. When the two waves have opposite propagation directions, the Raman-type processes, responsible for the creation of the σ_{12} coherence, have a strong velocity dependence. When integrated over velocity their net effect vanishes.

At $t = 0$, $\text{Re} \xi(-)$ is a Lorentzian of width γ_B^0 . If $\gamma_B^0 > \gamma_0$ then the $e^{-\gamma_B^0 t}$ terms will decay away in a time $\sim 1/\gamma_B^0$ leaving only the $e^{-\gamma_0 t}$ contribution, a Lorentzian of width $\gamma_B^0 - \gamma_0$. As explained in Sec.

III B 1, this term is induced by the decaying population of level 0. Its linewidth is narrower than that of the steady-state contribution because this term arises from a contribution to $\Delta\sigma_{01}^{(1)}$, driven by a decaying population transient [cf. Eq. (25)], thus causing narrowing. The narrowing of the $\xi(-)$ line shape in the time decay of the $\epsilon = -1$ change signal can be seen in Fig. 4(a).

If $\gamma_0 > \gamma_B^0$ the decaying change signal evolves in an entirely different way. The $e^{-\gamma_0 t}$ contribution decays rapidly, leaving the $e^{-\gamma_B^0 t}$ contributions, which oscillate at frequency $\delta(-)$. These terms are associated with free decay of the initial polarization. As explained earlier, the emitted radiation, which decays at the natural frequency of the prepared velocity group, $\omega_1 + k_1 v_1$, beats with the probe field

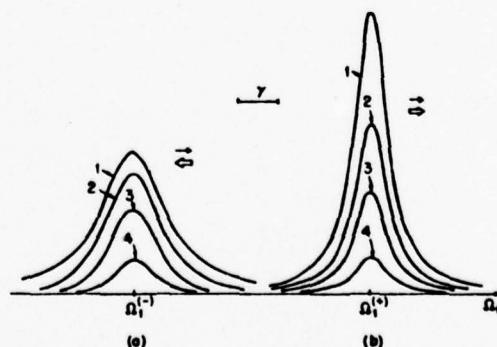


FIG. 4. Backward (a) and forward (b) change signals for weak saturation and no phase-changing collisions. The parameters are $k_1 = k_2$, $N_{10} = N_{20}$, $\gamma_{ij} = \gamma$, and $\beta = 0.1\gamma$. Time delays: $t_1 = 0$, $t_2 = 0.5/\gamma$, $t_3 = 1/\gamma$, and $t_4 = 2/\gamma$.

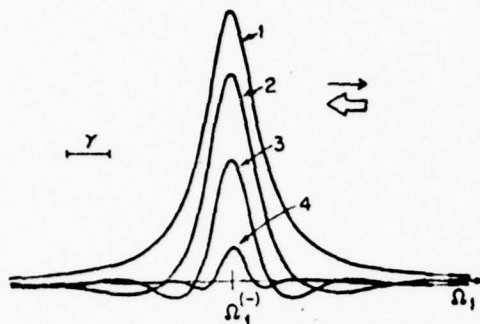


FIG. 5. Backward change signal for weak saturation and $\gamma_0 > \gamma_B^0$. The parameters are $k_1 = \frac{1}{2}k_2$, $\gamma_0 = \gamma$, $\gamma_1 = \gamma_2 = \frac{1}{10}\gamma$ (no phase-changing collisions), $\beta = 0.001\gamma$. Time delays: $t_1 = 0$, $t_2 = 1/\gamma$, $t_3 = 2/\gamma$, and $t_4 = 4/\gamma$.

to produce a gain component at $\delta(-)$. This type of beatnote is a characteristic feature of free-induction decay. Its counterpart in the frequency domain (at a fixed delay time) is a narrowing of the change-signal line shape accompanied by interference fringes. For example, the second term of Eq. (53) gives a line-shape contribution of the form

$$\frac{\gamma_B^0 \cos \delta t - \delta \sin \delta t}{(\gamma_B^0)^2 + \delta^2} \exp(-\gamma_B^0 t). \quad (54)$$

This expression behaves like a Lorentzian for $t \ll 1/\gamma_B^0$, but for longer time delays it narrows and develops fringes of width $\delta \approx \pi/t$. This narrowing occurs because, by observing change signals at delay times $\gg (\gamma_B^0)^{-1}$ one is selecting molecules whose lifetimes are longer than the average, and whose linewidths are correspondingly narrower. Therefore, this method can be used to produce change signals much narrower than the natural widths, although in practice extreme line narrowing is limited by the intensity reduction occurring because of the decaying exponential factor $e^{-\gamma_B^0 t}$. Line shapes having similar physical origins have been exploited by Ramsey³¹ in magnetic resonance experiments. Recently there have been several observations of this effect in the optical region.³² The same type of line shape has been observed in time-delayed level crossing experiments.³³

The actual line shape of Eq. (53) is composed of two such contributions, each of which exhibits fringes. It is plotted in Fig. 5 for $\gamma_B^0 = 0.825\gamma_0$, which corresponds to the case $k_1 = \frac{1}{2}k_2$ and $\gamma_1 = \gamma_2 = \frac{1}{10}\gamma_0$ [cf. Eq. (50)]. The observation of narrow resonances of this type opens interesting possibilities.

B. Co-propagating waves

For co-propagating fields the effect of Raman-type processes becomes important. The term in brackets in Eq. (48) is equal to

$$\xi(+) = \frac{\exp(-\gamma_0 t)}{\gamma_B^0 - \gamma_0 + i\delta} + \frac{\gamma_0(\gamma_{01} + \gamma_{02} - \gamma_{12} - \gamma_0) \exp[-(\gamma_B^0 + i\delta)t]}{(\gamma_B^0 - \gamma_0 + i\delta)(\gamma_B^0 + i\delta)(\gamma_0^0 + i\delta)}. \quad (55)$$

The transient evolution of the gain line shape for $k_1 \geq k_2$ is proportional to $\text{Re}\xi(+)$. As can be seen, Eq. (55) is a sensitive function of the presence of phase-changing collisions (see discussion below). When they are absent, $\gamma_{01} + \gamma_{02} = \gamma_{12} + \gamma_0$ [cf. discussion following Eq. (6)] and $\xi(+)$ reduces to

$$e^{-\gamma_0 t} / (\gamma_B^0 - \gamma_0 + i\delta). \quad (56)$$

Thus, the contribution arising from the decay of the initial polarization completely cancels and the gain line shape decays as a simple exponential. The change signal remains Lorentzian throughout the decay, and Ramsey-type fringes are absent [Fig. 4(b)]. Note that in Eq. (56) the decay rate is completely governed by population relaxation and is independent of Doppler dephasing, in contrast to ordinary two-level free-induction decay.⁷ By comparing Figs. 4(a) and 4(b) it can be seen that the areas of forward and backward change signals are equal at any given value of t , as expected.

For $k_2 > k_1$ there is an additional contribution to the change signal [cf. Eqs. (40) and (49)], entirely due to Raman-type processes. Indeed, when $k_2 \neq k_1$ the Raman-type processes are velocity dependent and can only occur for molecules in the \tilde{v}_{12}^0 velocity group, defined by the Raman resonance condition $L_{12}(v) = 0$

$$\tilde{v}_{12}^0 = (\Omega_2 - \Omega_1 - \omega_2 + \omega_1 + i\gamma_{12}) / (k_2 - k_1). \quad (57)$$

The real part of Eq. (57) is the statement of energy conservation for the Raman-type process in which a molecule undergoes a transition between levels 2 and 1 by emitting a photon Ω_2 and absorbing a photon Ω_1 . The imaginary part of \tilde{v}_{12}^0 gives the width of the resonant velocity group. The decay of the \tilde{v}_{12}^0 velocity group after $t=0$ leads to the $\Delta g(\tilde{v}_{12}^0, t, +)$ contribution. Since this contribution is associated with Raman-type processes, it can occur even if the molecular medium is transparent to the saturating field ($N_{20} = 0$). In this case the contribution given by Eq. (55) vanishes and the net change signal is proportional to the real part of

$$N_{10}(\tilde{\gamma} + i\delta)^{-2} e^{-(\tilde{\gamma} + i\delta)t} / \kappa. \quad (58)$$

The unusual time dependence of this expression can be understood by noting that the initial polar-

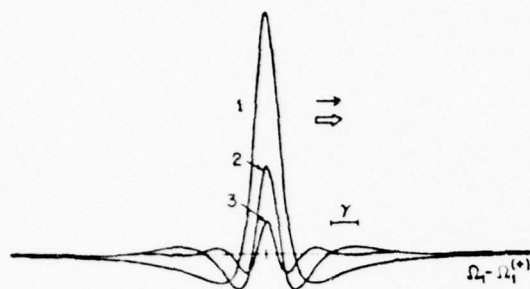


FIG. 6. Forward change signal, N_{10} contribution, for weak saturation. The parameters are $k_1 = \frac{1}{2} k_2$, $\gamma_{12} = \gamma$, and $\beta/\gamma = 0.1$. Time delays: $t_1 = 0$, $t_2 = 0.5/\gamma$, and $t_3 = 1/\gamma$.

ization undergoes free decay according to $\exp[-(\omega_1 + k_1 \tilde{\gamma}_{12}^0)t] \exp(-\gamma_{01}t)$. The resulting reradiated field then beats with E_1 to produce the time behavior of Eq. (58).

The time evolution of this change signal is plotted in Fig. 6. As can be seen, the change-signal area remains zero throughout the decay. Also note the development of Ramsey-type fringes as the decay progresses. The peculiar shape of this change signal has been experimentally verified by Hänsch *et al.*³⁴ in the steady-state regime.

C. Influence of phase changing collisions

Phase-changing collisions strongly affect both the line shape and time evolution of the change signals. In the presence of phase-changing collisions the forward change signal is no longer given by the simple expression (56) and Doppler dephasing effects appear [see Eq. (55)]. In contrast, strong phase-interrupting collisions ($\gamma_B \gg \gamma_0$) actually simplify the backward change signal, since Eq. (53) then reduces to $e^{-\gamma_0 t}(\gamma_B^0 + i\delta)^{-1}$. Thus, in this limit the evolution of the change signal is completely determined by population decay processes. The contribution arising from the decaying polarization is negligible and Ramsey-type fringes are absent.

A case of special interest occurs when the transition frequencies are close ($\omega_1 \approx \omega_2$) and the decay of the optical polarization is rapid compared to the other decay rates (fast T_2 processes):

$$\gamma_{02}, \gamma_{01} \gg \gamma_0, \gamma_{12}. \quad (59)$$

In many atomic and molecular transitions these conditions can be achieved by using a linearly polarized saturating field and a probe field having a different polarization. In this case levels 1 and 2 are two magnetic sublevels of the same energy level and γ_{12} represents the relaxation rate of the coherence between them ("Zeeman coherence"),

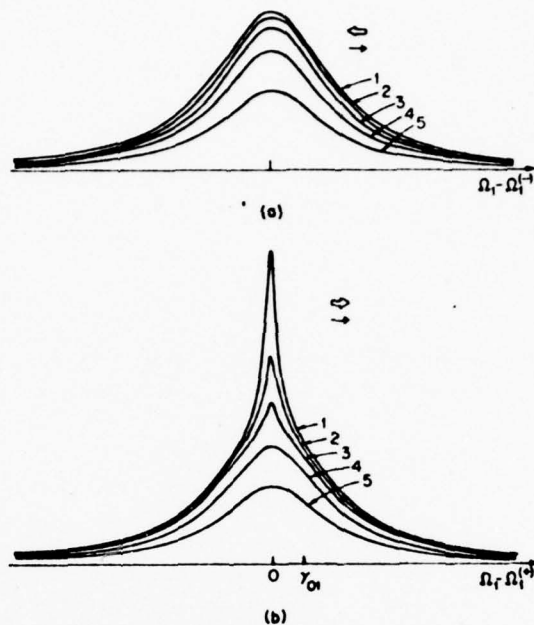


FIG. 7. Backward (a) and forward (b) change signals for strong phase-changing collisions and weak saturation. The parameters are $k_1 = k_2$, $\gamma_0 = \gamma_2 = \gamma_{12} = \gamma$, $\gamma_{01} = \gamma_{02} = 5\gamma$, and $\beta/\gamma = 0.1$. Time delays: $t_1 = 0$, $t_2 = 0.5/\gamma_{01}$, $t_3 = 1/\gamma_{01}$, $t_4 = 2/\gamma_{01}$, and $t_5 = 4/\gamma_{01}$.

which is typically of the same order of magnitude as γ_0 , the population decay rate, but much smaller than the decay rate of the induced optical polarization. When condition (59) is fulfilled $\xi(\epsilon)$ can be approximated by [cf. Eqs. (53) and (55)]

$$\xi(\epsilon) = \frac{\exp(-\gamma_0 t)}{\gamma_B^0 + i\delta(\epsilon)} + \frac{1 + \epsilon}{2} \frac{\gamma_0 \exp(-\gamma_B^0 t)}{\gamma_B^0 [\gamma_{12} + i\delta(\epsilon)]}. \quad (60)$$

The first term of Eq. (60) describes a broad resonance, width $\gamma_{01} + \gamma_{02}$, induced by the population saturation of level 0, which decays at characteristic rate γ_0 . This is the only contribution to the backward decay [Fig. 7(a)]. However, in the forward direction there is an additional contribution [second term of Eq. (60)] in the form of a narrow resonance of width γ_{12} , induced by Raman-type processes [Fig. 7(b)]. This narrow contribution decays at a much faster rate, $\gamma_{01} + \gamma_{02}$, determined by the optical-polarization decay rate.

Steady-state (i.e., $t=0$) forward change signals exhibiting both broad and narrow features have been observed recently.³⁵ This type of line shape is very similar to the Zeeman-tuned saturation resonances observed in the intensity of the fluorescence emitted from a transition with degenerate magnetic sublevels resonating with a single-mode laser.³⁶ Such resonances, observed as a function of Zeeman tuning, consist of a narrow component,

associated with Zeeman coherence ("Hanle effect"), superimposed on a broader "population effect" resonance. These features are the counterparts of the Raman-type and population-saturation features, respectively, of Eq. (60), $\epsilon = +1$.³⁷

The study of the transient behavior of the change signals in such a system provides a unique way of distinguishing population saturation and Raman-type processes, owing to their very different decay constants. A remarkable consequence of Eq. (60) is that after a time $\approx (\gamma_{01} + \gamma_{02})^{-1}$ the narrow contribution decays away, and the forward change signal is reduced to a broad resonance identical to the backward signal. This type of behavior, in which a broad resonance decays slowly and a narrow resonance rapidly, is different from the usual frequency-time domain behavior of linear systems. It is a good example of the fact that in three-level free-decay frequency and time behavior are not connected in a simple way.

The results of recent experiments in which such behavior is observed in NH_3 will be reported elsewhere.⁴¹

V. SATURATION EFFECTS

When the intensity of the saturating field is large enough [saturation parameter $s \approx 1$, Eq. (19)], new features appear including power broadening of the resonances, power dephasing of the decay rates and, in some cases, a new type of oscillatory behavior in the decaying change signals.

A. Power broadening and power dephasing

When $k_1 \geq \epsilon k_2$ (either counter-propagating waves or co-propagating waves with $k_1 > k_2$), the signal is given by $\Delta g(\bar{\nu}_2, t, \epsilon)$, Eq. (31). As the intensity of the saturating field increases two features are noteworthy: (i) The change signals become power broadened and their amplitudes saturate; (ii) of the two decay rates, the one associated with population relaxation (γ_0) remains unchanged, while the one associated with polarization decay (γ_B) increases. This increase is due to power broadening of the velocity group excited during the preparative stage. The growing range of interacting molecular velocities increases the velocity ("Doppler") dephasing contribution to the relaxation rate. For large saturating intensities γ_B can exceed γ_0 by an order of magnitude, and the decaying change signal evolves in two distinct stages. For the sake of simplicity let us consider the case in which phase-changing collisions are absent, Eq. (38).

(i) For $t \ll 1/\gamma_B$ the change signal is a Lorentzian of width $\gamma(\epsilon)$ [Eq. (39)]. This signal exhibits the well-known directional anisotropy between forward ($\epsilon = +1$) and backward ($\epsilon = -1$) scattering [Figs.

8(a) and 8(b)]. However, the areas of forward and backward change signals are equal. For high intensities ($s \gg 1$) $Q \approx (s)^{1/2} = \beta/(\gamma_0 \gamma_2)^{1/2}$, and we have

$$\Delta g(\bar{\nu}_2, t=0, \epsilon) \approx \frac{-(N_{20}/N_{10})g_0}{1 + (\gamma_0/\gamma_2)[1 - \epsilon(k_2/k_1)]} \times \text{Re} \frac{\gamma(\epsilon)}{\gamma(\epsilon) + i\delta(\epsilon)}, \quad (61a)$$

with

$$\gamma(\epsilon) \approx [(k_1/k_2)\gamma_{02} - \epsilon(\gamma_0/2)]Q. \quad (61b)$$

Thus, the change-signal amplitude saturates and its linewidth increases linearly with δ_2^0 .

(ii) In a time of order of γ_B^{-1} the $e^{-(\gamma_B + i\delta)t}$ contribution vanishes, and both forward and backward signals are reduced to the same Lorentzian line shape,

$$\Delta g(\bar{\nu}_2, t, \epsilon) \approx \frac{-(N_{20}/N_{10})g_0}{1 + (\gamma_0/\gamma_2)} \text{Re} \left[\frac{\gamma_B - \gamma_0}{\gamma_B - \gamma_0 + i\delta(\epsilon)} \right] e^{-\gamma_0 t}, \quad (62a)$$

with

$$\gamma_B - \gamma_0 \approx (k_1/k_2)\gamma_{02}Q. \quad (62b)$$

(This result is valid even if phase-changing collisions occur.) As can be seen by comparing Eqs. (61) and (62), as the backward signal decays from $t=0$ its amplitude increases and its linewidth narrows, while the forward signal decreases and broadens! This behavior is clearly seen in Figs. 8(a), 8(b), and 9, where the time decay of forward

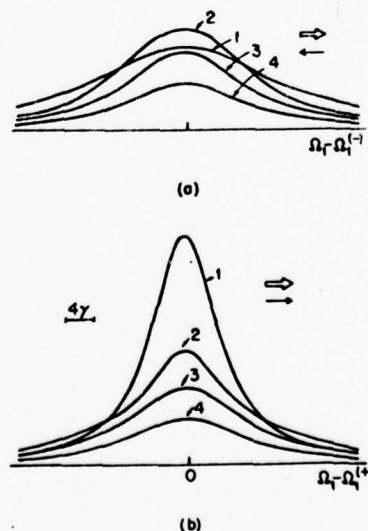


FIG. 8. Backward (a) and forward (b) change signals for strong saturation. The parameters are $k_1 = k_2$, $N_{10} = N_{20}$, $\gamma_{1j} = \gamma$, and $\beta/\gamma = 10$. Time delays: $t_1 = 0$, $t_2 = 0.2/\gamma$, $t_3 = 0.5/\gamma$, and $t_4 = 1/\gamma$.

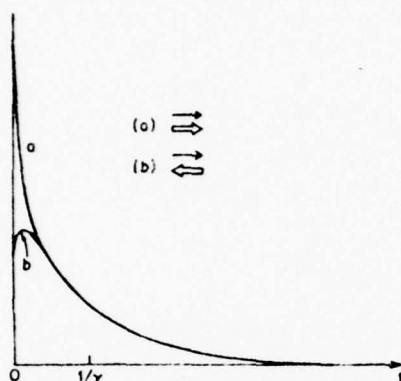


FIG. 9. Time decay of forward (a) and backward (b) change signals at line center ($\delta = 0$). The parameters are the same as in Fig. 8.

and backward change signals is plotted at line center.

This behavior occurs because in the steady-state the contribution from Raman-type processes broadens the backward change signal and narrows the forward one, as compared to the population saturation value. When the initial polarization (which contains the Raman contribution) has decayed away, in a time of order γ_B^{-1} , this influence is removed and the linewidths change. Furthermore, it follows from the equal-area property that rapid line narrowing automatically implies an increase in amplitude, and vice versa. Any process destroying the phase of the induced polarization—such as phase-changing collisions, Doppler dephasing or power dephasing—increases γ_B and thus accelerates the decay of the initial polarization. The remaining signal, due to population saturation, then decays away slowly with a time constant γ_0^{-1} .

Narrowing of this type has been reported by Shahin and Hänsch²¹ in a time-delayed Lamb-dip experiment using a short-pulse dye laser. It should be noted that pulsed lasers are not ideal for such studies. The present method has the advantage that the system can be prepared in a well-defined steady state, and the weak cw field can precisely probe its decay.

Another interesting type of behavior can occur in the backward change signal when the initial saturation is large but $k_1 \ll k_2$ (reduced Doppler dephasing), so that $\gamma_B = \gamma_0 + (k_1/k_2)\gamma_0 Q$ is of the same order as γ_0 . However, the initial linewidth $\gamma(-) \approx \frac{1}{2}\gamma_0 Q$ is still power broadened [Eq. (39)]. In this case the decay rates of the initial polarization and the population are comparable, giving rise to narrowing at line center and Ramsey-type fringes at the wings. An example is given in Fig. 10. As can be seen, the central portion of the line nar-

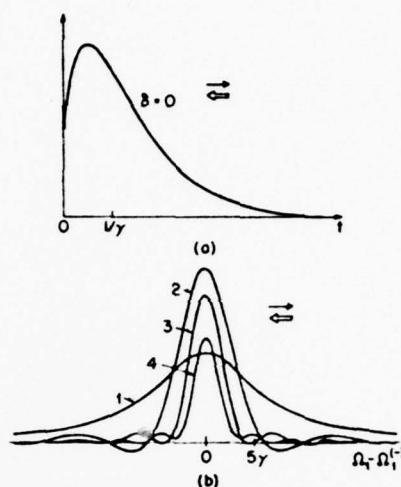


FIG. 10. Backward change signal for strong saturation and $k_1 \ll k_2$. The parameters are $k_1 = 0.1 k_2$, $\gamma_{ij} = \gamma$, and $\beta/\gamma = 10$. Time delays: $t_1 = 0$, $t_2 = 0.5/\gamma$, $t_3 = 1/\gamma$, and $t_4 = 2/\gamma$.

rows from $\gamma(-)$ to γ_B , with a corresponding increase in amplitude, in a time of order γ_B^{-1} , and narrow fringes appear at the wings of the resonance, in accord with Eq. (38).

B. Dynamical Stark splitting and oscillatory decay

When the two e.m. fields are co-propagating and k_2 is larger than k_1 , a new steady-state feature appears at high saturating intensities: the resonance splits symmetrically into two distinct peaks.²⁸ As will be seen in the following, the decay of this signal exhibits a novel type of oscillatory behavior. The steady-state splitting has been observed recently by Toschek and co-workers.³⁸ Its line-shape features have been analyzed by Skribanowitz *et al.*,³⁹ particularly in the case of transitions with level degeneracy.

This type of behavior comes from the $\Delta g(\bar{r}_{12}, t, +)$ contribution, Eq. (41), which increases as $\beta^{1/2}$ at high intensities and thus predominates over the $\Delta g(\bar{r}_2, t, +)$ contribution, whose amplitude saturates. In the vicinity of the peaks Λ , Eq. (41b), is a slowly varying function proportional to iS , and so for $\beta \gg \gamma_{ij}$,

$$\Delta g(t, +) \propto \xi_{12}(t) = S \operatorname{Im} \frac{e^{-(\Gamma + i\Delta)t/\kappa}}{\Gamma + i\Delta} \quad (63)$$

$$= S \frac{\Gamma \sin(\Delta' t/\kappa) + \Delta \cos(\Delta' t/\kappa)}{\Gamma^2 + \Delta^2} e^{-\Gamma t/\kappa} \quad (64)$$

The resonant behavior of the signal occurs through the denominator of Eq. (64). Using Eq. (42a) one

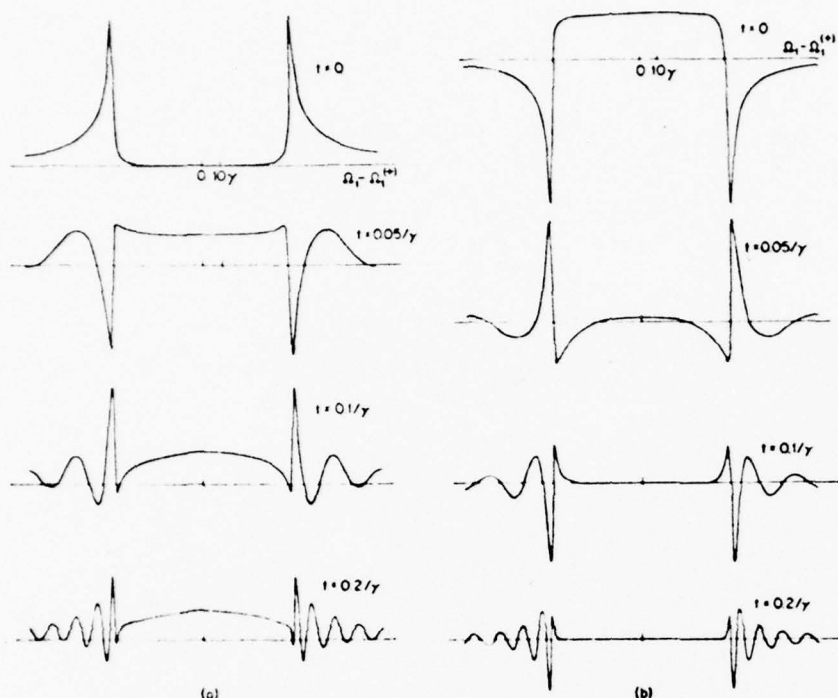


FIG. 11. Forward change signals for strong saturation, exhibiting dynamic Stark splitting. (a) N_{20} contribution; (b) N_{10} contribution. The parameters are $k_1 = \frac{1}{2}k_2$, $\gamma_{ij} = \gamma$, and $\beta = 10^4\gamma$. The time delays are as shown.

can show that³⁹

$$\frac{1}{\Gamma^2 + \Delta^2} = \frac{1}{(4\delta S)^{1/2}} \left(\frac{1}{\bar{\gamma}^2 + (\delta - S)^2} - \frac{1}{\bar{\gamma}^2 + (\delta + S)^2} \right)^{1/2}. \quad (65)$$

For $S \gg \bar{\gamma}$ this quantity undergoes a resonant enhancement around $\delta = +S$ (and a symmetrical one around $\delta = -S$):

$$(\Gamma^2 + \Delta^2)^{-1} \approx (2S)^{-1} [\bar{\gamma}^2 + (\delta - S)^2]^{-1/2}. \quad (66)$$

Also note that in this vicinity Γ and Δ , Eq. (42a), can be approximated by

$$\Gamma \approx S^{1/2} \{ [(\delta - S)^2 + \bar{\gamma}^2]^{1/2} - (\delta - S) \}^{1/2}, \quad (67)$$

and

$$\Delta \approx S^{1/2} \{ [(\delta - S)^2 + \bar{\gamma}^2]^{1/2} + (\delta - S) \}^{1/2}. \quad (68)$$

As seen in Eq. (64) the steady-state ($t = 0$) signal, proportional to $\Delta(\Gamma^2 + \Delta^2)^{-1}$, exhibits two resonant peaks separated by $\approx 2S$. The line shape of the $\delta = +S$ peak is given by

$$\xi_{12}(t=0) = \frac{S^{1/2}}{2} \left(\frac{[(\delta - S)^2 + \bar{\gamma}^2]^{1/2} + (\delta - S)}{(\delta - S)^2 + \bar{\gamma}^2} \right)^{1/2}. \quad (69)$$

This line shape is asymmetrical, the signal decreasing as $|\delta - S|^{-3/2}$ for $S > \delta \gg \bar{\gamma}$ and as $|\delta - S|^{-1/2}$ for $\delta - S \gg \bar{\gamma}$. The peak occurs at $\delta = S + \bar{\gamma}/\sqrt{3}$. Its amplitude is proportional to $S^{1/2}$

and its linewidth [full width at half maximum (FWHM)] is approximately $7\bar{\gamma}$.⁴⁰ This behavior is illustrated in the $t = 0$ plots of Fig. 11.

The origin of this splitting lies in the high-frequency Stark effect³⁸ or "dynamical Stark splitting," which is caused by the mixing of the two wave functions of the energy levels of a transition saturated by a resonant e.m. field. In the optical region this frequency splitting is velocity dependent and is usually washed out by the Doppler effect. Thus, when averaged over a wide velocity distribution the splitting is transformed into a power broadening, which contributes to the linewidth of the resonance.⁴¹ However, in the particular case considered here the velocity dependence can be substantially reduced over a wide velocity range, leading to the line shape splittings of Fig. 11.

The frequency features of the Stark splitting for a particular velocity group are determined by the resonant denominator $L_1 L_{12} + \frac{1}{4}\beta^2$ appearing in the initial polarization $\Delta\sigma_{01}^{(1)}(0)$, Eq. (24). It can be written in the form

$$L_1 L_{12} + \frac{1}{4}\beta^2 = -(\Omega_1 - \nu_+)(\Omega_1 - \nu_-), \quad (70)$$

with ν_{\pm} the velocity-dependent center frequencies of the two Stark peaks. For $\beta \gg \gamma_{ij}$,

$$\nu_{\pm}(\nu) = \omega_1 + k_1 \nu + \frac{1}{2}[\Delta_2 \pm (\Delta_2^2 + \beta^2)^{1/2}], \quad (71)$$

with $\Delta_2(\nu)$, the detuning of the saturating field from

resonance,

$$\Delta_2 = \Omega_2 - \omega_2 - \epsilon k_2 v. \quad (72)$$

This resonant behavior is due to the coupling between σ_{01} and σ_{21} , as can be seen by determining their eigenfrequencies from Eq. (3) in the limit $\alpha \rightarrow 0$. A solution of the form $\sigma \propto e^{i\lambda t}$ gives

$$(\lambda - iL_{12})(\lambda - iL_{21}) = \frac{1}{4}\beta^2, \quad (73)$$

which has roots (for $\beta \gg \gamma_{ij}$)

$$\lambda_{\pm} = -\Omega_1 + \nu_{\pm}. \quad (74)$$

The corresponding normal modes of the optical polarization P_1 oscillate at eigenfrequencies $\Omega_1(\nu) = \lambda_{\pm} + \Omega_1$ [see Eq. (2), ρ_{01} equation]. Resonant enhancement occurs when $\Omega_1(\nu)$ is Doppler shifted into resonance with the probe frequency. Setting $\Omega_1(\nu) = \Omega_1$, i.e., $\lambda = 0$, Eq. (73) then reduces to (70).⁴²

For $k_1 > \epsilon k_2$ the velocity dependence of the term in brackets in Eq. (71) adds to the Doppler shift $k_1 v$. However, for $\epsilon = +1$ and $k_2 > k_1$ the velocity dependence of these two terms are opposite, leading to a partial cancellation of the velocity dependence of ν_{\pm} . The resonant velocity groups contributing to the Stark splitting may be obtained from the condition $\Omega_1 = \nu_{\pm}(\nu)$. For the case $k_2 = 2k_1$ we have

$$k_1 v_{\pm} = \Omega_1^{(*)} - \omega_1 \pm (\delta^2 - S^2)^{1/2}. \quad (75)$$

(The considerations are similar for $k_2 \neq 2k_1$.) For $|\delta| = |\Omega_1 - \Omega_1^{(*)}| \gg S$, v_{\pm} varies linearly with Ω_1 , but as $|\delta|$ approaches S the dependence is much weaker. In fact, near $|\delta| \approx S$ the velocity groups $v_{\pm} \approx v_{\pm}$ are essentially independent of Ω_1 over an interval $\Delta\nu \approx S/k_1$. The washout effect is thus diminished, since all of the velocity groups in this interval can contribute to the high-frequency Stark resonance occurring at the corresponding value of Ω_1 . This value is determined by the condition that the quantity $\delta^2 - S^2$ in Eq. (75) be close to zero,

$$|\delta| = S, \quad (76)$$

which gives the center frequencies of the Stark-split components [cf. Eq. (69)]. Note that because of the velocity dependence the Stark components are split by $2S$ rather than by 2β , as they would be in the homogeneously broadened case.^{42,43} Also note from (75) that the resonance condition cannot be satisfied for any velocity group when Ω_1 is in the range

$$\Omega_1^{(*)} - S < \Omega_1 < \Omega_1^{(*)} + S. \quad (77)$$

This lack of resonant molecules explains why in this range of probe frequencies the molecular medium is nearly transparent to the probe. Outside this range there are always velocities satisfying $\Omega_1(\nu) = \Omega_1$, and the interaction of the probe with the molecular medium is nonvanishing.⁴⁴

As can be seen in Eq. (64), when the saturating laser is terminated the resonance undergoes oscillations at frequency Δ'/κ as it decays with time constant Γ'/κ . In the vicinity of the resonance [Eqs. (42e)]

$$\Gamma' \approx \frac{1}{2}\Gamma \quad (78)$$

where Γ is given by Eq. (67), and

$$\Delta' \approx \frac{1}{2}S. \quad (79)$$

The number of oscillations is of the order of

$$\Delta'/\Gamma' \approx (S/\bar{\gamma})^{1/2}. \quad (80)$$

Notice that this behavior is different from the well-known Rabi oscillations observed in optical nutation transients, since after $t = 0$ the saturating field is absent. The appearance of this new frequency is due to the dynamic Stark effect, which causes the resonant interaction between the molecules and the probe field to be shifted from $\Omega_1^{(*)}$ to a new value. When the saturating field is switched off, the v_{\pm} velocity group, prepared before $t = 0$, radiates at its natural frequency $\omega_1 + k_1 v_{\pm}$.⁴⁵ The re-emitted field then beats with the probe field to give a beat at $\Omega_1 - \omega_1 - k_1 v_{\pm} = \Delta'/\kappa$.⁴⁶

Some typical delayed line shapes are plotted in Fig. 11. A noteworthy feature is the distortion of the envelope of the decay curve, which enhances the outer shoulders of the resonance as the delay time increases. This effect occurs because the decay rate,

$$\Gamma'/\kappa \approx (\sqrt{S/2\kappa}) \{[(\delta - S)^2 + \bar{\gamma}^2]^{1/2} - (\delta - S)\}^{1/2}, \quad (81)$$

is frequency dependent. This dependence is due to the fact, explained earlier, that the range of interacting velocities, and hence the Doppler-dephasing contribution to the decay, varies with Ω_1 . It can be seen in Eq. (81) that the decay is faster on the inner sides of the resonance than on the outer sides. Thus, the asymmetry of the peaks is enhanced during the decay.

Figures 11(a) and 11(b) show the N_{20} and N_{10} contributions, respectively. Notice that while the N_{20} curve is initially transparent in the region between the Stark peaks (i.e., $|\delta| \ll S$), the N_{10} curve exhibits small gain over a broad region. The sign of this gain is opposite to that of the Stark peaks, as it must be to maintain zero area. After a short time delay ($t \sim S^{-1}$) the situation is reversed, the N_{20} curve exhibiting a broad central gain region and the N_{10} curve becoming transparent there. Also note that the area of the N_{10} curve remains zero throughout the decay, as it must.

The change-signal expression in this region can be obtained by considering Eqs. (31) and (41) in the limit $|\delta| \ll S$. For example, in the case of no phase-changing collisions, $k_2 = 2k_1$ and γ_0

$= \gamma_2$ [Eqs. (38) and (43)] one finds

$$\Delta g(t, +) = -g_0 e^{-S t} + \frac{g_0}{2} \frac{N_{20}}{N_{10}} (e^{-S t} - e^{-\gamma_0 t}), \quad (82)$$

which exhibits the features discussed above.

Finally, notice that whereas all contributions associated with the decay of initial polarization exhibit power dephasing for $\beta \gg \gamma_{12}$, the contributions associated with population decay do not. Therefore, for very long delays ($t \sim \gamma_1^{-1}$) the line-splitting disappears. The remaining broad N_{20} contribution decays as $e^{-\gamma_0 t}$ (population effect) and evolves similarly to the backward resonance (Sec. VA).

VI. TIME-DELAYED FLUORESCENCE CHANGE SIGNALS

Three-level free-decay resonances can also be observed by monitoring the side fluorescence originating from level 1 as the probe field is tuned through the 0-1 transition. As explained in Sec. IIB, the fluorescence intensity I_F is directly proportional to $\langle \sigma_{11} \rangle$, the velocity-integrated population of level 1 [Eq. (10)]. Thus, this type of experiment directly measures the time evolution of the level population changes induced by the probe field. For a weak probe these occur in second order in α . We will now calculate $\langle \sigma_{11}^{(2)} \rangle$ for a saturating field of arbitrary β .

A. Calculation of $\langle \sigma_{11} \rangle$

In the second order in α , σ_{11} is determined by Eq. (16). The solution can be written in the form

$$\sigma_{11}^{(2)}(t) = -\frac{1}{2} \alpha^2 (\gamma_{01}/\gamma_1) (n_{10}/|L_1|^2) + \Delta \sigma_{11}^{(2)}(t), \quad (83)$$

where the first term describes the time-indepen-

dent population change induced by the probe field. The second term, which describes the modification of the 0-1 transition rate induced by the saturating field, satisfies

$$\Delta \dot{\sigma}_{11}^{(2)} + \gamma_1 \Delta \sigma_{11}^{(2)} = \frac{1}{2} i \alpha \Delta \sigma_{01}^{(1)}(t) + \text{c.c.}, \quad (84)$$

where $\Delta \sigma_{01}^{(1)}(t)$ is given by Eq. (26). The resulting expression for $\langle \sigma_{11}(t) \rangle$, complete up to order α^2 , can then be written in the form

$$\langle \sigma_{11}(t) \rangle = \bar{n}_1 - \Delta \bar{n}_1 + \Delta \bar{n}_1(t, \epsilon), \quad (85)$$

with $\Delta \bar{n}_1^0$ the broad Gaussian background population change induced by the probe field for $\beta = 0$,

$$\Delta \bar{n}_1^0 = \alpha^2 N_{10} / 2 k_1 \gamma_1,$$

and $\Delta \bar{n}_1(t, \epsilon) = \langle \Delta \sigma_{11}^{(2)} \rangle$ the population change signal.

One way of obtaining $\Delta \bar{n}_1$ would be to solve Eq. (84) and then integrate the resulting expression over the velocity distribution. A simpler approach is to integrate Eq. (84) over velocity, thus obtaining an expression relating $\Delta \bar{n}_1$ to Δg :

$$\Delta \dot{\bar{n}}_1 + \gamma_1 \Delta \bar{n}_1 = -\gamma_1 \Delta \bar{n}_1^0 \Delta g(t, \epsilon) / g_0, \quad (86a)$$

where Eq. (28b) has been used. This equation has the solution

$$\Delta \bar{n}_1(t, \epsilon) = -\frac{\Delta \bar{n}_1^0}{g_0} \left(\Delta g(0, \epsilon) e^{-\gamma_1 t} + \int_0^t \Delta g(t', \epsilon) e^{-\gamma_1(t-t')} \gamma_1 dt' \right). \quad (86b)$$

Thus the expression for the population change signal follows directly from that of the gain change signal, without the necessity of doing additional velocity integrals. As could be expected, the transient signal exhibits a new time constant γ_1^{-1} related to the relaxation of the population of level 1.

$$1. \quad k_1 - \epsilon k_2 > 0$$

In this case Eq. (31) is used in (86b) to obtain

$$\Delta \bar{n}_1(\bar{v}_2, t, \epsilon) = \Delta \bar{n}_1^0 \left(\frac{k_1}{2k_2} \frac{\beta^2}{\gamma_0 Q} \frac{N_{20}}{N_{10}} \right) \text{Re} \gamma_0 \gamma_1 \left[\frac{L_N + \frac{1}{2} \gamma_0 (1 + \epsilon Q)}{L_B L_N + \frac{1}{4} \beta^2} \left(\frac{e^{-\gamma_1 t}}{\gamma_1} + \frac{e^{-\gamma_1 t} - e^{-L_B t}}{L_B - \gamma_1} \right) - \frac{1}{L_B - \gamma_0} \left(\frac{e^{-\gamma_1 t} - e^{-L_B t}}{L_B - \gamma_1} - \frac{e^{-\gamma_1 t} - e^{-\gamma_0 t}}{\gamma_0 - \gamma_1} \right) \right]. \quad (87)$$

In Eq. (87) the complex Lorentzian denominators L_B and L_N have been introduced to simplify the form of the expression,

$$L_B = \gamma_B + i\delta(\epsilon), \quad L_N = \gamma_N + i\delta(\epsilon), \quad (88)$$

with γ_B and γ_N given by Eqs. (36) and (37), respectively.

$$2. \quad k_1 - \epsilon k_2 < 0$$

In this case Eq. (41), used in (86b), leads to

$$\Delta \bar{n}_1(t, +) = \Delta \bar{n}_1(\bar{v}_2, t, +) + \Delta \bar{n}_1(\bar{v}_{12}, t, +), \quad (89)$$

with

$$\Delta \bar{n}_1(\bar{v}_{12}, t, +) = \frac{1}{2} \Delta \bar{n}_1^0 S^2 \text{Re} \left[\frac{\gamma_1}{(\Gamma + i\Delta)\Lambda} \left(\frac{e^{-\gamma_1 t} - e^{-(\Gamma + i\Delta)t/\kappa}}{(\Gamma' - \kappa\gamma_1 + i\Delta')/\kappa} + \frac{e^{-\gamma_1 t}}{\gamma_1} \right) \right]. \quad (90)$$

The notation used in Eq. (90) is the same as in Eqs. (41) and (42).

As can be seen in Eqs. (87) and (89), the steady-state line-shape behavior of $\Delta\bar{n}_1(t, \epsilon)$ is identical to that of $\Delta g(t, \epsilon)$. [This follows from Eq. (86a) with $\Delta\bar{n}_1 = 0$. See also the discussion following Eq. (16).] However, the time-delayed line shapes are not the same. In the following, the $\Delta\bar{n}_1(t, \epsilon)$ change signals are analyzed in the limits of weak and strong saturation of E_2 .

B. Weak field response

1. $k_1 > \epsilon k_2$

The response for $\beta \ll \gamma_{1f}$ is obtained by setting $\beta = 0$ and $Q = 1$ in Eq. (87), and replacing L_B and L_N by their unsaturated values,

$$L_B^0 = \gamma_B^0 + i\delta(\epsilon), \quad L_N^0 = \gamma_N^0 + i\delta(\epsilon), \quad (91)$$

with γ_B^0 and γ_N^0 defined as in Eqs. (50) and (51).

For counter-propagating waves, $\Delta\bar{n}_1$ is independent of L_N , indicating the cancellation of Raman-type processes. For $\epsilon = -1$ the term in brackets in Eq. (87) becomes

$$\xi(-) = \frac{1}{L_B^0} \left(\frac{e^{-\gamma_1 t}}{\gamma_1} + \frac{e^{-\gamma_1 t} - e^{-L_B^0 t}}{L_B^0 - \gamma_1} \right) - \frac{1}{L_B^0 - \gamma_0} \left(\frac{e^{-\gamma_1 t} - e^{-L_B^0 t}}{L_B^0 - \gamma_1} - \frac{e^{-\gamma_1 t} - e^{-\gamma_0 t}}{\gamma_0 - \gamma_1} \right). \quad (92)$$

In the co-propagating case, $\Delta\bar{n}_1$ is given by Eq. (87) with $\epsilon = +1$. This expression dramatically simplifies when phase-changing collisions are absent, in analogy with the $\Delta g(t, +)$ change signal [see Eq. (55)]. We then have

$$L_B^0 = L_N^0 + \gamma_0, \quad (93)$$

and so the quantity in brackets in Eq. (87) reduces to

$$\xi(+)=\frac{1}{\gamma_1 L_N^0} \left(\frac{\gamma_0 e^{-\gamma_1 t} - \gamma_1 e^{-\gamma_0 t}}{\gamma_0 - \gamma_1} \right). \quad (94)$$

As in the $\Delta g(t, +)$ change signal, the influence of Doppler dephasing is absent, but the decay of the $\Delta\bar{n}_1(t, +)$ change signal is governed by γ_1 , as well as by γ_0 . For the special case $\gamma_0 = \gamma_1$ the quantity in parentheses in Eq. (94) reduces to $(1 + \gamma_1 t)e^{-\gamma_1 t}$.

Next, consider the case of strong phase-changing collisions and close transition frequencies ($\omega_1 \approx \omega_2$), treated for Δg in Sec. IV C. In this limit,

$$\gamma_1 \xi(\epsilon) = \frac{\gamma_0 e^{-\gamma_1 t} - \gamma_1 e^{-\gamma_0 t}}{(\gamma_0 - \gamma_1) L_B^0} + \frac{1 + \epsilon}{2} \frac{\gamma_0 e^{-\gamma_1 t}}{\gamma_B L_N^0}. \quad (95)$$

Just as in the Δg change signals, Eq. (60), the first term of Eq. (95) describes a broad population-saturation resonance of width $\gamma_B^0 = \gamma_{01} + \gamma_{02}$, while the second term is a narrow resonance, width γ_{12} , induced by Raman-type processes. But in contrast

to the narrow resonance of Δg change signal, which decays rapidly at the rate γ_B^0 , the narrow contribution of $\Delta\bar{n}_1$ decays at the much slower rate γ_1 . This difference occurs because the narrow contribution to the $\Delta\bar{n}_1$ change signal is caused by the buildup of population in level 1 due to the completion of 2-1 and 0-1 Raman-type transitions.²² Although the information about these processes is contained in both the initial polarization [$\sigma_{01}^{(1)}(0)$] and population [$\sigma_{11}^{(2)}(0)$], the latter contribution is dominant when the polarization relaxation rate is rapid. Thus, the narrow $\Delta\bar{n}_1$ component decays at the population decay rate. This implies that the backward-forward asymmetry cannot be eliminated during the decay of the fluorescence change signal, in contrast to the behavior of the probe-field decay signal. Also note that the fluorescence change signal is not a simple exponential, and depends on the population relaxation rates of both levels 0 and 1.

2. $k_1 < \epsilon k_2$

For co-propagating waves there is an additional contribution to $\Delta\bar{n}_1$ for $k_2 > k_1$, which may be obtained from Eq. (90) using Eq. (52). Just as in the Δg change signal, this term arises from Raman-type transitions, which can lead to a population buildup in level 1. Thus, it can occur even when there is complete transparency at the saturating field ($N_{20} = 0$). In this case the $\Delta\bar{n}_1$ change signal is proportional to the real part of

$$\frac{N_{10}}{(\gamma + i\delta)(\gamma - \kappa\gamma_1 + i\delta)} \left[e^{-\gamma_1 t} - \frac{\kappa\gamma_1}{\gamma + i\delta} e^{-(\gamma + i\delta)t/\epsilon} \right]. \quad (96)$$

As compared to the corresponding Δg change signal, Eq. (58), Eq. (96) contains an additional term associated with the $\sigma_{11}^{(2)}(0)$ contribution, which decays at a rate γ_1 . Thus, although the two change signals are identical at $t = 0$, the fringes occurring in the time-delayed Δg change signals are less pronounced in the corresponding $\Delta\bar{n}_1$ signals.

C. Saturation effects

At high saturation intensities the decay rate of the initial polarization is very large due to power dephasing. Thus, all of the terms in Eqs. (87) and (90) associated with the initial polarization are diminished since, as compared to the corresponding Δg expressions, each term has an extra factor in the denominator proportional to the polarization decay rate.¹⁷ Accordingly, for $\beta \gg \gamma_{1f}$ the time evolution of the $\Delta\bar{n}_1$ change signals is completely determined by the terms decaying at the population relaxation rates. Equations (87) and (90) thus reduce to

$$\Delta \bar{n}_1(\bar{v}_2, t, \epsilon) = \Delta \bar{n}_1 \left(\frac{k_1}{k_2} \frac{\gamma_1 \gamma_2 Q}{1 + \gamma_0/\gamma_2} \frac{N_{20}}{N_{10}} \right) \\ \times \operatorname{Re} \left(\frac{L_A \cdot \frac{1}{2} \epsilon \gamma Q}{L_B L_A \cdot \frac{1}{2} \beta^2} \frac{e^{-\gamma_1 t}}{\gamma_1} \right. \\ \left. + \frac{1}{L_B} \frac{e^{-\gamma_1 t} - e^{-\gamma_0 t}}{\gamma_0 - \gamma_1} \right), \quad (97)$$

$$\Delta \bar{n}_1(\bar{v}_{12}, t, +) = \frac{1}{2} \Delta \bar{n}_1^0 S^2 \operatorname{Re} \left(\frac{1}{(\Gamma + i\Delta)\Lambda} \right) e^{-\gamma_1 t}. \quad (98)$$

The disappearance of the contribution associated with the initial polarization is responsible for the following differences in the behavior of the $\Delta \bar{n}_1$ change signal, as compared to that of the $\Delta \bar{n}_2$ change signal discussed in Sec. V: (i) There are no rapidly decaying terms. (ii) The forward-backward asymmetry does not decrease as the $\Delta \bar{n}_1$ change signals decay. (iii) In the $\Delta \bar{n}_1(\bar{v}_{12}, t, +)$ change signal, which gives rise to the dynamical Stark splitting, the Stark peaks decay slowly. The line-shape deformation and oscillatory behavior characteristic of the $\Delta \bar{n}_1(\bar{v}_{12}, t, +)$ change signal are absent.

VII. CONCLUSION

This paper has presented a theoretical analysis of the change signals induced by the free-induction decay of a Doppler-broadened molecular transition, observed as a weak probe field is tuned through a coupled transition. The evolving line shapes can be studied either by monitoring the gain at the coupled transition or by studying the side fluorescence. As has been shown, the time-delayed change signals manifest a rich range of features including forward-backward line-shape asymmetries, Doppler-dephasing effects, Ramsey-type fringes, power broadening and dephasing, and dynamical Stark splittings exhibiting oscillatory decay. It was also shown that the time-delayed line shapes provide a unique way of distinguishing population saturation effects from Raman-type processes, owing to their different decay times.

The experimental observation of time-delayed change signals of the type discussed here requires that the saturating field be terminated in a time τ which is small compared to the characteristic decay times of the optical polarization,

$$\tau \ll \gamma_B^{-1}, \beta^{-1}, \quad (99)$$

(conditions for validity of the sudden approximation). Otherwise, the initially prepared polarization cannot freely decay, and instead will tend to follow the time behavior of the saturating field. If, however, $\tau \ll \gamma_1^{-1}$, the change-signal contribution associated with the saturated level populations will still decay at its characteristic rate.

In the present study the applied fields have been assumed to fall within the Doppler profiles of their respective transitions:

$$|\delta_j| < k_j u,$$

with $\delta_j = \Omega_j - \omega_j$ the detuning of E_j from the 0- j molecular center frequency. Thus, the Raman-type processes occur in the presence of a resonant intermediate state. However, the two-photon (Raman) condition can be satisfied even if the intermediate state is nonresonant, i.e., for

$$|\delta_j| > k_j u. \quad (100)$$

In this limit, certain simplifications occur. For example, the velocity spread of the molecules can be ignored in the single-quantum resonant denominators (L_1 and L_2), since $|k_j u| \ll |\delta_j|$ for all velocities. Furthermore, for a given value of β the transition probabilities for both single- and double-quantum processes are reduced. However, the double-quantum transitions (i.e., Raman-type processes involving the exchange of two quanta with the radiation fields²²) predominate, so the buildup of population in the intermediate state is small. Thus, unlike the case of a resonant intermediate state, there is no interference between single- and double-quantum events, and the form of the change signals is simplified.²⁹ However, when the intermediate state is nonresonant an additional condition must be satisfied in order for the sudden approximation to hold,

$$\tau \ll |\delta_j|^{-1}. \quad (101)$$

Otherwise, the induced polarization will tend to respond adiabatically to the saturating field. In practice, Eqs. (100) and (101) are difficult to fulfill simultaneously, since they require $\tau \ll (ku)^{-1}$. However, the regime in which

$$|\delta_j|^{-1} \ll \tau \ll \gamma_1^{-1} \quad (102)$$

is readily achievable. In this case the contribution to the change signal coming from the initially prepared polarization will adiabatically follow the saturating field,⁴⁸ and so will vanish when $E_2 \rightarrow 0$, but the population contribution persists and will decay at its characteristic rate.

Several recent publications have investigated the transient behavior of cascade and folded three-level systems when the two-quantum (or Raman) transition is resonant or near-resonant and condition (102) is satisfied. Theoretical studies^{17,19} have shown that in this limit the equations of motion simplify and reduce to those of an effective two-level system, so that the time evolution can be described by a vector model in which a two-photon Bloch vector precesses about an effective field. Experiments^{18,49,50} have verified the different

time behavior expected from the double-quantum (Raman) and single-quantum ("stepwise") processes. Their different frequency behavior has also been studied experimentally.³¹

In summary, when the intermediate state is nonresonant and the adiabatic approximation holds the theoretical description simplifies, resulting in relatively simple line shapes. Double-quantum transitions predominate over stepwise processes and all information about the relaxation of the initially prepared polarization is lost. There is no interplay between population-saturation effects and Raman-type processes. Thus, the backward change signal is negligible compared to the forward signal.³² On the other hand, when the intermediate state is resonant the line shapes, which are more complicated, give rise to a richer range of effects, including detailed information about the polarization decay and other relaxation processes.

The fundamental premise of this paper, the time-delayed probing of a resonance line shape, is a basic one in quantum mechanics. The idea of preparing a system in a given initial state and then probing it at a later time goes directly to the process of quantum measurement. Thus, time-delayed laser saturation spectroscopy can provide a direct analysis of the dynamics of atomic and molecular systems—scattering and diffusion mechanisms, thermalization in the gaseous phase by velocity-changing collisions and radiative transfer, laser interactions, and M -changing collisions in degenerate systems^{13,35} can all be studied. The extension to four-level systems, where pump and probe transitions have no common level, should lead to similar information about inelastic collisions.

ACKNOWLEDGMENTS

We wish to thank Claude Cohen-Tannoudji for several stimulating discussions on this subject, and Dan Seligson for preparing the computer figures. One of us (M.D.) wishes to thank Ali Javan and Michael Feld for their kind hospitality during his stay at MIT. One of us (M.S.F.) wishes to acknowledge support from the Alfred P. Sloan Foundation. This work was supported in part by the National Science Foundation and the U.S. Army Research Office (Durham).

APPENDIX: POLES OF $(L_1 L_{12} + \frac{1}{4}\beta^2)^{-1}$

This appendix analyzes the solutions of the equation

$$L_1 L_{12} + \frac{1}{4}\beta^2 = 0, \quad (\text{A1})$$

where L_1 and L_{12} are given by Eqs. (4). Equation (A1) can be written in the form

$$(x - \delta_1 + i\gamma_{01})(x + \delta_{12} - i\gamma_{12}) + \frac{1}{4}\beta^2 = 0, \quad (\text{A2})$$

where

$$\delta_1 = \Omega_1 - \omega_1, \quad \delta_{12} = \delta_1 - \delta_2, \quad (\text{A3})$$

$$\chi = (\epsilon k_2 - k_1)/k_1, \quad (\text{A4})$$

$$x = k_1 v. \quad (\text{A5})$$

The solution of Eq. (A2) is straightforward,

$$x_{\pm}(\beta) = \frac{1}{2} \left[\delta_1 - \frac{\delta_{12}}{\chi} - i \left(\gamma_{01} - \frac{\gamma_{12}}{\chi} \right) \pm \left\{ \left[\delta_1 + \frac{\delta_{12}}{\chi} - i \left(\gamma_{01} + \frac{\gamma_{12}}{\chi} \right) \right]^2 - \frac{\beta^2}{\chi} \right\}^{1/2} \right]. \quad (\text{A6})$$

The sign of the complex square root is determined by the condition

$$x_{+}(\beta=0) = \delta_1 - i\gamma_{01}, \quad x_{-}(\beta=0) = (-\delta_{12} + i\gamma_{12})/\chi, \quad (\text{A7})$$

as required by Eq. (A2). Thus, for $\beta=0$ the quantity in curly brackets must approach

$$(\delta_1 + \delta_{12}/\chi) - i(\gamma_{01} + \gamma_{12}/\chi).$$

The sign of $\text{Im}(x)$ gives the position of the corresponding pole in the complex $k_1 v$ plane. $\text{Im}[x_{+}(0)]$ is always negative, whereas the sign of $\text{Im}[x_{-}(0)]$ is the same as that of χ . Since $x(\beta)$ is determined by continuity from $x(0)$, $\text{Im}(x)$, a continuous function of β , can change sign only if it vanishes for a given value of β . It is easily shown that Eq. (A2) cannot have a real solution, since γ_{01} and γ_{12} are always positive. Thus $\text{Im}[x_{+}(\beta)]$ is always negative and $\text{Im}[x_{-}(\beta)]$ has the sign of χ .

As explained in Sec. III B of the text, only the poles of x lying in the upper half of the complex plane can contribute in the velocity integrations. Thus, the x_{+} pole never contributes, and the x_{-} pole can contribute only for $\chi > 0$ ($\epsilon = +1, k_2 > k_1$).^{24(a)}

Using the definitions of δ , $\bar{\gamma}$ and κ introduced in the text, this pole can then be written in the form

$$x_{-}(\beta) = k_1 \bar{v}_{12} = \frac{1}{2\kappa} \left(\kappa \delta_1 - \frac{k_1}{k_2} \delta_{12} \right) - i \left(\kappa \gamma_{01} - \frac{k_1}{k_2} \gamma_{12} \right) + i \left[(\bar{\gamma} + i\delta)^2 + S^2 \right]^{1/2}. \quad (\text{A8})$$

- *This work was performed while the author was a Visiting Scientist at MIT.
- †Present address: Univ. Fed. de Pernambuco, Recife, Brazil.
- ¹W. E. Lamb, Jr., Phys. Rev. **134**, 1429 (1964); A. Szöke and A. Javan, Phys. Rev. Lett. **10**, 521 (1963); R. A. McFarlane, W. R. Bennett, and W. E. Lamb, Jr., Appl. Phys. Lett. **2**, 189 (1963).
 - ²P. H. Lee and M. L. Skolnik, Appl. Phys. Lett. **10**, 303 (1967); R. L. Barger and J. L. Hall, Phys. Rev. Lett. **22**, 4 (1969); N. G. Basov, I. N. Kompanets, V. S. Letokhov, and V. V. Nikitin, Zh. Eksp. Teor. Fiz. Pis. Red. **9**, 568 (1969) [JETP Lett. **9**, 345 (1969)].
 - ³For a review, see P. E. Toschek in *Spectroscopie sans Largeur Doppler de Systèmes Moléculaires Simples*, Colloque No. 217 (CNRS, Paris, 1974), pp. 13-27; and V. S. Letokhov and V. P. Chebotayev, *Nonlinear Laser Spectroscopy*, Vol. 4, edited by D. L. McAdam (Springer, Berlin, 1977).
 - ⁴G. E. Notkin, S. G. Nautian, and A. A. Feoktistov, Zh. Eksp. Teor. Fiz. **52**, 1673 (1967) [Sov. Phys. JETP **25**, 1112 (1967)]; M. S. Feld and A. Javan, Phys. Rev. **177**, 540 (1969); T. Hänsch and P. Toschek, Z. Phys. **236**, 213 (1970); B. J. Feldman and M. S. Feld, Phys. Rev. A **5**, 899 (1972).
 - ⁵R. H. Corlough, P. A. Darczyk, and A. Javan, Phys. Rev. Lett. **18**, 730 (1967); H. K. Holt, Phys. Rev. Lett. **20**, 410 (1968); T. Hänsch, R. Keil, A. Schabert, and P. Toschek, Z. Phys. **266**, 293 (1969); I. M. Beterov and V. P. Chebotayev, Zh. Eksp. Teor. Fiz. Pis. Red. **9**, 216 (1969) [JETP Lett. **9**, 127 (1969)]; A. Schabert, R. Keil and P. Toschek, Opt. Commun. **13**, 265 (1975); Appl. Phys. **6**, 181 (1975).
 - ⁶For a review, see M. S. Feld in *Fundamental and Applied Laser Physics*, edited by M. S. Feld, N. A. Kurnit, and A. Javan (Wiley, New York, 1973), pp. 369-420; and I. M. Beterov and V. P. Chebotayev in *Progress in Quantum Electronics 3*, edited by J. H. Sanders and S. Stenholm (Pergamon, Oxford, 1974).
 - ⁷R. G. Brewer and R. L. Shoemaker, Phys. Rev. A **6**, 2001 (1972).
 - ⁸B. Hocker and C. L. Tang, Phys. Rev. **184**, 356 (1969); R. G. Brewer and R. L. Shoemaker, Phys. Rev. Lett. **27**, 631 (1971).
 - ⁹N. A. Kurnit, I. D. Abella, and S. R. Hartmann, Phys. Rev. Lett. **13**, 567 (1964); C. K. N. Patel and E. E. Slusher, Phys. Rev. Lett. **20**, 1089 (1968).
 - ¹⁰I. J. Lowe and R. E. Norberg, Phys. Rev. **107**, 46 (1957); S. B. Grossman, A. Schenzle, and R. G. Brewer, Phys. Rev. Lett. **33**, 275 (1977).
 - ¹¹Similar effects can also be achieved with Stark switching or laser-frequency switching techniques (Refs. 7, 8, 10). However, if the switching leaves the laser frequency inside the Doppler profile, additional effects due to interference between free decay and optical nutation can occur.
 - ¹²M. Ducloy and M. S. Feld, J. Phys. Lett. (Paris) **37**, L-173 (1976).
 - ¹³J. R. R. Leite, M. Ducloy, A. Sanchez, D. Seligson, and M. S. Feld, Phys. Rev. Lett. **30**, 1469 (1973). See also M. Ducloy and M. S. Feld in *Laser Spectroscopy III, Springer Series in Optical Sciences*, edited by J. L. Hall and J. L. Carlsten (Springer, Berlin, 1977), Vol. 7, pp. 243-247.
 - ¹⁴R. L. Shoemaker and R. G. Brewer, Phys. Rev. Lett. **28**, 1430 (1972); R. G. Brewer and E. L. Hahn, Phys. Rev. A **8**, 464 (1973); **11**, 1641 (1975).
 - ¹⁵J. R. R. Leite, R. L. Sheffield, M. Ducloy, R. D. Sharma, and M. S. Feld, Phys. Rev. A **14**, 1151 (1976).
 - ¹⁶A. Corney and G. W. Series, Proc. Phys. Soc. Lond. **83**, 207 (1964); W. Gornik, D. Kaiser, W. Lange, J. Luther, and H. H. Schultz, Opt. Commun. **6**, 327 (1972); S. Haroche, J. A. Paisner, and A. L. Schawlow, Phys. Rev. Lett. **30**, 948 (1973).
 - ¹⁷D. Grischkowsky, M. Loy, and P. Liao, Phys. Rev. A **12**, 2514 (1975).
 - ¹⁸M. Bassini, F. Biraben, B. Cagnac, and G. Grynberg, Opt. Commun. **21**, 263 (1977).
 - ¹⁹E. Courtens and A. Szöke, Phys. Rev. A **15**, 1588 (1977) and references therein; Y. R. Shen, Phys. Rev. B **9**, 622 (1974).
 - ²⁰G. M. Dobbs, R. H. Michaels, J. I. Steinfeld, J. H. S. Wang, and J. M. Levy, J. Chem. Phys. **63**, 1904 (1975).
 - ²¹T. W. Hänsch, I. S. Shahin, and A. L. Schawlow, Phys. Rev. Lett. **27**, 707 (1971); I. S. Shahin and T. W. Hänsch, Opt. Commun. **5**, 312 (1973).
 - ²²The term "Raman-type processes," as used here, includes both single- and double-quantum processes. For a discussion of this point see the Feld article of Ref. 6.
 - ²³L. S. Vasilenko, V. P. Chebotayev, and A. V. Shishaev, Zh. Eksp. Teor. Fiz. Pis. Red. **12**, 161 (1970) [JETP Lett. **12**, 113 (1970)]; B. Cagnac, G. Grynberg, and F. Biraben, J. Phys. (Paris) **34**, 845 (1973); for a review on Doppler-free two-photon spectroscopy, see N. Bloembergen and M. D. Levenson, in *High Resolution Laser Spectroscopy*, edited by K. Shimoda (Springer, Berlin, 1976); B. Cagnac, Ann. Phys. (Paris) **2**, 223 (1975).
 - ²⁴The way of transposing the results from the "V" configuration [Fig. 3(a)] to the other configurations ["inverted V", Fig. 3(b), or cascade, Fig. 3(c)] has been discussed in detail by Feld and Javan (Ref. 4, pp. 560-562, Appendices C-D and Table II). For the "inverted V" configuration, the results are essentially the same as for the "V" configuration (change of an over-all sign, to transpose absorption and stimulated emission). On the other hand, for cascade transitions, the cases of co-propagating ($\epsilon = +1$) and counter-propagating ($\epsilon = -1$) beams reverse. This means: (i) Two-photon absorption processes are important for counter-propagating beams (instead of Raman-type processes for co-propagating beams in "V" and "inverted V" configurations). (ii) In the velocity integration (Sec. III B), the important quantity is now $k_1 + \epsilon k_2$, instead of $k_1 - \epsilon k_2$. The resonant velocity group, \tilde{v}_{12} , [Sec. III B 2 and Eq. (A5)] contributes to the signal for $k_1 + \epsilon k_2 < 0$ only. Then, for cascade transitions, the dynamic Stark splitting and related oscillatory decay (Sec. V B) appear for $\epsilon = -1$ and $k_2 > k_1$.
 - ²⁵A detailed calculation leading to Eqs. (3)-(9) is given in Ref. 15.
 - ²⁶W. Heitler, *The Quantum Theory of Radiation* (Oxford, Univ., London, 1960), Sec. 20; C. Cohen-Tannoudji, Ann. Phys. (Paris) **7**, 423 (1962).
 - ²⁷B. J. Feldman and M. S. Feld, Phys. Rev. A **12**, 1015 (1975).
 - ²⁸The velocity integration of signals observed in transient processes has been analyzed in Ref. 16. The reader is referred to this work for more detail. (see,

- in particular, Sec. IV and the Appendix of Ref. 15).
- ²⁸S. H. Autler and C. H. Townes, *Phys. Rev.* **100**, 703 (1955).
- ²⁹M. S. Feld and A. Javan, Ref. 4.
- ³⁰Reference 26, Eq. (29) and footnote 23.
- ³¹N. F. Ramsey, *Molecular Beams* (Oxford Univ., London, England, 1956), p. 124.
- ³²J. C. Bergquist, S. A. Lee, and J. L. Hall, *Phys. Rev. Lett.* **38**, 159 (1977); M. M. Salour and C. Cohen-Tannoudji, *Phys. Rev. Lett.* **38**, 757 (1977).
- ³³I. J. Ma, J. Mertens, G. zu Putlitz, and G. Schütte, *Z. Phys.* **208**, 352 (1968); G. Copley, B. P. Kibble, and G. W. Series, *J. Phys. B* **1**, 724 (1968).
- ³⁴Hänsch *et al.*, Ref. 5.
- ³⁵See J. R. R. Leite, M. Ducloy, A. Sanchez, D. Seligson, and M. S. Feld, *Phys. Rev. Lett.* **39**, 1465 (1977) and references therein. Also M. Ducloy and M. S. Feld, Ref. 13.
- ³⁶M. Dumont, *J. Phys. (Paris)* **33**, 971 (1972); M. Gorlicki and M. Dumont, *Opt. Commun.* **11**, 166 (1974).
- ³⁷In the experiments of Ref. 36 both Zeeman coherence and population saturation are destroyed by splitting the magnetic sublevels, whereas in the present technique the Raman coherence and population saturation are reduced as the probe field is detuned from resonance.
- ³⁸A. Schabert, R. Keil, and P. Toschek, Ref. 5.
- ³⁹N. Skribanowitz, M. J. Kelly, and M. S. Feld, *Phys. Rev. A* **6**, 2302 (1972).
- ⁴⁰Note that the linewidth value quoted in Ref. 39 is too small by a factor of 2.
- ⁴¹E. V. Baklanov and V. P. Chebotayev, *Zh. Eksp. Teor. Fiz.* **60**, 552 (1971) [*Sov. Phys. JETP* **33**, 300 (1971)]; **34**, 450 (1972)] have interpreted the saturated absorption line shape in a Doppler-broadened transition in terms of the high-frequency Stark effect.
- ⁴²This condition is derived in another way in C. H. Townes and A. L. Schawlow, *Microwave Spectroscopy* (McGraw-Hill, New York, 1955), Sec. 10-9.
- ⁴³A. Javan, *Phys. Rev.* **107**, 1579 (1957).
- ⁴⁴The high-frequency Stark splitting appears naturally when the electromagnetic field is quantized and one looks for the energy levels of the total system, molecule plus field (formalism of the "dressed" molecule). C. Cohen-Tannoudji and collaborators recently have calculated the steady-state Doppler-averaged response using this formalism (C. Cohen-Tannoudji, private communication).
- ⁴⁵The v_+ velocity groups are obtained from the equation $\Omega = v_+(\mathbf{r})$, as in Eq. (75). The oscillatory behavior comes from the v_- group. The pole associated with v_+ lies outside the contour in the complex v plane and does not contribute to the velocity integration.
- ⁴⁶Using Eqs. (68) and (42c) one can show that
- $$k \cdot v_- = \Omega_1 - \omega_1 - \Delta' / \kappa.$$
- ⁴⁷Note the similar effect caused by strong phase-changing collisions, which led to the simplified line-shape of Eq. (95).
- ⁴⁸To ensure adiabaticity one also must have $|\delta_2| \gg \beta$. (See, for example, Courtens and Szöke, Ref. 19).
- ⁴⁹D. Grischkowsky, *Phys. Rev. A* **14**, 802 (1976).
- ⁵⁰P. F. Williams, D. L. Rousseau, and S. H. Dworketsky, *Phys. Rev. Lett.* **32**, 196 (1974).
- ⁵¹J. L. Carlsten and A. Szöke, *Phys. Rev. Lett.* **36**, 667 (1976); *J. Phys. B* **9**, L231 (1976).
- ⁵²This statement holds for a folded system. In the case of a cascade configuration the forward signal is absent. This is because in the cascade case the roles of forward and backward signals are interchanged [see footnote 24a].

SATURATED ABSORPTION SPECTROSCOPY OF CH_3OH
J.R.R. Leite, A. Sanchez, M. Ducloy and M.S. Feld
Physics Department and Spectroscopy Laboratory
Massachusetts Institute of Technology
Cambridge, Massachusetts 02139

Up to now methyl alcohol has been the most fertile molecule for generating far infrared laser radiation via CO_2 laser optical pumping [1]. Nevertheless, of the numerous CH_3OH submillimeter emission lines and their corresponding pump transitions, most of the spectroscopic assignments have yet to be made. Detailed knowledge of the quantum numbers, relaxation rates and dipole matrix elements is essential for assessing further potential of these lasers as sources and for new fundamental studies of the physics of three level systems.

In what follows we report some high resolution spectroscopic studies on two CH_3OH infrared transitions in near coincidence with the CO_2 P(34) and P(36) 9.7 μm lines. Their special interest lies in the fact that both can be pumped with a low power ($\sim 3\text{W}$) CW CO_2 laser to emit strong CW submillimeter radiation. In the experiments saturated absorption resonances (Lamb dips) were observed in a low pressure CH_3OH cell using a stable CO_2 laser, from which precise measurements of the pressure broadening coefficients, linear absorption coefficients and frequency detunings between the CO_2 and CH_3OH lines were obtained. In subsequent experiments a Stark field was applied, leading to partial assignment of the transitions.

The experimental set up used to observe the Lamb dips [2] is shown in Fig. 1. The CO_2 laser, with linearly polarized emission, was set at 100 mW power level to eliminate power broadening effects. A piezoelectric crystal, on which the laser mirror was mounted, permitted a 90 MHz tunability of each CO_2 line. An NaCl beam splitter was used to divide the laser output into two components, one intense (saturating beam) and one weak (probe beam), which were passed through the 1.5m CH_3OH sample cell in opposite directions. The Lamb dip occurs as a decrease in probe absorption as the laser is tuned across the CH_3OH line center. By measuring the frequency separation between the Lamb dip and the center of the CO_2 emission profile, the CH_3OH transition frequency could be obtained with a resolution much better than its 50 MHz Doppler width. For the P(34) CO_2 line, the methanol transition lies 38 \pm 5 MHz above the CO_2 center frequency. The transition overlapping the P(36) line lies 25 \pm 5 MHz above the corresponding CO_2 line center. The absence of Lamb dips for the P(32) and P(38) CO_2 lines indicates that the corresponding CH_3OH transitions are detuned by at least 45 MHz.

The linear absorption coefficient for

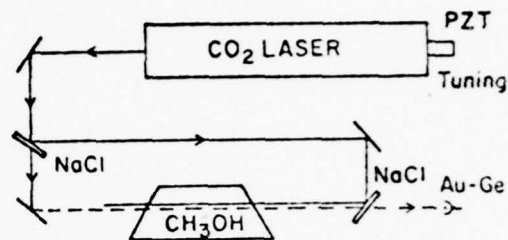


Figure 1. Experimental set up.

the P(34) overlapping line is $\alpha = 3.1 \pm 0.5 \text{ m}^{-1} \text{ Torr}^{-1}$. By observing the linewidth of the Lamb dip with increasing pressure, the collision broadening coefficient was found to be $\gamma = 18 \pm 4 \text{ MHz/Torr}$ (HWHM). The respective numbers for the P(36) overlapping line are $\alpha = 1.6 \pm 0.3 \text{ m}^{-1} \text{ Torr}^{-1}$ and $\gamma = 26 \pm 5 \text{ MHz/Torr}$.

From early low-resolution studies [3] it could be established that the CO_2 9.7 μm band overlaps the Q branch of the $\text{C}=\text{O}$ parallel stretching mode of CH_3OH . However, the rotational quantum numbers for the various coincidences were unknown. Their identification was the subject of our Stark effect experiments. Applying a static electric field to the CH_3OH gas sample splits the magnetic (m) sublevels of the rotational manifold. Consequently, each Lamb dip will split into a series of dips, reflecting the character of the Stark effect (linear or quadratic) and the level degeneracy (J value). In our experiments P(34) and P(36) coincidences both exhibited linear Stark effect. The following discussion is valid only in this case. When the polarization of the saturating field is parallel to the Stark field and the probe field polarization is perpendicular to it, the Lamb dip splits into two multiplets, the structure of which are not resolved if $\Delta e \cdot \Delta g$ is small compared to γ [$\Delta e(\Delta g)$ is the splitting between adjacent m-states in the excited (ground) levels]. The separation between the two components is then $\Delta = (\Delta e + \Delta g)/2$. This relation results from the fact that the saturating field is inducing $\Delta m = 0$ transitions while the probe couples to the $\Delta m = \pm 1$ transitions.

If, on the other hand, both probe and saturating beams are polarized along the Stark field, the Lamb dip splits into a series of $2J+1$ components, separated by $\delta = |\Delta e - \Delta g|$. Figure 2 shows the Stark patterns obtained for the P(34) and P(36) coincidences. In these traces a 30 V/cm, 10 kHz modulation was added to the static ($\sim 300 \text{ V/cm}$) Stark field, Es, and phase sensitive detection was used. In conse-

quence, the observed signal occurs as the derivative of the Lorentzian dips, and the central component is absent. The J value of the transition follows directly from the number of dips. From data like Fig. 2 taken at different values of E_s and both polarization configurations we obtain for the P(34) coincidence: $J=1$, $\Delta=28\pm 3\text{ MHz/(kV/cm)}$, $\delta=3.3\pm 0.3\text{ MHz/(kV/cm)}$. The corresponding values for the P(36) coincidence are $J=7$, $\Delta=25\pm 3\text{ MHz/(kV/cm)}$ and $\delta=3.5\pm 0.3\text{ MHz/(kV/cm)}$.

Further work is under way to complete the assignments. Preliminary estimates for the transition dipole matrix element, using symmetric top partition functions, are ~ 0.03 Debye for both transitions. Definitive values will be obtained after the K quantum numbers have been determined. As for the permanent dipole moments, we can conclude from δ/Δ that the vibrationally excited and ground state values differ by $\sim 10\%$.

Experiments are also in progress to assign the submillimeter emitting transitions and study their properties. These experiments employ a low pressure CH_3OH sample cell, saturated by the pump laser and probed by the submillimeter emission of an optically pumped CH_3OH laser. Both steady state and transient experiments are planned.

References

1. M. Rosenbluh, R.J. Temkin and K.J. Button, "Submillimeter Laser Wavelength Tables" to be published in *Applied Optics*, Nov. 1976.
2. See for example, P.E. Toschek in "Spectroscopie sans Largeur Doppler de Systèmes Moléculaires Simples" (Colloque No. 217-CNRS-Paris, 1974), pp. 13-27.
3. A. Borden and R. F. Barker, *J. of Chem. Phys.* **6**, 553, 1938.

* Work supported by U.S. Army Research Office (Durham).
 ** Partially supported by Universidade Federal de Pernambuco and CNPq-Brazil.
 + Present address: Laboratoire de Physique des Lasers, Université Paris Nord, Av. J.B. Clément 93430 Villetaneuse (France).
 § Alfred P. Sloan Fellow.

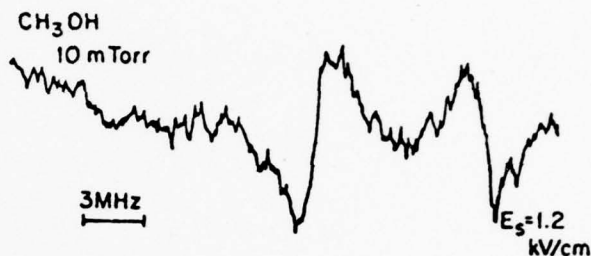


Figure 2a. Lamb dip Stark splitting of $\text{CO}_2\text{P}(34)\text{-CH}_3\text{OH}$ coincidence.

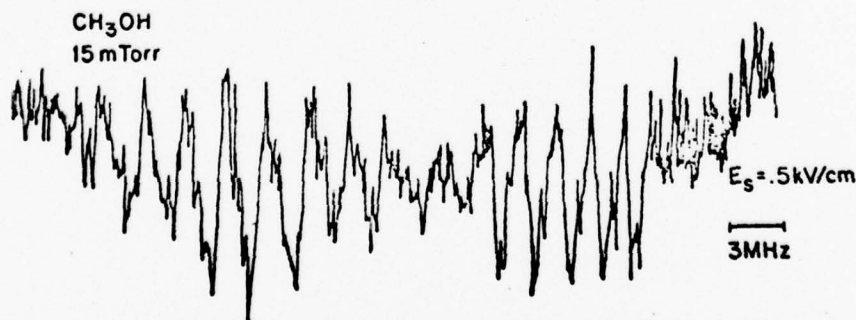


Figure 2b. Lamb dip Stark splitting of $\text{CO}_2\text{P}(36)\text{-CH}_3\text{OH}$ coincidence.

IV. Optically Pumped Far Infrared Lasers

QUANTUM MECHANICAL FEATURES OF OPTICALLY PUMPED FIR C.W. LASERS*

J.R.R. Leite^{**}, D. Seligson, J.J. Mickey, M. Ducloy[†], A. Sanchez and M.S. Feld[‡]
 Physics Department and Spectroscopy Laboratory
 Massachusetts Institute of Technology
 Cambridge, Massachusetts 02139

Generation of far infrared (FIR) laser radiation by means of optical pumping of molecules has received increasing attention over the past few years [1]. In the course of the development of FIR sources two important features have been largely neglected; (i) the assignment of the pump and FIR transitions; (ii) the detailed tuning behavior of the FIR emission. Knowledge of these two points is essential for a complete understanding of the optical pumping mechanism, and for assessing the full potential of various FIR laser sources and their extension to new spectral ranges. The assignment of CH_3OH transitions is presented in another talk. This communication discusses the frequency characteristics of the FIR emission.

Analysis of the optical pumping process is usually based on rate equations (RE) [2]. However, it is well known that two-quantum Raman-type processes, which are not accounted for in RE treatments, play an important role in three level systems of the type employed in FIR optical pumping [3]. For instance, these processes give rise to a directional anisotropy in the reemission of radiation. The way in which Raman-type processes manifest themselves depends on whether the transitions are homogeneously or inhomogeneously broadened. For these different cases, we will analyze the frequency dependence of the linear gain at the FIR 0-1 transition (frequency ω_1) when the excited level 0 is optically pumped via the 2+0 transition (ω_2) [$\omega_2 > \omega_1$].

1. Fully Doppler-broadened systems

This case is now well understood [3]. For weak pump intensities, the gain curve is Lorentzian, narrower in forward emission ($\epsilon=+1$) than in backward emission ($\epsilon=-1$), and is centered at frequency $\omega_1 \times (1+\epsilon\delta_2/\omega_2)$, where δ_2 is the frequency detuning of the pump.² The full widths at half maximum (FWHM) are respectively $\gamma(\pm) = \gamma_0 + \gamma_1 \pm \omega_1(\gamma_2 + \gamma_0)/\omega_2$, where γ_i is the decay rate of level i [4]. In addition, the peak forward gain is greater than the backward gain, so that the "areas" under the two Lorentzians are equal. The forward-backward anisotropy increases with ω_1/ω_2 . For large pump intensities the forward reemission line splits in two components because of the dynamical Stark splitting. The line splitting is given by $2\delta \omega_2 \sqrt{\omega_1(\omega_2 - \omega_1)}$, where δ is the Rabi nutation frequency on the 0-2 transition ($\delta = \mu E/\hbar$). The splitting in maximum for $\omega_1 = \omega_2/2$.

2. Systems in which only the pump transition is Doppler-broadened

This is the case in which the Doppler effect at the FIR frequency is negligible compared to the pressure-broadened linewidth, but the pump transition is still Doppler-broadened. Then the single-quantum 2-0 transition and the double-quantum transition have the same Doppler shift, causing the forward-backward anisotropy to disappear. Furthermore, the gain curve is centered at the FIR molecular frequency. Only its overall amplitude depends on the detuning of the pump frequency. The line-shape of the gain curve is given by

$$g = \beta^2 (2\gamma_2 Q)^{-1} \times$$

$$\text{Re} \left[\frac{\gamma_{12} + \gamma_{01} Q + \frac{\gamma_2}{2}(1-Q) + i\delta_1}{(\gamma_{01} + i\delta_1)(\gamma_{12} + \gamma_{01} Q + i\delta_1) + \beta^2/4} \right]$$

where γ_{ij} is the relaxation rate of the i - j coherence, δ_1 is the FIR frequency detuning and the saturation parameter is $Q = (1 + \beta^2/\gamma_0\gamma_2)^{1/2}$. When phase-changing collisions are absent [$\gamma_{ij} = (\gamma_i + \gamma_j)/2$], the lineshape is a Lorentzian of width $\gamma_1 + \gamma_0 Q$ (FWHM). The linewidth increases with increasing pump intensity, and, at high intensities, the gain saturates ($Q \rightarrow 1$). The RE approximation corresponds to making γ_{12} infinitely large in Eq. (1), in order to cancel the 1-2 coherence (absence of Raman-type processes). Thus, for weak pump intensities RE gives the correct result, but not for an intense pump, where RE predicts a gain curve whose width does not power broaden (FWHM = $2\gamma_{01}$) and whose peak increases linearly with β . The correct behavior [Eq. (1)] is a direct consequence of the occurrence of two-quantum transitions. Notice also the absence of dynamical Stark splitting, which vanishes in the velocity integration.

3. Homogeneously-broadened systems

When the Doppler effect is negligible for both transitions the gain curve reverts to the well-known results observed in microwave-microwave and microwave-RF double resonance experiments. In particular, at high pump intensities the FIR line splits in two resonances, the splitting depending on the pump intensity and the detuning of the pump frequency [5].

4. Experimental observations

The experimental study of the FIR tuning behavior for different cases is under way. The sample is a methyl alcohol cell placed

inside a 1m waveguide cavity and optically pumped by a 10W c.w. CO₂ laser. Preliminary studies of c.w. FIR emission at $\lambda = 120 \mu\text{m}$ (pump $\lambda = 9.7 \mu\text{m}$, P(36) line), $\lambda = 80 \mu\text{m}$ [P(34) pump] and other wavelengths are in progress. The emission frequency is tuned with a PZT mounted on one of the FIR cavity mirrors. At both 80 μm and 120 μm , for low (< 100 mTorr) pressures (case 1), two narrow bands of FIR emission are observed when the CO₂ pump frequency is detuned from the CH₃OH center frequency. These correspond to forward and backward reemission components of the standing-wave FIR field, and are symmetrically located around the FIR transition frequency. Due to the small values of ω_1/ω_2 (0.08 \sim 0.12), the forward-backward asymmetry is very weak. Reemission at $\lambda = 40 \mu\text{m}$ [P(34) CO₂ pump] should exhibit more pronounced asymmetries. Cases (2) and (3) will be studied by going to higher pressures and longer FIR wavelengths ($\lambda = 500 \mu\text{m}$). Observation of transient FIR emission, obtained when the pump laser is suddenly turned on or off, is also under way, in order to check the theoretical predictions of a previously performed analysis [6].

References

1. T.Y. Chang, IEEE Trans. Microwave Theory and Tech., MTT-22 (1974), 983.
2. e.g., J.R. Tucker, *ibid*, MTT-22 (1974), 1117.
3. For a review on three-level spectroscopy, see M.S. Feld in Fundamental and Applied Laser Physics, edited by M.S. Feld, A. Javan and N.A. Kurnit (Wiley, New York 1973), pp. 369-420.
4. For simplicity of this discussion, phase-changing collisions are not taken into account in this section.
5. S.H. Autler and C.H. Townes, Phys. Rev. 100 (1955), 703.
6. M. Ducloy and M.S. Feld, Journal de Physique-Lettres 37 (1976), L-173; M. Ducloy, J.R.R. Leite and M.S. Feld, Phys. Rev. A, to be published.

- * Work supported by Army Research Office (Durham).
- ** Partially supported by Universidade Federal de Pernambuco and CNPq-Brazil.
- + Present address: Laboratoire de Physique des Lasers, Université Paris Nord, Av. J.B. Clément, 93430, Villetaneuse (France).
- ‡ Alfred P. Sloan Fellow.

Quantum Mechanical Features of Optically Pumped CW FIR Lasers

D. SELIGSON, MARTIAL DUCLOY, J. R. R. LEITE, A. SANCHEZ, AND M. S. FELD

Abstract—Quantum mechanical predictions for the gain of an optically pumped CW FIR laser are presented for cases in which one or both of the pump and FIR transitions are pressure or Doppler broadened. The results are compared to those based on the rate equation model.

Some of the quantum mechanical predictions are verified in CH_3OH .

Manuscript received February 4, 1977. This work was supported in part by the U.S. Army Research Office (Durham), the National Aeronautics and Space Administration, the Universidade Federal de Pernambuco and the CNPq-Brazil under grants to one of the authors (J. R. R. L.), and an Alfred P. Sloan Fellowship (M.S.F.).

D. Seligson, J. R. R. Leite, A. Sanchez, and M. S. Feld are with the Department of Physics and the Spectroscopy Laboratory, Massachusetts Institute of Technology, Cambridge, MA 02139.

M. Ducloy was with the Department of Physics and the Spectroscopy Laboratory, Massachusetts Institute of Technology, Cambridge, MA 02139. He is now with the Laboratoire de Physique des Lasers, Université Paris Nord, Villetaneuse, France.

GENERATION of far infrared (FIR) laser radiation by means of optical pumping of molecules has received increasing attention over the past few years [1]. Analysis of the optical pumping process is usually based on rate equation (RE) treatments [2]. Such treatments neglect important contributions to the FIR gain due to multiple quantum processes and modulation of the time-dependent wave function. From the quantum-mechanical (QM) point of view an optically pumped laser can be considered as a coupled three-level system interacting with applied radiation fields. It is well known that in such systems Raman-type processes [3] play an impor-

tant role. For example, double quantum transitions can occur in which a molecule initially in the ground state undergoes a coherent transition to the lower level of the FIR transition by simultaneously absorbing a pump photon and emitting a FIR photon. Such processes can modify the gain and, in some cases, give rise to directional anisotropy in the FIR laser emission [3], [4]. Accordingly, a complete understanding of the quantum mechanical features makes it possible to optimize the output characteristics of such lasers. For example, in one case [5] it has been possible to achieve gain and laser oscillation in the absence of population inversion. The way in which Raman-type processes manifest themselves depends on whether one or both of the coupled transitions are pressure or Doppler broadened. In Sections I-III the predictions of the QM treatment for the gain of an optically pumped laser are discussed for the various cases. Section IV presents some FIR laser experiments in which QM features, not predicted by rate equations, are observed.

The theoretical model [6] considers a three-level system composed of a pump transition, 2-0, center frequency ω_2 , coupled to a FIR transition, 0-1, center frequency ω_1 , via the common level, 0 (Fig. 1). It is assumed that in the absence of the pump laser only the ground state, level 2, is populated (total population n_2). The pump field, E_2 , at frequency Ω_2 , can be arbitrarily large, but the field E_1 , frequency Ω_1 , generated at the 0-1 transition is considered to be weak [7]. Different relaxation rates (γ 's) are included in the theory: population decay ($\gamma_0, \gamma_1, \gamma_2$), polarization decay (γ_{01}, γ_{02}), and decay of the Raman coherence (γ_{12}). The quantity of interest is the gain induced at the 0-1 transition by a weak probe field E_1 propagating either parallel or antiparallel to E_2 . Let $W(v)$ be the normalized velocity distribution of molecules with velocity component v along the propagation direction of the fields:

$$W(v) = \frac{1}{u\sqrt{\pi}} \exp(-v^2/u^2), \quad u^2 = 2kT/M$$

(u = thermal velocity, M = molecular mass). The probe field gain is then given by [8]

$$G(\Omega_1) = G_0 \beta^2 \operatorname{Im} \gamma_{10} \int \left[\frac{L_2 - 2R\gamma_{20}/\gamma_0}{AB} \right] W(v) \alpha v, \quad (1)$$

where

$$G_0 = 4\pi \frac{\omega_1}{c} \frac{\mu_1^2}{h} \frac{N_2}{\gamma_{10}},$$

$$\beta = \mu_2 E_2 / (2h),$$

$$L_1 = \Delta'_1 + i\gamma_{10},$$

$$L_2 = -\Delta'_2 + i\gamma_{20},$$

$$R = (\Delta'_1 - \Delta'_2) - i\gamma_{21},$$

$$A = |L_2|^2 + 4\beta^2 \gamma_{20}^2 / (\gamma_0 \gamma_2),$$

$$B = -RL_1^* + \beta^2,$$

$$\Delta'_j = \Omega'_j - \omega_j, \quad j = 1, 2,$$

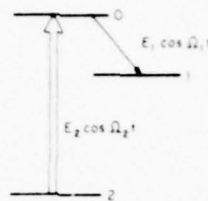


Fig. 1. Three-level system used to describe an optically pumped FIR laser. The pump field resonates with the 2-0 transition, molecular center frequency ω_2 . The FIR laser emission occurs at the 0-1 transition, molecular center frequency ω_1 .

$$\Omega'_1 = \Omega_1 - k_1 v,$$

$$\Omega'_2 = \Omega_2 - \epsilon k_2 v,$$

$$k_j = \Omega_j/c.$$

The frequencies Ω'_1 and Ω'_2 are those seen by the molecules in their rest frames and are Doppler shifted by $k_1 v$ and $\epsilon k_2 v$, respectively. For copropagating (counterpropagating) beams we have $\epsilon = +1$ ($\epsilon = -1$). Depending on whether pump and probe transitions are pressure or Doppler broadened, any of the cases described in the following three sections can occur.

1. HOMOGENEOUSLY BROADENED SYSTEMS (HIGH-PRESSURE REGIME)

When both transitions are pressure broadened ($\gamma \gg k_{1,2} u$) the velocity dependence at both pump and probe frequencies may be neglected (i.e., $\Omega'_1 = \Omega_1$, $\Omega'_2 = \Omega_2$), so the factor in brackets in (1) becomes velocity independent and the remaining integration over $W(v)$ gives unity. In this case the gain curve reverts to the well-known result of microwave-microwave and microwave-RF double resonance experiments. For simplicity, let us inspect the case in which all relaxation rates are equal. Equation (1) can be written in the following form, first given by Javan [9]:

$$G = G_0 \frac{\gamma^2 \beta^2}{2a^2} \left\{ \frac{1}{2} \left[\frac{1}{\gamma^2 + (a+b)^2} + \frac{1}{\gamma^2 + (a-b)^2} \right] + \frac{(a^2 - b^2)(2a^2 + \gamma^2) - \gamma^4}{(4a^2 + \gamma^2)[\gamma^2 + (a+b)^2][\gamma^2 + (a-b)^2]} \right\}, \quad (2)$$

where

$$G_0 = 4\pi \frac{\omega_1}{c} \frac{\mu_1^2}{h} \frac{N_2}{\gamma},$$

$$a = (\Delta_2^2 + 4\beta^2)^{1/2}/2,$$

$$b = \Delta_2/2 - \Delta_1,$$

and

$$\Delta_j = \Omega_j - \omega_j.$$

The first two terms give rise to a doublet with resonant frequencies at

$$\Omega_1(\pm) = \omega_1 + \frac{1}{2} [\Delta_2 \pm (\Delta_2^2 + 4\beta^2)^{1/2}].$$

The third term, which is due to interference originating from overlap of the components of the doublet, is important only at low intensities ($\beta \ll \gamma$), when the splitting is small. For very large intensities ($\beta \gg \gamma, \Delta_2$) the doublet separation is 2β .

This splitting is a manifestation of the dynamical Stark effect (Autler-Townes effect).

Let us first analyze the gain expression for the case of resonant pumping ($\Delta_2 = 0$), where G is always largest. At low intensities a peak gain of $3G_0\beta^2/\gamma^2$ occurs at $\Delta_1 = 0$. The peak gain increases with increasing pump intensity, reaching a maximum value $G_0/3$ for $\beta = \gamma/2$. At a slightly higher intensity ($\beta = 5\gamma/7$) the line begins to split. As β continues to increase the splitting increases, and for $\beta \gg \gamma$ the peak gain at each doublet component approaches a limiting value $G_0/4$.

For off-resonance pumping ($\Delta_2 \gg \beta \gg \gamma$) the gain curve is again in the form of a doublet with peaks of equal magnitude $G_0\beta^2/\Delta_2^2$ occurring at $\Delta_1 = 0$ and $\Delta_1 = \Delta_2$.

The corresponding expression in the RE limit can be obtained from (1) by setting $\gamma_{12} \rightarrow \infty$, which has the effect of completely destroying the Raman coherence, i.e., no double quantum processes can then occur. Setting all other decay rates equal we then obtain

$$G_{RE} = G_0 \frac{2\beta^2\gamma^2}{(\Delta_1^2 + \gamma^2)(\Delta_2^2 + \gamma^2 + 4\beta^2)}.$$

In contrast to (2), this expression is always a Lorentzian function of Δ_1 of width 2γ (FWHM), which has a peak value at $\Delta_1 = \Delta_2 = 0$ of magnitude

$$G_0 \frac{2\beta^2}{\gamma^2 + 4\beta^2}.$$

Therefore, for weak pumping the RE predicts a peak gain $2G_0\beta^2/\gamma^2$, somewhat smaller than the QM result. For strong saturation the RE limit predicts no splitting and a peak gain that is twice as large as that of each doublet component.

II. SYSTEMS IN WHICH ONLY THE PUMP TRANSITION IS DOPPLER BROADENED

This is the case in which the Doppler effect at the FIR frequency is negligible compared to the pressure-broadened linewidth, but the pump transition is still Doppler broadened ($k_1 u \ll \gamma \ll k_2 u$). Therefore, in the velocity integration of (1) the $k_1 v$ velocity dependence may be neglected ($\Omega'_1 = \Omega_1$, $\Omega'_2 = \Omega_2 - \epsilon k_2 v$). This gives

$$G(\Delta_1) = G'_0 \frac{2\beta^2}{\gamma_0 Q} \cdot \text{Re} \left[\frac{\gamma_{21} + \gamma_{20} Q - \gamma_0(Q-1)/2 + i\Delta_1}{\beta^2 + (i\Delta_1 + \gamma_{10})(i\Delta_1 + \gamma_{21} + \gamma_{20} Q)} \right], \quad (3)$$

with

$$G'_0 = 4\pi \frac{\omega_1}{c} \frac{\mu_1^2}{h} \frac{N_2 \exp[-(\Delta_2/k_2 u)^2]}{k_2 u / \sqrt{\pi}},$$

and saturation parameter

$$Q = [1 + 4\beta^2/\gamma_0\gamma_2]^{1/2}.$$

When phase changing collisions are absent [i.e., for $\gamma_{ij} = (\gamma_i + \gamma_j)/2$] the numerator becomes a factor of the denominator, and the line shape becomes a Lorentzian of width $\gamma_1 + \gamma_0 Q$ (FWHM).

The RE approximation corresponds, again, to setting $\gamma_{12} = \infty$ in (3). For weak pump intensities the RE limit agrees with the QM result but not for an intense pump, where the RE predicts an emission line that does not power broaden (FWHM = $2\gamma_{01}$), and whose peak gain increases as β/γ . In contrast, for large β/γ the QM expression, (3), predicts that the gain reaches a limiting value $G'_0(2\gamma_{20}/\gamma_0 - 1)$. This behavior is a direct consequence of the occurrence of two quantum transitions. Notice also the absence of dynamical Stark splitting, which vanishes in the velocity integration.

When the pump field becomes so intense that $\beta \sim k_2 u$ the Doppler shift at the 2-0 transition is no longer important, and the system reverts to the homogeneously broadened case of Section I.

III. FULLY DOPPLER-BROADENED SYSTEMS

The fully Doppler-broadened limit has been studied extensively over the past few years [6]. In this case $\gamma \ll k_{1,2} u$, and so the Doppler shift at both transitions is important. This gives rise to a directional anisotropy in the gain. The integration can be performed analytically in the limit $\beta^2 \ll \gamma(ku)$. Complete expressions may be found in [10].

For weak pump intensity and no dephasing collisions the emission line shape is a Lorentzian, narrower in the forward direction ($\epsilon = +1$) than in the backward direction ($\epsilon = -1$), and is centered at frequency $\Omega_1^0(\epsilon) = \omega_1(1 + \epsilon\Delta_2/\omega_2)$. The respective linewidths (FWHM) are

$$\gamma(\epsilon) = \gamma_1 + \gamma_0 + (\gamma_2 - \epsilon\gamma_0)\omega_1/\omega_2. \quad (4)$$

The peak gain, located at frequency $\Omega_1^0(\epsilon)$ for $\epsilon = \pm 1$, is given by

$$G(\epsilon) = 4G'_0\beta^2/[\gamma_0\gamma(\epsilon)]. \quad (5)$$

Note that the gain in the forward direction exceeds that in the backward direction [$G(+)>G(-)$], and that because $\gamma(+)G(+)=\gamma(-)G(-)$ the "areas" under the two Lorentzians are equal. The gain anisotropy has made it possible to construct a unidirectional optically pumped laser amplifier in a ring cavity configuration [11].

The gain anisotropy $G(+)/G(-)$ increases with the ratio ω_1/ω_2 . In the case when all the γ 's are equal

$$G(+)/G(-) = 1 + \omega_1/\omega_2. \quad (6)$$

In the limit of $\omega_1/\omega_2 \ll 1$

$$G(+)\simeq G(-)\simeq 2G'_0\beta^2/\gamma^2,$$

and the anisotropy disappears.

For large pump intensities ($ku > \beta > \gamma$) the anisotropy between forward and backward emission line shapes becomes even more pronounced. The backward emission line shape remains Lorentzian, with a linewidth $\gamma_1 + Q[\gamma_0 + (\gamma_2 + \gamma_0)\omega_1/\omega_2]$ (FWHM). Accordingly, for large β/γ the backward gain profile power broadens. At the same time its peak value approaches a limiting value

$$G'_0\gamma_2/[\gamma_0 + (\gamma_2 + \gamma_0)\omega_1/\omega_2].$$

In contrast, at large pump intensities the forward emission line shape splits symmetrically into two components separated by

$4\beta[\omega_1(\omega_2 - \omega_1)]^{1/2}$. The splitting of this doublet is maximum for $\omega_1 = \omega_2/2$. This splitting is another manifestation of the dynamic Stark effect, discussed in Section I, which is preserved in the fully Doppler-broadened limit when E_1 and E_2 are copropagating. Note, however, that although the splitting increases linearly with β , as in the pressure-broadened case, its magnitude is different. In contrast to the counter-propagating case, the peak gain of each component does not saturate with increasing pump intensity, but instead continues to increase $\propto (\beta/\gamma)^{1/2}$ up to the point $\beta \sim k\omega$, where the system is no longer Doppler broadened and the gain saturates, as described in Section I.

In comparison with the above results, the RE approach in the fully Doppler-broadened limit predicts identical Lorentzian gain profiles centered at $\Omega_1^0(\pm)$. There is no forward-backward anisotropy, since Raman-type processes are neglected [3]. For weak pump intensities the gain curves are identical to the backward gain curve of the QM case. For large pump intensities the Lorentzians power broaden. In the case of no dephasing collisions the linewidths are $\gamma_1 + \gamma_0 + Q(\gamma_0 + \gamma_2)\omega_1/\omega_2$ (FWHM), somewhat narrower than the $\epsilon = -1$ QM linewidth. With increasing pump intensity the peak gain (for both $\epsilon = \pm 1$) approaches the limiting value $G'_0(\omega_2/\omega_1)\gamma_2/(\gamma_2 + \gamma_0)$, which is larger than that of the $\epsilon = -1$ QM peak gain, but smaller than the gain peaks of the $\epsilon = +1$ doublet.

IV. EXPERIMENTS

We have studied the emission characteristics of an optically pumped FIR system which is fully Doppler broadened. Two types of experiments will be described. In the first a weak tunable field is used to probe the gain line shape at the FIR transition in an optically pumped external cell. Subsequent experiments study the frequency characteristics of the output of an optically pumped FIR laser. In this case the laser field itself serves as the probe.

In the gain line shape studies a CH₃OH sample cell was pumped with a CO₂ laser and probed with the radiation from a FIR CH₃OH laser. The CO₂ laser, capable of delivering 12 W CW at 9.7 μ m, had a 1-m discharge and used a diffraction grating for line selection. Power was coupled out of the cavity via the zeroth diffraction order. The frequency of the CO₂ laser could be controlled by adjusting the voltage of a PZT attached to the end cavity mirror.

Most of the CO₂ laser power was used to pump the FIR laser. The FIR laser cavity was of the waveguide type with two flat mirrors, one of which was mounted on a second PZT. The FIR cavity modes could be tuned by adjusting the PZT voltage. The CO₂ pump beam was focused inside the FIR cavity through a 2-mm-diam hole in one of the mirrors. This hole also served to couple out the FIR radiation. The FIR cavity was filled with CH₃OH in the pressure range 50–500 mtorr. Using different CO₂ pump lines, CW FIR radiation at several wavelengths could be generated [1]. The experiments reported below studied the FIR emission of the 70.5- μ m line, [P(34) 9.7- μ m CO₂ pump].

In the external cell experiments about 1 W of the CO₂ laser power was split off from the main beam and sent unfocused to pump a 60-cm cell filled with low-pressure (<100 mtorr)

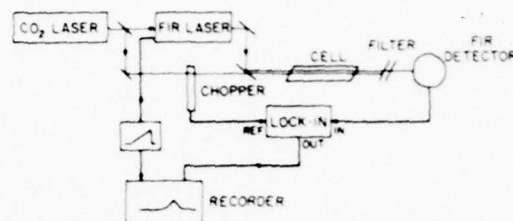


Fig. 2. Experimental setup for studying the CH₃OH FIR gain induced in an external, optically pumped sample cell.

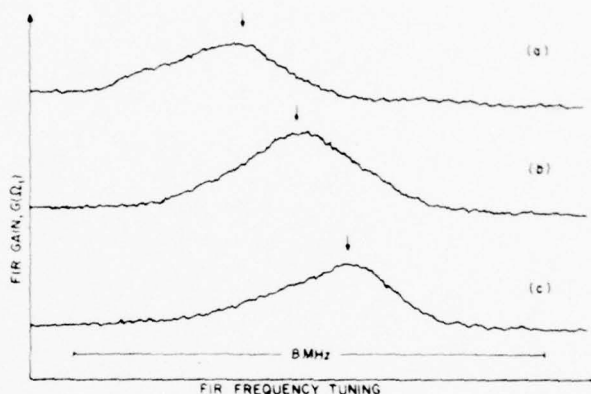


Fig. 3. Observed FIR gain profiles. Lock-in amplifier output versus FIR probe frequency is shown. In traces (a), (b), (c) the frequency setting of the CO₂ pump laser is successively incremented by 7 MHz.

CH₃OH (Fig. 2). The collimated output of the FIR laser, aligned to coincide with the CO₂ beam, was used to probe the gain at the coupled transition of the CH₃OH sample cell in the forward direction. A TPX filter placed after the sample cell was used to reject the pump beam and transmit the FIR signal. A He-cooled InGe detector was used to detect the FIR radiation. The CO₂ laser was chopped at 100 Hz, and synchronous detection was used to measure the gain.

Fig. 3 shows the output of the lock-in detector as the FIR frequency is swept. The sample cell pressure was 50 mtorr. In gain profiles (a), (b), and (c) the CO₂ pump frequency was successively increased by increments of 7 MHz. The distortion in the line shapes is due to the power change of the probe laser (operated at 300 mtorr) as it is tuned over its ~ 10 -MHz range. The gain profiles are found to be 2.4-MHz wide (FWHM). Power broadening was negligible at the available pumping power, so that if we assume $\gamma_1 = \gamma_0 = \gamma$ in (4) (with $\epsilon = \pm 1$) we obtain $\gamma = 24(\pm 6)$ MHz/torr. Under these experimental conditions a peak FIR gain of 5 percent/m was measured.

The forward-backward gain anisotropy is one of the most interesting predictions of the QM treatment in the fully Doppler-broadened limit. Equation (5) predicts a higher gain in the forward direction than in the backward direction, the gain anisotropy ratio being $1 + \omega_1/\omega_2$, (6). For the 70- μ m FIR transition $\omega_1 = 0.08\omega_2$, yielding a small anisotropy ratio which would be difficult to observe in forward/backward probe experiments. Instead, the gain anisotropy was investigated by studying the tuning characteristics of the FIR laser itself, because near threshold the power output is very sensi-

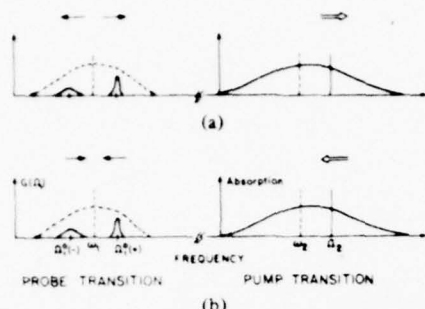


Fig. 4. Frequency profile of FIR gain induced by a standing-wave pump field. The dashed lines show the Doppler profile of the 0-1 transition. (a) and (b) show the gain contributions from the right- and left-propagating traveling wave components of the standing wave field. Peaks occur at $\Omega_2(\pm) = \omega_1 \pm \Delta_2 \omega_1 / \omega_2$. Note that in both (a) and (b) for $\Delta_2 > 0$ ($\Delta_2 < 0$) the emission component above (below) ω_1 has higher gain.

tive to small changes in gain. In these experiments the FIR laser was operated in the low-pressure (80 mtorr) range. In order to resolve the forward and backward emission line shapes the pump laser was detuned from the center of the CH_3OH transition. It is important to realize that the gain anisotropy, usually described for the traveling wave pump field, is not destroyed when the pump field is in the form of a standing wave, as is the case in our FIR cavity (Fig. 4). If the pump laser is set at the high- (low-) frequency side of the CH_3OH absorbing transition, the high- (low-) frequency component of the FIR emission line shape should exhibit higher gain, and this gain asymmetry should give rise to a corresponding asymmetry in the FIR laser output as the FIR cavity is tuned.

This is verified in the experimental results of Fig. 5: when the pump is tuned to the center of the absorbing transition ($\Delta_2 = 0$) 1) forward and backward line shapes overlap, giving rise to a single symmetrical profile of the FIR laser output tuning curve. For a pump frequency detuning of $\Delta_2 = 7$ MHz 2) the components begin to split and the gain asymmetry becomes apparent. With increased detuning 3) the splitting becomes larger and both peaks decrease in magnitude, but the backward peak decreases more rapidly since its gain is closer to oscillation threshold. Eventually only the forward emission component has enough gain for laser oscillation.

Similar effects have been observed in the visible in a three-level system in neon in which the common level (level 0) is lowest in energy [12].

Further experiments to explore the QM features of optically pumped CH_3OH FIR lasers are in progress. Studies are planned using transitions having shorter FIR wavelengths, where the gain anisotropy is more pronounced. Cases (1) and (2) will be studied by going to higher pressures and using longer FIR wavelengths ($\lambda \sim 500 \mu\text{m}$). Studies of the transient behavior of the FIR emission, obtained when the pump laser is suddenly turned on or off, are also under way.

ACKNOWLEDGMENT

We would like to thank J. Mickey and C. Duda for their help in the experiments, and W. Ryan for expert technical assistance.

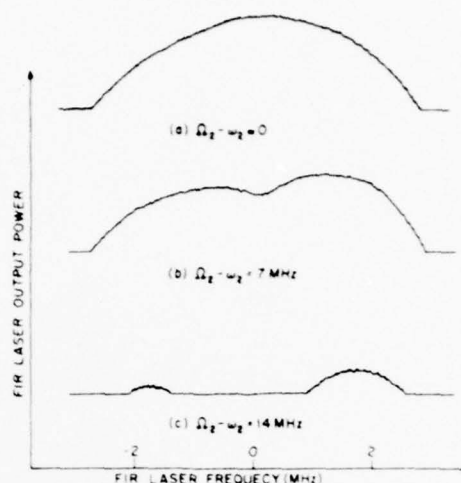


Fig. 5. FIR laser output tuning curve. Laser output intensity versus cavity tuning is shown. (a) on-resonance pumping ($\Delta_2 = 0$); (b) $\Delta_2 = 7$ MHz; (c) $\Delta_2 = 14$ MHz.

REFERENCES

- [1] T. Y. Chang, "Optically pumped submillimeter-wave sources," *IEEE Trans. Microwave Theory Tech.*, vol. MTT-22, p. 983, 1974.
- [2] See, for example, T. A. DeTemple and E. Danielewicz, "Continuous-wave CH_3F waveguide laser at $496 \mu\text{m}$: Theory and experiment," *IEEE J. Quantum Electron.*, vol. QE-12, p. 40, 1976.
- [3] M. S. Feld, "Laser saturation spectroscopy in coupled Doppler-broadened systems: How to find a needle in a haystack," in *Fundamental and Applied Laser Physics*, M. S. Feld, A. Javan, and N. A. Kurnit, Ed. New York: Wiley, 1973, p. 369.
- [4] V. P. Chebotayev, "Three-level laser spectroscopy," in *Topics in Applied Physics*, vol. 13, K. Shimoda, Ed. New York: Springer, 1976, p. 201.
- [5] N. Skribanowitz, I. P. Herman, and M. S. Feld, "Laser oscillation and anisotropic gain in the $1 \rightarrow 0$ vibrational band of optically pumped HF gas," *Appl. Phys. Lett.*, vol. 21, p. 466, 1972. For the case of off-resonant pumping, see the recent work of T. Y. Chang and J. D. McGee, "Off-resonant infrared laser action in NH_3 and C_2H_2 without population inversion," *Appl. Phys. Lett.*, vol. 29, p. 725, 1976.
- [6] See reviews [3] and [4] and references therein.
- [7] The case of strong FIR fields (E_1) has recently been analyzed for a coupled homogeneously broadened system by R. J. Temkin, "Rate equations and theory of optically-pumped submillimeter lasers," in *Conf. Dig. Second Int. Conf. and Winter School on Submillimeter Waves and their Applications*, Puerto Rico, 1976, p. 43; and R. L. Panock and R. J. Temkin, "Interaction of two laser fields with a three level molecular system," this issue, pp. 425-434.
- [8] M. S. Feld and A. Javan, "Laser-induced line narrowing effects in coupled Doppler-broadened transitions," *Phys. Rev.*, vol. 177, p. 540, 1969.
- [9] A. Javan, "Theory of a three-level maser," *Phys. Rev.*, vol. 107, p. 1579, 1957.
- [10] B. J. Feldman and M. S. Feld, "Laser induced line-narrowing effects in coupled Doppler-broadened transitions, II. Standing wave features," *Phys. Rev.*, vol. A5, p. 899, 1972.
- [11] N. Skribanowitz, M. S. Feld, R. E. Francke, M. J. Kelly, and A. Javan, "Possibility of a unidirectional laser amplifier produced by monochromatic optical pumping of a coupled Doppler-broadened transition," *Appl. Phys. Lett.*, vol. 19, p. 161, 1971; N. Skribanowitz, I. P. Herman, R. M. Osgood, Jr., M. S. Feld, and A. Javan, "Anisotropic ultra-high gain emission observed in rotational transitions in optically pumped HF gas," *Appl. Phys. Lett.*, vol. 20, p. 428, 1972.
- [12] I. M. Beterov and V. P. Chebotayev, "Three level gas lasers," *JETP Lett.*, vol. 9, p. 127, 1969.

ENERGY STORAGE AND VIBRATIONAL HEATING IN CH_3F FOLLOWING INTENSE LASER EXCITATION

R.E. McNAIR*, S.F. FULGHUM, G.W. FLYNN**, M.S. FELD†

Physics Department and Spectroscopy Laboratory, Massachusetts Institute of Technology, Cambridge, Massachusetts 02139, USA

and

B.J. FELDMAN

Los Alamos Scientific Laboratory, Los Alamos, New Mexico 87545, USA

Received 15 March 1977

Fundamental relations for energy storage among the modes of a polyatomic molecule are derived in terms of γ_{VV} , the V-V collision parameter and the energy flow path. A new method is introduced for making absolute measurements of vibrational energy.

This paper explores energy absorption and energy transfer induced by vibrational (V-V) collisions following intense laser excitation[†]. A theoretical model is derived which predicts that under appropriate conditions several quanta per molecule can be absorbed in vibrational energy. This is confirmed using a pulsed CO_2 laser to vibrationally heat $^{13}\text{CH}_3\text{F}$. In addition, we directly measure the energy stored in the vibrational modes and show that a steady state exists. These findings are basic to the use of molecular gases as energy storage media. Furthermore, a complete knowledge of the energy distribution of vibrationally hot but rotationally cold gases opens interesting possibilities for achieving laser oscillation and for studying chemical reactions in excited vibrational states.

Consider an intense pulse of laser radiation reso-

nantly interacting with one of the ground state ($v = 0 \rightarrow 1$) rotational-vibrational transitions of a diatomic molecular gas. When the laser pulse time (τ_p) is long compared to the rotational bottleneck time (τ_B), the entire rotational manifold of the $v = 1$ state can be populated[‡]. If τ_p is short compared to the characteristic V-V collision time (τ_{VV}), the energy flow into the system will be limited by the condition that not more than half of the ground state population can be transferred into the $v = 1$ vibrational state. However, if $\tau_p \gg \tau_{VV}$ additional energy can flow into the system. This comes about because the normal V-V processes as they occur in thermal equilibrium are unbalanced by the presence of the intense laser field. The laser continually acts to equalize the $v = 0$ and $v = 1$ level populations, and resonant V-V processes can then lead to additional vibrational heating. For example, consider the process in which two molecules in the $v = 1$ state collide to produce a $v = 2$ molecule and a $v = 0$ molecule. The $v = 2$ molecules thus created will be carried up the vibrational ladder by subsequent

* Present address: Hughes Research Laboratory, Malibu, California, USA.

** John Simon Guggenheim Memorial Fellow 1974-75; permanent address: Department of Chemistry, Columbia University, New York City, New York, USA.

† Alfred P. Sloan Fellow.

‡ Many energy transfer and relaxation studies have been made using weak laser excitation. See for example, ref. [1] and references therein.

[‡] $\tau_B = \tau_R/f$, with τ_R the rotational thermalization time, and f the fractional population of the lower level of the laser transition. Letokhov and Makarov [2] have considered the regime where $\tau_B \gg \tau_{VV}$. See also ref. [3].

V-V collisions. The molecules transferred to the $v = 0$ level unbalance the population equality of the $v = 0$ and $v = 1$ states. However, the laser maintains this equality, thereby bringing additional energy into the system. This build-up of stored vibrational energy can continue until V-T relaxation (characteristic time τ_{VT}) sets in.

The theoretical model assumes: (1) $\tau_B \ll \tau_P$, (2) $\tau_P \ll \tau_{VT}$ (to prevent thermal heating) and (3) a pulse sufficiently intense to equalize $v = 0$ and 1 level populations for molecules of all velocities. Assuming resonant binary V-V processes, and dipole-dipole collisions in the harmonic oscillator approximation, the vibrational heating of a diatomic molecule can be described by coupled rate equations of the form[†]

$$\begin{aligned} dP_v/dt + \frac{1}{2}\gamma_{VV} \sum_{v'=0}^{\infty} \{[(v+1)v' + v(v'+1)] P_v P_{v'} \\ - vv' P_{v-1} P_{v'} - (v+1)(v'+1) P_{v+1} P_{v'}\} \\ = \sigma I (P_0 - P_1)(\delta_{v,1} - \delta_{v,0}), \quad v = 0, 1, 2, \dots \end{aligned} \quad (1)$$

Here P_v is the fraction of molecules in the v th level, γ_{VV} is the V-V rate constant ($\tau_{VV} \approx \gamma_{VV}^{-1}$). The right-hand side of eq. (1) describes the pumping of the $v = 0 \rightarrow 1$ transition (absorption cross section σ) by a laser field of photon flux I . For full saturation of the laser transition $\hat{P}_0 \approx \hat{P}_1$ and we assume that a quasi-equilibrium is established among states $v \geq 1$ having an effective temperature which increases with time. The number of quanta per molecule, ϵ , is then

$$\epsilon = \sum v P_v = (1 - P_1)^2 / P_1. \quad (2a)$$

Using eq. (1) and initial conditions $P_0(0) = P_1(0) = 1/2$, $P_1(t)$ is then given by

$$1/P_1^2 + 4 \ln(2P_1) = 4 + \gamma_{VV} t, \quad (2b)$$

from which $\epsilon(t)$ can be obtained. Computer solutions of eq. (1) agree with eqs. (2) and confirm that an effective temperature is established [5].

In polyatomic molecules, where other modes are present, the energy absorption process is modified by V-V cross-over collisions, which lead to energy transfer to other modes. However, when the $v = 1$ level of

a closely coupled mode, ν_b , is at least $\approx kT$ above that of the mode being pumped, ν_a (as in the CH_3F experiments), a temperature relationship [eq. (5), below] is rapidly established between the modes during the pumping process, and the number of quanta within the modes, ϵ_a and ϵ_b , increases with $\epsilon_a \gg \epsilon_b$. As a result, the net vibrational energy deposited in a polyatomic molecule is very nearly the same as in the diatomic case, so that eqs. (2) still hold, with $\epsilon = \epsilon_a + \epsilon_b$ and γ_{VV} being the V-V rate constant of the mode being pumped. Computer calculations [5] confirm these findings. As seen below, eqs. (2) give good agreement with the data.

The 9.65 μm P(32) CO_2 laser line falls within the Doppler width of the ν_3 ($v = 0 \rightarrow 1$) R(4, 3) transition of $^{13}\text{CH}_3\text{F}$. The large transition matrix element leads to full saturation at moderate laser intensities, and $\tau_R \ll \tau_{VV} \ll \tau_{VT}$ [1]. Spontaneous emission from several modes is readily observable, providing a means of observing stored vibrational energy. Laser pulse durations were typically 2–4 μs . Pulse energies (< 0.25 J) were kept well below the threshold for collisionless absorption [6], but sufficiently high to ensure complete saturation of the $^{13}\text{CH}_3\text{F}$ Doppler profile.

In the energy absorption experiments the laser beam traversed an 18 cm CH_3F sample cell. Incident and transmitted pulse energies were monitored with calibrated Au:Ge detectors. Given the energy absorbed by the sample and the beam volume, the number of CO_2 quanta absorbed per molecule, $\epsilon(P)$, can be obtained as a function of the $^{13}\text{CH}_3\text{F}$ pressure, P (fig. 1a). For $P < 5$ torr $\epsilon(P)$ rose monotonically, reaching a maximum of 2.6 quanta. At higher pressures it slowly decreased due to incomplete laser saturation over the cell length. A best fit to $\epsilon(P)$, obtained from eqs. (2), gives a value of $\gamma_{VV} = 0.8 \pm 0.2 \mu\text{s}^{-1} \text{ torr}^{-1}$. This result agrees with Earl and Ronn's value [7] of $1.2 \pm 0.3 \mu\text{s}^{-1} \text{ torr}^{-1}$, measured via laser fluorescence, and confirms that eq. (2) is a good approximation for predicting energy absorption in a polyatomic.

If a rotational bottleneck [2,3] is present it can be eliminated by adding a buffer gas which reduces τ_R . In CH_3F , however, no bottleneck is present, as evidenced by the fact that the energy absorbed did not change when up to 500 torr of argon was added to a fixed amount of CH_3F .

To establish that for times $\ll \tau_{VT}$ the absorbed energy resides in the vibrational degrees of freedom, the time evolution of the fluorescence from the 9.6 μm

[†] The left-hand side of this equation is given by Shuler [4].

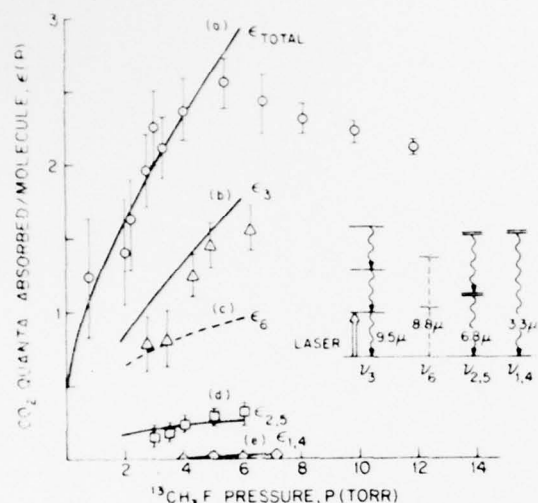


Fig. 1. CO_2 quanta stored versus pressure. (a) Total quanta stored. The theoretical fit gives $\gamma_{\text{VT}} = 0.8 \pm 0.2 \mu\text{s}^{-1} \text{ torr}^{-1}$. (b) (c) Quanta stored in ν_n . The curves were calculated from (a). The insert shows relevant vibrational levels.

C—F stretch mode (ν_3) was monitored by a Cu:Ge detector. In the pressure range of the experiments the fluorescence signal was always in the form of a rapid rise, governed by the duration of the laser pulse, followed by a long (\approx ms) decay, determined by the V—T relaxation processes. The $3.3 \mu\text{m}$ C—H stretch (ν_1, ν_4) and $6.8 \mu\text{m}$ bend (ν_2, ν_5) fluorescence bands exhibited the same temporal behavior as ν_3 . This indicates fast intermode V—V transfer rates, and that soon after the laser pulse terminates a vibrational steady state among the modes is established.

Since the absorbed energy is distributed among all the modes, it is important to determine how much is stored in each. However, absolute measurement of fluorescence intensities would be difficult and imprecise. A new technique, which utilizes the fact that a steady state is rapidly established among the vibrational modes, was employed to measure the energy stored in ν_3 . In this technique the peak fluorescence is first observed after it passes through an empty "cold gas filter" cell to give $I(0)$. Then, methyl fluoride gas at room temperature is introduced into this cell to remove the $\nu = 1 \rightarrow 0$, giving $I(0) - I_{10}$. This "cold" (room temperature) gas is an ideal filter for the $\nu = 1 \rightarrow 0$ fluorescence, since the absorption band matches the emission frequencies line for line, and the small

anharmonicity (18 cm^{-1}) is sufficient to prevent absorption of ν_3 fluorescence from higher lying levels*. Describing the vibrational level populations by a Boltzmann distribution at temperature T_3 ($T_3 >$ room temperature), and assuming harmonic oscillator transition moment matrix elements, we obtain

$$I_{10}/I(0) = (1 + \epsilon_3)^{-2}, \quad \epsilon_3 = [\exp(\hbar\omega_3/kT_3) - 1]^{-1}, \quad (3)$$

where ω_3 is the ν_3 frequency. The measured ratio $I_{10}/I(0)$ determines ϵ_3 , the number of quanta stored in ν_3 .

In practice, care must be taken in obtaining the ratio $I_{10}/I(0)$. The $\nu = 1 \rightarrow 0$ emission occurs over the entire rotational manifold. The intense emission lines are absorbed strongly; conversely, the weak emission lines are absorbed weakly. As a result the curve of transmitted intensity $I(P')$ versus cold gas filter pressure, P' has a long tail rather than a sharp cut-off. One finds

$$I(P')/I(0) = 1 + [I_{10}/I(0)] [\chi(P') - 1], \quad (4a)$$

where $\chi(P')$ is a function of the symmetric top matrix elements and absorption coefficients. For a cold gas filter cell of length L containing Doppler-broadened CH_3F , $\chi(P')$ is closely approximated by

$$\chi(P') = 0.567 e^{-0.614 P' L} + 0.331 e^{-0.145 P' L} + 0.102 e^{-0.019 P' L}. \quad (4b)$$

Fig. 2 shows the transmitted fluorescence intensity as a function of cold gas filter pressure for several values of sample cell pressure. In each case the solid line gives a best fit to the theoretical expression for $I(P')/I(0)$ [eq. (4)], from which ϵ_3 is obtained [eq. (3)]. Note that with increasing sample cell pressure, P , $I(P')$ falls off more slowly, indicating increased population of the upper vibrational states and thus higher T_3 .

The observed values of ϵ_3 at various pressures are given in fig. 1b. Note that 40–50% of the total energy (fig. 1a) resides in ν_3 . Since τ_{VT} is long the remaining energy must be shared among other modes.

In order to determine more precisely the partitioning of energy, the vibrational energies ϵ_n of the $\nu_{2,5}$

* Pressures of both sample and cold gas filter cells were kept below 10 torr to avoid overlap of lines due to excessive pressure broadening.

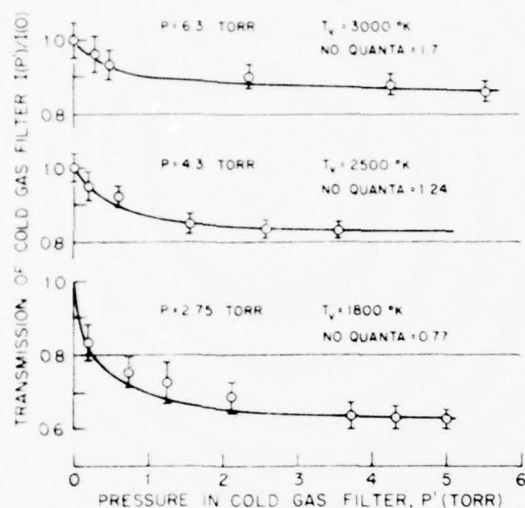


Fig. 2. Cold gas filter measurements. The theoretical fits give the temperature of the ν_3 mode.

and $\nu_{1,4}$ modes were also measured. (ϵ_6 was too weak to measure.) This was done by taking ratios of the corresponding fluorescence intensities to that of ν_3 . Knowing the ratios of the mode frequencies and transition moments, and the detector efficiency, ϵ_n could then be obtained in terms of ϵ_3 (fig. 1). Cold gas filter experiments performed on the $\nu_{1,4}$ fluorescence, which are less accurate because of its weak transition moment, establish a firm upper bound for $\epsilon_{1,4}$ which agrees with fig. 1.

The steady state partitioning of energy among the modes may be determined from a knowledge of the path by which energy is transferred among the modes. The temperature of two modes, energies E_a and E_b , in vibrational equilibrium are related by [8]

$$E_a/T_a = E_b/T_b = (E_a - E_b)/T, \quad (5)$$

with T the kinetic temperature. Therefore, by assuming a dominant energy flow path, eq. (5) can be successively applied to each pair of modes collisionally coupled in the energy flow process. The smooth curves of figs. 1b-1e were obtained from eq. (5) using the theoretical

curve of fig. 1a and the energy flow path of ref. [9]. The agreement with the experimental points is indicative of the accuracy of our absolute measurements of vibrational temperatures, and supports the energy flow assignments [9]. No other path assignments led to good agreement with the data.

In conclusion, this is the first time that the energy storage and partitioning of a highly excited polyatomic have been measured. The confirmation of the simple prediction of laser induced vibrational heating [eq. (2)] and subsequent vibrational energy redistribution shows that these relationships can be applied with confidence in other molecules. Finally, a comparison of the present results with weak excitation experiments [9] strongly suggests that the dominant path for vibrational energy redistribution does not change in CH_3F for vibrational excitation up to ≈ 7 kcal/mole.

The authors wish to thank Rick Forber, Vladik Letokhov, Bill Ryan, Howard Schlossberg and Ramesh Sharma for useful discussions and Ali Javan for his support and encouragement.

References

- [1] E. Weitz and G.W. Flynn, *Ann. Rev. Phys. Chem.* 27 (1973) 81.
- [2] V.S. Letokhov and A.A. Makarov, *Soviet Phys. JETP* 36 (1973) 1091.
- [3] B.J. Feldman, *IEEE J. Quantum Electron.* QE-9 (1973) 1070.
- [4] K.E. Shuler, *J. Chem. Phys.* 32 (1960) 1692.
- [5] R.E. McNair, R. Forber, S.F. Fulghum, G.W. Flynn, B.J. Feldman and M.S. Feld, to be published.
- [6] R.V. Ambartsumian, V.S. Letokhov, E.A. Ryabov and N.V. Chekalin, *JETP Letters* 20 (1975) 275; J.L. Lyman, R.J. Jensen, J. Rink, C.P. Robinson and S.D. Rockwood, *Appl. Phys. Letters* 27 (1975) 87.
- [7] B.L. Earl and A.M. Ronn, *Chem. Phys. Letters* 39 (1976) 95.
- [8] C.E. Treanor, J.W. Rich and R.G. Rehm, *J. Chem. Phys.* 48 (1968) 1798.
- [9] I. Shamah and G.W. Flynn, *J. Chem. Phys.*, to be published.

V. Non-Linear Characteristics of Tunnelling
Diodes

Proceedings of the 31st Annual Frequency Control Symposium, Fort
Monmouth, N.J. (1977)

OPTICAL ELECTRONICS, EXTENSION OF MICROWAVE TECHNIQUES INTO THE OPTICAL REGION

C. F. Davis, Jr., G. Elchinger, A. Sanchez, K. C. Liu and A. Javan

Massachusetts Institute of Technology

Infrared diode work began some ten years ago with point contact MOM junctions. These were used as harmonic generators and mixers, often of fairly high order. They have even been used in stabilized harmonic generator chains through $2\ \mu\text{m}$.¹ Such devices can form the basis of active far infrared (FIR) elements and circuits for reradiation of laser sidebands, signal processing in this region of the spectrum and studying extremely short pulse phenomena. Recently work has been done on MOM devices evaporated through masks or photolithographically defined. I will show you why small area devices are essential to extending the operating frequency and how such devices can perform active circuit functions in the FIR and perhaps someday on into the visible; already MOM diodes are responding non-thermally to visible radiation. A study we are just completing shows that a point contact MOM behaves according to classical antenna theory in the FIR. Some of our latest work is described on printing MOM circuits for a real time holographic array.

The MOM devices operate by nonlinearities in their conductance, which must be the order of the signal source (the antenna at about $100\ \Omega$). This junction is then shunted by its own capacitance which restricts its high frequency operation. Junction conductance decreases exponentially with thickness while capacitance goes as the reciprocal; hence the thinnest junction must have the most favorable conductance capacitance ratio. A junction with barrier thickness about the typical $10\ \text{\AA}$ would have resistance of $10^2\ \Omega/\text{\AA}$ (\AA in μm^2) requiring about $1\ \mu\text{m}^2$ to match the typical antenna resistance. Orders of magnitude change in the area can be compensated for by small changes in barrier thickness to maintain junction impedance comparable to the antenna resistance ($100\ \Omega$) while adjusting the capacitance. The response time would then be given by $RC = 10^{-12}\ \text{A.}$ (\AA in μm^2)

We have considered several FIR functional circuits; these have not yet been built. However, fabrication would require two successive photolithographically defined metalizations, the first capable of forming and supporting a stable barrier layer about $10\ \text{\AA}$ thick and the second of adhering to the substrate and making good contact to the barrier layer. One circuit usable as a parametric subharmonic generator might consist of a circle half made of each metal, overlapping at one intersection to form a small area MOM diode and at the other a large area ohmic contact. Inherent inductance and capacitance of this circuit and junction can make it resonant in the FIR. With appropriate input driving signal and bias leads and a realizable junction nonlinearity, a Q of 5 would be adequate to cause oscillation at half the signal frequency.

Some particularly interesting work has been with high speed deposited negative resistance junctions formed by evaporating a narrow lead stripe on tin with a thin surface oxidation. This junction is cooled to about 2°K where both metals are superconducting and irradiated with a focused argon laser

beam; definite non-thermal response was observed. Responses of lead on aluminum junctions were observed, again at 2°K (aluminum above its superconducting transition). The response to X-band and $5145\ \text{\AA}$ argon laser radiation was very similar showing peaks in exactly the same locations. The principal structural response occurs at dc bias voltage less than $20\ \text{mV}$ and is due to the superconducting transition and photon scattering in the lead film.

A theoretical analysis² of the MOM antenna/diode as a detector of microwave and infrared radiation is being conducted and FIR experiments evaluated to examine the consistency of the theory. The antenna is coupled directly into the diode. An equivalent circuit is used to represent the system of the antenna and its coupling to the diode. A Stratton³ tunneling model represents the nonlinear character of the junction. Detector performance is shown to obey experimentally verified laws and determine an optimum junction thickness and area for each frequency. It is shown that the detectivity at room temperature can be as high as $10^{10}\ \text{watts}^{-1}\ \text{Hz}^{1/2}$ at frequencies of $10^{14}\ \text{Hz}$ in the infrared. Experimental results show that for small focusing angles, $\theta_f = D/f$ (where $f = 12.7\ \text{cm}$ in this case), the efficiency η is proportional to θ_f^2 (see Fig. 1) consistent with the concept of effective aperture. The proportionality constant (at $337\ \mu\text{m}$ wavelength) agrees within a factor of two with that expected from our theory; this discrepancy may be caused by uncertainty in the calorimetric laser power measurement. As the focusing angle is increased to the width of the major radiation lobe, the coupling efficiency saturates to about 3%, in agreement again with the theory. Different antenna lengths give proportionally different coupling efficiencies for small focusing angles and the same saturated value for larger angles.

To confirm that the FIR detection arises from the same mechanism as that for rf detection (i.e. rectification), we checked, using a balancing technique, that the same detected voltage comes from an rf signal as from a preadjusted ir signal, as the bias is increased up to about $100\ \text{mV}$.

This balancing technique has been applied to the study of the type of printed diodes integrated to an antenna described in Ref. 4. Preliminary results show that some structures have coupling efficiencies as high as 2 or 3%, comparable to that of the mechanical point contact diode. This technique is applicable regardless of the nature of the rectification mechanism as long as it is the same at rf and ir frequencies. For example, we have also fabricated antenna structures where the detecting element is an evaporated micron-sized, thin-film wire without a junction. A weak bolometric response, with the same bias dependence, was observed at both frequencies and the best coupling efficiency was found to be around 1%.

We have studied the behavior of the point contact diode nonlinearities by observing the bias dependence of the rectified signal when a known

amount of rf power is coupled to the diode. These results can be compared with the predictions of the tunneling model. Values for the barrier parameters are found to be reasonable.

The diode's I-V characteristic up to the third order can be expressed as:

$$I = \frac{1}{R} (V + mV^2 + nV^3)$$

Then the rectified voltage, V_r , when an rf voltage $V_D \cos \omega t$ is coupled to these diode nonlinearities is given by

$$V_r = (m + 3n V_b) \frac{V_D^2}{2}$$

The experimental dependence of V_r on V_D shown in Fig. 2, can be approximated by a straight line in the low bias region. We can then obtain for the 2 K-ohm diode, $m = .16 \text{ V}^{-1}$ and $n = 1.8 \text{ V}^{-2}$.

These values for m and n , which are independent of the contact area, are in general agreement with those obtained from the model assuming reasonable values for the barrier parameters. From the tunneling model, we can express the average potential, ϕ_0 , and thickness of barrier, L , as:

$$\phi_0 = \frac{1}{4\sqrt{6n}} \ln \frac{324 R_D a}{4\sqrt{6n}}$$

$$L = \frac{4\sqrt{6n\phi_0}}{1.025}$$

By estimating the value of contact area as $a = .1 \mu\text{m}^2$, we can then obtain $\phi_0 = .65 \text{ eV}$ and $L = 10.3 \text{ \AA}$ which are quite reasonable and change only logarithmically with the estimated area. Furthermore, the value of the asymmetry factor, α , according to the theory is given by

$$\alpha = m\sqrt{6/n}$$

which, in the case of Fig. 2, is equal to 0.29 and does not depend on the estimated area.

As the resistance of the diode is lowered by adjusting the pressure of contact, the value for n decreased monotonically. For example; if $R_D = 50 \text{ ohms}$ we get $n = 1.39$ so that $\phi_0 = 0.43 \text{ eV}$ and $L = 7.3 \text{ \AA}$. At these low values of L and ϕ_0 , the W.K.B. approximation used in calculating the tunneling probability begins to lose its applicability.

We have shown that in agreement with the theory, the zero bias responsivity, $B_i (=m)$, remains nearly constant as the resistance is varied over two orders of magnitude. By studying the laser rectification as the resistance of the diode, R_D , "relaxes" continuously and slowly (presumably keeping the same asymmetry factor α) from 10 to few thousand ohms, we were able to fit the result to the expression:

$$V_r = V_0 \left(\frac{R_D}{R_D + R_A} \right)^2$$

with two adjustable parameters, V_0 and R_A (antenna

resistance).

A 2×2 array of antenna/diodes has been fabricated for ultimate use as a real time holographic imaging array. This is now being evaluated as individual infrared rectifier/mixers. In operation, two infrared beams differing by a microwave frequency will irradiate the array. From the amplified difference frequency we can obtain relative phase information of the two signals. This provides the information required to define and construct a real time hologram.

1. D. A. Jennings, F. R. Peterson, K. M. Evenson, Appl. Phys. Letts. 26, 510 (1975).

2. To be published.

3. R. Stratton, J. Phys. Chem. Solids 23, 1177 (1962).

4. J. Small, G. M. Elchinger, A. Javan, A. Sanchez, F. L. Bachner, D. L. Smythe, Appl. Phys. Letts. 24, 275 (1974).

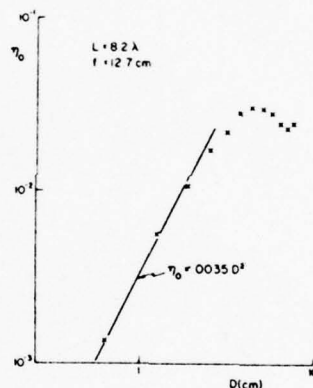


Figure 1. The antenna/diode efficiency is plotted as a function of iris diameter, D . It should be noted that saturation at high values of D comes from a combination of approaching the beam diameter and exceeding the width of the first lobe. The proportionality constant, .0035, is within a factor of two of the theoretical value.

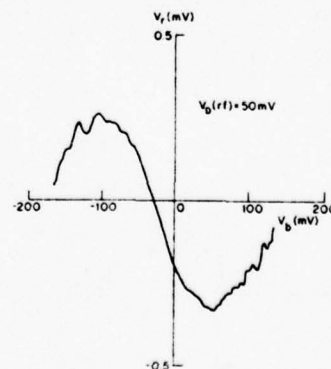


Figure 2. The experimental dependence of V_r on V_b is presented. Diode resistance was measured as 2 K Ω and values of $m = .16 \text{ V}^{-1}$ and $n = 1.81 \text{ V}^{-2}$ were calculated from this plot.

THE MOM TUNNELING DIODE: THEORETICAL ESTIMATE
OF ITS PERFORMANCE AT MICROWAVE AND INFRARED FREQUENCIES*

A. Sanchez, C. F. Davis, Jr., K. C. Liu
and A. Javan

Department of Physics
Massachusetts Institute of Technology
Cambridge, Massachusetts 02139

(To be published J. of Appl Phys. Aug. 1978)

ABSTRACT

A theoretical analysis of the metal-oxide-metal (MOM) antenna/diode as detector of microwave and infrared radiation is presented with experimental verification conducted in the far infrared. It is shown that the detectivity at room temperature can be as high as $10^{10} \text{ watts}^{-1} \text{ Hz}^{1/2}$ at frequencies of 10^{14} Hz in the infrared. As a result, design guidelines are obtained for the lithographic fabrication of thin film MOM structures that are to operate in the 10 micron region of the infrared spectrum.

* This work has been supported by the Air Force ARPA and, in part, by NASA and Army Research Office.

I. INTRODUCTION

The metal-oxide-metal diode has been used extensively over the past decade for frequency measurements in the infrared.⁽¹⁻⁴⁾ In fact, frequencies up to the 2.0 micron region have been measured.⁽⁵⁾ Electron tunneling across an oxide layer separating the sharply tipped tungsten wire from the metal (typically nickel) post, has been recognized as the dominant (nonlinear) conduction mechanism in the dc regime. Previously it has been shown that the conduction mechanism at low frequencies is also responsible for rectification in the 10 micron region.⁽⁶⁾ Radiation is coupled from an electromagnetic wave to the nonlinear junction by means of an antenna that in the case of the point contact diode is the tungsten wire.^(7,8) Several theoretical analyses of the metal-oxide-metal point contact detector have dealt either with the nonlinearities of the junction^(9,10,11) or with the antenna characteristics.⁽¹²⁾ These theoretical results are consequently not easy to compare with the measured values of detector characteristics such as responsivity and noise equivalent power. For instance, in the analysis followed by Green⁽⁹⁾ and Kwok⁽¹⁰⁾ the junction's nonlinearities are thoroughly discussed but the problem of matching the junction to the antenna is ignored. Other analyses based only on the antenna model⁽¹²⁾ predict a frequency dependence of the diode responsivity that is not in good agreement with experimental observations.⁽¹³⁾

In the present paper a model is chosen for the antenna (Section II) where the load contains a capacitive component due to the small contact area. Electron tunneling theory is briefly reviewed in Section III to obtain expressions for the responsivity in the case of a trapezoidal tunneling barrier. The results from these two sections are combined in Sections IV and V to yield actual numerical results for optimum expected power conversion efficiency ($\sim 10^{-2}$) and detector NEP at room temperature ($\sim 10^{-10}$ W.Hz $^{-1/2}$). Further, it is seen that the quantum efficiency factor can be as high as 10^{-2} in the 10μ region.

Section VI contains the results of computer calculations that support the validity of the simplified analytical results of the previous two sections.

II. ANTENNA MODEL

The antenna, as a receiver, is represented by an ac voltage source $v \cos \omega t$ with an internal real impedance R_A .

The non-linear resistance, R_D , in parallel with the junction capacitance represents the diode whose series resistance is assumed negligible compared to both R_A and R_D . The effective voltage (see Fig. 1) developed across the diode is

$$v_D = v \frac{Z_D}{R_A + Z_D} = v \frac{R_D}{R_A + R_D + j\omega R_A R_D C}$$

where Z_D is the parallel combination of R_D with X_C . The junction capacitance, $C = \epsilon_0 \epsilon \frac{a}{L}$ is due to the finite contact area, a , and dielectric thickness, L .

Introducing the "reduced frequency," $q = \omega C R_A$, the "reduced diode resistance," $x = R_D / R_A$ and the "incident power" $P = \frac{V^2}{8R_A}$, then

$$V_D = V \frac{x}{1 + (1 + jq)x}$$

The power dissipated in R_D (effectively the receiver load) is

$$P_r = \frac{|V_D|^2}{2R_D} = 4P \frac{x}{1 + 2x + (1 + q^2)x^2} \quad [1]$$

It is of interest to find the value of the diode resistance that maximizes P_r , the power coupled to the load. The condition $\frac{\partial P_r}{\partial x} = 0$ leads to $x_m^2 = \frac{1}{1 + q^2}$, and then

$$P_r(x_m) = 2P \frac{1}{1 + \sqrt{1 + q^2}}$$

At high frequency ($q \gg 1$), there is a roll off where $P_r(x_m) \sim q^{-1}$.

In the low frequency regime ($q \ll 1$), the maximum value of P_r occurs for $R_D = R_A$, ($x = 1$) and is

$$P_r(\max) = P$$

We then say that the antenna is matched to the load. This optimum received power, P , is related to the Poynting Vector, \bar{S} , of the incident field.

$$P = \sigma(\theta, \phi) |\bar{S}|$$

This relationship defines the effective aperture of the antenna⁽¹⁴⁾. Calculation of the aperture and antenna impedance for different antenna geometries is a subject that belongs to antenna theory. For certain simple geometries (e.g. dipole), the maximum effective aperture is about $0.1\lambda^2$. (See Section VII a). In what follows, and for reasons that will become evident later, we will want to study the effect on the diode as the radiation frequency is changed. In order to still couple the same power P , we will require that: a) the linear dimensions of the antenna be scaled with the wavelength (that means same R_A , same σ/λ^2); b) the power incident in $\lambda^2 (= \lambda^2 |\bar{S}|)$ also be kept constant. In the case of two lasers of equal power and different frequencies this implies that their beams are focused with the same f number.

III. DIODE MODEL

Electrical conduction between the two metallic electrodes forming the MOM diode is due to electron tunneling through a potential barrier formed by a metal oxide layer on the order of 10°\AA or less. This mechanism produces the non-linearities in the I-V characteristic. In order to

calculate the I-V characteristic, we choose a model consisting of a trapezoidal potential barrier with thickness L and heights ϕ_1 and ϕ_2 on each side. The WKB approximation is used⁽¹⁵⁾ to calculate the tunneling probability for an electron that has a certain energy associated with its motion normal to the barrier.

The total current density for an applied voltage V is obtained by integrating the contributions of electrons with all possible energies. This can be done with the help of a computer. However, some analytical approximations⁽¹⁵⁾ allow us to obtain a closed form expression for the I-V characteristic. A series expansion up to V^3 leads to

$$I = \frac{1}{R_D} (V + mV^2 + nV^3)$$

Introducing the average barrier height $\phi_0 = \frac{\phi_1 + \phi_2}{2}$, the asymmetry factor $\alpha = \frac{\phi_1 - \phi_2}{\phi_1 + \phi_2}$ and the dimensionless parameter $S = 1.025 L \sqrt{\phi_0}$, where L is given in angstroms and ϕ_0 in electron volts, the theory (see Appendix A) gives the following results

$$R_D = \frac{Se^S}{324\phi_0} \frac{1}{a(\mu m^2)} \quad (a = \text{junction area}) \quad [2]$$

$$m = \frac{\alpha S}{24\phi_0} \quad \text{and} \quad [3]$$

$$n = \frac{1}{6} \left(\frac{S}{4\phi_0} \right)^2 \quad [4]$$

If a voltage of amplitude $v_D \cos \omega t$ is applied to the diode simultaneously with a bias voltage V_b , there will be a rectified current whose value is

$$i_r = \frac{1}{2} \left. \frac{\partial^2 I}{\partial V^2} \right|_{V_b} \overline{v_D^2 \cos^2 \omega t} = (m + 3nV_b) \frac{v_D^2}{2R_D} \\ = (m + 3nV_b) P_r$$

The current responsivity is defined as $\beta_i = \frac{i_r}{P_r}$. In what follows we will consider only the case of the unbiased diode so that $\beta_i = m$.

IV. RECTIFICATION AND POWER CONVERSION

a) Rectification

The rectified voltage appearing on the diode (with given parameters α, L, ϕ_0, a) is

$$V_r = R_D \beta_i P_r$$

where P_r is the power delivered by the antenna to the diode (load)

Therefore

$$V_r = \beta_i 4P R_A \frac{x^2}{1 + 2x + (1 + q^2) x^2} \quad [5]$$

It should be noted that both β_i and q are relatively insensitive functions of the barrier thickness, L , while x has an exponential dependence. With that in mind we can see from Eq. (5) that v_r is a monotonically increasing function of x . The limiting value is

$$v_r(x=\infty) = v_0 \frac{1}{1+q^2} \quad \text{where } v_0 = 4\beta_i R_A P \quad [6]$$

Fig. 2 displays the rectified voltage given by Eq. (5) as a function of the reduced resistance x and for various values of the reduced frequency q .

From Eq. (6) we can get some numerical results for a practical case. Consider a barrier with $L = 10 \text{ \AA}$, $\phi_0 = 1 \text{ eV}$, $\alpha = 0.2$ so that $S \approx 10$ and $\beta_i = m = 1/12 \text{ amp/watt}$. If $R_A = 100 \Omega$ and $q \ll 1$ (frequency below the roll off) we obtain for an incident power $P = 1 \text{ mW}$ that the maximum rectified voltage is about $v_0 = 30 \text{ mV}$.

b) Power Conversion

An incident power P generates a rectified voltage v_r , according to Eq. (5). The rectified power P_{DC} associated with v_r is given by

$$P_{DC} = \frac{v_r^2}{R_D} = (4\beta_i P)^2 R_A F(x, q) \quad [7]$$

$$\text{where } F(x, q) = \frac{x^3}{[1 + 2x + (1 + q^2)x^2]^2} \quad [8]$$

The maximum value of P_{DC} occurs at

$$x_o = \frac{1 + \sqrt{4 + 3q^2}}{1 + q^2} \quad [9]$$

so that the optimum conversion efficiency η_e is:

$$\eta_e = \frac{P_{DC}(x_o)}{P} = (4\beta_i)^2 P R_A F(x_o, q) \quad [10]$$

$$\text{where } F(x_o, q) = \frac{[1 + \sqrt{4 + 3q^2}]^3}{(1 + q^2) [q^2 + (2 + \sqrt{4 + 3q^2})^2]^2} \quad [11]$$

In Fig. 3 the dependence on the reduced frequency, q , of the optimum reduced diode resistance, x_o , and of the function $F(x_o, q)$ are displayed. For the typical value of $\beta_i = 1/12$ amp/watt used in the previous section η_e/P is also displayed as a function of q in Fig. 3. It should be noted that for frequencies below roll off $\eta_e/P \approx 1 \text{ watt}^{-1}$.

The maximum power P that can be used in Eq. (10) is determined by the burn out level of the diode. Voltages across the diode on the order of 0.3 volts can already burn the junction (the electric field in the oxide would be on the order of 3×10^6 volts/cm). This would result from a maximum incident power, P , of about 10 mwatts and, therefore, for $q \leq 1$ we would obtain a conversion efficiency of 1%.

It should be remembered, however, that when the diode is driven with such high power levels, the rectified current depends quite strongly on higher order derivatives of the I-V characteristic. The simple model used to calculate the nonlinear I-V characteristic cannot predict the correct behavior of the fourth order derivative. Available experimental data on MOM diodes, however, show that the fourth derivative contribution is already important at $V = 0.1$ volt.

At frequencies lying in the roll off ($q \gg 1$) the conversion efficiency goes as q^{-3} (see Fig. 3). It is, therefore, evident that in order to have good conversion efficiency in the infrared we should reduce the junction area to minimize C and have $q = \omega RC \leq 1$ at the frequency of interest. In what follows we will estimate the junction area a , and barrier thickness, L , to achieve that condition at a given frequency.

At the corner frequency ($q = 1$) and for optimum conversion we have from Eq. (9) that $x_o = \frac{R_D}{R_A} = 1.82$. This together with Eq. (2) gives a condition relating the area, a , and the barrier parameter S ,

$$1.82 R_A = \frac{1}{324} \frac{S}{\phi_o} \frac{e^S}{a} \quad [12]$$

A second relation involving S and a is obtained from the

requirement $q = 1$, so that $2\pi f_C R_A C = 1$ where the junction capacitance, C , is given in farads by

$$C = \epsilon_0 \epsilon \frac{a}{L} = .835 \times 10^{-13} \epsilon \frac{a}{L} \quad [13]$$

with a in $(\mu m)^2$ and L in \AA . This second relation can therefore be expressed as

$$a = .177 \times \frac{L}{R_A} \frac{10^{13}}{\epsilon f_C} \quad [14]$$

From Eqs. (12) and (14) we have that

$$e^S = 103 \sqrt{\phi_0} \frac{10^{13}}{\epsilon f_C} \quad [15]$$

$$L = \frac{1}{1.025\sqrt{\phi_0}} \ln \left(103 \sqrt{\phi_0} \frac{10^{13}}{\epsilon f_C} \right) \quad [16]$$

The results given by Eqs. (14) and (16) are displayed in Fig. 4 for the typical case of $\phi_0 = 1$ and $R_A = 100$.

It should be noticed that the values for L in Fig. 4 do not depend on the antenna resistance (see Eq. (16)) while those for contact area, a , are inversely proportional to R_A (Eq. (14)).

Also, since the value of L changes by not more than a factor of 5, so does the current responsivity $\beta_i = \frac{\alpha S}{24\phi_0}$.

The above guidelines are important to consider in the design of high speed MOM junction structures in which, using photolithographic techniques, an antenna is printed^(16,17) and integrated with the small area junction.

As the corner frequency of the diode goes up to $f_c = 10^{14}$ Hz we see that the required L and a decrease. The decrease in a , although a difficult technical problem with the present photolithographic techniques could be achieved with some further sophistication (e.g. electron beam lithography). It should be mentioned that areas on the order of $.0004 \mu m^2$ can be obtained in a mechanical point contact diode. The reduction in L down to 2.27 \AA , on the other hand, brings into question the validity of the WKB approximation used in calculating the electron tunneling. The condition for its validity is that this probability ($\sim e^{-S}$) is small compared to unity. Substituting this condition into Eq. (15) requires:

$$f_c \ll 103 \sqrt{\phi_0} 10^{13} \approx 10^{15} .$$

We will not attempt at this point to make any quantitative estimates on the modifications to the model due to the breakdown of the WKB approximation in the optical and near infrared region. In addition, in this frequency region, photon energy is comparable to the barrier height ($\sim \phi_0$) and other interesting effects may set in and dominate the rectification process. ²⁴

V. DETECTOR PERFORMANCE

Let us consider thermal noise to be the dominant one.

Then

$$V_n = \sqrt{4KT R_D \Delta\nu} = \sqrt{4KT R_A \Delta\nu} \sqrt{x}$$

Using the rectified voltage given by Eq. (7) we obtain the signal to noise ratio where $F(x)$ is given by Eq. (8) .

$$\frac{V_r}{V_n} = \frac{4\beta_i P \sqrt{R_A}}{\sqrt{4KT \Delta\nu}} F^{1/2}(x) \quad [17]$$

The noise equivalent power (NEP) is the value of the power P that gives a unity signal to noise ratio for a bandwidth of $\Delta\nu = 1\text{Hz}$. The inverse of the NEP is known as the detectivity, D , and therefore, is given by

$$D(x) = \frac{4\beta_i \sqrt{R_A}}{\sqrt{4KT}} F^{1/2}(x) \quad [18]$$

With the same considerations that we used previously we can obtain, by optimizing $F(x)$, the barrier thickness that for a given junction area yields the optimum detectivity.

Replacing $F(x_0)$ as given by Eq. (11), we obtain:

$$D = D(x_0) = \frac{4\beta_i \sqrt{R_A}}{\sqrt{4KT}} F^{1/2}(x_0) \quad [19]$$

Using $\beta_i = 1/12$, $R_A = 100$ ohms and $T = 300^\circ\text{K}$ we obtain

$$D = 2.6 \times 10^{10} f^{1/2} (X_0)$$

The dependence of D on the frequency is given in Fig. 3.

It is of interest to compare the detector responsivity of the MOM diode with those of existing infrared quantum-type detectors. The detection mechanism in the MOM diode arises from rectification of ac currents induced across the junction at infrared frequencies. The mechanism in the second type of detectors arises from generation of free carriers due to absorption of infrared photons. For this type of detectors the current responsivity, β_i , and the quantum efficiency, η_q , are related by

$$\eta_q = \frac{h\nu}{e} \beta_i$$

For comparison purposes let us estimate the quantum efficiency, η_q , of an MOM diode operating, below roll off, in the 10 microns region. The energy $h\nu$ of a photon at this wavelength is about .1 ev and taking the typical responsivity $\beta_i \approx .1$ amp/watt, we get that $\eta_q \approx 10^{-2}$. In the average, there is a transfer of one electron across the barrier for an energy coupled to the diode corresponding to 100 infrared photons. As the frequency increases, so does the quantum efficiency, but remains

below unity everywhere in the infrared. It is this fact that provides the theoretical justification for using the low frequency I-V characteristic in order to estimate the rectification at infrared frequencies. (18)

VI. COMPUTER CALCULATIONS

In order to get the results of the previous sections, approximations were necessary. In Eq. (5), (7), and (18), the values for v_r , P_{DC} and $D(x)$ were optimized by varying the barrier thickness. In one instance the maximum of the rectified power P_{DC} is obtained by maximizing $F(x)$ in Eq. (9). In this approximation the fact that β_i has a linear dependence on S was ignored because $x \sim R_D \sim e^S$ has an exponential dependence. More exact computer calculations have been carried out to check the validity of these approximations. The results will be compared with those of Fig. 3.

Figure 5 shows the calculated detectivities at different frequencies as the barrier thickness is changed. For this calculation it was assumed $R_A = 100$ ohm, and $a = 1\mu m^2$. Eq. (18) was used where $F(x)$ is taken from Eq. (8) and for β_i we take the value of m given by Eq. (3). The important result in Figure 5 is that for each frequency there is a value of the barrier thickness that optimizes the NEP. For a given contact area we have that to each frequency corresponds an optimum NEP leading to the results of Figure 6. These results are very much in agreement with those in Fig. 3, obtained analytically, where $D(x_0)$ is plotted as a function of the frequency q .

In comparing Figure 3 with Figure 6, we would like to comment on two points. In the low frequency region ($q \ll 1$)

Figure 6 predicts detectivities ranging from 10^{10} to $1.2 \times 10^{10} \text{ Watts}^{-1} \times \text{Hz}^{1/2}$, depending on contact area, while Figure 3 predicts $.85 \times 10^{10}$ independently of the contact area. This is so because the small dependence of β_i on barrier parameters was not taken care of in calculations leading to Figure 3. The second remark is about the roll off region ($q \gg 1$). Figure 3 predicts a dependence $D \sim \omega^{-1.5}$ while more exact calculations predict $D \sim \omega^{-1.78}$. Considering the type of approximations involved the agreement is satisfactory.

VII. EXPERIMENTS AND TEST OF THE THEORY

a) Experiments in support of antenna theory

We have measured the efficiency in coupling the radiation from a focused HCN laser beam ($\lambda = 377 \mu\text{m}$, $P_L = 5 \text{ mw}$) into the antenna/diode and studied the dependence of this efficiency on the diode resistance and focusing angle of the laser beam. A balancing technique is used for measuring the FIR coupled power (Fig. 7). The focused beam and an adjustable amount of rf (at 400 KHz) are coupled alternately to the diode at a rate of 80 Hz so that a null signal is obtained when the rectified signal due to the FIR laser rectification equals that due to the rf.

The, otherwise unknown, AC voltage at FIR frequency induced on the junction equals that of the balancing rf voltage, easily measurable on an oscilloscope. The received laser power, $P_r = v_{AC}^2 / 2R_D$ on the junction can then be measured when a laser beam with total power P_L is focused on the antenna/diode and the dependence of the coupling efficiency, $\eta = P_r/P_L$, on the diode resistance can be studied and compared to the theory (Eq. 1). In the experiment, the antenna is formed by a thin tungsten wire several wavelengths long so that the radiation impedance is predominantly resistive. Also the radius of the point contact ($\approx 1000 \text{ \AA}$) is sufficiently small that capacitive loading is negligible ($q \ll 1$). The resistance of the diode is varied by adjusting the pressure on the point contact and the coupling efficiency is measured for each value of the resistance. A typical set of experimental results is presented in Fig. 8 and found to agree with the theoretical prediction: $\eta = 4 n_0 R_A \frac{R_D}{(R_D + R_A)^2}$

In this way, a value of $R_A = 162 \pm 10$ ohm was obtained for the antenna whose radiation pattern was also measured (Fig. 9) by using a previously described technique.⁷

The dependence $\eta_0(\theta_f)$ on the focusing angle was then investigated. If the focusing angle is much smaller than the width of the first lobe ($\theta_f \ll \theta_d$), the laser radiation appears essentially as a plane wave and the coupling can be described by an effective antenna aperture $\sigma = \frac{\lambda^2}{4\pi} G$ where the gain, G , for $L \gg \lambda$ is given by $G = \frac{120}{R_A} \frac{L}{\lambda}$

(See Appendix B). In this regime, ($\theta_f \ll \theta_d$), the efficiency is given by the ratio $\eta_0 \approx \sigma / \pi w_0^2$ (where $2w_0 = \lambda / \theta_f$ is the focused spot diameter). Then $\eta_0 = \sigma / (\pi w_0^2) = \frac{120}{\pi^2 R_A} \frac{L}{\lambda} \theta_f^2$

has a θ_f^2 dependence in agreement with the experimental results in Fig. 10.

The experimental results of Fig. 10 show that for small focusing angles ($\theta_f = D/f$ where $f = 12.7$ cm. in this case) the efficiency η_0 is in fact proportional to θ_f^2 , consistent with the concept of effective aperture. That proportionality constant agrees within a factor of two with the one expected from the theory when in the above expression for η_0 we replace L and R_A by their experimentally measured values. Considering the simplifications involved and uncertainty in our calorimetric laser power measurements, the above agreement is satisfactory. As the focusing angle is increased to a value comparable to the width of the first radiation lobe, the coupling efficiency saturates to about 3%, in agreement again with the theory. (Appendix B) The experiment was repeated for a different antenna length and a proportionally different coupling efficiency (or antenna gain) was observed for small focusing angles. At larger focusing angles, however, the same saturated value of the coupling efficiency is reached.

To confirm that the FIR detection is due to the same mechanism as that of rf detection (i.e. rectification), we checked that the balancing condition remains when a bias, up to about 100 mV, is applied to the diode. (i.e. FIR and rf detection have the same bias dependence.)

A major recent advance has been photolithographic fabrication of a high-speed metal-oxide-metal junction.¹⁶ With a two-stage thin film vacuum evaporation method, a high-speed junction is deposited on a substrate, along with a small antenna integrated to it. We have applied the balancing technique to the study of such a diode junction (integrated to an antenna). Preliminary results show that in some structures the coupling efficiency is as high as 2 or 3%, comparable to that of the mechanical point contact diode.

We should recall that the technique is applicable regardless of the nature of the rectification mechanism as long as it is the same at rf and ir frequencies. For example, we have also fabricated antenna structures where the load is an evaporated micron-sized, thin-film wire without a junction. A weak bolometric response was observed at both frequencies and the best coupling efficiency was found to be around 1%.

b) Experiments in support of tunneling as the rectification mechanism

We have studied the behavior of the point contact diode nonlinearities by observing the bias dependence of the rectified signal when a known amount of rf power is coupled to the diode. These results can be compared with the predications of the tunneling model (Section III) yielding values for the barrier parameters that are found to be reasonable.

The diode's I-V characteristic up to third order can be expressed as:

$$I = \frac{1}{R} (V + mV^2 + nV^3)$$

Due to these nonlinearities, the rectified voltage, V_r , when an rf voltage $V_D \cos \omega t$ is coupled to the diode is given by

$$V_r = (m + 3n V_b) \frac{V_D^2}{2}$$

The experimental dependence of V_r on V_b shown in Fig. 11, can be approximated by a straight line in the low bias region. We can then obtain for the 2 K-ohm diode, $m = .16 \text{ V}^{-1}$ and $n = 1.81 \text{ V}^{-2}$.

Note that these values for m and n , which are independent of the contact area, are in general agreement with those obtained from the tunneling model assuming reasonable values for the barrier parameters.

We can invert equations (2) and (4) to obtain:

$$\phi_0 = \frac{1}{4\sqrt{6n}} \ln \frac{324 R_D a}{4\sqrt{6n}}$$

$$S = 4\phi_0 \sqrt{6n}$$

$$L = \frac{4 \sqrt{6n} \phi_0}{1.025}$$

By estimating the value of contact area as $a = .1 \text{ } \mu\text{m}^2$, we can then obtain $\phi_0 = .65 \text{ eV}$ and $L = 10.3 \text{ } \text{\AA}$ which are quite reasonable and change only logarithmically with the estimated area. Furthermore, the value of α according to the theory is given by

$$\alpha = m \sqrt{6/n}$$

which, in the case of Fig. 11, is equal to 0.29 and does not depend on the estimated area.

As the resistance of the diode is lowered by adjusting the pressure of contact, the value for n decreases monotonically. For example; if $R_D = 50 \text{ ohms}$ we get $n = 1.39$ so that $\phi_0 = 0.43 \text{ eV}$ and $L = 7.3 \text{ } \text{\AA}$. At

these low values of L and ϕ_0 , the W.K.B. approximation used in calculating the tunneling probability begins to lose its applicability.

On the other hand, the value of the barrier asymmetry factor can vary over a very wide range for diodes with the same resistance. Some of the other characteristics reported in the literature^{6,11,13,20} correspond only to nearly symmetric diodes.

We have shown that in agreement with the theory, the zero bias responsivity, β_i ($=m$), remains nearly constant as the resistance is varied over two orders of magnitude. This statement was previously made in section IV (a) without experimental support. We have, however, verified Eq. 5 at FIR frequencies (where $q < 1$) by studying the laser rectification as the resistance of the diode "relaxes" continuously and slowly (presumably keeping the same asymmetry factor α) from 10 to few thousand ohms. We were able to fit the result to the expression:

$$V_r = V_0 \left(\frac{R_D}{R_D + R_A} \right)^2$$

with two adjustable parameters, V_0 and R_A .

This method of determining R_A is, however, more tedious and difficult than the previously described balancing technique, where the changes in R_D need not be continuous.

The authors would like to acknowledge several valuable discussions on this subject with G. Elchinger.

APPENDIX A

The problem of calculating the I-V characteristic of a metal-insulator-metal structure^(15,21,22) has been treated by different authors. We will summarize the treatment given in reference 15. However, we should point out that when the I-V characteristic is expanded up to the V^3 term, the same results are obtained from reference 21..

The current is due to quantum mechanical tunneling of electrons through the potential barrier presented by the thin insulating layer. When a voltage V is applied across the junction the barrier shape is $\phi(x,V) = \phi(x) - \frac{x}{L} eV$. An electron approaching the barrier with an energy E_x in the direction perpendicular to the barrier has a transmission probability given by the WKB approximation

$$P(E_x, V) = e^{-\alpha_e \int_0^L \sqrt{\phi(x,V) - E_x} dx}$$

$$\text{where } \alpha_e = \frac{2\sqrt{2m}}{\hbar} = 1.025 \text{ eV}^{-1/2} \text{\AA}^{-1}$$

carrying out a Taylor expansion:

$$\ln P(E_x, V) = -[b_1 + c_1 \epsilon_x + f_1 \epsilon_x^2 + \dots] \text{ where } \epsilon_x = \xi_1 - E_x, \text{ and } \xi_1 \text{ is the Fermi energy in metal 1 and the } V \text{ dependence appears in the coefficients } b_1, c_1, f_1 \dots.$$

The total tunneling current density is obtained by integration over the contribution of electrons with different energies E_x .

$$J(V) = \frac{4\pi me kT}{h^3} \int_{-\infty}^{+\infty} P(E_x, V) F(E_x, V) dE_x$$

$$\text{and } F = \ln \frac{1 + \exp(-E_x/kT)}{1 + \exp(-(E_x + eV)/kT)}$$

AD-A058 441

MASSACHUSETTS INST OF TECH CAMBRIDGE DEPT OF PHYSICS
MEASUREMENT OF FREQUENCY OF LIGHT AND ITS APPLICATION.(U)
AUG 78 A JAVAN, M S FELD

F/G 17/5

UNCLASSIFIED

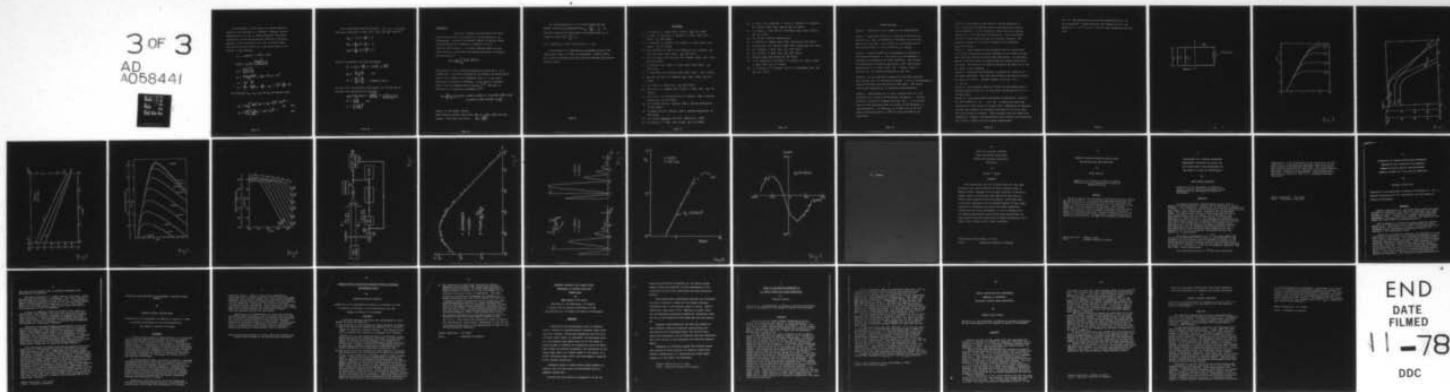
ARO-13227.12-P

DAAG29-75-C-0026

NL

3 OF 3

AD
A058441



END
DATE
FILMED

11-78

DDC

It is possible, at this point, to obtain numerical solutions with the help of a computer. However, further approximations will let us obtain analytical solutions. A discussion of the approximations involved in different methods is best discussed in ref. 22. A series expansion of the current density up to the third power of the voltage is then obtained.

$$J = G(T) (V + mV^2 + nV^3)$$

$$G(T) = j_0 c_{10} \frac{\pi c_{10} k T}{\sin(\pi c_{10} k T)}$$

$$j_0 = \frac{A e^{-b_{10}}}{(c_{10} k T)^2}$$

$$A = \frac{4\pi m_e e (kT)^2}{h^3} = 120 T^2 \text{ amp} \cdot \text{cm}^{-2}$$

$$m = b_{11} - \frac{c_{10}}{2}$$

$$n = \frac{b_{11}^2}{2} - \frac{c_{10} b_{11}}{2} + \frac{c_{10}^2}{6} - b_{12} = \frac{m^2}{2} + \frac{c_{10}^2}{24} - b_{12}$$

The parameters b_{10} , b_{11} , b_{12} and c_{10} are obtained from

$$b_1 = \alpha e \int_0^L \sqrt{\phi(x)} dx = b_{10} - b_{11}V + b_{12}V^2 \dots \quad \text{and} \quad [\text{A1}]$$

$$c_1 = \frac{\alpha e}{2} \int_0^L \frac{dx}{\sqrt{\phi(x)}} = c_{10} + c_{11}V \dots \quad [\text{A2}]$$

For a trapezoidal barrier we have $\phi(x) = \phi_1 - (\phi_1 - \phi_2) \frac{x}{L}$ that when substituted in Eqs. (A3), (A1), and (A2) leads to:

$$b_{10} = S \left(1 - \frac{\alpha^2}{24} + \dots \right)$$

$$b_{11} = \frac{S}{4\phi_0} \left(1 + \frac{\alpha}{6} + \dots \right)$$

$$c_{10} = \frac{S}{2\phi_0} \left(1 + \frac{\alpha^2}{8} + \dots \right)$$

where the parameter S has been introduced

$$S = \alpha_e L \sqrt{\phi_0} = 1.025 L \sqrt{\phi_0}$$

$$\phi_0 = \frac{\phi_1 + \phi_2}{2} \quad \text{and}$$

$$\alpha = \frac{\phi_1 - \phi_2}{\phi_1 + \phi_2} = \text{asymmetry factor}$$

For zero bias and neglecting high powers in α we get the resistance and responsivity of the diode

$$a (\mu m^2) \cdot R_D (\text{ohms}) = \frac{S e^S}{324 \phi_0} = \frac{1}{G (\text{ohm}^{-1} \cdot \mu m^{-2})}$$

$$m = \frac{\alpha S}{24 \phi_0} \quad \text{and}$$

$$n = \frac{1}{6} \left(\frac{S}{4 \phi_0} \right)^2$$

APPENDIX B

We shall estimate the efficiency with which power focused from an infrared laser can be coupled to the antenna/diode. Using the reciprocity theorem of antenna theory and considering the antenna as a radiator, we will calculate the fraction, γ , of power radiated under the same solid angle, Ω_0 , with which the infrared radiation is focused. The efficiency is

$$\gamma = \frac{1}{4\pi} \int_{\Omega_0} G(\theta, \phi) d\Omega$$

where $G(\theta, \phi)$ is the orientation-dependent antenna gain. It is assumed that the load is matched to the antenna. By definition of gain if Ω_0 is taken as 4π steradians, then $\gamma = 1$ (all power delivered to antenna is radiated). In the case of a whisker diode, long wire antenna theory applies.^(7,8) The gain in the case of a standing wave antenna is⁽²⁵⁾

$$G = \frac{30}{R_A \sin^2 \theta} \left\{ \cos^2 kL + \cos^2 \theta \sin^2 kL + 1 - 2 \cos kL \cos(kL \cos \theta) - 2 \cos \theta \sin kL \sin(kL \cos \theta) \right\}$$

where L is the whisker length.

This radiation pattern has a main lobe at a small angle from the antenna. The first null is at:

$$\theta_1 = \sqrt{\frac{2\lambda}{L}}$$

For long antennas ($L \gg \lambda$) it can be shown that the maximum gain can be approximated by $G_m \approx \frac{120}{R_A} \frac{L}{\lambda}$ so that the coupling efficiency when the focusing angle θ_f is comparable with θ_e is $\gamma \approx \frac{30}{R_A} \frac{1}{\pi}$

For a typical $R_A = 150 \Omega$ we would get $\gamma = .06$

In principle it is possible to use phased arrays in the same context that it is done in microwaves. A horn antenna or an end-fire phased array would provide coupling efficiencies close to unity.

REFERENCES

1. L.O. Hocker, A. Javan, Phys. Letters 26A, 255 (1968).
2. V. Daneu, D. Sokoloff, A. Sanchez, A. Javan, Appl. Phys. Letts. 15, 398 (1969).
3. D. Sokoloff, A. Sanchez, R.M. Osgood, A. Javan, Appl. Phys. Letts. 17, 257 (1970).
4. K.M. Evenson, J.S. Wells, F.R. Peterson, B.L. Davidson, and G.W. Day, Appl. Phys. Letts. 22, 192 (1973).
5. D.A. Jennings, F.R. Peterson, K.M. Evenson, Appl. Phys. Letts. 26, 510 (1975).
6. A. Sanchez, S.K. Singh, A. Javan, Appl. Phys. Letts. 21, 240 (1972).
7. L. Matarrese, K.M. Evenson, Appl. Phys. Letts. 17, 8 (1970).
8. Bor-long Twu and S. E. Schwarz, Appl. Phys. Letts. 26, 672 (1975).
9. S.J. Green, J. Appl. Phys. 42, 1166 (1971).
10. S.P. Kwok, G.J. Haddad and G. Lobov, J. Appl. Phys. 42, 544 (1971).
11. S.M. Faris, T.K. Gustafson and J.C. Wiesner, IEEE J. Quantum Electronics 7, 737 (1973).
12. C.C. Bradley and G.J. Edwards, IEEE J. Quantum Electronics 7, 548 (1973).
13. E. Sakuma and K.M. Evenson, IEEE J. Quantum Electronics 8, 599 (1974).
14. J.D. Kraus, Antennas, New York: McGraw Hill (1966).
15. R. Stratton, J. Phys. Chem. Solids 23, 1177 (1962).

16. J. Small, G.M. Elchinger, A. Javan, A. Sanchez, F.J. Bachner, D.L. Smythe, Appl. Phys. Letters 24, 275 (1974).
17. S.Y. Wang, T. Izawa and T.K. Gustafson, Appl. Phys. Letters 27, 481 (1975).
18. J.R. Tucker, private communication.
19. W. Gandrud, R. Abrams, Appl. Phys. Letters 17, 150 (1970).
20. Bor-long Twu, S.E. Schwarz, Appl. Phys. Letters 25, 595 (1974).
21. J.G. Simmons, J. Appl. Phys. 34, 1793 (1963).
22. T.E. Hartman, J. Appl. Phys. 35, 3283 (1964).
23. Shyh Wang, Appl. Phys. Letters 28, 303 (1976).
24. G. M. Elchinger, A. Sanchez, C. F. Davis, Jr., and A. Javan, J. Appl. Phys. 47, 591 (1976).
25. P. S. Carter, C. W. Hansell, and N. E. Lindenblad, Proc. IRE 19, 1773 (1931).

FIGURE CAPTIONS

Figure 1. Equivalent circuit model of the antenna/diode.

Figure 2. Rectified voltage as a function of the diode resistance, $R_D = xR_A$, at frequencies from below ($q < 1$) to well above ($q > 1$) roll off. The voltage, v_o , is proportional to the incident power, P , and is given by $v_o = 4\beta_i R_A P$.

Figure 3. Several quantities are plotted as a function of the reduced frequency, q . The value x_o is the reduced resistance that optimizes the power conversion. This conversion efficiency is given by η_e/P in Eq. (10). The optimum detectivity, D , is given by Eq. (19). Finally, $F(x_o)$ is given by Eq. (11) appears frequently in the text.

Figure 4. As the operating frequency of the diode increases the junction area, a , and oxide thickness, L , have to be decreased in order to optimize the detectivity of the diode. The resulting current responsivity, β_i , decreases logarithmically.

Figure 5. The detectivity, D , for a junction area of $1 \mu m^2$, is plotted as a function of dielectric thickness, L . The calculation is done on a computer using Eq. (18). It is noticed that for each frequency there is a value of the thickness, L , that optimizes D . In addition, it is seen that as the frequency increases beyond 3×10^{11} Hz, roll off effects are noticeable.

Figure 6. The maxima of the family of curves displayed in Fig. 5 shows how the optimum value of the detectivity depends on the frequency. In this manner we obtain the curve labeled above as $a = 1 \mu\text{m}^2$ (the area for which Fig. 5 was calculated). Curves for other junction areas are similarly obtained. The optimum thickness at the corner frequencies are displayed above the curves.

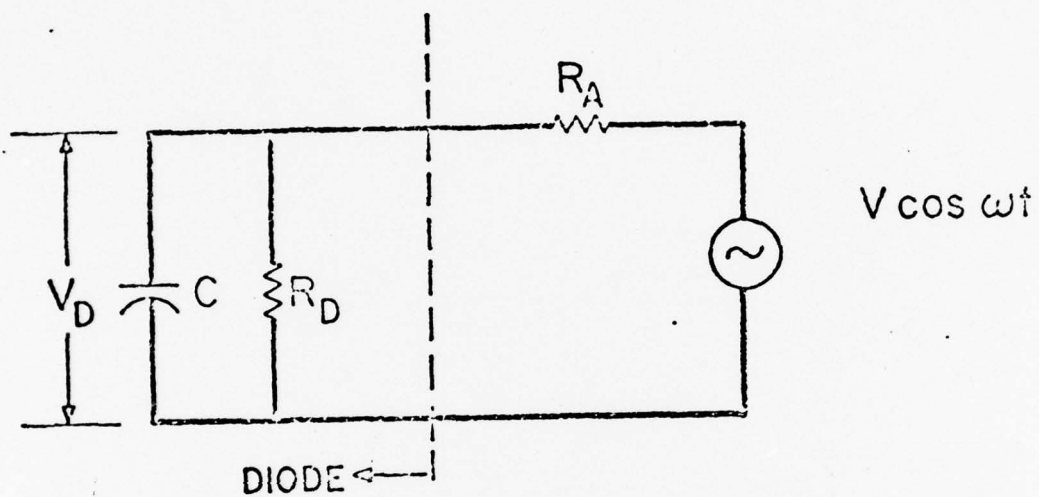
Figure 7. Block diagram of the equipment used for establishing an rf level that gives equivalent response to an incident focused laser beam for various measured diode resistances. An adjustable amount of 400 kHz signal is coupled when the chopper blade blocks the laser. The lock-in is nulled by adjusting the amplitude of the rf, which is then measured.

Figure 8. Antenna/diode efficiency is plotted as a function of the diode resistance. The curve was fitted to the data by varying R_A ; best fit is 162Ω . Whisker length is $1.95 \text{ mm} = 5.8 \lambda$, $\lambda = 337 \mu\text{m}$.

Figure 9. The radiation pattern is given for the antenna used in the measurement of Fig. 8. In this case, the pattern for $311 \mu\text{m}$ is also given.

Figure 10. The antenna/diode efficiency is plotted as a function of iris diameter, D , for $\lambda = 12.7 \text{ cm}$. It should be noted that saturation at high values of D comes from a combination of approaching the beam diameter and exceeding the width of the first lobe. The proportionality constant, .0035 coincides with the theoretical prediction. However, the experimental value contains an uncertainty of a factor of about two due to power measurements.

Fig. 11. The experimentally determined dependence of V_r on V_b is presented. Diode resistance was measured as $2\text{ K}\Omega$ and values of $m = .16\text{ V}^{-1}$ and $n = 1.81\text{ V}^{-2}$ were calculated from this plot.



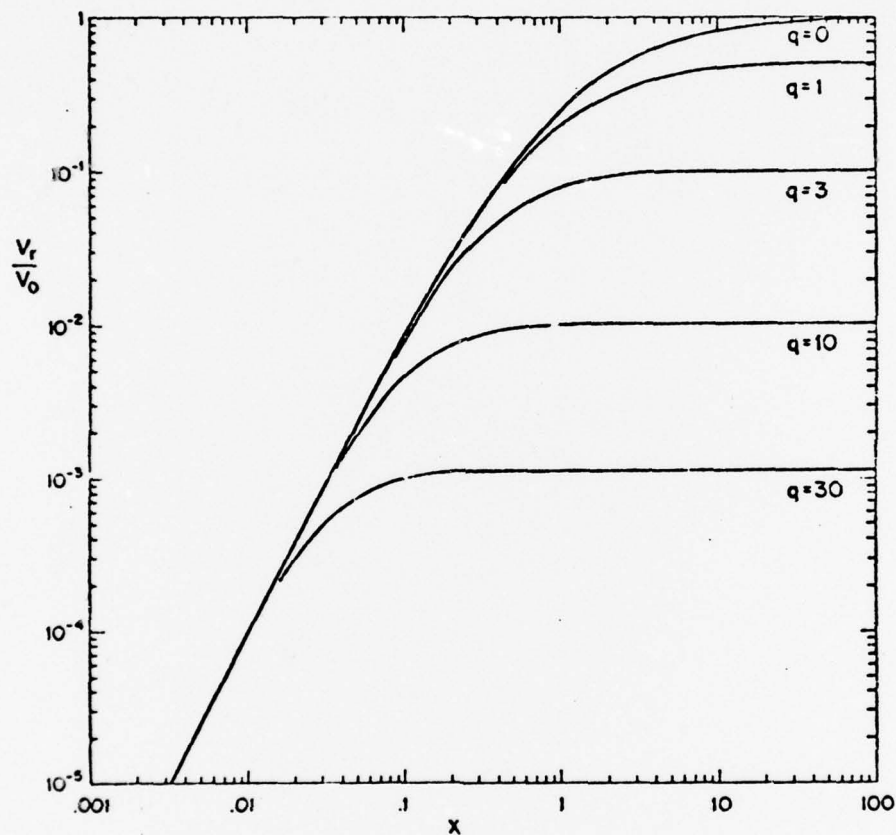


Fig 2

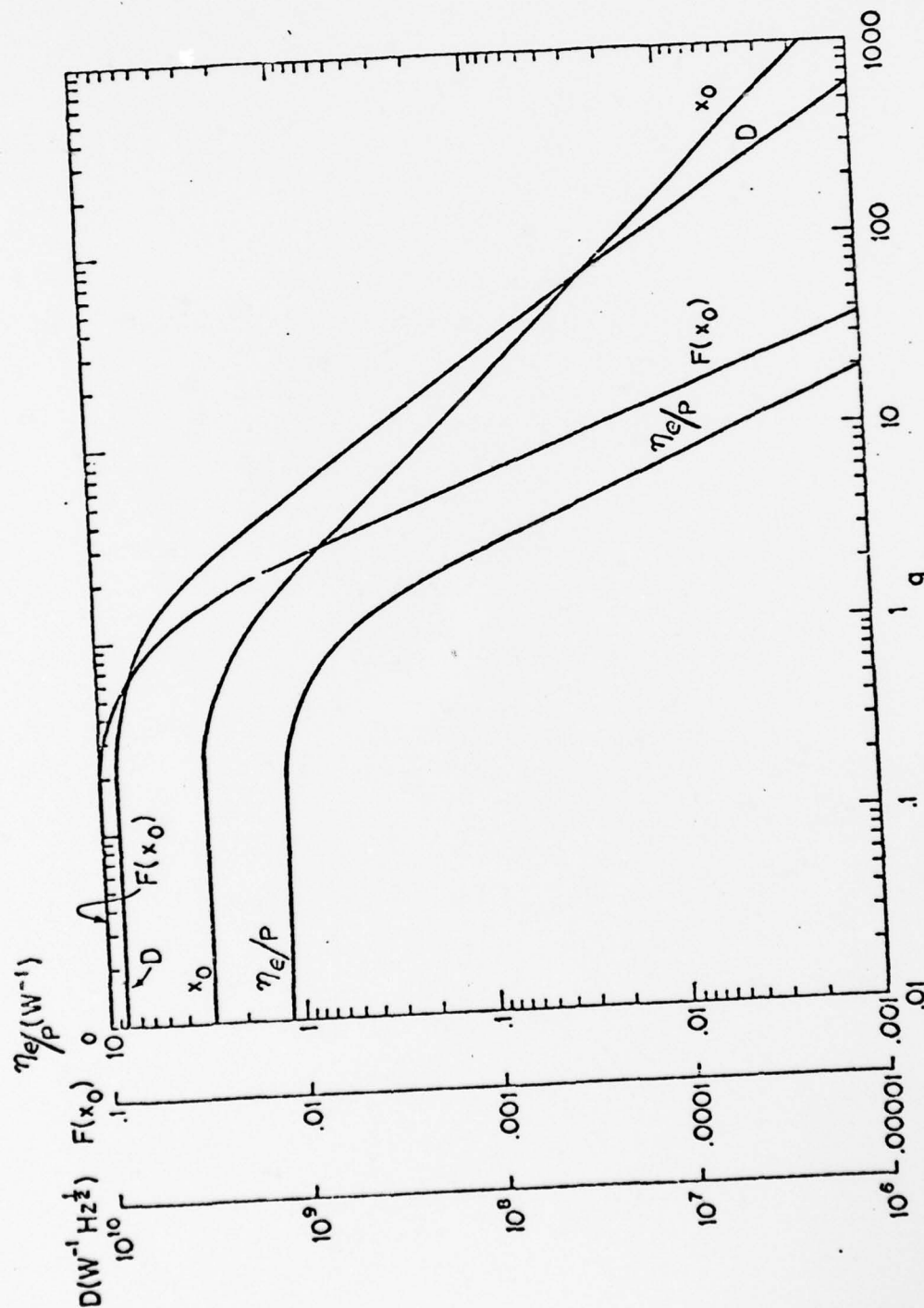


Fig 3

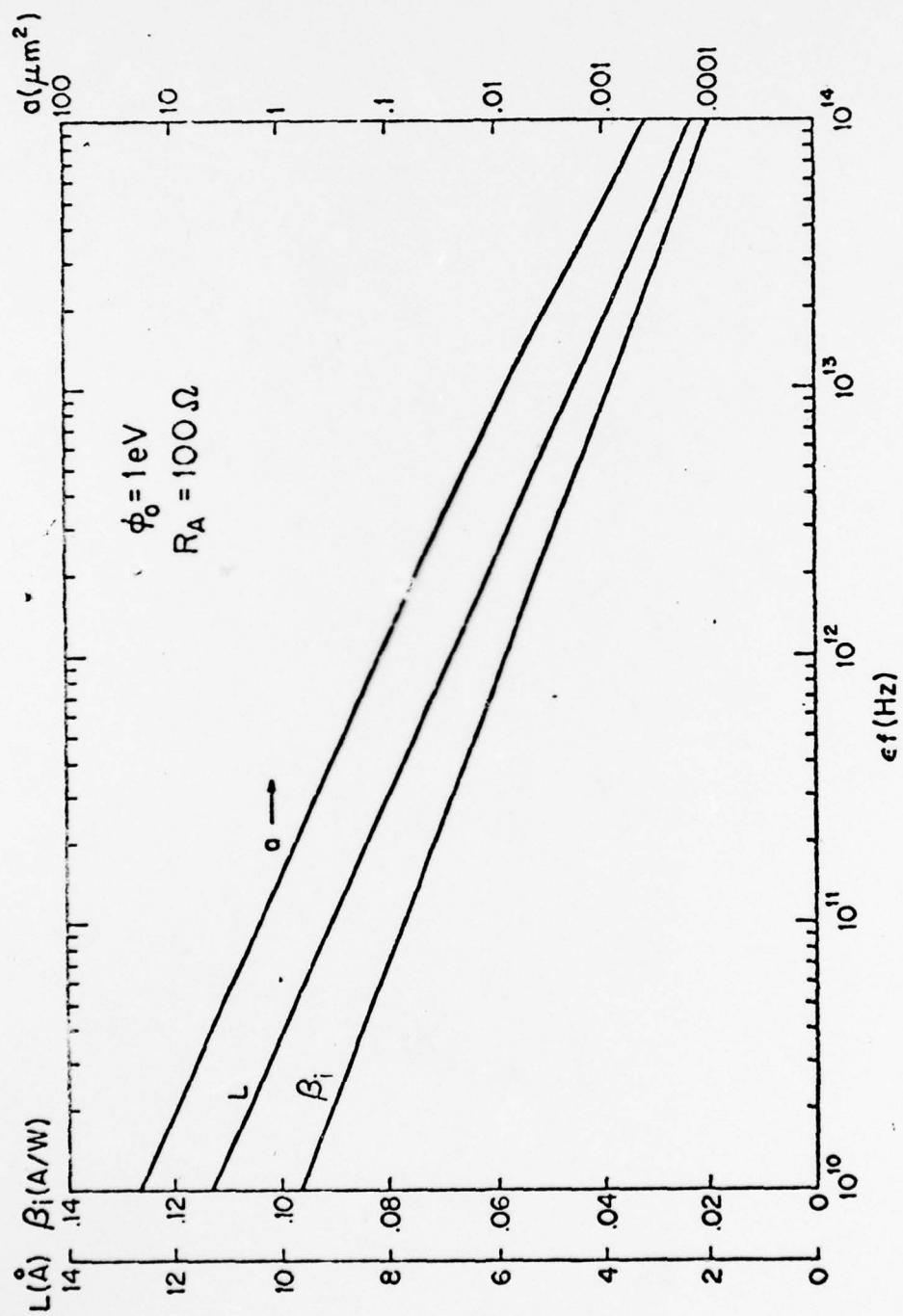


Fig 4

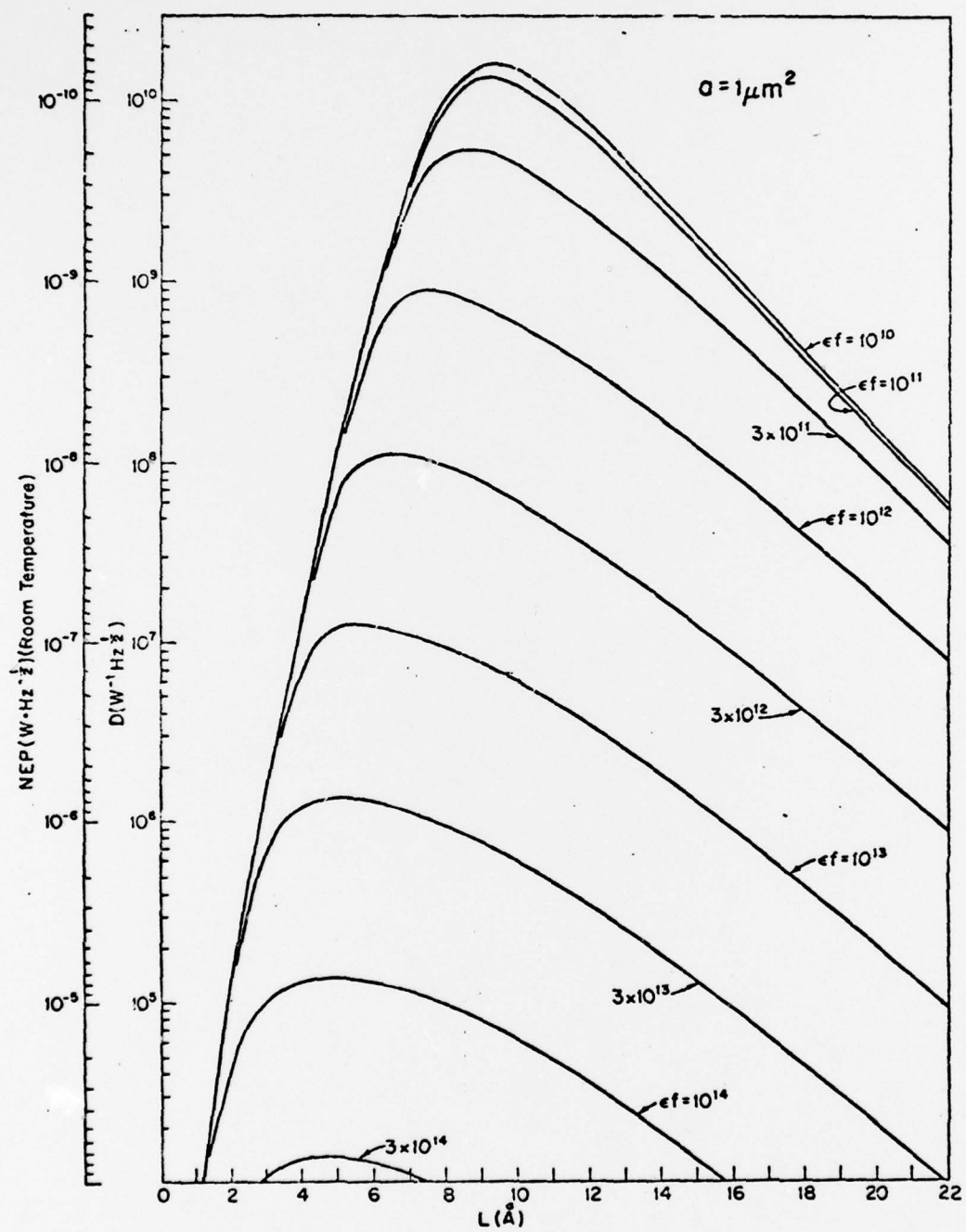


Fig 5

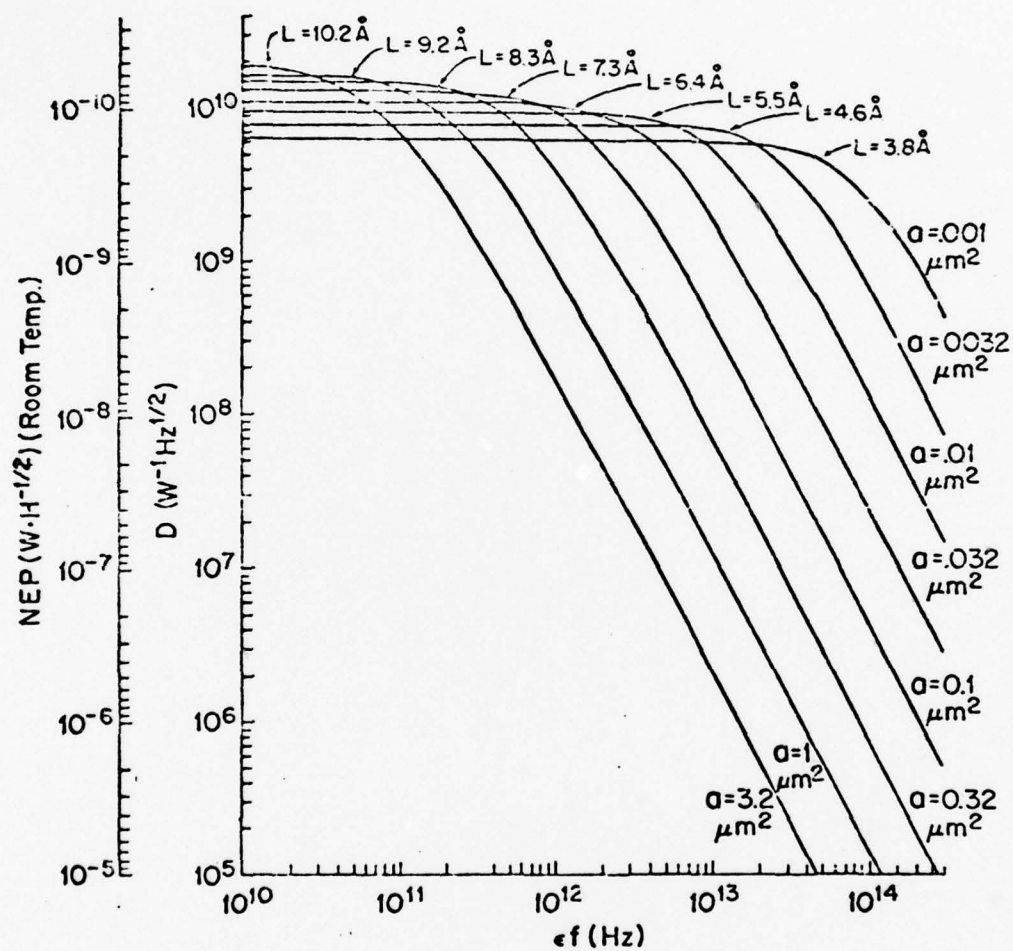


Fig 6

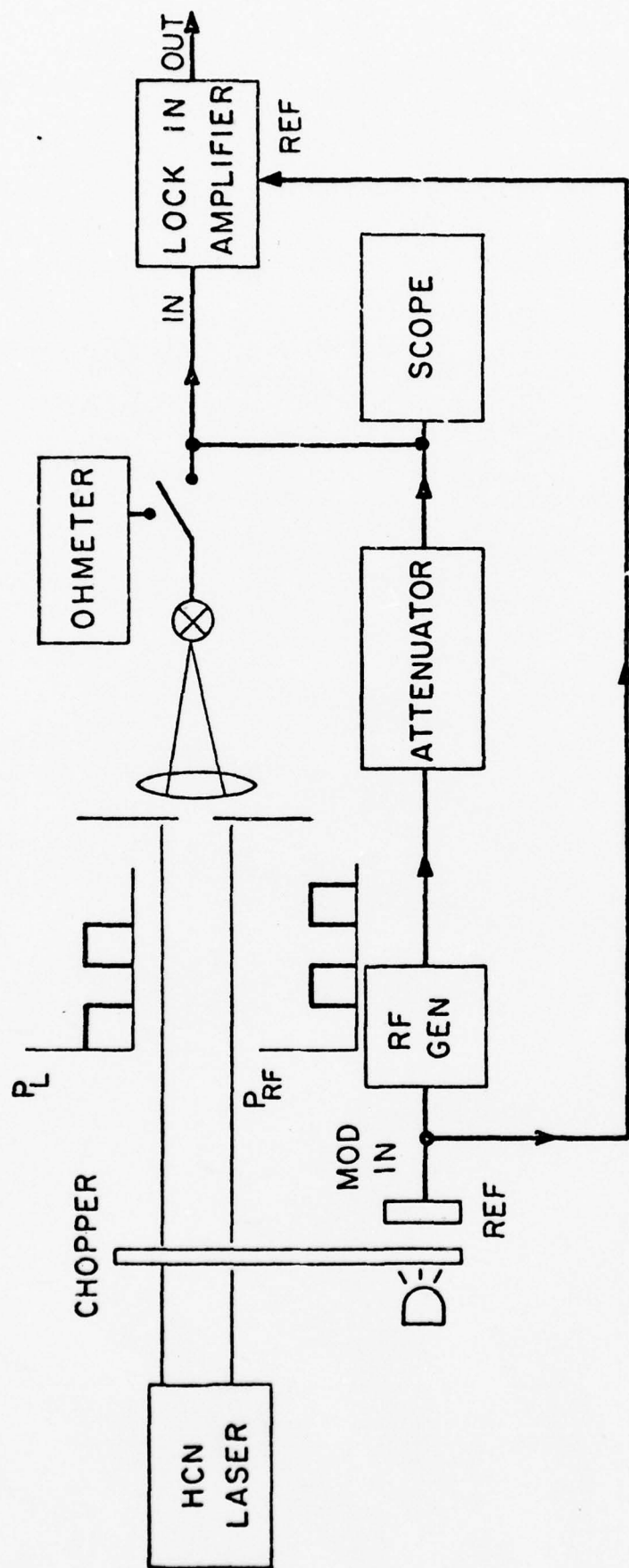


Fig 7

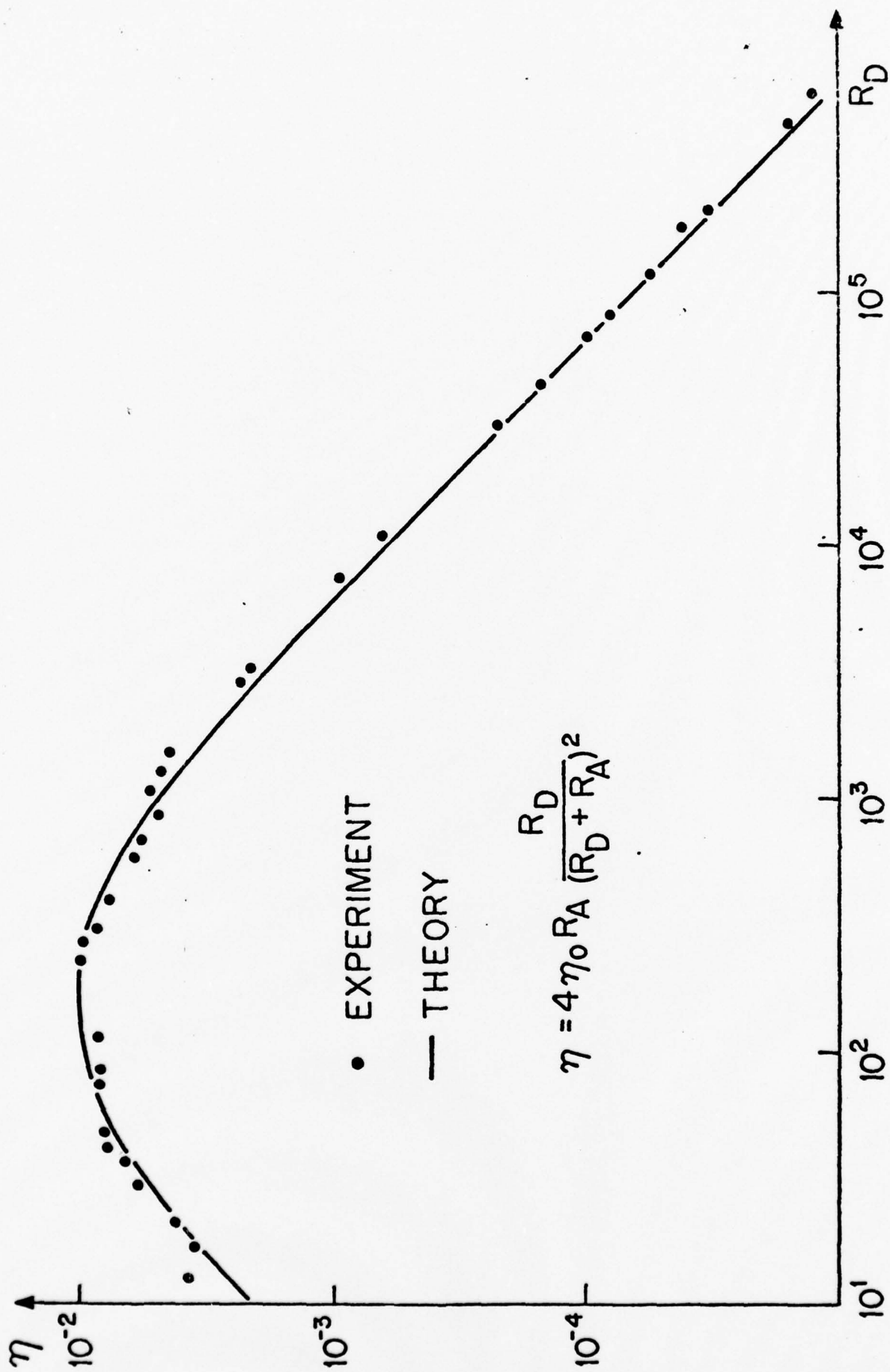
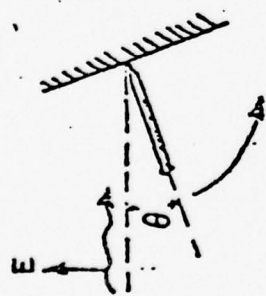


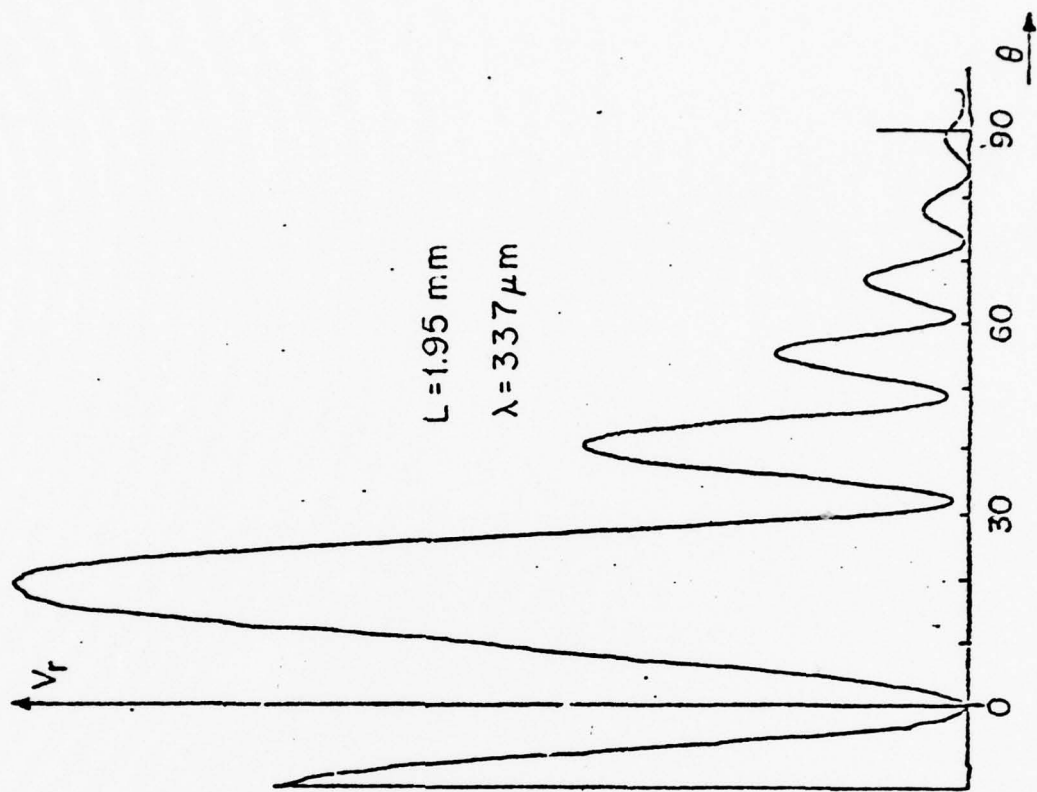
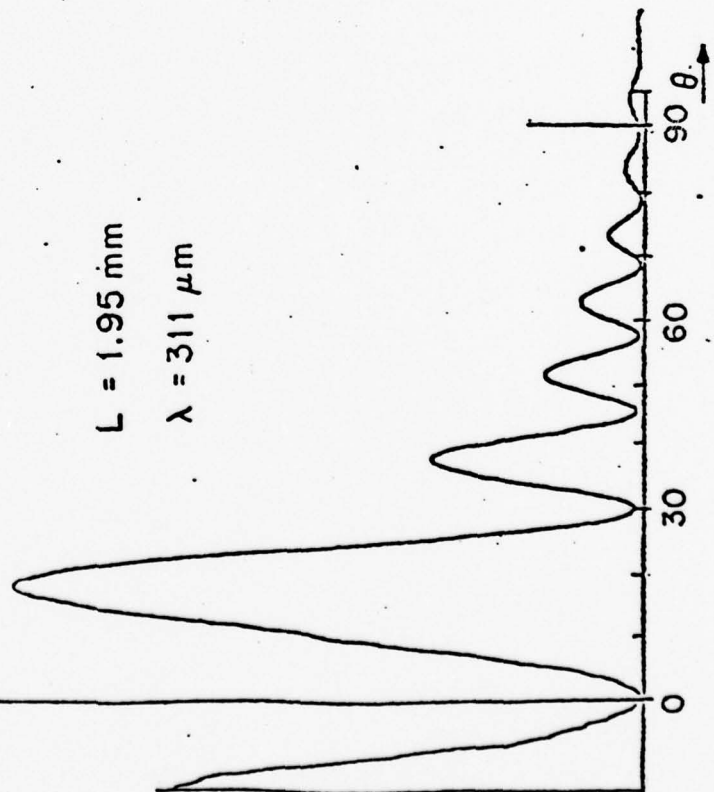
Fig 8



V_r

$L = 1.95 \text{ mm}$

$\lambda = 311 \mu\text{m}$



$L = 1.95 \text{ mm}$

$\lambda = 337 \mu\text{m}$

Fig 9

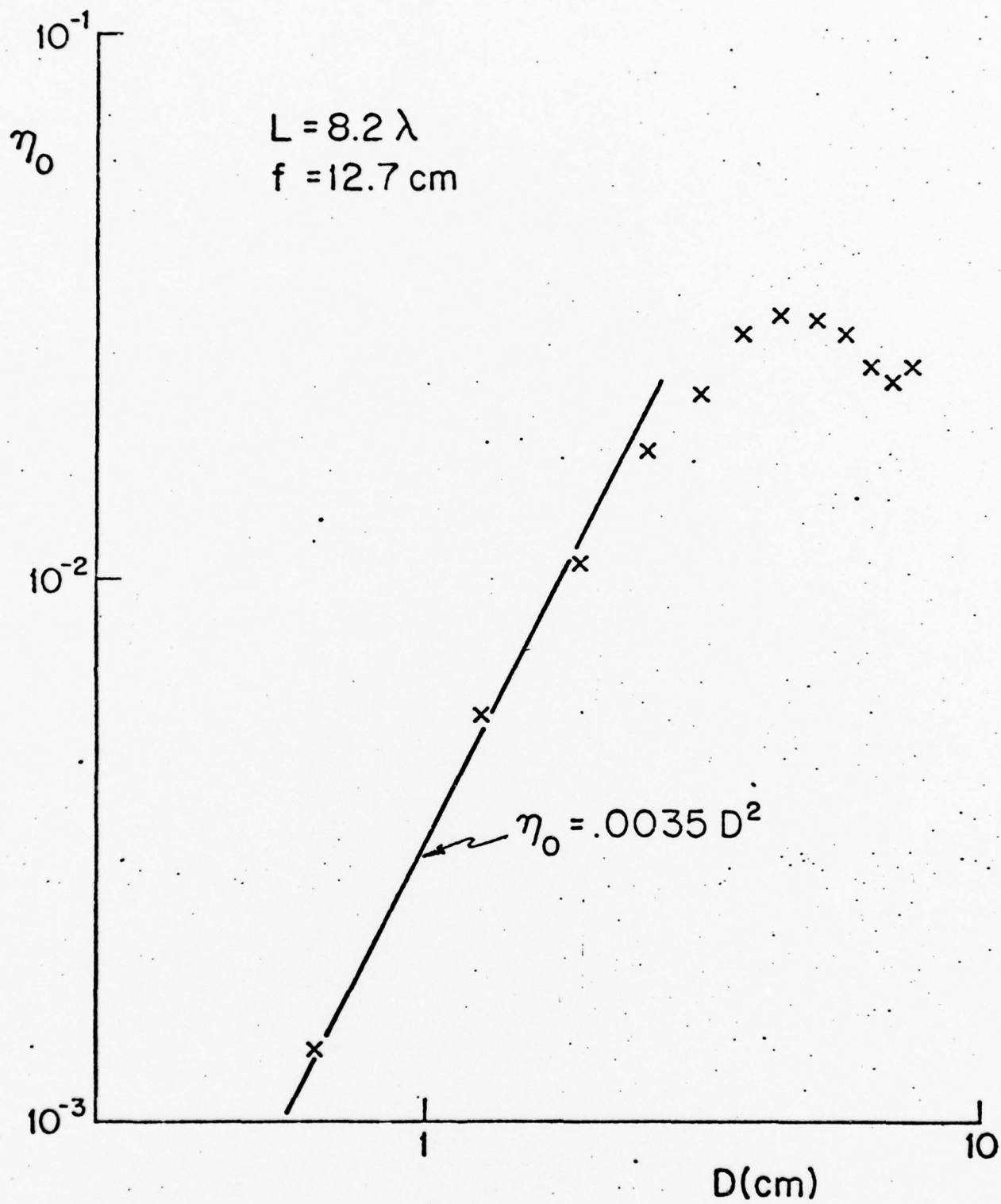


Fig 10

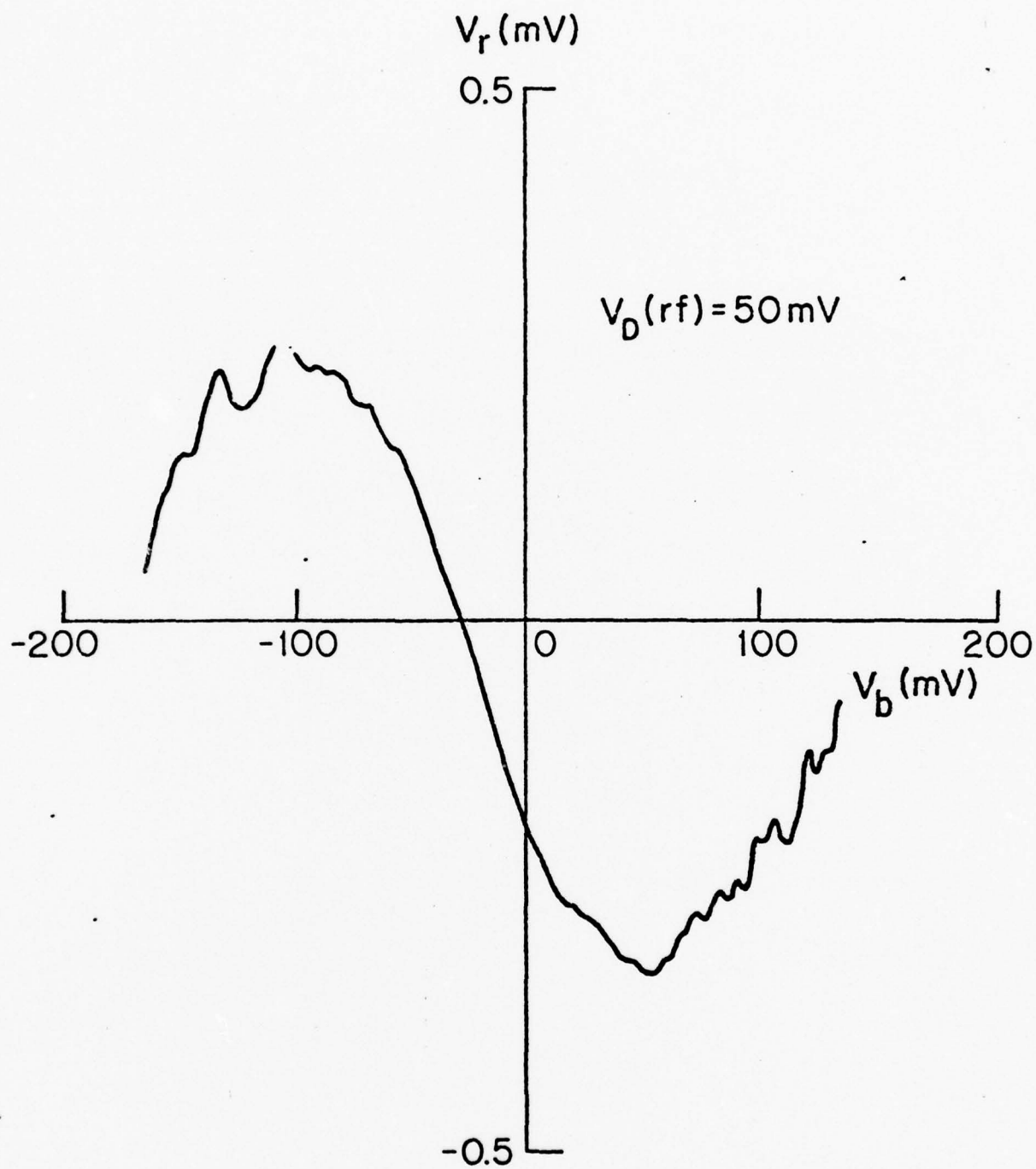


Fig 11

VI. Theses

-ii-

Study of CH_3OH Far Infrared
Pump Transitions Using Stark
Effect and Saturated Absorption
Techniques

by

Joseph J. Mickey

ABSTRACT

It is well known that the 9 micron band of a CO_2 laser overlaps the Q and R branches of the C-O stretch band of Methyl Alcohol. Because of the current interest in optically pumped lasers, we have made high resolution Lamb dip and Stark effect studies of the coincidences. From these data, we can make assignments of the quantum numbers of some CH_3OH transitions. Hennigson and others have made theoretical predictions for these assignments. It is our purpose here to compare experimental results with these predictions. We have results from data taken for the CH_3OH coincidences with P(36), P(34), P(32), P(30), P(24), and R(10).

Thesis Supervisor: Michael S. Feld

Title: Associate Professor of Physics

SATURATED ABSORPTION STUDIES OF METHYL ALCOHOL
FAR INFRARED LASER PUMP TRANSITIONS

by

DANIEL SELIGSON

Submitted to the Department of Physics in partial
fulfillment of the requirements for the Degree of
Bachelor of Science

ABSTRACT

The $9\ \mu\text{m}$ band of a CO_2 laser overlaps the Q branch of the C-O stretch band of methyl alcohol. We have made high resolution Lamb dip and Stark Lamb dip studies of the coincidence with the CO_2 laser lines 9P(34) and 9P(36). We found that the CH_3OH resonances lie $25 \pm 5\ \text{MHz}$ and $38 \pm 5\ \text{MHz}$, respectively, above the centers of the CO_2 lines. Also, we made measurements of linear absorption, pressure broadening, and Stark tuning rates. From these data, we made tentative assignments of the quantum numbers of the methanol transitions. Because of current activity in the field of optically pumped Far Infrared lasers, researchers are trying to assign this transition also. We compare our assignment with some others.

Thesis Supervisor: Michael S. Feld
Title: Associate Professor of Physics

DEVELOPMENT OF A PRECISE WAVELENGTH
MEASUREMENT TECHNIQUE FOR LASERS AND
ITS APPLICATION TO THE MEASUREMENT OF
THE SPEED OF LIGHT AND SPECTROSCOPY.

by

JEAN-PIERRE MONCHALIN

Submitted to the Department of Physics on
August 9, 1976 in partial fulfillment of the
requirements for the degree of Doctor of
Philosophy.

ABSTRACT

A scanning Michelson interferometer has been used to compare the wavelengths of 2 lasers, one of them being a length standard. The fundamental limitation to the accuracy originates from diffraction; the correction due to diffraction is calculated for the TEM₀₀ mode, higher order modes, astigmatic and uncollimated beams. The experimental set-up is fully described including the interferometer, the CO₂ lasers, the He-Ne lasers, the stabilization technique and all the optics. The alignment technique is given in detail. The instrumental corrections and the instrumental errors are discussed; these include the correction due to the diffraction by the corner reflector of the interferometer and the errors introduced by feedback effects. The technique used for recording and processing the data is also described. Using the He-Ne laser stabilized on the i component of ¹²⁷I₂ as a standard, the system has been the object of 2 applications.

The ratio of wavelength of a ¹²C¹⁶O₂ laser stabilized on R14 of the 0001-[1000,0200]_{II} band to the wavelength of the standard has been measured with an accuracy of 6 parts in 10⁹. Using the value of the frequency given by the National Bureau of Standards of Boulder, a value for the speed of light has been calculated $c = 299792457.6 (2.2) \text{ m/s}$ in excellent agreement with the other recent measurements.

The wavelengths given by a ¹²C¹⁶O₂ laser stabilized

successively on 26 transitions of the P branch of the $01^1_1 - [11^1_0, 03^1_0]_1$ band have been measured. These data and two other frequency measurements have been used to calculate the molecular constants for this band ; the values obtained have been compared to their previous best estimates and represent a significant improvement . Using the values of the constants tables of the P, Q , R branches have been calculated.

Thesis Supervisor : Ali Javan
Title : Professor of Physics.

LINESHAPES OF NARROW DOPPLER-FREE SATURATION
RESONANCES AND OBSERVATION OF ANOMALOUS
ZEEMAN SPLITTING ARISING FROM ROTATIONAL
MAGNETIC MOMENT IN $^1\Sigma$ CO₂ AND N₂O MOLECULES

by

Michael James Kelly

Submitted to the Department of Physics on February 20, 1976 in
partial fulfillment of the requirements for the degree of
Doctor of Philosophy.

ABSTRACT

Several experiments are described which extend the possibilities of performing high resolution nonlinear laser spectroscopy by utilizing Doppler-free standing wave saturation resonances (SWSR). Theoretical lineshape calculations are performed on two and three level systems. The resulting lineshapes are then fitted to experimental data.

The lineshape of a three level system with two closely spaced levels interacting with a weakly saturating plane standing wave laser field is derived. It is shown that this lineshape can be considerably simplified before it is compared to the experimental data.

Using the rate equation approach, the lineshape of a two level system interacting with a strongly saturating standing wave field is calculated. This calculation includes a derivation of the 30% theoretical maximum depth of the saturation resonance observed in fluorescence. This lineshape is averaged over a Gaussian intensity distribution and yields a closed form solution. This solution permits the derivation of an expression for the half-width at half-maximum (HWHM) which is not limited to third- or fourth-order perturbation theory. Hence, this expression contains the effects of saturation broadening. The intensity averaged lineshape has

3.

the interesting property that it predicts anomalous line narrowing at low pressure.

The design features of a highly stable 4-rod laser, useful for precision spectroscopy, is presented. The laser structure can be operated as either a CO₂ or N₂O laser. It oscillates on several hundred transitions in the 9², 10-, and 11-micron bands. Also, the development of a large area (2 cm x 2 cm) liquid helium cooled Cu:Ge detector with a cold filter which has a S/N comparable to InSb is presented.

A study of feedback effects on CO₂/N₂O laser stability demonstrated that feedback can effect the laser cavity power by as much as $\pm 10\%$ without producing any measurable frequency pulling effects. Several techniques of feedback isolation were investigated. The technique of misaligning the standing wave mirror was shown to produce a 35 kHz per mrad broadening of the HWHM of a saturation resonance.

Collision- and power-broadening measurements of CO₂ and N₂O fluorescence saturation resonances in the 0 to 70 mTorr region are presented. The slope of the collision-broadening data in this region varies from 6 to 16 kHz/mTorr. The data indicates that the transit time is not responsible for the anomalous line narrowing observed at low pressures. A fivefold reduction in the linewidth of these resonances is achieved. The experimental results demonstrate that there are no barriers which would prevent the use of these narrow Doppler-free fluorescence resonances in future clock applications.

The observation of Zeeman splitting of excited vibrational states of CO₂ (10⁰⁰, 02⁰⁰, 00⁰¹) and N₂O (10⁰⁰, 00⁰¹) using the SWSR technique is reported. Observation of the small Zeeman splitting (~ 60 kHz/kg) in these $^1\Sigma$ molecules is made possible by the narrow linewidth obtained by this technique. The existence of hundreds of lasing transitions in CO₂ and N₂O enables investigation of molecular g-factors across the whole vibrational band. The anomalous Zeeman effect resulting from the small difference in the g-factors of the two levels ($\sim 1-2\%$), due primarily to molecular vibration, produces a large difference in the observed lineshapes for P- and R-branch transitions. Experiments with linearly and circularly polarized light determine g and Δg to be: CO₂, 10-micron band, $g = -0.053 \pm 0.003$, $\Delta g = 0.00100 \pm 0.00006$; CO₂, 9-micron band, $g = -0.052 \pm 0.003$, $\Delta g = 0.00100 \pm 0.00006$; N₂O, 10-micron band, $g = -0.077 \pm 0.008$, $\Delta g = 0.00077 \pm 0.00008$ where the magnitude of the lower level g-factor is greater than the magnitude of the upper level g-factor.

Thesis Supervisor: Ali Javan
Title: Professor of Physics

THEORY OF SUPERRADIANCE IN AN EXTENDED, OPTICALLY THICK
MEDIUM

by

JEFFREY CHARLES MACGILLIVRAY

Submitted to the Department of Physics on August 11, 1978
in partial fulfillment of the requirements for
the degree of Doctor of Science

ABSTRACT

A semiclassical theory of superradiance in an optically thick two-level medium is presented in terms of coupled Maxwell-Schrödinger equations which can be integrated numerically. The evolution of this model is followed from Dicke's original description of superradiance through more recent theories. A description of superradiance experiments is given, and they are compared to this and other theories. While good qualitative agreement has been achieved, some controversy regarding the choice of appropriate values of the initial parameters to correspond to a given set of experimental conditions.

The semiclassical model, described in detail, simulates spontaneous emission in the form of a distributed source of randomly phased polarization the amplitude of which is calculated using the Einstein equation. Methods used for computer solutions of the semiclassical equations are described in detail, and simple analytical formulas for experimentally relevant parameters are derived. Experimental implications of the assumptions made in deriving both the original equations and the simple analytical formulas are discussed in detail.

Expressions are given which limit the length and density of a high gain system which can superradiate, or equivalently, which limit the shortness of its output

radiation pulses. Limits arising from experimental conditions such as finite inversion time, finite decay and dephasing times, finite transit time (cooperation length), feedback, diffraction, and Fresnel number not approximately one are discussed. Both swept and uniform excitation configurations are considered. Modifications to the simple analytical expressions for the output radiation which result from each of these effects are described in detail. Detailed computer results are also given.

Applications of superradiance to x-ray laser design, ultrashort pulse generation, and analogous radiation which may be possible in paramagnetic spin systems are described. The need for further study of non-plane wave behavior, especially transverse effects, is discussed. Finally a new class of experiments is proposed in which a superradiant state is prepared directly, rather than by inverting a system and allowing a superradiant state to evolve.

Thesis Supervisor: Michael S. Feld, Associate Professor of
Physics and Director of the Spectroscopy Laboratory

INVESTIGATION OF TRANSIENT COHERENT OPTICAL PHENOMENA
IN RESONANT MEDIA

by

SIAVOSH MOSHFEGH HAMADANI

Submitted to the Department of Physics on January 15, 1976
in partial fulfillment of the requirements for the
degree of Doctor of Philosophy.

ABSTRACT

Transient coherent phenomena are investigated in this thesis by means of studying

- a) The evolution of the envelope of short duration (2-40nsec) N_2O laser pulses in resonant NH_3 absorber for a variable number of absorption lengths ($\alpha L < 14$). Zero degree pulses ($\int_{-\infty}^{+\infty} \epsilon(z,t) dt = 0$) are observed to propagate with enhanced transmission for both short-duration low intensity pulses and longer pulses of intensity sufficient to allow observation of optical nutation effects. The reshaping of pulses which contain a rapid amplitude or phase variation is observed to result in pulses of subnanosecond duration. A rapid phase reversal gives rise to amplification for times comparable to the transverse relaxation time.
- b) The evolution of the envelope of short-duration (2-40nsec) CO_2 laser pulses in a low pressure (~ 5 Torr) CO_2 amplifier in the linear regime for a variable number of gain lengths ($\alpha L < 7$). Single pulses grow considerably in duration as well as amplitude in agreement with theoretical considerations. Analysis of the observed pulse evolution is used to obtain experimental values for the transverse relaxation parameter T_2 and the number of gain lengths αL in agreement with values obtained by other methods. Zero degree pulses are observed to terminate much of the long tail which occurs in single pulse amplification. Off-resonant amplification of short duration pulses is shown to lead to dramatic changes in the zero-degree pulse evolution. Numerical calculations relating to the use of these techniques in the nonlinear regime for high pressure CO_2 amplifiers are also presented.

- c) The properties of population inversion by optical Adiabatic Rapid Passage (ARP) using laser saturation spectroscopy techniques. In these investigations, a direct attempt to measure T_1 in the time domain for an infrared transition in NH_3 is undertaken. The population change produced by sweeping the frequency of a strong saturating N_2O laser field through the center of a Doppler-broadened absorption line is probed by a weak counterpropagating field as in a Lamb-dip experiment. When the ARP conditions are satisfied, inversion of population is detected as amplification of the probe wave near the line center. As the inverted population relaxes to equilibrium, the amplification decays back to the unsaturated absorption with a time constant given by T_1 . The pressure dependence of this decay below 40 mTorr is measured to be $T_1 P = 24.3 (\mu\text{sec} \cdot \text{mTorr})$ indicating that $T_1 \approx 3.6 T_2$. The results are discussed in terms of molecular dipole-dipole interactions, responsible in NH_3 for the collision-induced decay of the polarization as well as that of the population inversion.

Thesis Supervisor: Ali Javan

Title : Professor of Physics

COHERENT TRANSIENT AND STEADY STATE
PHENOMENA IN COUPLED MOLECULAR
TRANSITIONS

by

JOSE ROBERTO RIOS LEITE

Submitted to the Department of Physics
on April 1977 in partial fulfillment of the
requirements for the Degree of Doctor of Philosophy

ABSTRACT

A theoretical and experimental study of coherent optical effects in coupled Doppler broadened three-level molecular systems, interacting resonantly with two monochromatic laser beams, is presented. The phenomena occur in a low pressure gas sample when one of the beams is strong enough to saturate one transition while the other beam probes the coupled transition. The saturation by the strong beam leads to a change signal in the probe, in a narrow frequency range within the wide Doppler linewidth of the coupled transition.

Transient decay of these narrow change signals is studied, for the case where the saturating field is suddenly turned off.

Parallel and anti-parallel propagation of the two

beams give different lineshapes for the narrow change signals which are analyzed in their dependence on the relaxation rates of the transitions and high saturation effects.

From steady state experiments with NH_3 the lineshapes are used to extract a value for the Zeeman coherence relaxation rate in the excited state of the ν_2 $Q(8,7)$ transition. This rate of 7.2 MHz/Torr is almost twice the corresponding population relaxation. Relaxation rates for NH_3 in the presence of He buffer gas are also measured.

Transient experiments with the same NH_3 transition were observed. Features predicted theoretically are verified for the lineshapes' decay. The excited state population relaxation rate is measured from the transients, the result being in good agreement with previous measurements.

Properties of Optically pumped Far-Infrared Lasers are studied in their relation to coherent three-level effects. Experiments in a continuous wave CH_3OH laser, pumped by a CO_2 laser, are presented.

Thesis Supervisor: M. S. Feld

Title: Associate Professor of Physics

STUDY OF RELAXATION PROCESSES IN
He₂ USING PULSED DYE LASER TECHNIQUES

by

Ricardo Francke

Submitted to the Department of Physics in partial fulfillment of the requirements for the degree of Doctor of Philosophy.

ABSTRACT

The technique of laser-induced fluorescence using a pulsed dye laser has been applied to study processes in ground and excited triplet states of molecular helium. The technique is simple and generally applicable. In the present work it was used to study the formation and quenching of the ground triplet state $\text{He}_2(a^3\Sigma_u^+) = \text{He}_2^m$ and the relaxation processes of the $\text{He}_2(e^3\Pi_g)$.

In the experiment, a pulsed discharge in He is used to produce different excited species, some of which become He_2 , which is then quenched by different mechanisms. In order to study the formation and decay of He_2 , the electrical pulses were made purposely short, so the species of interest are created after the gas discharge. A nitrogen laser pumped dye laser was used to excite the $a^3\Sigma_u^+(v,N) \rightarrow e^3\Pi_g(v,N')$ $\lambda=4650\text{\AA}$ vibronic transitions of He in the afterglow of the gas discharge. The excitation was measured by monitoring the fluorescence emitted from the $e^3\Pi_g$ level of He_2 . The detection system consisted of an optical system to collect light, and a monochromator followed by a cooled photomultiplier. The monochromator used as a filter is necessary to isolate the laser induced fluorescence from the noise of the discharge. The signal to noise ratio was further increased by using a gated integrator with an adjustable gate aperture time. A scanning device was incorporated into the system which varies the delay between the dye laser pulse and the helium discharge. In this way all the time evolution of He_2^m was obtained in one single scan. The high intensity and the short pulse of the dye laser (6 nsec FWHM) acted as a delta function excitation of the upper level. These features of this laser simplified the detection and data analysis of relaxation processes of the upper level being populated.

It was found that under the conditions used here, He_2^m is produced during the first 400 μsec of the afterglow from excited helium atoms. Also the formation rate of He_2^m coincides with the destruction rate of He^+ through transformation to He_2^+ and dielectronic recombination. This model also explains the variation of peak current during the glow with peak population of He_2^m . Furthermore, it also accounts for the time evolution of He_2^m . The rate of formation of He_2^m from He^+ was found to be (2.20 ± 0.40) times the concentration of He^+ . Of course the formation of He_2^m from He^+ could involve many other intermediate steps. In the experimental conditions of this work, other mechanisms that produce He_2^m are found to make very small contributions to the formation of He_2^m .

The main loss mechanism of He_2^m is diffusion to the walls. Another loss mechanism is electron quenching. The $v=1$ state was found to be quenched faster than $v=0$. The first one has a rate of $(9.00 \pm 2.90) \times 10^{-9} \text{ cm}^3/\text{sec}$, while the $v=0$ has a rate of $(2.2 \pm 0.70) \times 10^{-9} \text{ cm}^3/\text{sec}$. The dependence of this quenching rate on the vibrational quantum number was seen here for the first time.

It was also found that the lifetime " τ " of the $e^3\Pi_g$ state is given by $1/\tau = [37.22 \pm 8.5 + (4.30 \pm 1.20)p] 10^6 \text{ sec}^{-1}$ where " p " is the pressure in torr. It was also found that a collision of an excited molecule with a helium atom could change the electronic state of the molecule. This collision transfer allowed me to measure the radiative lifetime of the $e^3\Pi_g$, $d^3\Sigma_u^+$, $f^3\Sigma_u^+$ and $f^3\Pi_u$ states as being 27 ± 6 , 53 ± 5 , 27 ± 6 , and 40 ± 13 nsec, respectively. The collision transfer rate from the $e^3\Pi_g$ to the $d^3\Sigma_u^+$, $f^3\Pi_u$ and $f^3\Delta_u$ was measured as being $(6.70 \pm 1.39) \times 10^6$, $(1.00 \pm 0.23) 10^6$ and $(22.6 \pm 5.2) 10^3 \text{ sec}^{-1} \text{ torr}^{-1}$ respectively. The collision transfer rate from the $e^3\Pi_g$ to the $f^3\Sigma_u^+$ was found to be extremely fast and such that at pressures above 3 torr the two levels were in thermal equilibrium. This rate was determined as being over $30 \times 10^6 \text{ sec}^{-1} \text{ torr}^{-1}$.

Ratios of Franck-Condon factors between the $e^3\Pi_g$ and $a^3\Sigma_u^+$ states were measured as $q_{00}/q_{01} = 21.1$ and $q_{11}/q_{12} = 9.84 \pm 0.39$,

Thesis Supervisors: Ali Javan and Michael S. Feld
Title: Professors of Physics

ENERGY ABSORPTION AND VIBRATIONAL
HEATING IN MOLECULES
FOLLOWING INTENSE LASER EXCITATION

by

Ronald Erwin McNair

Submitted to the Department of Physics in partial fulfillment
of the requirements for the degree of Doctor of Philosophy.

ABSTRACT

Studies are made of the energy flow into and among the vibrational degrees of freedom of polyatomic molecules due to vibration-vibration (V-V) collisions following intense laser excitation. These studies have been made theoretically, by computer analysis, and experimentally.

Simple closed form expressions are derived for predicting the energy absorbed by an oscillator from an intense saturating laser pulse. This analysis treats the regime where high vibrational excitation is accomplished via V-V exchange collisions. The fundamental results obtained employ the novel assumption of a time dependent quasi-equilibrium distribution existing among the upper vibrational states. This assumption is verified by detailed computer simulations.

A similar formalism is applied to a simple polyatomic molecule with one mode under laser irradiation. Theoretical, computer, and experimental evidence are presented supporting the remarkable finding that: the energy absorbed by a polyatomic can be predicted by the simple expressions derived for a diatomic molecule.

Energy absorption of CO_2 laser radiation by CH_3F gas have shown that at 5.0 Torr CH_3F pressure, ~ 2.5 quanta per molecule is absorbed by the gas. For a known laser pulse duration (3.0 μsec) the simple theoretical expressions yield a V-V up-

the-ladder rate for the ν_3 (C-F stretch) mode of $0.8 \pm 0.2 \mu\text{sec}^{-1}$ -
torr⁻¹ which agrees well with measurements by laser fluores-
cence techniques. This shows that an energy absorption ex-
periment is now a method for determining V-V rates.

A new method for measuring the energy stored in the
vibrational degrees of freedom is introduced. Using this
technique--the "cold gas filter" method--approximately 50%
of the total energy absorbed is found to reside in the C-F
stretch mode of CH_3F at about $9.6 \mu\text{m}$. Vibrational tempera-
tures of $\sim 3000^\circ\text{K}$ are observed after all the modes reach a
vibrational steady state while the translational tempera-
ture remains a constant.

The re-distribution of energy by intra-mode V-V colli-
sional coupling is observed and presented in the transient
and steady state regimes. The energy stored in the modes
of CH_3F that are collisionally coupled to the laser pumped
mode is measured, again, by laser induced fluorescence. By
calibrating the spontaneous emission intensity of the n^{th}
mode by that of ν_3 , which is measured by the cold gas fil-
ter, the intensity ratios I_n/I_3 are used to obtain the ener-
gy storage. I_n is the intensity of any mode in CH_3F and I_3
is the ν_3 intensity.

A model for predicting the steady state partitioning of
energy in polyatomics is presented and applied to CH_3F . The
good agreement between the model predicted partitioning of
energy and the measured energies prove that the modes equi-
librate at different vibrational temperatures and that the
energy flow path used is the dominant and most probable one.

These findings manifest some of the heretofore unobser-
ved behavior of polyatomics and their interaction with strong
resonant laser pulses. In addition, new possibilities are
opened in the areas of laser induced photochemistry and
intra-mode and inter-molecular energy transfer lasers.

Thesis Supervisor: Michael S. Feld
Title: Associate Professor of Physics

PROPERTIES OF METAL-BARRIER-METAL HIGH SPEED TUNNELING
JUNCTIONS RESPONDING TO INFRARED AND VISIBLE RADIATIONS

by

GILBERT MICHAEL ELCHINGER

Submitted to the Department of Physics on July 17, 1978, in partial fulfillment of the requirements for the degree of Doctor of Philosophy.

Abstract

The conduction mechanisms of metal evaporated tunnel junctions are examined for applied electric field frequencies from RF to the visible. For optical frequencies, responses were measured when a laser source directly illuminated the junction. Responses of both normal and superconducting junctions were measured.

In the metal-oxide-metal junction, two frequency dependent regimes of conductivity exist. At RF, where the frequency is smaller than the junction's $(RC)^{-1}$ the conduction scheme is electron tunneling. At photon energies in the range of the tunnel barrier height the conduction scheme is photo-induced tunneling. Expressions for the tunnel barrier parameters (width, height, and asymmetry factor) in terms of the RF rectified response are derived from the tunneling formalism. It is shown that the tunnel current, for photo-induced tunneling, is a function of the barrier shape through the energy dependent tunneling probability function. Tunneling theory is used to derive the photocurrents, as a function of incident photon energy, for different barrier shapes; square, trapezoidal, parabolic, and image force lowered. Estimates of barrier shapes for three junctions (Al-Mg, Al-Al, and Mg-Mg) were obtained by matching measured photocurrents to those calculated from the barrier models. Barrier parameters obtained from RF rectification measurements were used as bounds for the barrier models.

Responses to optical fields of the Al-Pb, metal-oxide-superconducting junction were found to be of two types; the thermal, or heating response, and a rectification-like response. The nonthermal responses were found to be independent of radiation frequency, and closely resemble the RF rectified response of the junction. Examination of the non-thermal response characteristics shows that rectification at optical frequencies does not occur. A conduction scheme based on a laser-induced nonequilibrium electron distribution

in the superconductor is presented. This model is an extension of a recently proposed model explaining the conduction scheme in superconductor-superconductor junctions. The model proposes that a population inversion of electrons and holes exists about the edges of the superconducting gap when the laser illuminates the junction. The response of the junction, as a function of bias, changes sign at $V_b = \Delta_{pb}/e$, resembling the rectification response.

Thesis Supervisor: Ali Javan

Title: Professor of Physics